Amundsen Sea sea-ice variability, atmospheric circulation, and spatial variations in snow isotopic composition from new West Antarctic firn cores

by

Alison Sara Criscitiello

B.A., Wesleyan University, 2003
M.A., Columbia University, 2006

Submitted in partial fulfillment of the requirements for the degree of

Doctor of Philosophy

at the
MASSACHUSETTS INSTITUTE OF TECHNOLOGY
and the
WOODS HOLE OCEANOGRAPHIC INSTITUTION

February 2014

Signature of Author

Joint Program in Oceanography/Applied Ocean Science and Engineering
Massachusetts Institute of Technology
and Woods Hole Oceanographic Institution
December 19, 2013

Certified by

Sarah B. Das
Thesis Supervisor

Accepted by

Timothy L. Grove
Chair, Joint Committee for Marine Geology and Geophysics
Woods Hole Oceanographic Institution

Amundsen Sea sea-ice variability, atmospheric circulation, and spatial variations in snow isotopic composition from new West Antarctic firn cores

by

Alison Sara Criscitiello

Submitted to the Department of Marine Geology and Geophysics, MIT/WHOI Joint Program in Oceanography/Applied Ocean Science and Engineering on December 19, 2013 in partial fulfillment of the requirements for the degree of Doctor of Philosophy

Abstract

Recent work has documented dramatic changes in the West Antarctic Ice Sheet (WAIS) over the past 30 years (e.g., mass loss, glacier acceleration, surface warming) due largely to the influence of the marine environment. WAIS is particularly vulnerable to large-scale atmospheric dynamics that remotely influence the transport of marine aerosols to the ice sheet. Understanding seasonal- to decadal-scale changes in the marine influence on WAIS (particularly sea-ice concentration) is vital to our ability to predict future change. In this thesis, I develop tools that enable us to reconstruct the source and transport variability of marine aerosols to West Antarctica in the past. I validate new firn-core sea-ice proxies over the satellite era; results indicate that firn-core glaciochemical records from this dynamic region may provide a proxy for reconstructing Amundsen Sea and Pine Island Bay polynya variability prior to the satellite era. I next investigate the remote influence of tropical Pacific variability on marine aerosol transport to West Antarctica. Results illustrate that both source and transport of marine aerosols to West Antarctica are controlled by remote atmospheric forcing, linking local dynamics (e.g., katabatic winds) with large-scale teleconnections to the tropics (e.g., Rossby waves). Oxygen isotope records allow me to further investigate the relationship between West Antarctic firn-core records and temperature, precipitation origin, sea-ice variability, and large-scale atmospheric circulation. I show that the tropical Pacific remotely influences the source and transport of the isotopic signal to the coastal ice sheet. The regional firn-core array reveals a spatially varying response to remote tropical Pacific forcing. Finally, I investigate longer-term (~200 year) ocean and ice-sheet changes using the methods and results gleaned from the previous work. I utilize sea-ice proxies to reconstruct long-term changes in sea-ice and polynya variability in the Amundsen Sea, and show that the tropics remotely influence West Antarctica over decadal timescales. This thesis utilizes some of the highest-resolution, most coastal records in the region to date, and provides some of the first analyses of the seasonal- to decadal-scale controls on source and transport of marine aerosols to West Antarctica.

Thesis Supervisor: Sarah Das
Title: Associate Scientist, Woods Hole Oceanographic Institution

Acknowledgments

First and foremost I would like to thank my advisor Sarah Das. I could not have asked for a better advisor, mentor or friend. My success during this crucial part in my career is thanks to her guidance, support, and patience. She has taught me the most valuable lessons of my scientific career thus far, perhaps most importantly – how to find the questions most worth asking, and how to take risks in order to find the answers.

I owe a big thank you to my committee members. Kris Karnauskas, Patrick Heimback, Weifu Guo, and Matt Evans helped guide my research, lab work, and writing. I am also grateful to Delia Oppo who served as the Chair of my defense, and has been a help and inspiration during my years in the program.

I have been lucky to have incredible collaborators. Ian Joughin, Eric Steig, Howard Conway, and Brooke Medley at University of Washington, and Karen Frey and Luke Trusel at Clark University, have been invaluable to me during this process – at home and in the deep field. The research presented in this thesis would not have been possible without our ice-core drilling team, and RPSC Antarctic science support staff.

To my incredible friends in Boston, Woods Hole, and across the country and world – my life is so much richer because of you.

This thesis is dedicated to my amazing sisters, Ra and Shana, and to my parents. You have lovingly supported and encouraged me my entire life, and have instilled in me the belief that I can do absolutely anything I set my mind to.

This research was supported by an award from the Department of Energy Office of Science Graduate Fellowship Program (DOE SCGF) to ASC, a James E. and Barbara V. Moltz Research Fellowship, and by grants from the National Science Foundation Office of Polar Programs (NSF-OPP; #ANT-0632031 & #ANT-0631973), the National Science Foundation Major Research Instrumentation Program (NSF-MRI; #EAR-1126217), the NASA Cryosphere Program (#NNX10AP09G), and a WHOI Andrew W. Mellon Foundation Award for Innovative Research.

Table of Contents

Chapter 1

Introduction

The marine portion of the West Antarctic Ice Sheet (WAIS) is potentially unstable and may be susceptible to rapid disintegration as a result of relatively modest changes in climatic boundary conditions [e.g., *Hughes*, 1975]. The instability of WAIS is largely a consequence of its bedrock, which lies below sea level and slopes downward from the margins of the ice sheet to its interior. Removal of the fringing ice shelves may result in the rapid and irreversible inland migration of the grounding line [*Thomas et al.*, 1979]. While collapse is a low-probability, high-impact event, its potential contribution to sea-level rise (SLR) combined with recent changes in mass balance and outlet glacier velocities highlight the importance of focusing efforts on better understanding the dynamics in this key region. Pine Island and Thwaites Glaciers are two of the largest Antarctic contributors to recent SLR [*Rignot et al.*, 2008; *Shepherd et al.*, 2012] and will likely continue contributing substantially over the next century [*Joughin et al.*, 2010].

The rapid dynamical changes observed on Pine Island and Thwaites Glaciers are largely the result of variations in ocean heat transport beneath their buttressing ice shelves [*Jacobs et al.*, 2011; *Jenkins et al.*, 2010; *Steig et al.*, 2012]. This region of WAIS is also susceptible to marine intrusions of warm, moist air [*Nicolas and Bromwich*, 2011]. Widespread mass losses along the Bellingshausen and Amundsen Seas have increased the ice sheet loss by 59% between 1998–2008 alone [*Rignot et al.*, 2008]. Understanding recent (~200 year) changes and seasonal- to decadal-scale variability in

the marine influence on WAIS (including changes in atmospheric circulation, ocean temperatures, sea-ice cover, and moisture source) is vital to our ability to predict future change. Polar ice cores contain an extraordinary archive of climate information that extends far beyond the satellite and instrumental periods, making them a valuable tool for interpreting climate trends such as those observed in West Antarctica over longer time periods. In particular, soluble impurity records in polar ice cores can provide evidence for past changes in marine productivity [e.g., *Legrand et al.*, 1997], sea-ice extent [e.g., *Welch et al.*, 1993], and atmospheric circulation [e.g., *Kreutz et al.*, 1997].

The primary goal of my thesis is to examine the dynamic marine influence on WAIS with a multi-disciplinary approach, utilizing a suite of new firn cores from Pine Island and Thwaites Glaciers along the Amundsen Coast. These cores offer some of the highest-resolution, most coastal records in the region to date. In Chapter 2, I focus on sea-ice proxy development (methanesulfonic acid (MSA) and sea salts) over the high-resolution satellite era (1979–2010) in the most coastal firn core of the suite, located 180 km from Pine Island Bay. This has allowed me to characterize how glaciochemical records at this site capture changes in Amundsen Sea sea-ice variability. Additionally, firn-core glaciochemical records from this region prove to be a potential proxy for reconstructing Amundsen Sea and Pine Island Bay polynya variability prior to the satellite era. In Chapter 3, I examine the effect of large-scale atmospheric variability in the tropical Pacific on the transport of marine aerosols to West Antarctica (1979–2010), utilizing four cores from across the Amundsen Coast. My work has shown that both source and transport of marine aerosols to West Antarctica are modulated by similar atmospheric dynamics in response to remote forcing. The regional firn-core array

suggests there is both a temporally and spatially varying response to remote tropical forcing. Taken together, Chapters 2 and 3 give a comprehensive view of recent (1979–2010) changes in source and transport of marine aerosols to the Amundsen Coast of West Antarctica. A particular strength of this work is the multi-core, multi-species approach used when looking to reconstruct sea-ice variability as well as spatial and temporal patterns of atmospheric variability and biological productivity near the sites. In Chapter 4, I provide a first assessment of three new stable isotope records from West Antarctica, focusing on relationships between $\delta^{18}O$ and deuterium excess (*d*) and local temperature, regional sea-ice concentration and polynya variability, and remote tropical Pacific forcing. The array of cores along the Amundsen Coast allows me to investigate the spatial variability in these relationships. I find that the most coastal core exhibits patterns in moisture source location distinct from the other two sites, and is more strongly affected by local polynya variability than the sites farther inland. My results indicate a shift from predominantly Amundsen-Bellingshausen Sea moisture source regions in spring toward Ross Sea moisture source regions in fall, concurrent with a shift (from fall to spring) toward predominantly cyclonic transport pathways, likely a result of the position of the Amundsen Sea Low (ASL). In agreement with results from Chapter 3, the source and transport of the isotopic signal to all sites, and ultimately local winds, are remotely influenced by the tropical Pacific.

Chapter 4 serves as an analog to Chapters 2 and 3, as all three together give a complete view of regional surface ocean and ice-sheet changes over the last ~20 years, with a particular focus on how the glaciochemical records associated with these processes are deposited and preserved in the ice-sheet stratigraphy at various locations across West

Antarctica. In Chapter 5, I apply the methods and tools developed in the previous three chapters to the full length of the three long firn cores (1786–2010, 1918–2010, and 1867–2010), enabling me to investigate longer-term ocean and ice-sheet changes near Pine Island Bay. During the twentieth century, the West Antarctic firn-core records indicate strong linkages to sea surface temperature and sea level pressure variations in the tropical Pacific on decadal time scales. In addition, glaciochemical records from the core site farthest inland appear to be most influenced by remote atmospheric dynamics, while glaciochemical records from the most coastal site (180 km from Pine Island Bay) are most influenced by local sea-ice and polynya variability. Each chapter in this thesis builds upon the previous chapters, together providing a comprehensive view of how recent changes in surface ocean conditions (in particular sea-ice and polynya variability) influence the adjacent ice-sheet surface, and how this marine influence on the ice sheet has changed through time.

References

Hughes, T. (1975), The West Antarctic Ice Sheet: Instability, disintegration, and initiation of ice ages, *Rev. Geophys.*, *13*(4), 502-526.

Jacobs, S., A. Jenkins, C. F. Giulivi, and P. Dutrieux (2011), Stronger ocean circulation and increased melting under Pine Island Glacier ice shelf, *Nature Geosci*, *4*(8), 519-523.

Jenkins, A., P. Dutrieux, S. S. Jacobs, S. D. McPhail, J. R. Perrett, A. T. Webb, and D. White (2010), Observations beneath Pine Island Glacier in West Antarctica and implications for its retreat, *Nature Geosciences*, *3*(7), 468-472.

Joughin, I., B. E. Smith, and D. M. Holland (2010), Sensitivity of 21st century sea level to ocean-induced thinning of Pine Island Glacier, Antarctica, *Geophysical research letters*, *37*(20), L20502.

Kreutz, K. J., P. A. Mayewski, L. D. Meeker, M. S. Twickler, S. I. Whitlow, and I. I. Pittalwala (1997), Bipolar changes in atmospheric circulation during the Little Ice Age, *Science*, *277*(5330), 1294-1296.

Legrand, M., C. Hammer, M. De Angelis, J. Savarino, R. Delmas, H. Clausen, and S. J. Johnsen (1997), Sulfur-containing species (methanesulfonate and SO4) over the

last climatic cycle in the Greenland Ice Core Project (central Greenland) ice core, *J. Geophys. Res.*, *102*(C12), 26663-26679.

Nicolas, J. P., and D. H. Bromwich (2011), Climate of West Antarctica and influence of marine air intrusions, *Journal of Climate*, *24*(1), 49-67.

Rignot, E., J. L. Bamber, M. R. van den Broeke, C. Davis, Y. Li, W. J. van de Berg, and E. van Meijgaard (2008), Recent Antarctic ice mass loss from radar interferometry and regional climate modelling, *Nature Geosciences*, *1*(2), 106-110.

Shepherd, A., et al. (2012), A reconciled estimate of ice-sheet mass balance, *Science*, *338*(6111), 1183-1189.

Steig, E. J., Q. Ding, D. S. Battisti, and A. Jenkins (2012), Tropical forcing of circumpolar deep water inflow and outlet glacier thinning in the Amundsen Sea Embayment, West Antarctica, *Annals of Glaciology*, *53*(60), 19-28.

Thomas, R. H., T. J. O. Sanderson, and K. E. Rose (1979), Effect of climatic warming on the West Antarctic Ice Sheet, *Nature*, *277*(5695), 355-358.

Welch, K. A., P. A. Mayewski, and S. I. Whitlow (1993), Methanesulfonic acid in coastal Antarctic snow related to sea-ice extent, *Geophys. Res. Lett.*, *20*(6), 443-446.

Chapter 2

Ice sheet record of recent sea-ice behavior and polynya variability in the Amundsen Sea, West Antarctica *

Abstract

Our understanding of past sea-ice variability is limited by the short length of satellite and instrumental records. Proxy records can extend these observations but require further development and validation. We compare methanesulfonic acid (MSA) and chloride (Cl^-) concentrations from a new firn core from coastal West Antarctica with satellite-derived observations of regional sea-ice concentration (SIC) in the Amundsen Sea (AS) to evaluate spatial and temporal correlations from 2002–2010. The high accumulation rate (~39 $g \cdot cm^{-2} \cdot yr^{-1}$) provides monthly resolved records of MSA and Cl^-, allowing detailed investigation of how regional SIC is recorded in the ice-sheet stratigraphy. Over the period 2002–2010 we find that the ice-sheet chemistry is significantly correlated with SIC variability within the AS and Pine Island Bay polynyas. Based on this result, we evaluate the use of ice-core chemistry as a proxy for interannual polynya variability in this region, one of the largest and most persistent polynya areas in Antarctica. MSA concentrations correlate strongly with summer SIC within the polynya regions, consistent with MSA at this site being derived from marine biological productivity during the spring and summer. Cl^- concentrations correlate strongly with winter SIC within the polynyas as well as some regions outside the polynyas, consistent with Cl^- at this site originating primarily from winter sea-ice formation. Spatial correlations were generally insignificant outside of the polynya areas, with some notable exceptions. Ice-core glaciochemical records from this dynamic region thus may provide a proxy for reconstructing AS and Pine Island Bay polynya variability prior to the satellite era.

* Published as: Criscitiello, A.S., S.B. Das, M.J. Evans, K.E. Frey, H. Conway, I. Joughin, B. Medley, and E.J. Steig (2013). Ice sheet record of recent sea-ice behavior and polynya variability in the Amundsen Sea, West Antarctica, *Journal of Geophysical Research – Oceans*, 118: 118–130, doi:10.1029/2012JC008077.

Ice sheet record of recent sea-ice behavior and polynya variability in the Amundsen Sea, West Antarctica

Alison S. Criscitiello,[1,2] Sarah B. Das,[2] Matthew J. Evans,[3] Karen E. Frey,[4] Howard Conway,[5] Ian Joughin,[5,6] Brooke Medley,[5] and Eric J. Steig[5,7]

Received 22 March 2012; revised 26 October 2012; accepted 3 November 2012; published 25 January 2013.

[1] Our understanding of past sea-ice variability is limited by the short length of satellite and instrumental records. Proxy records can extend these observations but require further development and validation. We compare methanesulfonic acid (MSA) and chloride (Cl^-) concentrations from a new firn core from coastal West Antarctica with satellite-derived observations of regional sea-ice concentration (SIC) in the Amundsen Sea (AS) to evaluate spatial and temporal correlations from 2002–2010. The high accumulation rate (~39 $g \cdot cm^{-2} \cdot yr^{-1}$) provides monthly resolved records of MSA and Cl^-, allowing detailed investigation of how regional SIC is recorded in the ice-sheet stratigraphy. Over the period 2002–2010 we find that the ice-sheet chemistry is significantly correlated with SIC variability within the AS and Pine Island Bay polynyas. Based on this result, we evaluate the use of ice-core chemistry as a proxy for interannual polynya variability in this region, one of the largest and most persistent polynya areas in Antarctica. MSA concentrations correlate strongly with summer SIC within the polynya regions, consistent with MSA at this site being derived from marine biological productivity during the spring and summer. Cl^- concentrations correlate strongly with winter SIC within the polynyas as well as some regions outside the polynyas, consistent with Cl^- at this site originating primarily from winter sea-ice formation. Spatial correlations were generally insignificant outside of the polynya areas, with some notable exceptions. Ice-core glaciochemical records from this dynamic region thus may provide a proxy for reconstructing AS and Pine Island Bay polynya variability prior to the satellite era.

Citation: Criscitiello, A. S., S. B. Das, M. J. Evans, K. E. Frey, H. Conway, I. Joughin, B. Medley, and E. J. Steig (2013), Ice sheet record of recent sea-ice behavior and polynya variability in the Amundsen Sea, West Antarctica, *J. Geophys. Res. Oceans*, *118*, 118–130, doi:10.1029/2012JC008077.

1. Introduction

[2] The Amundsen Sea (AS) has experienced a significant decline in sea-ice extent (SIE) over the last quarter century [*Comiso and Nishio*, 2008; *Turner et al.*, 2009], in contrast to increasing SIE trends around the rest of Antarctica and coincident with regional ice-sheet surface warming [*Steig et al.*, 2009; *Schneider et al.*, 2011]. The West Antarctic Ice Sheet (WAIS) is susceptible to both marine intrusions of warm, moist air [*Nicolas and Bromwich*, 2011] and changes in ocean heat transport beneath its ice shelves [*Jenkins et al.*, 2010; *Jacobs et al.*, 2011; *Steig et al.*, 2012]. This has resulted in the highest rates of mass loss and glacier acceleration in Antarctica outside of the Antarctic Peninsula. Widespread mass losses along the Amundsen-Bellingshausen Sea have increased the ice-sheet loss by nearly 60% between 1996 and 2006 alone [*Rignot et al.*, 2008]. The most significant rates of mass loss and acceleration have occurred in the Pine Island and Thwaites Glacier regions of WAIS (Figure 1) [*Rignot et al.*, 2008].

[3] Antarctic coastal polynyas can affect regional ocean-atmosphere heat exchange and play an important role in winter sea-ice production, upwelling, deep-water formation, and biological productivity. In West Antarctica, polynya variability may be particularly important in the context of recent sea-ice decline in the AS and mass loss of the adjacent WAIS [e.g., *Rignot et al.*, 2008]. Polynya variability within the AS and Pine Island Bay (PIB) polynyas may contribute to these observed ice-sheet changes, most notably by influencing

All Supporting Information may be found in the online version of this article.

[1]MIT/WHOI Joint Program in Oceanography/Applied Ocean Sciences and Engineering, Woods Hole Oceanographic Institution, Woods Hole, Massachusetts, USA.
[2]Department of Geology and Geophysics, Woods Hole Oceanographic Institution, Woods Hole, Massachusetts, USA.
[3]Department of Chemistry, Wheaton College, Norton, Massachusetts.
[4]Graduate School of Geography, Clark University, Worcester, Massachusetts, USA.
[5]Department of Earth and Space Sciences, University of Washington, Seattle, Washington, USA.
[6]Applied Physics Laboratory, University of Washington, Seattle, Washington, USA.
[7]Quaternary Research Center, University of Washington, Seattle, Washington, USA.

Corresponding author: A. S. Criscitiello, Department of Geology and Geophysics, Woods Hole Oceanographic Institution, Woods Hole, MA 02543, USA. (acriscitiello@whoi.edu)

2169-9275/13/2012JC008077

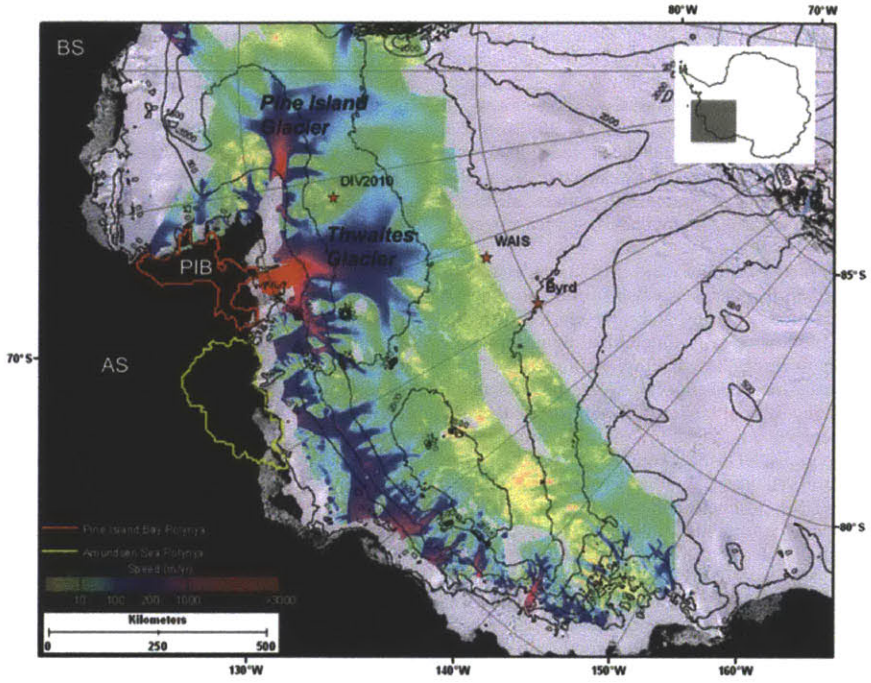

Figure 1. Regional setting of coastal West Antarctica. Grey box in inset shows map location. Glacier speeds ($m \cdot yr^{-1}$) derived from InSAR data [*I. Joughin*]. Background MODIS mosaic of Antarctica is shown with 500 m contour intervals. The DIV2010 drill site on the divide between Thwaites and Pine Island Glaciers is at an elevation of 1292 m. Byrd and WAIS Divide are also shown. PIB = Pine Island Bay, AS = Amundsen Sea, BS = Bellingshausen Sea. The PIB polynya mask is shown in red, and the AS polynya mask is shown in yellow. This region has experienced rapid change since 1979 which has been attributed to increased subglacial melting, warming surface temperatures, and susceptibility to intrusions of warm, moist marine air [e.g., *Zwally et al.*, 2002].

coastal sea-ice production, ocean circulation, ice-shelf melting and retreat, and ice-sheet dynamics. Polynyas are often considered to be wintertime phenomena since they are, by definition, areas of open water or reduced sea-ice cover located in a region where surrounding waters are ice-covered. In spring, surface waters associated with polynyas are often biologically productive because they are the first polar marine systems to be exposed to springtime solar radiation, either because they are ice free or their thin sea-ice cover is more susceptible to early breakup in the spring [*Mundy and Barber*, 2001]. While technically no longer polynyas, these non-winter features are biogeochemically and thermodynamically important. Owing to their close relationship to winter polynyas, these areas in spring and summer will be referred to here as post-polynyas following others [e.g., *Arrigo and van Dijken*, 2003].

[4] Winter sea-ice production, local biology, and regional ocean-atmosphere heat exchange can be strongly impacted by the presence of polynyas, even though they make up only a small fraction of the coastal Southern Ocean [*Maykut*, 1982]. Surface waters associated with coastal polynyas are regions of enhanced primary and secondary production [*Grebmeier and Cooper*, 1995; *Mundy and Barber*, 2001; *Arrigo and van Dijken*, 2003]. Growth and accumulation of phytoplankton biomass are much greater within polynyas than in adjacent waters, with rates of primary production often exceeding $1\ g \cdot C \cdot m^{-2} \cdot d^{-1}$ [*Arrigo et al.*, 2000] and the proportion of new to regenerated production generally high [*Smith et al.*, 1990]. Polynya dynamics for some Antarctic polynyas have been quantified over the satellite era [e.g., *Massom et al.*, 1998; *Fichefet and Goosse*, 1999; *Bindoff et al.*, 2001; *Arrigo and van Dijken*, 2003], increasing our understanding of their spatial and temporal variability. Obtaining longer-term, pre-satellite-era records of both sea-ice and polynya variability is critical to our understanding of the climate system, ocean circulation, and biological productivity across the Antarctic.

[5] Previous efforts have attempted to develop sea-ice proxies using ice- and firn-core records. Sea salt sodium ($ssNa^+$) and other sea-salt aerosol ions (Cl^-, Mg^+, K^+, Ca^{2+}, SO_4^{2-}) have been used as qualitative proxies for regional SIE around Antarctica. Some studies have proposed that sea-ice formation processes, including frost flower formation and brine production, as well as blowing snow released from sea-ice surfaces, are the dominant source of sea-salt aerosol transport to Antarctic glacial ice [*Rankin et al.*, 2002; *Wolff et al.*, 2003;

Kaleschke et al., 2004; *Wolff et al.*, 2006; *Fischer et al.*, 2007; *Yang et al.*, 2008; *Roscoe et al.*, 2011]. Other studies, however, have instead suggested that open water in the marginal sea-ice zone, particularly during stormy seasons, promotes increased production, transport, and deposition of sea-salt aerosols [*Petit et al.*, 1999; *Kinnard et al.*, 2006; *Abram et al.*, 2011]. Observations of enhanced sea-salt aerosol fluxes are difficult to interpret with respect to their ultimate drivers, as enhanced fluxes can reflect increased open water in some cases, or increased sea-ice cover in other cases.

[6] The use of methanesulfonic acid (MSA) concentrations in Antarctic ice and firn cores has also been explored as a potential sea-ice proxy. During and after sea-ice breakup, phytoplankton blooms release dimethylsulfoniopropionate (DMSP) which degrades to dimethyl sulfide (DMS) by several biologically-mediated processes (e.g., phytoplankton cell lysis or grazing by zooplankton) [*Dacey and Wakeham*, 1986]. It has been shown that in low-nutrient, subtropical, oligotrophic regions, DMS production results from physiological stress such as UV radiation [*Toole and Siegel*, 2004], whereas DMS production in polar regions is bloom-forced and therefore directly linked to phytoplankton activity [*Curran and Jones*, 2000]. In the Southern Ocean, DMS-producing phytoplankton are dominated by sea-ice algae [*Curran et al.*, 2003]. Changes in brine volume associated with increased permeability of sea-ice cover as it warms and thins have been shown to directly affect DMS and DMSP migration through the brine network in Antarctic sea ice, significantly contributing to the atmospheric sulfur budget [*Tison et al.*, 2010]. DMS is oxidized in the atmosphere to MSA [*Ravishankara et al.*, 1997], which is then deposited by solid precipitation onto the adjacent ice sheet [*Saigne and Legrand*, 1987; *Gibson et al.*, 1990]. While oxidation of MSA is greatly reduced during polar darkness, the process has still been shown to occur year-round, depending primarily on the BrO oxidation pathway [*Jourdain and Legrand*, 2001; *Breider et al.*, 2010].

[7] The timing, duration, and spatial extent of sea-ice breakup should therefore exert a control on the timing and amount of both DMSP produced and MSA precipitated on the ice sheet. There is no other known source of MSA [*Mulvaney et al.*, 1992]. Previous studies have shown there are both strong negative correlations [*Pasteur et al.*, 1995; *Isaksson et al.*, 2005; *Abram et al.*, 2007; *Rhodes et al.*, 2009; *Abram et al.*, 2011] and strong positive correlations [*Welch et al.*, 1993; *Legrand et al.*, 1997; *Curran et al.*, 2003; *Abram et al.*, 2010] between time series of MSA concentrations and SIE, suggesting that MSA concentrations are influenced by many factors including local sea-surface and air temperatures, precipitation, winds, and general sea-ice conditions [*Hezel et al.*, 2011]. Precipitation and winds in particular may confound the interpretation of MSA records, as high MSA production does not necessarily mean high MSA concentrations reaching the ice sheet if precipitation is low or winds are offshore. These regional studies vary in local meteorology, climate, elevation, and distance from the coast. Additionally, previous studies have not always clearly defined whether their proxies indicate annual mean or maximum sea ice, nor whether their proxies are indicative of sea-ice concentration (SIC) or extent. The recent use of sea-salt and MSA records from the International Trans-Antarctic Scientific Expedition (ITASE) cores collected across WAIS revealed that maximum and mean annual concentrations for both species correlated significantly with maximum, mean, and minimum annual SIE in the Amundsen-Bellingshausen Sea (230°–290°) [*Sneed et al.*, 2011], and highlighted the effectiveness of combining MSA and sea-salt records when investigating the marine influence on ice-sheet chemistry.

[8] Our understanding of modern climate and past change in the AS and PIB requires attaining reliable records of sea-ice behavior and biological production prior to the satellite era. While aforementioned studies have used sea-salt aerosols and/or MSA to investigate sea-ice extent, here we examine how such glaciochemical records may provide additional insight into polynya behavior. In this study, we present new high temporal resolution (monthly) records of MSA and Cl^- from the divide between Thwaites and Pine Island Glaciers (Figure 1) over the past decade (2001–2010), and investigate the use of MSA and Cl^- records as proxies for variability within the Amundsen Sea, specifically within the AS and PIB polynya regions. In this study we explicitly explore the relationships between several sea-ice and ice-sheet variables in a more rigorous way than has been done in previous studies. This work allows for reconstructions of SIC and polynya activity using measurements of ice cores extending beyond the satellite era, bridging a critical gap in our understanding of past climate and sea-surface conditions.

2. Methods

2.1. Site Description

[9] The DIV2010 core site (76.768°S, 101.735°W) is located on the drainage divide between Thwaites and Pine Island glaciers (Figure 1). This site is 1292 m above sea level and 180 km from the coast of PIB. The ice speed at this location is ~10–20 $m \cdot yr^{-1}$ [*Joughin et al.*, 2003]. The DIV2010 firn core used in this study was collected in December 2010 using a 3 inch diameter Pico hand auger and is 7.94 m long, with a corresponding bottom age of October 2001. Age-depth relationship and accumulation rates were established by matching the $\delta^{18}O$ firn-core record (Figure 2) with regional surface temperature data. Using this method we calculated a mean accumulation rate of ~39 $g \cdot cm^{-2} \cdot yr^{-1}$ ($\sigma = 8.7$ $g \cdot cm^{-2} \cdot yr^{-1}$) and determined that annual accumulation is relatively equally distributed seasonally. The high accumulation rates allow for sub-seasonal resolution of the DIV2010 core records, as well as limit post-depositional loss of MSA [*Weller et al.*, 2004]. Further detail on core handling, core physical properties, and core dating is included in the Supporting Information.

2.2. Lab Methods and Glaciochemical Time Series

[10] The outer 2 cm of each core was removed, and the core was then subsampled into 3–5 cm thick slices (~14 samples/yr) depending on the location of core breaks. These slices were cut in half longitudinally, one sample used for analysis of oxygen isotopes, the other sample used for MSA and Cl^- analyses. Samples were kept frozen until the day of analysis. $\delta^{18}O$ analyses were run on a Picarro cavity ring-down spectroscopy analyzer (precision for $\delta^{18}O$ of water samples is $\leq 0.1‰$). The $\delta^{18}O$ time series was used to derive an age-depth scale for the geochemical records, further described in the Supporting Information.

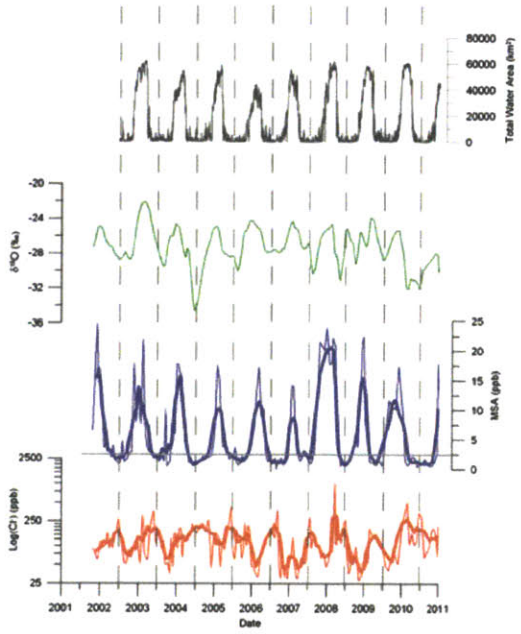

Figure 2. Chemical time series in the DIV2010 core and total open water area within AS and PIB polynyas. Total polynya open water area (grey), $\delta^{18}O$ (green), MSA (blue), and Cl^- (red; shown as log(Cl^-)) are shown. Thick red and blue lines are a 5-point running mean. Vertical black dashed lines indicate mid-winter (June 1) of each year, and the horizontal grey line indicates the MSA detection limit (the entire Cl^- time series lies above the Cl^- detection limit of 0.8 ppb). *X*-axis years indicate the start (January) of a year.

[11] MSA and Cl^- analyses were performed simultaneously on a Dionex ICS1000 Ion Chromatograph (IC) using suppressed ion chromatography after *Curran and Palmer* [2001]. The IC is equipped with small-bore tubing and columns (2 mm) and a 240 µL sample loop to increase sensitivity. MSA analyses were performed using Dionex AG/AS 14 columns and a 2 µM sodium-borate eluent [*Curran and Palmer*, 2001; *Morganti et al.*, 2007]. Standards were prepared daily and blanks were evaluated before and after each sample. A daily 5-point calibration curve was calculated to determine concentrations. Analytical precision is 2.8% (MSA) and 5.5% (Cl^-), with detection limits of 2.5 ppb (MSA) and 0.8 ppb (Cl^-).

[12] MSA and Cl^- fluxes were calculated from the measured MSA and Cl^- concentrations, firn-sample volumes, and firn-sample densities. Monthly MSA and Cl^- data were calculated by linearly interpolating between measured concentrations, which are not evenly spaced in time (due to irregular core breaks, variations in accumulation rate, etc.), and then averaging these interpolated time series. Seasonal MSA and Cl^- values were calculated by averaging the monthly time series; for the purposes of this study we define winter = April to September, summer = October to March.

2.3. Satellite-Derived Sea-Ice Concentration and Polynya Masks

[13] The regional development of sea-ice proxies requires direct validation utilizing satellite imagery. We used Advanced Microwave Scanning Radiometer – EOS (AMSR-E) spatial data of SIC from 2002 to 2010 [*Spreen et al.*, 2008]. Based on passive microwave brightness temperatures, the daily AMSR-E product provides 6.25 km × 6.25 km resolution gridded SIC, ranging from 0% to 100%. While we use a standard, consistent satellite sea-ice product, we note that there may be some ambiguity in the interpretation of thin ice which can effect SIC values [*Markus and Cavalieri*, 2000]. Minimal data gaps were spatially or temporally linearly interpolated. Monthly SIC was calculated by averaging daily SIC (January 2003 to December 2010). Summer SIC was calculated by averaging October to March monthly SIC (October 2002 to March 2010), and winter SIC was calculated by averaging April to September monthly SIC (April 2003 to September 2010). Monthly and seasonal spatial correlation maps were then generated between monthly and seasonal AMSR-E sea-ice time series and monthly and seasonal ice-core glaciochemical time series, respectively. Monthly correlations had 96 pairwise comparisons, whereas seasonal correlations had 8 pairwise comparisons. All correlations reported are statistically significant ($p < 0.1$, monthly threshold $|r| > 0.169$ and seasonal threshold $|r| > 0.622$, accounting for differing degrees of freedom).

[14] Previous work used daily SIC images to map the number of ice-free winter days (June to October) at each pixel location [*Arrigo and van Dijken*, 2003]. Such maps were in turn used to identify the location of coastal polynyas by assuming that polynyas experience the greatest number of ice-free days (using a threshold of 50% ice-free winter days to qualify as a polynya) [*Arrigo and van Dijken*, 2003]. Based on these masks, the AS polynya had a winter area of 3670 km^2, a summer post-polynya area of 38,000 km^2, a January chlorophyll-*a* concentration of 6.98 ± 3.32 $mg \cdot m^{-3}$, and an annual primary production rate of 160.7 ± 36.9 $g \cdot C \cdot m^{-2}$ (data are based on 5 year averages, 1997–2001) [*Arrigo and van Dijken*, 2003]. The PIB polynya had a winter area of 1090 km^2, a summer post-polynya area of 16,890 km^2, a January chlorophyll-*a* concentration of 4.36 ± 3.28 $mg \cdot m^{-3}$, and an annual primary production rate of 151.1 ± 77.8 $g \cdot C \cdot m^{-2}$ (same 5 year average as previous) [*Arrigo and van Dijken*, 2003].

[15] Our AS and PIB polynya masks (Figure 1, 62,344 km^2 maximum total summer water area) are similar (within 7400 km^2 maximum total summer water area) to the summer post-polynya areas of *Arrigo and van Dijken* [2003], but target the areas of significant correlation (*r*-values of –0.4 or better ($p < 0.1$)) between monthly SIC (across all pixels) and monthly-averaged DIV2010 MSA concentrations. These high correlations are driven largely by the strength of correlations in summer. Our chosen threshold r-value of $|r| > 0.4$ is greater than the minimum for monthly statistical significance ($|r| > 0.169$) because this minimum encompasses a large part of the Amundsen Sea. An $|r|$ of 0.4 or better results in reasonable polynya regions that are comparable to *Arrigo and van Dijken* [2003]. These polynya masks show the characteristic spring and summer open-water (break-out) pattern for the AS region, which is particularly evident by midsummer (indicating post-polynya

behavior). Within these polynya masks we then extracted daily open water areas by summing the pixels (6.25 km 6.25 km) that had <15% SIC. We also calculate days with <50% sea-ice cover within both polynyas. This was determined by first creating for each day a binary ice/no-ice dataset, where pixels with >15% sea-ice cover are defined as ice, and pixels with <15% sea-ice cover are defined as no ice. We then calculated the number of days in which <50% of pixels in the polynya areas had sea-ice cover.

[16] Although these two polynya areas (AS and PIB) are geographically distinct, they generally open and close within a week of each other (this holds for summer and winter seasons as well). The percent of open water area within the two polynyas positively covaries ($r^2 = 0.8$). Additionally, the ice-core record does not allow us to distinguish between these two source regions, thus we focus on combined AS +PIB polynya activity in much of the following results and discussion. When we refer to the AS and PIB post-polynyas, we refer to these same mask regions. We note that the monthly polynya SIC and monthly MSA correlations we present below will naturally be high, as this is how we have defined the polynya masks, but emphasize that the overall spatial correlation pattern shown in Figure 7 highlighting the strong correlation between monthly polynya SIC and monthly MSA is from cross-pair analyses across the entire region, and is independent of any masking.

3. Results

3.1. Satellite-Derived Polynya Sea-Ice Reconstructions

[17] AMSR-E data show strong seasonal and interannual variability in open water as well as in the timing of sea-ice breakup and formation in AS+PIB polynya regions over the 2002–2010 period (Figure 3). Generally, sea-ice breakup within AS+PIB polynya regions begins at the end of October, with seasonal sea-ice cover minimum occurring by the end of February. The process of sea-ice formation occurs much more rapidly than breakup and typically occurs over the month of March. The rate of sea-ice breakup is generally slower than the rate of sea-ice formation. There is also more seasonal and more interannual SIC variability during breakup than during formation within AS+PIB polynya regions (over 2002–2010, mean summer total open water $\sigma = 7313\,km^2$, mean winter total open water $\sigma = 823\,km^2$, maximum interannual summer open water $\sigma = 12{,}006\,km^2$, and maximum interannual winter open water $\sigma = 1433\,km^2$).

[18] There is notable variability in interannual summer post-polynya activity during our study period. In particular, the lowest SIC within the post-polynyas (and the earliest onset of breakup) occurred during the austral summer of 2002/2003. Other years with notably low SIC within the post-polynyas are 2007/2008 and 2009/2010. The greatest summertime sea-ice cover occurred during the summer of 2005/2006. There is also variability in the timing that peak polynya size is attained. Postpolynyas reach their maximum size as early as the beginning of January (as in 2006/2007) and as late as the beginning of March (as in 2002/2003). The AS and PIB post-polynyas closed most rapidly and steadily in 2010 (mid-March to mid-April). There is also significant interannual variability in the number of days with <50% sea-ice cover (as defined above). Year 2002/2003 had 129 days with <50% sea-ice cover, which steadily decreased to 67 days by 2005/2006. Following 2005/2006, the number of days with <50% sea-ice cover increased to 115 days by 2008/2009 and remained near-constant through 2010. Annual maximum open polynya water area followed the same trend, with 61,875 km^2 in 2002/03 decreasing steadily to 43,984 km^2 in 2005/2006, followed by an increase to 61,914 km^2 in 2007/2008, which remained near-constant through 2010. While AS and PIB polynyas generally open and close within a week of each other, the percent open water within AS polynya is greater than the percent open water within PIB polynya for all summers between 2002–2010.

[19] There are also wintertime polynya events in AS and PIB polynyas, with considerable interannual variability (Figure 3). Openings have been observed in all months between April and September. Small openings (6000–12,000 km^2) occur annually, sometimes multiple times per year, occurring most often in April, May, and September. Large openings (>12,000 km^2) occurred in July 2002, September 2004, and April 2006. Year 2005 was notable for being the only year over the length of record without a wintertime event. The winter polynya activity is discussed below (section 4.3) in the context of the glaciochemical records.

3.2. Cl^- and MSA Concentrations

[20] We use Cl^- as the representative sea-salt species and present the log value of Cl^- (owing to the non-linear character of seasonal changes in sea-salt concentration) following the recent work of others [e.g., *Röthlisberger et al.*, 2010;

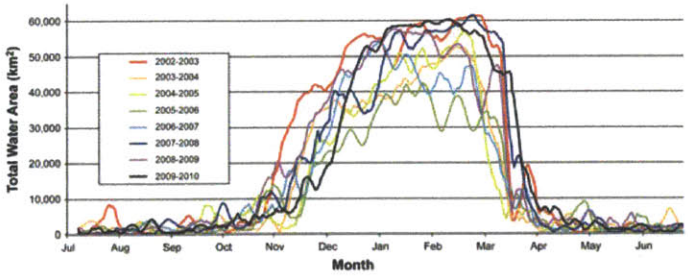

Figure 3. Total water area (km^2) within the AS and PIB polynya masks (as defined in this study, where total water area within the masks = 62,344 km^2) combined, 2002–2010. Only 7-point running means of daily total water area are shown.

Abram et al., 2011]. Measured Cl^- concentrations at the DIV2010 core site range from 28.3–1010 ppb (Figure 2). The mean Cl^- concentration over the length of the core is 128 ppb ($\sigma = 106$ ppb). There is a strong seasonal signal in the Cl^- concentrations (Figure 2). Annual maxima occur in winter months and annual minima occur in early to mid summer (November to December, Figure 4). We also find a smaller late summer (February to March) peak in Cl^- coincident with the initiation of sea-ice formation that occurs during this time. The highest measured Cl^- concentrations in the core occur during June 2005 (428 ppb), February 2010 (514 ppb), and March 2008 (1.01 ppm). Winter mean Cl^- maxima occur earlier in 2008–2010 than in previous years (Figure 2).

[21] Measured MSA concentrations in the DIV2010 core range from 0 to 25 ppb (Figure 2). The mean MSA concentration over the length of the core is 6 ppb ($\sigma = 6$ ppb). The minimum, maximum, and mean MSA concentrations are comparable to concentrations found in other recent Antarctic cores such as the James Ross Island core [*Abram et al.*, 2011]. Annual maxima in MSA occur consistently during the austral summers (Figure 4). Austral winters correspond with annual minima in MSA concentration (Figure 4). The highest MSA concentrations occur during November 2001 (24 ppb), February 2003 (22 ppb), November/December 2007 (23–25 ppb), and February and December 2008 (22 ppb). For most years, there is also one or more smaller winter peaks in MSA concentration (2.5–10 ppb) that coincide with midwinter openings within the AS and PIB polynyas (Figure 5). The largest winter MSA peaks occur during May 2002 (4 ppb), August 2002 (5 ppb), September 2003 (10 ppb), July 2005 (4 ppb), and May/June 2007 (3 ppb, Figure 5). MSA concentrations associated with winter polynya events that occur during months of nonzero insolation south of latitude 70°S (April/August/September, 5–12 ppb) are higher than the winter MSA peaks that occur during months of zero insolation south of latitude 70°S (May/June/July, 3–4 ppb).

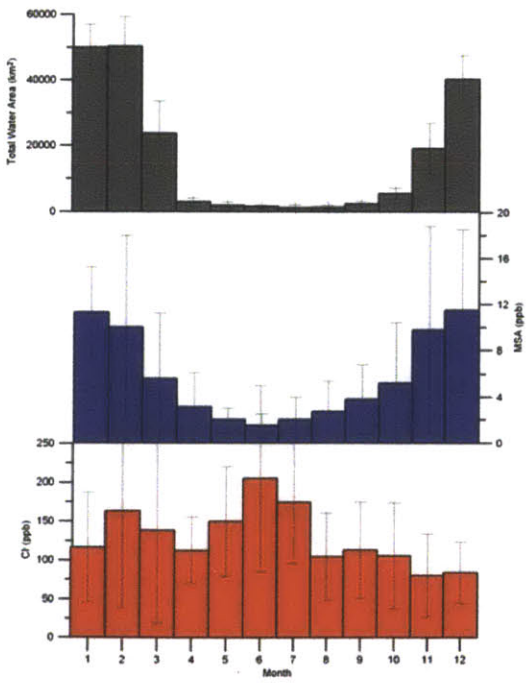

Figure 4. The composite annual cycles of Cl^- (red), MSA (blue), and total polynya water area (grey) for 2002–2010. Error bars give the 1σ range on the composite monthly means. Annual Cl^- maxima occur in winter, corresponding to formation of new sea-ice surfaces within the polynyas. Annual MSA maxima occur in summer, corresponding to sea-ice breakup and phytoplankton blooms within the polynyas.

3.3. Cl^- and MSA Spatial Correlations With Sea-Ice Concentration

[22] Cl^- and MSA concentrations from the DIV2010 site (2002–2010) exhibit correlation patterns with SIC inside the AS and PIB polynya areas, as well as some regions outside the polynyas (Figures 6 and 7, hatch pattern indicates areas statistically significant at $p < 0.1$, monthly threshold $|r| > 0.169$ and seasonal threshold $|r| > 0.622$, accounting for differing degrees of freedom). Focusing first within these masked polynya areas (as defined in section 2.3 above) we find that monthly- and seasonally-averaged MSA and Cl^- concentrations show significant correlation with monthly and seasonal SIC for some areas within the polynyas (Table 1). Cl^- concentrations show a moderate positive correlation with monthly SIC in the AS polynya ($r_{max} = 0.25$), a strong positive correlation with winter SIC in the AS polynya ($r_{max} = 0.65$), and no correlation with summer SIC at $p < 0.1$ (Figure 6). MSA concentrations show a strong negative correlation with monthly SIC in both polynyas ($r_{max} = -0.65$) as expected from our definition of the polynya masks, a strong negative correlation with winter SIC in the AS polynya ($r_{max} = -0.8$), and a strong negative correlation with summer SIC in both polynyas ($r_{max} = -0.8$, Figure 7) at $p < 0.1$ (Table 1).

[23] Monthly and seasonal correlations between sea-ice outside of these polynya areas and ice-sheet chemistry are

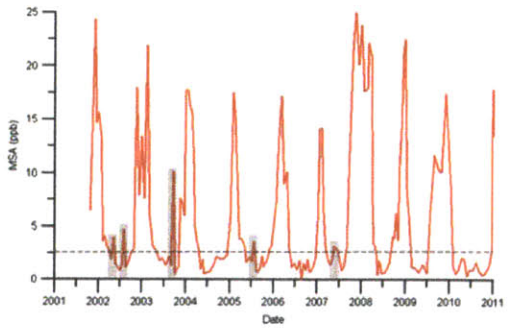

Figure 5. MSA in the DIV2010 core. Winter months (April–September) discussed are highlighted by the grey shading. The small but consistent winter peaks in MSA at the DIV2010 site correspond to winter polynya activity (MSA detection limit is 2.5 ppb, indicated by the dashed black line). *X*-axis years indicate the start (January) of a year.

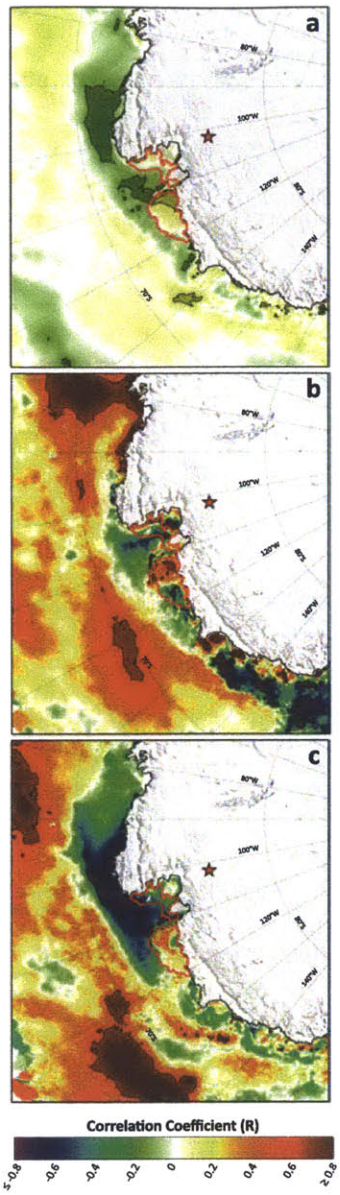

Figure 6. Spatial correlation map of (a) monthly, (b) winter (April to September), and (c) summer (October to March) Cl^- concentrations in the DIV2010 core with AMSR-E SIC around Antarctica. Figures show the AS and PIB masks outlined in red for reference. Hatch pattern indicates areas statistically significant at $p < 0.1$ (monthly threshold $|r| > 0.169$, seasonal threshold $|r| > 0.622$, accounting for differing degrees of freedom). There are positive monthly and winter correlations between Cl^- concentrations at the core site and sea ice within the AS and PIB polynyas, driven primarily by winter sea-ice formation.

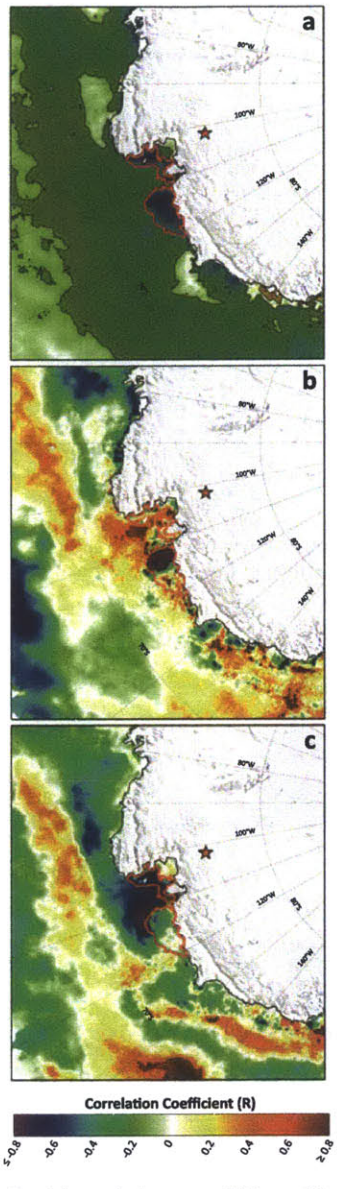

Figure 7. Spatial correlation map of (a) monthly, (b) winter (April to September), and (c) summer (October to March) MSA concentrations in the DIV2010 core with AMSR-E SIC around Antarctica. Figures show the AS and PIB masks outlined in red for reference. Hatch pattern indicates areas statistically significant at $p < 0.1$ (monthly threshold $|r| > 0.169$, seasonal threshold $|r| > 0.622$, accounting for differing degrees of freedom). There are strong negative monthly and summer correlations between MSA concentrations at the core site and sea ice within the AS and PIB polynyas, driven primarily by annual integrated polynya open water area and associated phytoplankton blooms.

Table 1. Correlations ($p < 0.1$) Between MSA/Cl^- and Water Area/SIC Parameters Within the Polynyas, at/north of 70°S, and Northeast of PIB (nc = Not Statistically Significant at $p < 0.1$, SIC = Sea-ice Concentration, TWA = Total Polynya Open Water Area, OW Days = Annual Days With Less Than 50% Sea-ice Cover, OW(max) = Maximum Annual Polynya Open Water Area, IWA = Annual Integrated Total Polynya Open Water Area, MSA/Cl^-(sum) = Annual Integrated MSA/Cl^-, MSA/Cl^-(max) = Maximum Annual MSA/Cl^-). *R*-values Reported Are the Maximum *r*-value Within the Geographic Region Described

	Within Polynyas	AS at/north of 70°S	NE of PIB
Monthly SIC and monthly MSA	–0.65	–0.20	–0.20
Winter SIC and winter MSA	–0.80 (AS)	–0.60	nc
Summer SIC and summer MSA	–0.80	0.80	–0.80
Monthly SIC and monthly Cl^-	0.25 (AS)	nc	–0.30
Winter SIC and winter Cl–	0.65 (AS)	0.60	nc
Summer SIC and summer Cl^-	nc	0.80	–0.80
Monthly TWA and monthly MSA	0.57		
Summer TWA and summer MSA	0.41		
Winter TWA and winter Cl^-	–0.22		
OW days and MSA(max)	0.65		
IWA and MSA(max)	0.66		
IWA and MSA(sum)	0.54		
OW(max) and MSA(sum)	0.50		
OW(max) and MSA(max)	0.49		
OW(max) and Cl^-(max)	0.68		

generally weaker ($|r| < 0.2$), although with notable exceptions. Winter Cl^- concentrations and winter SIC show strong positive correlation ($r = 0.6$) in two regions in the AS north of 70°S (Figure 6). Cl^- and SIC in these two regions correlate in summer and winter, and are most strongly correlated and cover a larger area in the AS in summer. Summer Cl^- concentrations and summer SIC also show strong negative correlations with the coastal AS region northeast of the PIB polynya (between ~70°S–72°S and ~97°W–107°W, $r = –0.8$, Figure 6). Monthly and summer MSA concentrations and monthly and summer SIC also show strong correlations ($r = –0.3$ and –0.8, respectively) northeast of PIB polynya, and north of 70°S between ~130°W–140°W in summer ($r = 0.8$) in the AS (Figure 7, Table 1).

3.4. Cl^- and MSA Correlations With Interannual Polynya Open Water Area

[24] We next investigate the temporal relationship between the masked polynyas and glaciochemical time series from 2002–2010 (Figure 2) to determine how well the DIV2010 ice-core chemical records capture the interannual variability in polynya open water (defined as <15% SIC). We note that while it is assumed that sea-ice breakup leads MSA increase, we cannot say for all years whether one lags the other because we would need resolution of better than 7 days, which cannot be achieved using ice cores (global annual lifetimes of DMS and MSA are 1.8 and 6.7 days, respectively [e.g., *Hezel et al.*, 2011]). For some years (2003, 2007–2009), however, MSA increase clearly does lead sea-ice breakup (Figure 2), suggesting the marine aerosols must also have a source outside of the polynya regions (discussed in section 4). All *r*-values reported are statistically significant ($p < 0.1$). There is a negative correlation between mean winter Cl^- and mean winter total polynya open water area ($r = –0.22$), suggesting that polynyas could be contributing to higher rates of sea-ice production in winter and higher Cl^- concentrations. Mean summer Cl^- and mean summer total polynya open water area are not significantly correlated. Monthly mean Cl^- concentration and monthly mean total polynya water area are also not significantly correlated. A strong relationship was found between the maximum annual open water area within the polynyas and the maximum annual Cl^- concentration ($r = 0.68$, Table 1). No significant correlations were found between annual Cl^- flux and any polynya variables (annual integrated open water area, maximum annual open water area, or annual number of days with <50% sea-ice cover).

[25] Monthly mean MSA concentration and monthly mean total polynya water area are significantly positively correlated ($r = 0.57$) as are mean summer MSA concentration and mean summer total polynya water area ($r = 0.41$, Figure 2). There is a strong relationship between the annual integrated open water area within the polynyas and the maximum annual MSA concentration ($r = 0.66$), and between the annual number of days with <50% sea-ice cover and the maximum annual MSA concentration ($r = 0.65$). Strong relationships were also found between the annual integrated open water area within the polynyas and the annual integrated MSA concentration ($r = 0.54$), the maximum annual open water area within the polynyas and the annual integrated MSA concentration ($r = 0.50$), and the maximum annual open water area within the polynyas and the maximum annual MSA concentration ($r = 0.49$, Figure 2). No statistically significant correlations ($p < 0.1$) were found between annual MSA flux and any polynya variables (annual integrated open water area, maximum annual open water area, or annual number of days with <50% sea-ice cover).

4. Discussion

4.1. Sea-Salt Variability and Polynya Activity

[26] Our results show that the strongest correlations between regional SIC and Cl^- concentrations over the period 2002–2010 occur during winter within the AS polynya (positive correlation), year-round in the AS north of 70°S (positive correlation), and during summer in the AS northeast of the PIB polynya (between ~70°S–72°S and ~97°W–107°W, negative correlation). This area of strong negative correlation northeast of the PIB polynya during summer generally retains thick multiyear sea ice, and

summer openings therefore may generate sea-ice production instead of melt. These results indicate that Cl^- may result from sea-ice production in both summer and winter (Figure 4), and open water sources (including wind-blown sea spray) northeast of the PIB polynya primarily in summer (Figure 6).

[27] In winter, the area of strong positive correlation lies along and offshore of the continental shelf break, whereas over the continental shelf (outside of the polynyas), correlations are negative. Offshore, high sea-ice production is likely associated with ice-edge advance, resulting in high SIC and explaining the positive correlations. In contrast, farther south over the continental shelf, sea ice is typically more consolidated pack ice. Thus new sea-ice production likely follows new openings (leads), which could explain the negative correlations between SIC and Cl^- in this area.

[28] New winter sea-ice surfaces within the AS polynya may also contribute to the sea-salts in the DIV2010 core. Winter polynyas can produce substantial amounts of sea ice, as newly-formed ice is quickly removed by offshore winds, making way for additional sea-ice formation [*Cavalieri*, 1985; *Wagenbach et al.*, 1998]. The presence of polynyas during winter has been suggested to be the largest source of marine aerosols in West Antarctica from both sea spray and frost flowers [*Kaspari et al.*, 2005]. Blowing snow released from sea-ice surfaces has also been suggested to be a large source of marine aerosols [*Yang et al.*, 2008]. This study, however, finds that the rapid, continual development of new sea ice within polynyas (and at the leading ice edge) is likely a significant source of sea-salt aerosols to the DIV2010 site during winter months. Furthermore, the timing of the highest sea-salt concentrations (i.e., winter) coincides with the season of greatest storminess and strongest winds along the Amundsen Coast [*Kreutz et al.*, 2000]. This suggests that there is also a strong wind-driven influence on sea salts deposited at the DIV2010 site. Future investigations of regional wind-driven transport are needed to help differentiate between the different source regions.

[29] Our results are consistent with findings of others, who have also found that seasonal maxima in firn-core sea salts correlate well with winter maxima in SIC [e.g., *Rankin et al.*, 2002; *Wolff et al.*, 2003; *Abram et al.*, 2011]. Some variations in seasonal and interannual variability of the Cl^- record at the DIV2010 site are also likely due to the impacts of varying winds and transport efficiency on sea-salt aerosol deposition. It has been previously suggested that storminess over the ocean and strength of inland transport, both of which are enhanced during winter, can explain the winter maxima in sea-salt records at many coastal sites [*Petit et al.*, 1999]. Therefore, the consistent winter maxima in sea-salt concentrations at the DIV2010 site (Figure 4) are likely the result of both intense sea-ice formation in the region (in the open ocean and polynya areas, as discussed above), as well as increased winds during winter. We note here that the timing of the Cl^- maxima post-2008, while still occurring during winter months as defined in this study, is less consistent than pre-2008 (Figure 2). As in other studies [e.g., *Wolff et al.*, 2003], we find that the transport of sea salts resulting from new ice formation likely represents an important process in the transfer of ocean sea salts to the core site, particularly during the time of winter sea-ice maximum. The source and transport effects on sea-salt variability likely combine to strengthen the signal preserved in the sea-salt concentration of the DIV2010 core. Analysis of nearby ITASE cores showed that the ice-core sea-salt records are controlled in large part by wind strength, whether the aerosols are derived from frost flowers or open-ocean surfaces [*Kaspari et al.*, 2005]. By examining the spatial distribution of marine aerosols across West Antarctica, the authors of this study also confirmed that the dominant source region for the Pine Island-Thwaites sector of WAIS is not the Ross Sea, but rather the Amundsen-Bellingshausen Sea. The quantitative effects of transport variability on the DIV2010 sea-salt record lie outside the scope of this paper (e.g., evaluation of reanalysis winds) but deserve future investigation.

4.2. MSA Variability and Polynya/Post-polynya Activity

[30] Our results show that the strongest negative correlations between regional SIC and MSA concentrations over the period 2002–2010 (monthly and summer) occur within the AS and PIB polynyas/post-polynyas (Figure 7). Our results also show that annual MSA maxima occur in summer when post-polynya open water is at a maximum, and annual MSA minima occur in winter when polynya open water is at a minimum (Figure 4). Monthly and summer MSA concentration and monthly and summer total polynya water area (the inverse of SIC, which is shown in Figure 7) are significantly positively correlated. These results suggest that sea-ice breakup within the post-polynyas in the austral summer, and size of the assumed associated annual phytoplankton bloom, is a primary source of MSA to the core site. This is similar in principle to the findings of *Curran et al.* [2003], who found that annual MSA concentrations were dependent on winter SIC (because summer SIC in their region of study was close to zero, and thus invariable from year to year). In this study, the MSA concentrations are dependent on the timing and variability of summer polynya activity, because there is little change in winter SIC (limited winter polynya activity) from year to year.

[31] In addition, the positive summer correlations noted previously lie along the continental shelf break. High SIC during summer months in this area may be associated with enhanced ice-edge blooms resulting from the retreating ice edge which can induce stratification and promote ice-edge productivity. The percent open water within the AS polynya is greater than the percent open water within the PIB polynya for all summers between 2002–2010, suggesting that the AS polynya may be a more significant source of DMS than the PIB polynya. This is consistent with the hypothesis that a larger sea-ice breakup and more open water in summer will often result in larger phytoplankton blooms and increased release of DMS, which others have shown [*Pasteur et al.*, 1995; *Isaksson et al.*, 2005; *Abram et al.*, 2007; *Rhodes et al.*, 2009; *Abram et al.*, 2011; *Arrigo et al.*, 2012]. This is also consistent with several studies that show that polynyas can produce more significant fluxes of DMS into the overlying atmosphere than adjacent waters in the sea-ice zone [*Zemmelink et al.*, 2005, 2008; *Tison et al.*, 2010; *Asher et al.*, 2011; *Brabant et al.*, 2011].

[32] Our results also show that there are significant correlations between annual integrated polynya open water area

and maximum annual MSA concentration, as well as annual number of days with <50% sea-ice cover (calculated from the open water time series) and maximum annual MSA concentration. Annual integrated polynya open water area (not the maximum polynya size attained), then, has a more significant effect on maximum annual MSA concentrations at the core site. These results suggest that the length of time the polynyas are at least partially open during spring and summer strongly affects the size of the summer phytoplankton bloom (shown by others, e.g., *Arrigo et al.*, 2012), amount of DMS produced in the polynyas/post-polynyas, and therefore the amount of MSA precipitated at the core site. High DMS concentrations and turnover rates in ice-free Antarctic polynya waters, particularly under late summer conditions of high solar irradiance and mixed layer stratification, have been documented in nearby polynyas [e.g., *Asher et al.*, 2011]. With sufficient sunlight and adequate upwelling, a polynya event that is small in area but of long duration may result in higher DMS production (and ultimately higher MSA concentrations) than a large but short-duration polynya event.

4.3. Winter MSA Variability

[33] Our results show wintertime increases in MSA coincident with openings within the AS polynya. As this is the first time wintertime peaks in MSA have been reported, we spend some time here to discuss proposed processes associated with these peaks. This winter polynya activity occurs during times of both nonzero and zero insolation in the polynya regions. Winter polynya events that occur during times of nonzero insolation result in higher MSA concentrations than winter polynya events that occur during times of zero insolation, however neither are as high as summer MSA concentrations. We propose different mechanisms that might explain these winter increases in MSA. During times of low but nonzero insolation, the wintertime MSA signal may originate from new, albeit reduced, primary production within the polynyas similar to summer. During times of zero insolation, the MSA signal may originate from release of previously stored DMS in sea ice within the polynyas, or from source regions farther offshore (north of 65°S) that do receive radiation year-round. In either case, the production of oxidants that convert DMS to MSA in the atmosphere is not a limiting factor, as oxidation is initiated by OH in sunny regions, and by NO_3 in dark regions [*Ravishankara et al.*, 1997] (although we note that the relative conversion of DMS to MSA and sulfate aerosols may be seasonally variable). We discuss the proposed mechanisms below.

[34] For years when winter polynya opening occurs when insolation is nonzero (before May or after July), the limited light may be sufficient to support biological productivity within the polynyas when other contributing factors such as adequate upwelling are present. This may be the case in August 2002, September 2003, and August 2005; times when insolation is weak but potentially sufficient to support new productivity in polynya surface waters with sea-ice breakup.

[35] For years when winter polynya opening occurs when insolation is zero (May 2002 and May 2007), an alternative explanation is required to explain the winter MSA peaks. It is improbable that DMS or DMSP from a previous summer would be present in deep water [*Matrai et al.*, 1995; *Rellinger et al.*, 2009]. Instead, winter MSA and winter SIC spatial correlation results indicate that part of the winter MSA source may come from farther offshore in the AS during winter (between ~64°S–67°S and ~107°W–115°W, Figure 7b). This region of moderate negative winter correlation receives sunlight year-round. While insolation from May to July in this region of the AS (north of 65°S) is severely limited, the small amount of radiation may be sufficient both for supporting productivity in open water and for oxidizing DMS to MSA in the atmosphere by several oxidation pathways. DMS emissions have been shown to peak at 66°S [*Hezel et al.*, 2011], further supporting the feasibility of a winter MSA source component from the AS north of 65°S.

[36] The wintertime peaks may additionally be attributed to release of previously stored DMS in sea ice that is in turn released upon wind-driven sea-ice fragmentation during winter polynya openings. This may be the case in May 2002 and May/June 2007. The MSA record, in such instances, may be indicative of a polynya opening, which can be seen both in reconstructions of polynya SIC as well as in AWS temperature data and the $\delta^{18}O$ record (Figure 2) showing midwinter warming during such polynya events. These polynya openings appear to allow for the transfer of stored DMS in sea ice to the atmosphere. It is possible that release of previously stored DMS in sea ice enhances both the summer and winter MSA signal. Several studies have shown evidence of "old" DMSP in winter sea ice from the previous spring/summer bloom, which can be released upon sea-ice breakup and surface flooding [*Trevena et al.*, 2003; *Elliott et al.*, 2009; *Nomura et al.*, 2011; *Tison et al.*, 2010]. It has been shown that the snow layer covering sea ice is important because it is the interface through which DMS needs to be transported to be emitted from the ice to the overlying atmosphere [*Zemmelink et al.*, 2008]. In Antarctic sea ice, flooding of this sea-ice snow cover allows infiltration of the surface layers [*Arrigo et al.*, 1997], which can permit release of DMSP within the sea ice. When sea ice becomes fragmented and is forced offshore by wind during polynya events, the breakup itself can be mechanism enough for release of DMS contained in the sea ice. While the oxidation pathways of DMS to MSA are greatly inhibited during times of zero solar radiation, DMS oxidation does occur year-round. During polar darkness, oxidation of DMS to MSA via BrO pathways increases in importance, and improves the potential for retaining local signals of DMS emissions in MSA deposition at coastal sites [*Breider et al.*, 2010].

5. Conclusions

[37] This work investigates the use of MSA and Cl^- concentrations in a new coastal firn core from the divide between Thwaites and Pine Island glaciers as proxies for sea-ice behavior and polynya variability in the AS and PIB. We compare MSA and Cl^- concentrations in the core with satellite-derived reconstructions of SIC (2002–2010) around coastal West Antarctica. The high annual accumulation rate at the core site (10 year mean ~39 $g \cdot cm^{-2} \cdot yr^{-1}$) results in a monthly- to seasonally-resolved record of MSA and Cl^-, allowing us to investigate how sea-ice and polynya variability is recorded in the firn-core record. Our key

findings are that: (1) firn-core records and regional SIC correlate strongly within AS and PIB polynyas, (2) monthly and summer MSA concentrations are significantly negatively correlated with monthly and summer polynya SIC ($r = -0.65$ and -0.8, respectively; $p < 0.1$), (3) monthly and winter Cl^- concentrations are positively correlated with monthly and winter polynya SIC ($r = 0.25$ and 0.65, respectively; $p < 0.1$), summer Cl^- concentrations are negatively correlated with SIC in the coastal AS northeast of the PIB polynya (between ~70°S–72°S and ~97°W–107°W, $r = -0.8$, $p < 0.1$), and winter and summer Cl^- concentrations and winter and summer SIC show strong positive correlation ($r = 0.6$) in the AS north of 70°S, and (4) interannual monthly and summer MSA concentration and interannual monthly and summer total polynya water area are significantly correlated ($r = 0.57$ and 0.41, respectively; $p < 0.1$). While significant correlations exist between MSA/Cl^- and SIC in some regions in the AS outside of the polynya areas, our results suggest that MSA peaks are in large part a result of new biological productivity in summer following polynya openings, with smaller winter MSA peaks reflecting stored DMS/DMSP in sea ice released during polynya sea-ice breakup, or transport of MSA from farther offshore in the AS. Our results also suggest that sea salts, predominantly deposited in the winter, are originating in large part from winter sea-ice formation within the AS polynya. In summer, sea salts appear to originate primarily from open water sources in the coastal AS northeast of PIB. The summer open water source along 70°S (Figure 6) likely reflects ice-edge advance which occurs predominantly in March and is marked by rapid sea-ice production.

[38] Our results are in agreement with many proxy development studies at other locations in Antarctica that have shown the primary source of MSA to coastal sites to be new summertime biological productivity following sea-ice breakup. Our results are also in agreement with previous work showing the presence of polynyas during winter to be one of the sources of marine aerosols in West Antarctica from both sea spray and frost flowers, owing to the continual development of new sea ice within polynyas. In addition, our results suggest that initiation of new sea-ice production in leads on the continental shelf, as well as new sea-ice production associated with ice-edge advance offshore of the continental shelf, may be other significant sources of marine aerosols to the DIV2010 core site.

[39] The location and temporal resolution of the DIV2010 core allow us to investigate how monthly to seasonal changes in AS SIC as well as AS and PIB polynya SIC are recorded in the adjacent ice sheet. Owing to the high resolution of the DIV2010 core, and its proximity to PIB, we are able to show that interannual MSA and sea-salt variability are driven in part by interannual AS and PIB polynya variability. Our results show that winter mean Cl^- concentrations from this region best capture winter polynya SIC and SIC in two regions in the AS north of 70°S ($r = 0.65$, Figure 6), while maximum annual Cl^- concentrations best capture the maximum annual open water in the polynyas ($r = 0.68$). Our results also suggest that maximum annual MSA concentrations at the core site best capture annual integrated AS and PIB post-polynya open water area variability ($r = 0.65$), although other influences (e.g., productivity outside the polynyas and atmospheric transport variability) undoubtedly also contribute to the MSA variability at DIV2010. This holds promise that the combined use of sea-salt and MSA records in future studies may allow us to reconstruct seasonal changes in regional sea-ice behavior and polynya variability beyond the satellite era, bridging a key gap in our understanding of past climate and sea-surface conditions. Analysis of ice-core records from other sites across the Amundsen Sea Embayment will additionally allow us to assess the reliability of similar proxy records across the ice sheet.

[40] Ice-core marine aerosol records are influenced by both source and transport variability. This study, which focuses on the spatial relationships between satellite-derived SIC (including polynya activity) and ice-sheet chemistry across the AS (including PIB), furthers our understanding of the source variability. Transport variability (including how these marine aerosol records relate to large-scale atmospheric circulation as well as tropical teleconnections) requires proper treatment of its own, and will be the focus of future work.

[41] **Acknowledgments.** Thanks to Luke Trusel, Lou Albershardt, and RPSC support staff for assistance in the field. Thanks to Emily Medeiros and Lauren Thompson for assistance with MSA and Cl^- measurements, and Δ*IsoLab at the University of Washington for assistance with the isotope measurements. Naomi Levine and Ted Maksym provided helpful discussions during the preparation of this manuscript. The authors thank the three anonymous reviewers, whose comments greatly helped improve the original manuscript. This research was supported by an award from the Department of Energy Office of Science Graduate Fellowship Program (DOE SCGF) to ASC, a James E. and Barbara V. Moltz Research Fellowship to SBD, and by grants from NSF-OPP (#ANT-0632031 & #ANT-0631973); NSF-MRI (#EAR-1126217); NASA Cryosphere Program (#NNX10AP09G); and a WHOI Andrew W. Mellon Foundation Award for Innovative Research.

References

Abram, N. J., R. Mulvaney, and C. Arrowsmith (2011), Environmental signals in a highly resolved ice core from James Ross Island, Antarctica, *J. Geophys. Res.*, *116*(D20), D20116, doi:10.1029/2011JD016147.

Abram, N. J., R. Mulvaney, E. W. Wolff, and M. Mudelsee (2007), Ice core records as sea ice proxies: An evaluation from the Weddell Sea region of Antarctica, *J. Geophys. Res.*, *112*(D15), D15101, doi:10.1029/2006JD008139.

Abram, N. J., E. R. Thomas, J. R. McConnell, R. Mulvaney, T. J. Bracegirdle, L. C. Sime, and A. J. Aristarain (2010), Ice core evidence for a 20th century decline of sea ice in the Bellingshausen Sea, Antarctica, *J. Geophys. Res.*, *115*(D23), D23101, doi:10.1029/2010JD014644.

Arrigo, K. R., and G. L. van Dijken (2003), Phytoplankton dynamics within 37 Antarctic coastal polynya systems, *J. Geophys. Res.*, *108*(C8), 3271.

Arrigo, K. R., D. L. Worthen, M. P. Lizotte, P. Dixon, and G. Dieckmann (1997), Primary Production in Antarctic Sea Ice, *Science*, *276*(5311), 394–397.

Arrigo, K. R., G. R. DiTullio, R. B. Dunbar, D. H. Robinson, M. VanWoert, D. L. Worthen, and M. P. Lizotte (2000), Phytoplankton taxonomic variability in nutrient utilization and primary production in the Ross Sea, *J. Geophys. Res.*, *105*(C4), 8827–8846.

Arrigo, K. R., K. E. Lowry, and G. L. van Dijken (2012), Annual changes in sea ice and phytoplankton in polynyas of the Amundsen Sea, Antarctica, *Deep Sea Research Part II: Topical Studies in Oceanography*, *71–76*(0), 5–15.

Asher, E. C., J. W. H. Dacey, M. M. Mills, K. R. Arrigo, and P. D. Tortell (2011), High concentrations and turnover rates of DMS, DMSP and DMSO in Antarctic sea ice, *Geophys. Res. Lett.*, *38*(23), L23609.

Bindoff, N. L., G. D. Williams, and I. Allison (2001), Sea-ice growth and water-mass modification in the Mertz Glacier polynya, East Antarctica, during winter, *Annals of Glaciology*, *33*(1), 399–406.

Brabant, F., S. El Amri, and J. L. Tison (2011), A robust approach for the determination of dimethylsulfoxide in sea ice, *Limnology and Oceanography: Methods*, *9*, 261–274.

Breider, T. J., M. P. Chipperfield, N. A. D. Richards, K. S. Carslaw, G. W. Mann, and D. V. Spracklen (2010), Impact of BrO on

dimethylsulfide in the remote marine boundary layer, *Geophys. Res. Lett.*, *37*(2), L02807.

Cavalieri, D. J. (1985), A passive microwave study of polynyas along the Antarctic Wilkes Land Coast, *Oceanology of the Antarctic Continental Shelf, Antarct.Res.Ser.*, *43*, 227–252.

Comiso, J. C., and F. Nishio (2008), Trends in the sea ice cover using enhanced and compatible AMSR-E, SSM/I, and SMMR data, *J. Geophys. Res.*, *113*(C2), C02S07.

Curran, M. A. J., and G. B. Jones (2000), Dimethyl sulfide in the Southern Ocean: Seasonality and flux, *J. Geophys. Res.*, *105*(D16), 20451–20459.

Curran, M. A. J., and A. S. Palmer (2001), Suppressed ion chromatography methods for the routine determination of ultra low level anions and cations in ice cores, *Journal of Chromatography A*, *919*(1), 107–113.

Curran, M. A. J., T. D. van Ommen, V. I. Morgan, K. L. Phillips, and A. S. Palmer (2003), Ice core evidence for Antarctic sea ice decline since the 1950s, *Science*, *302*(5648), 1203–1206.

Dacey, J. W. H., and S. G. Wakeham (1986), Oceanic dimethylsulfide: Production during zooplankton grazing on phytoplankton, *Science*, *233* (4770), 1314–1316.

Elliott, D., K. Tang, and A. Shields (2009), Mesozooplankton beneath the summer sea ice in McMurdo Sound, Antarctica: abundance, species composition, and DMSP content, *Polar Biology*, *32*(1), 113–122.

Fichefet, T., and H. Goosse (1999), A numerical investigation of the spring Ross Sea polynya, *Geophys. Res. Lett.*, *26*(8), 1015–1018.

Fischer, H., et al. (2007), Reconstruction of millennial changes in dust emission, transport and regional sea ice coverage using the deep EPICA ice cores from the Atlantic and Indian Ocean sector of Antarctica, *Earth and Planetary Science Letters*, *260*(1–2), 340–354.

Gibson, J. A. E., R. C. Garrick, H. R. Burton, and A. R. McTaggart (1990), Dimethylsulfide and the alga Phaeocystis pouchetii in Antarctic coastal waters, *Marine Biology*, *104*(2), 339–346.

Grebmeier, J. M., and L. W. Cooper (1995), Influence of the St. Lawrence Island Polynya upon the Bering Sea benthos, *J. Geophys. Res.*, *100* (C3), 4439–4460.

Hezel, P. J., B. Alexander, C. M. Bitz, E. J. Steig, C. D. Holmes, X. Yang, and J. Sciare (2011), Modeled methanesulfonic acid (MSA) deposition in Antarctica and its relationship to sea ice, *J. Geophys. Res.*, *116*(D23), D23214.

Isaksson, E., T. Kekonen, J. Moore, and R. Mulvaney (2005), The methanesulfonic acid (MSA) record in a Svalbard ice core, *Annals of Glaciology*, *42*(1), 345–351.

Jacobs, S., A. Jenkins, C. F. Giulivi, and P. Dutrieux (2011), Stronger ocean circulation and increased melting under Pine Island Glacier ice shelf, *Nature Geosci*, *4*(8), 519–523.

Jenkins, A., P. Dutrieux, S. S. Jacobs, S. D. McPhail, J. R. Perrett, A. T. Webb, and D. White (2010), Observations beneath Pine Island Glacier in West Antarctica and implications for its retreat, *Nature Geosciences*, *3*(7), 468–472.

Joughin, I., E. Rignot, C. E. Rosanova, B. K. Lucchitta, and J. Bohlander (2003), Timing of recent accelerations of Pine Island Glacier, Antarctica, *Geophys. Res. Lett.*, *30*(13), 1706.

Jourdain, B., and M. Legrand (2001), Seasonal variations of atmospheric dimethylsulfide, dimethylsulfoxide, sulfur dioxide, methanesulfonate, and non-sea-salt sulfate aerosols at Dumont d'Urville (coastal Antarctica) (December 1998 to July 1999), *J. Geophys. Res.*, *106*(D13), 14391–14408.

Kaleschke, L., et al. (2004), Frost flowers on sea ice as a source of sea salt and their influence on tropospheric halogen chemistry, *Geophys. Res. Lett.*, *31*(16), L16114.

Kaspari, S., D. A. Dixon, S. B. Sneed, and M. J. Handley (2005), Sources and transport pathways of marine aerosol species into West Antarctica, *Annals of Glaciology*, *41*(1), 1–9.

Kinnard, C., C. M. Zdanowicz, D. A. Fisher, and C. P. Wake (2006), Calibration of an ice-core glaciochemical (sea-salt) record with sea-ice variability in the Canadian Arctic, *Annals of Glaciology*, *44*, 383–390.

Kreutz, K. J., P. A. Mayewski, I. I. Pittalwala, L. D. Meeker, M. S. Twickler, and S. I. Whitlow (2000), Sea level pressure variability in the Amundsen Sea region inferred from a West Antarctic glaciochemical record, *J. Geophys. Res.*, *105*(D3), 4047–4059.

Legrand, M., C. Hammer, M. De Angelis, J. Savarino, R. Delmas, H. Clausen, and S. J. Johnsen (1997), Sulfur-containing species (methanesulfonate and SO4) over the last climatic cycle in the Greenland Ice Core Project (central Greenland) ice core, *J. Geophys. Res.*, *102*(C12), 26663–26679.

Markus, T., and D. J. Cavalieri (2000), An enhancement of the NASA Team sea ice algorithm, *IEEE Transactions on Geoscience and Remote Sensing*, *38*(3), 1387–1398.

Massom, R. A., P. T. Harris, K. J. Michael, and M. J. Potter (1998), The distribution and formative processes of latent-heat polynyas in East Antarctica, in Annals of Glaciology, Vol 27, 1998, edited by W. F. Budd, pp. 420–426, Int Glaciological Soc, Cambridge.

Matrai, P. A., M. Vernet, R. Hood, A. Jennings, E. Brody, and S. Saemundsdóttir (1995), Light-dependence of carbon and sulfur production by polar clones of the genus *Phaeocystis*, *Marine Biology*, *124*(1), 157–167.

Maykut, G. A. (1982), Large-scale heat exchange and ice production in the central Arctic, *J. Geophys. Res.*, *87*(C10), 7971–7984.

Morganti, A., S. Becagli, E. Castellano, M. Severi, R. Traversi, and R. Udisti (2007), An improved flow analysis-ion chromatography method for determination of cationic and anionic species at trace levels in Antarctic ice cores, *Analytica Chimica Acta*, *603*(2), 190–198.

Mulvaney, R., E. C. Pasteur, D. A. Peel, E. S. Saltzman, and P.-Y. Whung (1992), The ratio of MSA to non-sea-salt sulphate in Antarctic Peninsula ice cores, *Tellus B*, *44*(4), 295–303.

Mundy, C. J., and D. G. Barber (2001), On the relationship between spatial patterns of sea-ice type and the mechanisms which create and maintain the North Water (NOW) polynya, *Atmosphere-Ocean*, *39*(3), 327–341.

Nicolas, J. P., and D. H. Bromwich (2011), Climate of West Antarctica and influence of marine air intrusions, *Journal of Climate*, *24*(1), 49–67.

Nomura, D., N. Kasamatsu, K. Tateyama, S. Kudoh, and M. Fukuchi (2011), DMSP and DMS in coastal fast ice and under-ice water of Lützow-Holm Bay, eastern Antarctica, *Continental Shelf Research*, *31* (13), 1377–1383.

Pasteur, E. C., R. Mulvaney, D. A. Peel, E. S. Saltzman, and P.-Y. Whung (1995), A 340 year record of biogenic sulphur from the Weddell Sea area, Antarctica, *Annals of Glaciology*, *21*, 169–174.

Petit, J. R., et al. (1999), Climate and atmospheric history of the past 420,000 years from the Vostok ice core, Antarctica, *Nature*, *399*.

Rankin, A. M., E. W. Wolff, and S. Martin (2002), Frost flowers: Implications for tropospheric chemistry and ice core interpretation, *J. Geophys. Res.*, *107*(D23), 4683.

Ravishankara, A. R., Y. Rudich, R. Talukdar, and S. B. Barone (1997), Oxidation of atmospheric reduced sulphur compounds: Perspective from laboratory studies, *Philosophical Transactions of the Royal Society of London. Series B: Biological Sciences*, *352*(1350), 171–182.

Rellinger, A. N., R. P. Kiene, D. A. del Valle, D. J. Kieber, D. Slezak, H. Harada, J. Bisgrove, and J. Brinkley (2009), Occurrence and turnover of DMSP and DMS in deep waters of the Ross Sea, Antarctica, *Deep Sea Research Part I: Oceanographic Research Papers*, *56*(5), 686–702.

Rhodes, R. H., N. A. N. Bertler, J. A. Baker, S. B. Sneed, H. Oerter, and K. R. Arrigo (2009), Sea ice variability and primary productivity in the Ross Sea, Antarctica, from methylsulphonate snow record, *Geophys. Res. Lett.*, *36*(10), L10704.

Rignot, E., J. L. Bamber, M. R. van den Broeke, C. Davis, Y. Li, W. J. van de Berg, and E. van Meijgaard (2008), Recent Antarctic ice mass loss from radar interferometry and regional climate modelling, *Nature Geosciences*, *1*(2), 106–110.

Roscoe, H. K., B. Brooks, A. V. Jackson, M. H. Smith, S. J. Walker, R. W. Obbard, and E. W. Wolff (2011), Frost flowers in the laboratory: Growth, characteristics, aerosol, and the underlying sea ice, *J. Geophys. Res.*, *116*(D12), D12301.

Röthlisberger, R., X. Crosta, N. J. Abram, L. Armand, and E. W. Wolff (2010), Potential and limitations of marine and ice core sea ice proxies: an example from the Indian Ocean sector, *Quaternary Science Reviews*, *29*(1–2), 296–302.

Saigne, C., and M. Legrand (1987), Measurements of methanesulphonic acid in Antarctic ice, *Nature*, *330*(6145), 240–242.

Schneider, D. P., C. Deser, and Y. Okumura (2011), An assessment and interpretation of the observed warming of West Antarctica in the austral spring, *Climate Dynamics*, *38*(1–2), 323–347.

Smith, S. D., R. D. Muench, and C. H. Pease (1990), Polynyas and leads: An overview of physical processes and environment, *J. Geophys. Res.*, *95*(C6), 9461–9479.

Sneed, S. B., P. A. Mayewski, and D. A. Dixon (2011), An emerging technique: multi-ice-core multi-parameter correlations with Antarctic sea-ice extent, *Annals of Glaciology*, *52*(57), 347–354.

Spreen, G., L. Kaleschke, and G. Heygster (2008), Sea ice remote sensing using AMSR-E 89-GHz channels, *J. Geophys. Res.*, *113*(C2), C02S03.

Steig, E. J., Q. Ding, D. S. Battisti, and A. Jenkins (2012), Tropical forcing of circumpolar deep water inflow and outlet glacier thinning in the Amundsen Sea Embayment, West Antarctica, *Annals of Glaciology*, *53*(60), 19–28.

Steig, E. J., D. P. Schneider, S. D. Rutherford, M. E. Mann, J. C. Comiso, and D. T. Shindell (2009), Warming of the Antarctic ice-sheet surface since the 1957 International Geophysical Year, *Nature*, *457*(7228), 459–462.

Tison, J. L., F. Brabant, I. Dumont, and J. Stefels (2010), High-resolution dimethyl sulfide and dimethylsulfoniopropionate time series profiles in

decaying summer first-year sea ice at Ice Station Polarstern, western Weddell Sea, Antarctica, *J. Geophys. Res.*, *115*(G4), G04044.

Toole, D. A., and D. A. Siegel (2004), Light-driven cycling of dimethylsulfide (DMS) in the Sargasso Sea: Closing the loop, *Geophys. Res. Lett.*, *31*(9), L09308.

Trevena, A. J., G. B. Jones, S. W. Wright, and R. L. van den Enden (2003), Profiles of dimethylsulphoniopropionate (DMSP), algal pigments, nutrients, and salinity in the fast ice of Prydz Bay, Antarctica, *J. Geophys. Res.*, *108*(C5), 3145.

Turner, J., J. C. Comiso, G. J. Marshall, T. A. Lachlan-Cope, T. Bracegirdle, T. Maksym, M. P. Meredith, Z. Wang, and A. Orr (2009), Non-annular atmospheric circulation change induced by stratospheric ozone depletion and its role in the recent increase of Antarctic sea ice extent, *Geophys. Res. Lett.*, *36*(8), L08502.

Wagenbach, D., F. Ducroz, R. Mulvaney, L. Keck, A. Minikin, M. Legrand, J. S. Hall, and E. W. Wolff (1998), Sea-salt aerosol in coastal Antarctic regions, *J. Geophys. Res.*, *103*(D9), 10961–10974.

Welch, K. A., P. A. Mayewski, and S. I. Whitlow (1993), Methanesulfonic acid in coastal Antarctic snow related to sea-ice extent, *Geophys. Res. Lett.*, *20*(6), 443–446.

Weller, R., F. Traufetter, H. Fischer, H. Oerter, C. Piel, and H. Miller (2004), Postdepositional losses of methane sulfonate, nitrate, and chloride at the European Project for Ice Coring in Antarctica deep-drilling site in Dronning Maud Land, *Antarctica, J. Geophys. Res.*, *109*(D7), D07301.

Wolff, E. W., A. M. Rankin, and R. Röthlisberger (2003), An ice core indicator of Antarctic sea ice production?, *Geophys. Res. Lett.*, *30*(22), 2158.

Wolff, E. W., et al. (2006), Southern Ocean sea-ice extent, productivity and iron flux over the past eight glacial cycles, *Nature*, *440*(7083), 491–496.

Yang, X., J. A. Pyle, and R. A. Cox (2008), Sea salt aerosol production and bromine release: Role of snow on sea ice, *Geophys. Res. Lett.*, *35*(16), L16815.

Zemmelink, H. J., L. Houghton, J. W. H. Dacey, A. P. Worby, and P. S. Liss (2005), Emission of dimethylsulfide from Weddell Sea leads, *Geophys. Res. Lett.*, *32*(23), L23610.

Zemmelink, H. J., J. W. H. Dacey, L. Houghton, E. J. Hintsa, and P. S. Liss (2008), Dimethylsulfide emissions over the multi-year ice of the western Weddell Sea, *Geophys. Res. Lett.*, *35*(6), L06603.

Zwally, H. J., J. C. Comiso, C. L. Parkinson, D. J. Cavalieri, and P. Gloersen (2002), Variability of Antarctic sea ice 1979 – 1998, *J. Geophys. Res.*, *107*(C5), 3041.

Chapter 3

Tropical Pacific influence on source and transport of marine aerosols to West Antarctica *

Abstract

The climate of West Antarctica is strongly influenced by remote forcing from the tropical Pacific. For example, recent surface warming over West Antarctica reflects atmospheric circulation changes over the Amundsen Sea, driven by an atmospheric Rossby wave response to tropical sea surface temperature (SST) anomalies. Here, we demonstrate that tropical Pacific SST anomalies also influence the source and transport of marine-derived aerosols to the West Antarctic Ice Sheet. Using records from four firn cores collected along the Amundsen Coast of West Antarctica, we investigate the relationship between sea-ice modulated chemical species and large-scale atmospheric variability in the tropical Pacific from 1979–2010. We find significant correlation of marine biogenic aerosols and sea salts with SST and sea level pressure in the tropical Pacific. In particular, La Niña-like conditions generate an atmospheric Rossby wave response that influences atmospheric circulation over Pine Island Bay. Seasonal regression of atmospheric fields on MSA reveal a reduction in onshore wind velocities in summer at Pine Island Bay, consistent with enhanced katabatic flow, polynya opening, and coastal dimethyl sulfide production. Seasonal regression of atmospheric fields on Cl^- reveal an intensification in onshore wind velocities in winter, consistent with sea salt transport from offshore source regions. We find both source and transport of marine aerosols to West Antarctica are modulated by similar atmospheric dynamics in response to remote forcing. Finally, our regional ice-core array suggests there is both a temporally and spatially varying response to remote tropical forcing.

* Published as: Criscitiello, A.S., S.B. Das, K.B. Karnauskas, M.J. Evans, K.E. Frey, I. Joughin, E.J. Steig, J.R. McConnell, and B. Medley (2013). Tropical Pacific influence on source and transport of marine aerosols to West Antarctica, *Journal of Climate*, doi: 10.1175/JCLI-D-13-00148.1.

1. Introduction

Marine aerosols (biogenic and sea salts) play an important role in many atmospheric processes (Fitzgerald 1991), and directly affect Antarctic climate. Marine biogenic aerosols transported to Antarctica originate from oceanic areas of high primary productivity, which emit dimethyl sulfide (DMS) during and after sea-ice breakup (Dacey and Wakeham 1986). As such, atmospheric DMS concentrations peak in the austral summer when oceanic primary productivity is high (Ayers et al. 1997). DMS is subsequently oxidized in the atmosphere to methanesulfonic acid (MSA; Ravishankara et al. 1997). Maximum MSA concentrations found on the adjacent ice sheet occur in snowfall deposited during the austral summer (Criscitiello et al. 2013), as expected since the lifetimes of DMS and MSA in the polar atmosphere are short (<7 days; Hezel et al. 2011). Both DMS and MSA interact with incoming solar radiation, affecting cloud albedo and regional climate (Charlson et al. 1987). These biogenic marine aerosols significantly increase cloud droplet concentrations over phytoplankton blooms, resulting in a decrease in short-wave radiation flux at the top of the atmosphere and an enhancement of cloud condensation nuclei production (Meskhidze and Nenes 2006). Sulphur species such as DMS are also a large contributor to the acidity of the atmosphere (Legrand 1997).

In contrast to marine biogenic species, the seasonality of sea-salt aerosols varies regionally, as there are several processes associated with the production of sea-salt aerosols at high latitudes. Some studies have shown that processes associated with sea-ice formation (e.g., frost-flower formation, brine production, blowing snow released from sea-ice surfaces), primarily occurring from late summer through winter, are the dominant

source of sea-salt aerosols to Antarctica (Rankin et al. 2002; Wolff et al. 2003; Kaleschke et al. 2004; Wolff et al. 2006; Fischer et al. 2007; Yang et al. 2008; Roscoe et al. 2011; Criscitiello et al. 2013). Other studies have instead suggested that open water in the marginal sea-ice zone, particularly during stormy seasons, promotes increased production, transport, and deposition of sea-salt aerosols (Petit et al. 1999; Kinnard et al. 2006; Abram et al. 2011). Whether enhanced sea-salt aerosol fluxes reflect increased open water or increased sea-ice cover in a particular region, sea-salt aerosols ubiquitously affect climate by scattering and absorbing radiation and influencing the albedo of marine boundary layer clouds (Fitzgerald 1991).

The strong relationship between sea-surface conditions and marine aerosols also means that in coastal regions of Antarctica, where annual precipitation rates are high, high-resolution ice-core records allow for reconstruction of past ocean surface and sea-ice conditions (e.g., Thomas et al. 2009). MSA and sea-salt aerosols (Na, Cl, Mg, K, Ca, SO_4) have been used as qualitative proxies for regional sea-ice extent (SIE) around Antarctica (see Abram et al. (2013) for a review, and references therein). In a previous study we focused on the spatial relationships between ice-sheet chemistry adjacent to Pine Island Bay, West Antarctica, and satellite-derived sea-ice concentration (SIC) in the Amundsen Sea (including polynya activity), to further understanding of marine-aerosol source variability in this region (Criscitiello et al. 2013). Winds also affect the transport of marine aerosols to the ice sheet, and thus need to be considered in the interpretation of ice-core records.

Because winds are ultimately forced by remote large-scale atmospheric dynamics, the transport of marine aerosols may also be affected by regional- to global-scale

47 phenomena. The tropical Pacific strongly influences atmospheric circulation at high
48 northern and southern latitudes (Trenberth et al. 1998). Tropical Pacific sea surface
49 temperature (SST) variability influences the upper troposphere, enhancing convection
50 and upper tropospheric divergence near the equator (Trenberth et al. 1998). The resulting
51 wave train of alternating high and low pressure emanates both north and south. In the
52 southern hemisphere (SH), there is a strong teleconnection between the tropical Pacific
53 and West Antarctica as a result of this increased convection in the central tropical Pacific
54 during El Niño and La Niña conditions, which gives rise to a pattern of stationary Rossby
55 waves that propagate to the extratropical SH (e.g., Hoskins and Karoly 1981; Karoly
56 1989; Jin and Hoskins 1995; Trenberth et al. 1998; Turner 2004; Lachlan-Cope and
57 Connolley 2006). The widespread recent warming in continental West Antarctica has
58 been linked to SST changes in the tropical Pacific (Ding et al. 2011; Schneider et al.
59 2011; Ding et al. 2012; Steig et al. 2013).

60 Observational and modeling studies have also documented the strong influence of
61 the leading patterns of tropical and SH large-scale climate variability (El Niño Southern
62 Oscillation (ENSO) and the Southern Annular Mode (SAM)) on polar records including
63 melting events in West Antarctica (e.g., Trusel et al. 2012) and marine aerosols and SIC
64 around Antarctica (Yuan and Martinson 2001; Hall and Visbeck 2002; Kwok and Comiso
65 2002; Lefebvre et al. 2004; Liu et al. 2004; Stammerjohn et al. 2008; Yuan and Li 2008;
66 Simpkins et al. 2012). One recent study identified a highly significant ENSO signature
67 (during 1889–2009) in a sea-salt record from Law Dome, East Antarctica (Vance et al.
68 2012). Work is ongoing, but many studies suggest that the tropical-extratropical
69 connection between ENSO and Antarctica is highly variable, depending on the exact

70 pattern and zonal distribution of tropical SST anomalies and zonal winds in the South
71 Pacific (Turner 2004; Fogt and Bromwich 2006; Lachlan-Cope and Connolley 2006;
72 L'Heureux and Thompson 2006; Fogt et al. 2011). Tropical Pacific variability not
73 directly related to ENSO also influences high latitude circulation (Lachlan-Cope and
74 Connolley 2006; Ashok et al. 2007; Schneider and Steig 2008; Ding et al. 2011). In
75 particular, SST anomalies under areas of strong tropical convection have a significant
76 influence on atmospheric circulation in the Amundsen Sea region, through the generation
77 of a Rossby wave train (Lachlan-Cope and Connolley 2006). As our understanding of
78 low to high latitude Pacific Ocean teleconnections evolves, investigators are beginning to
79 examine scarce but potentially proxy-rich Antarctic data for tropical Pacific signatures
80 (e.g., Okumura et al. 2012; Vance et al. 2012; Steig et al. 2013). Several studies of
81 Pacific extratropical teleconnections to high southern latitudes have focused on West
82 Antarctica, where the extratropical signal is especially strong and has been linked to
83 variability in SST, precipitation, sea level pressure (SLP), SIE, and sea-ice thickness
84 (e.g., Cullather et al. 1996; Kwok and Comiso 2002; Turner 2004; Yuan and Li 2008;
85 Ding et al. 2011).

86 In this study, we provide a first assessment of the influence of the tropical Pacific
87 on the source and transport of marine aerosols to the West Antarctic Ice Sheet (WAIS).
88 We focus on the effects of large-scale atmospheric circulation on four new marine-
89 aerosol ice-sheet records from the Amundsen Coast of West Antarctica. We carry out
90 least-squares linear temporal regression analyses of global reanalysis fields on seasonally
91 stratified anomalies of firn-core chemical composition to investigate the large-scale
92 atmospheric processes that influence the transport of marine aerosols, and thus in turn

93 influence ice-sheet chemistry, in the region. This both aids in our interpretation of ice-
94 core marine-aerosol records in West Antarctica, and provides additional evidence of the
95 teleconnection between the tropical Pacific and the Amundsen Sea (previously shown
96 using SST, SLP, SIC) with independent ice-sheet variables.
97
98 **2. Methods and datasets**
99
100 *a. Site description and core collection*
101 The Amundsen Sea is characterized by a relatively narrow continental shelf, a
102 large amount of perennial sea ice, and several coastal polynyas located adjacent to large
103 ice shelves (Arrigo and van Dijken 2003). Surface waters associated with these polynyas
104 have enhanced rates of primary and secondary production (Arrigo and van Dijken 2003;
105 Arrigo et al. 2012), and some of the highest abundances of phytoplankton in the world
106 (Smith and Gordon 1997). The Amundsen Sea and Pine Island Bay polynyas (Fig. 1) are
107 latent heat polynyas, meaning that they are influenced largely by local katabatic winds
108 (Marshall and Turner 1997), and the associated transport of sea ice away from the coast
109 (Pease 1987). Pine Island, Thwaites, and Smith Glaciers are the principal drainage
110 systems of the Amundsen Sea sector of WAIS (Shepherd et al. 2002), with approximately
111 25% of the area of WAIS draining into the Amundsen Sea Embayment (Rignot et al.
112 2002). The highest rates of mass loss and glacier acceleration in Antarctica outside of the
113 Antarctic Peninsula have occurred along the Amundsen-Bellingshausen Sea in the Pine
114 Island and Thwaites Glacier regions, as a result of increases in ocean heat transport
115 beneath its ice shelves (Jenkins et al. 2010; Jacobs et al. 2011; Steig et al. 2012).

116 Continental West Antarctica has also experienced substantial warming in the past 50
117 years (Steig et al. 2009; Orsi et al. 2012; Bromwich et al. 2013). Trends in SIC provide
118 independent evidence of the observed warming over West Antarctica; the decrease in sea-
119 ice area in the Amundsen and Bellingshausen Seas has been shown to be congruent with
120 at least 50% of the inland warming of West Antarctica (Ding et al. 2011; Schneider et al.
121 2011). Owing to these recent changes, there is a strong need to develop longer histories
122 of environmental variability in this region, as well as a better understanding of the large-
123 scale, remote drivers of such variability.

124 In this study, we used new firn cores from Pine Island Glacier (PIG2010),
125 Thwaites Glacier (THW2010 and UPT2009), and the drainage divide between Pine
126 Island and Thwaites Glaciers (DIV2010) to reconstruct marine-aerosol histories (Fig. 1).
127 These core sites range in elevation from 1329 to 2020 m, and range from 180 to 500 km
128 in distance from the coast (Table 1). Accumulation rates at the sites are relatively high,
129 ranging from 0.28 to 0.42 $m \cdot we \cdot yr^{-1}$ (Table 1). Ice velocities at the core locations are low
130 (~10–20 $m \cdot yr^{-1}$; Joughin et al. 2003). We drilled the UPT2009 firn core in December
131 2010 using a 3-inch diameter Pico hand auger, and the DIV2010, PIG2010, and
132 THW2010 firn cores in December 2011 using the US Eclipse drill. For the purposes of
133 this study, we focus on ice-core records from 1979–2010 (where available) in order to
134 provide the best overlap with the ERA-Interim reanalysis dataset.
135
136 *b. Glaciochemical records*
137 Data for the DIV2010, PIG2010, and THW2010 cores include MSA, total soluble
138 plus insoluble S (S_{total}), Na, Cl^-, Ca, and Mg. Data for the UPT2009 core are limited to

139 MSA and Cl^-. We performed MSA and Cl^- ionic analyses using suppressed ion
140 chromatography (Curran and Palmer 2001; Morganti et al. 2007). The detection limits of
141 this procedure are 0.4 ppb (MSA) and 10 ppb (Cl^-), with analytical precision of <5%. We
142 performed analyses of S_{total}, Na, Ca, and Mg using mass spectrometry (detection limits
143 ~500 ppq for elements in this study; McConnell et al. 2001). To avoid timing uncertainty
144 generating errors in correlation with large-scale reanalysis fields, we applied a 3-point
145 running mean to all monthly glaciochemical time series. Normalized time series
146 presented in Fig. 2 are standard score normalizations ($Z = (X - \mu) / \sigma$). Composite annual
147 cycles of MSA and Cl^- presented in Fig. 3 are monthly climatology means of all months
148 available for each record (1979–2010 for DIV2010 and THW2010, 1992–2010 for
149 PIG2010, and 1992–2009 for UPT2009). Note that using the same time interval for all
150 records (1992–2009) reveals similar results.

151 To aid in dating, oxygen isotopes in all firn cores were measured at a minimum of
152 5-cm resolution following methods of Maselli et al. (2013). We established an age-depth
153 relationship and determined accumulation rates following standard methods (see
154 Appendix, and Criscitiello et al. (2013), for detailed methods). The high accumulation
155 rates at the core sites (Table 1) allow for seasonal resolution of the core records (~14
156 samples/year even at the lower accumulation sites on Thwaites Glacier), and limit post-
157 depositional loss of MSA (Weller et al. 2004). To allow investigation of chemical
158 species alongside reanalysis records, we produced monthly-resolution records (Fig. 2).
159 We calculated these monthly results by linearly interpolating between measured
160 concentrations (which are not evenly spaced in time due to irregular core breaks,
161 variations in accumulation rate, etc.), and then averaging these interpolated time series.

Finally, we created seasonal time series of the glaciochemical records. Because MSA deposition occurs almost entirely in summer, we created a time series of summertime MSA deposition. The summer season was defined as Nov–Mar to coincide with the peak MSA deposition month +/- 2 months (Fig. 3). Since there is a broad Cl^- peak in winter but it is deposited year-round, we created summer (Nov–Mar) and winter (Jun–Oct) time series, with the winter season centered on the peak Cl^- deposition month (Fig. 3).

c. Observational climate datasets

We utilized ERA-Interim reanalysis products from the European Centre for Medium-Range Weather Forecasts (ECMWF; Dee et al. 2011) to provide global monthly SLP, 500 hPa geopotential height (GH), SST, and zonal and meridional wind velocities over the study period. We analyzed these variables to investigate the spatial relationships between chemical signals recorded in the DIV2010, PIG2010, THW2010, and UPT2009 cores and climate fields. To improve results relative to the earlier ERA-40 reanalysis data, we used ERA-Interim reanalysis data (Berrisford et al. 2009; Dee et al. 2011) because it has a higher horizontal (0.75° x 0.75°) and vertical resolution and improved model physics and characterization of the hydrological cycle. Recent assessments for the Amundsen Sea region of Antarctica indicate that ERA-Interim is the most reliable reanalysis product for this region of Antarctica that is currently available (Bracegirdle 2012). ERA-40 is known to have limitations in the Antarctic Peninsula region because it insufficiently resolves the mountainous terrain (Miles et al. 2008). To reduce subseasonal noise unrelated to tropical forcing, we applied a 3-point running mean to all the monthly data as well (similar to the glaciochemical records). Seasonal reanalysis

185 fields were defined the same as for the glaciochemical records (described in 2.b above).
186 Our results are presented as seasonal anomalies (i.e., their deviation from the long-term
187 mean climatology). We conducted least-squares linear temporal regression analyses of
188 atmospheric fields on the seasonal anomalies of the firn-core glaciochemical records
189 (please see Appendix for monthly regression figures). Only linear regression maps for
190 positive MSA and Cl^- deposition are presented, though we note that anomaly patterns of
191 opposite sign for negative deposition anomalies inherently exist. Statistical significance
192 for the seasonal regressions was determined using the two-tailed Student's *t*-test ($p <$
193 *0.05*). In addition, we performed lead/lag tests (±0, 1 and 2-months) between
194 glaciochemical time series and reanalysis data. These did not reveal a systematic lead/lag
195 relationship;,therefore, only 0 lag results are presented. Finally, we created stacked
196 records of MSA and Cl^- (by averaging the monthly MSA and Cl^- data from the four
197 sites), which did not yield correlations or regressions (strength or spatial patterns) distinct
198 from individual site results and are therefore not presented.
199
200 *d. Polynya total open water area and regional SIE*
201 We created polynya and SIE time series to examine the link between remote
202 atmospheric forcing of regional winds and polynya and sea-ice variability specifically
203 relevant to this study. To examine polynya variability directly linked with local DMS
204 production and marine biogenic aerosol deposition on the ice sheet, we derived an open
205 water time series for the sea surface within the Pine Island Bay and Amundsen Sea
206 polynyas (Fig. 1), regions that previously have been shown to correlate significantly with
207 MSA at DIV2010 (Criscitiello et al. 2013). Polynya masks (Fig. 1) were defined using

methods outlined in Criscitiello et al. (2013), but here we utilized Scanning Multichannel Microwave Radiometer (SMMR) and Special Sensor Microwave Imager (SSM/I) passive microwave data of SIC from 1979–2010 rather than Advanced Microwave Scanning Radiometer – EOS (AMSR-E) data used previously (as AMSR-E data are only available 2002–present). Using these polynya masks, we extracted daily open water areas (1979–2010) by summing the pixels (25 km x 25 km) that had <15% SIC (our defined threshold value for open water). Next, we summed the daily open-water areas of the Pine Island Bay and Amundsen Sea polynyas, and then averaged these daily values to generate a monthly time series of polynya total open water area (TOWA) to produce a time series of the TOWA anomalies (please see Appendix for monthly regression figures of atmospheric fields on TOWA). Finally, we smoothed the monthly TOWA anomaly time series with a 3-month running mean, and created a summer (Nov–Mar) time series from these monthly data, as we did with the reanalysis data and MSA time series. We present regressions of reanalysis fields on summer TOWA, as summer is the deposition season for MSA.

The primary source of sea salts to this region is a much larger region around the leading seasonal ice edge as well as near 70°S between ~97°W–107°W, largely outside the polynyas described above (Criscitiello et al. 2013). Thus, to examine the relationship between remote atmospheric forcing of regional winds and SIE over this larger offshore region, we created a separate SIE time series. This time series also utilizes SMMR- and SSM/I-based SIC, but in this case we created a monthly time series (1979–2010) of SIE between 80°W and 140°W, and 60°S and 71°S, where SIE is defined as the total area within this defined region with SIC > 15% (please see Appendix for monthly regression

231 figures of atmospheric fields on SIE). We then created summer and winter time series
232 from this monthly data, as we did with the reanalysis data and Cl^- time series. We present
233 both summer and winter regressions of reanalysis fields on SIE, as sea salts have a broad
234 peak encompassing winter but with nontrivial deposition rates year-round (Fig. 3).
235
236 **3. Results**
237 *a. Glaciochemical records*
238 Our measured MSA and Cl^- concentrations in the DIV2010, PIG2010, THW2010,
239 and UPT2009 cores (Table 1) are comparable to concentrations found in other recent
240 Antarctic cores (e.g., Abram et al. 2011). The highest measured MSA concentrations are
241 from the two lower elevation sites: the DIV2010 core (the site closest to Pine Island Bay;
242 44.8 ppb) and the PIG2010 core (31.7 ppb), while the lowest concentrations are from the
243 UPT2009 core (the site farthest from Pine Island Bay; 22.6 ppb; Table 1). The opposite
244 is found in the Cl^- records, where the highest measured Cl^- concentrations are from the
245 UPT2009 core (503.3 ppb), and the lowest concentrations are from the DIV2010 core
246 (212.6 ppb; Table 1).
247 MSA has a strong seasonal cycle at all sites (Fig. 3), being deposited almost
248 entirely in summer (DJF) with annual minima during austral winter (JJA), while Cl^- has a
249 broad peak in winter but with substantial deposition year-round at all sites (Fig. 3).
250 These results are consistent with a previous study at the DIV2010 site that found MSA
251 maxima during summer months were derived from marine biological productivity during
252 spring and summer, while Cl^- maxima during winter months originated primarily from
253 winter sea-ice formation (Criscitiello et al. 2013). While maximum measured MSA

254 concentrations are highest in the DIV2010 record and lowest in the UPT2009 record, the
255 climatology reveals that PIG2010 has the highest composite summer MSA
256 concentrations, and UPT2009 has the lowest composite summer MSA concentrations
257 (Fig. 3). Similarly, while the maximum measured Cl^- concentrations are highest in the
258 UPT2009 record and lowest in the DIV2010 record (Table 1), the climatology reveals
259 that UPT2009 also has the highest composite winter Cl^- concentrations, but THW2010
260 and PIG2010 have the lowest composite winter Cl^- concentrations (Fig. 3).

261 There are significant correlations between normalized sea-salt species anomalies
262 (Na, Cl^-, Ca, Mg) at DIV2010, PIG2010, and THW2010 (Table 2), as has been found at
263 many other Antarctic sites (e.g., Artaxo et al. 1992; Abram et al. 2011). Correlations
264 between sea-salt species are generally weakest (though still significant at $p < 0.05$) at
265 THW2010 (Table 2). Correlations between Na, Cl^-, and Mg at each site are stronger ($r >$
266 0.60, $p < 0.05$) than correlations at each site between any of these sea-salt species and Ca
267 ($r > 0.30$, $p < 0.05$; Table 2), likely due to the large aerosol size of Ca which results in a
268 dilution effect at high accumulation rate sites (Herron 1982; Kreutz and Mayewski 1999).
269 Owing to the strong correlation between sea-salt species, we have chosen Cl^- as the
270 representative sea-salt ion in the results presented below. Similarly, owing to the
271 correlation ($r > 0.49$, $p < 0.05$) between MSA and S_{total} at all sites (Table 2), we have
272 chosen MSA as the representative biogenic species. This is further justified by the vast
273 body of work focused on the sulfur cycle in the Antarctic and the various pathways and
274 covariability between S_{total}, DMS, and MSA (e.g., Cunningham and Zoller 1981; Pszenny
275 et al. 1989). As with sea-salt species, correlations between marine biogenic species are
276 weakest (though still significant at $p < 0.05$) at THW2010 (Table 2).

277

278 *b. Global atmospheric anomalies*

279 At PIG2010, regressions of SLP and 500 hPa GH (Fig. 5) on summer MSA and
280 winter Cl^- reveal a low pressure anomaly over the western Antarctic Peninsula, which
281 alternates with a high pressure anomaly in the central south Pacific and a low pressure
282 anomaly in the western tropical Pacific (see also Appendix Figure 2). These same
283 patterns exist for DIV2010, though not statistically significant at $p < 0.05$. The
284 THW2010 summer regressions of SLP and 500 hPa GH on MSA are the only regressions
285 that shows low pressure over the entire polar region (indicative of the positive phase of
286 SAM), while the winter regressions of SLP and 500 hPa GH on Cl^- show a similar
287 Rossby wave pattern as seen at DIV2010 and PIG2010 but of opposite sign (Fig. 6). At
288 UPT2009, regressions of SLP and 500 hPa GH (Fig. 7) on summer MSA and winter Cl^-
289 show a Rossby wave pattern similar to the winter regression at THW2010 (with a high
290 pressure anomaly centered near the Amundsen Coast and the western Antarctic
291 Peninsula). Regressions using SLP and 500 hPa GH are similar to one another in pattern
292 outside the tropics, and both are significant at $p < 0.05$, but regions of statistical
293 significance tend to be larger and more coherent at 500 hPa, i.e., in the free troposphere
294 (indicated by shading in Figs. 4–7).

295 A similar hemispheric-scale pattern is found in regressions of SLP or 500 hPa GH
296 on TOWA (not statistically significant at $p < 0.05$; Fig. 8) and regional SIE (statistically
297 significant at $p < 0.05$; Fig. 9), where the regional SIE exhibits a distinct SAM-like
298 pattern with a wave train embedded, particularly in winter (see also Appendix Figures 5–
299 6). The alternating low and high pressure anomalies at both the surface as well as

300 throughout the atmospheric column suggest a barotropic response of the atmosphere
301 connecting the western tropical Pacific with the Antarctic Peninsula (Trenberth et al.
302 1998). These global regression fields of atmospheric variability on firn-core records are
303 evident year-round, but are generally stronger in winter (as seen in the Cl^- and SIE
304 regressions; Figs. 4-7 and 9). We note that significant regressions present in some cases
305 in the equatorial and south Atlantic basin are not discussed here, as they are due to the
306 fast tropical atmospheric adjustment (Matsuno 1966; Gill 1980). Regressions at high
307 north and south latitudes are often similar in strength and pattern (e.g., UPT2009 summer
308 MSA and SLP; Fig. 7A). It is encouraging that the significant regressions in the southern
309 hemisphere are mirrored in the northern hemisphere, as this provides additional evidence
310 of the tropical Pacific influence on both hemispheres (e.g., Trenberth et al. 1998; Lee et
311 al. 2011; and references therein).
312
313 *c. Global SST anomalies*
314 Regressions of SST on the marine aerosol records at some sites reveal a strong
315 Antarctic connection to SST anomalies in the equatorial Pacific. This is in agreement
316 with the initiation and propagation of a Rossby wave train (Hoskins and Karoly 1981; Jin
317 and Hoskins 1995; Zhang et al. 1997) as revealed by the SLP and 500 hPa GH analyses
318 described in section 3 above. UPT2009 (Fig. 7) summer and winter Cl^-, as well as
319 PIG2010 (Fig. 5) summer Cl^-, are positively correlated with SST in the eastern tropical
320 Pacific. PIG2010 summer MSA and winter Cl^-, and THW2010 summer MSA and winter
321 Cl^-, are negatively correlated with SST in the eastern tropical Pacific (La Niña-like
322 conditions). The most significant and organized patterns of SST regressions in the

323 equatorial Pacific are on winter Cl^- at PIG2010 and THW2010 (Figs. 5-6; see also
324 Appendix Figure 3E–F). Similarly, the summer and winter regional SIE time series are
325 negatively correlated with SST in the eastern tropical Pacific (Fig. 9; see also Appendix
326 Figure 6C). The THW2010 regressions of SST on MSA and Cl^- anomalies show a
327 horseshoe pattern in the North Pacific (the highest elevation site; Fig. 6). A horseshoe
328 pattern of opposite sign in the North Pacific is seen for summer MSA at PIG2010 (Fig.
329 5), and summer and winter Cl^- at UPT2009 (Fig. 7). There is less variability in SST in
330 the tropics than at high latitudes; therefore, the SST patterns we do see in the tropics are
331 particularly notable.
332
333 *d. Regional wind variability*
334 At all sites, regression of summer surface wind velocity on summer MSA
335 highlights offshore wind anomalies within Pine Island Bay and along the Amundsen
336 Coast (Fig. 10; see also Appendix Figure 4). The same relationship is found between
337 summer TOWA and summer winds (Fig. 8D; see also Appendix Figure 5D), and winter
338 regional SIE and winter winds (Fig. 9H; see also Appendix Figure 6D). At DIV2010 (the
339 lowest elevation site, closest to Pine Island Bay), regression of summer and winter
340 surface wind velocity on summer and winter Cl^- also show offshore wind anomalies
341 along the Amundsen Coast, similar to the pattern observed at this site with summer MSA
342 (Fig. 10B–C). At PIG2010, regression of summer surface wind velocity on summer Cl^-
343 shows easterly wind anomalies within Pine Island Bay (Fig. 10E). At PIG2010 and
344 UPT2009 (the sites farthest from the coast), regression of winter surface wind velocity on
345 winter Cl^- shows an opposite pattern to MSA, with onshore wind anomalies within Pine

346 Island Bay and along the Amundsen Coast (Figs. 10F&L). At THW2010, regression of
347 summer surface wind velocity on summer Cl^- shows neutral wind anomalies within Pine
348 Island Bay, and onshore wind anomalies along the Amundsen Coast (Fig. 10H);
349 regression of winter surface wind velocity on winter Cl^- shows onshore wind anomalies
350 within Pine Island Bay and neutral wind anomalies along the Amundsen Coast (Fig. 10I).
351
352 **4. Discussion**
353 In this section we discuss the broad seasonal relationships between regional wind
354 anomalies and the source and transport of marine biogenic and sea-salt aerosols to the ice
355 sheet indicated by our results above. Within that context, we take advantage of our
356 records from multiple core sites to begin to assess how locations across the Amundsen
357 catchment of WAIS are impacted spatially in response to atmospheric transport and
358 marine aerosol source variability. Finally, we discuss the SH teleconnection to the
359 tropical Pacific in the context of these new ice-sheet records from along the Amundsen
360 Coast.
361
362 *a. Regional wind anomalies and marine biogenic aerosol source and transport*
363 The strong annual cycle of MSA shown at all sites (Fig. 3) supports previous
364 findings that the marine biogenic compounds in ice cores from this region are derived
365 primarily from summer productivity in the sea-ice zone of the Amundsen Sea, with
366 particularly strong influence from seasonal sea-ice loss within the Pine Island Bay and
367 Amundsen Sea polynyas for the most coastal ice-core sites (Criscitiello et al. 2013).
368 Records from other Antarctic locations indicate negative correlations between MSA

369 concentrations and SIE more broadly, consistent with the source of MSA being derived
370 largely from summer productivity following sea-ice breakup (Pasteur et al. 1995; Abram
371 et al. 2007; Rhodes et al. 2009; Abram et al. 2011). The deposition of MSA on the ice
372 sheet requires both conditions favorable for phytoplankton blooms as well as effective
373 atmospheric transport of the resulting marine biogenic species onshore. Our results show
374 that during times of MSA deposition, offshore wind anomalies (weakened onshore
375 winds) are prevalent. We suggest that this anomaly increases both MSA source and
376 transport through a proposed link with regional katabatic winds and associated polynya
377 behavior (Fig. 11); this phenomena is best expressed at DIV2010, the most coastal site.
378 Additionally, these offshore wind anomalies may contribute to sea-ice breakup and thus
379 enhanced DMS production near the leading ice edge, impacting the MSA record over
380 parts of the ice sheet that receive precipitation from moisture source regions farther
381 offshore. The reduced onshore winds observed during times of MSA deposition
382 described above are in agreement with transport of marine biogenic aerosols to the ice
383 sheet, as the climatology confirms that winds are consistently onshore during MSA
384 deposition at all sites which is necessary for transmission of moisture to the ice sheet
385 (precipitation being the source of the marine signal; Fig. 11).

386 Previous work has shown that this region experiences persistent, strong katabatic
387 winds (Parish and Bromwich 1987) which can develop more easily when there is a
388 reduction in onshore winds (Nylen et al. 2004.) Furthermore, katabatic winds have been
389 shown to produce favorable conditions for polynya openings generally (Marshall and
390 Turner 1997) and along the Amundsen coast more specifically (Arrigo et al. 2012).
391 Along the Amundsen coast, katabatic winds push higher than normal volumes of sea ice

both northward in the Amundsen Sea and away from the coast yielding persistent polynya formation, resulting in high primary production rates (Smith Jr et al. 2000; Arrigo and van Dijken 2003) and strong air-sea heat fluxes (Fusco et al. 2009). Katabatic winds are not captured by the reanalysis data employed in this study, thus we cannot use the present study to test this hypothesis directly, but as detailed above the broad existing knowledge available about katabatic dynamics in this region supports this scenario, particularly for DIV2010, the most coastal site (Fig. 11).

We find that PIG2010 and THW2010 have the highest composite summer MSA concentrations and strongest seasonal cycles (Fig. 3). PIG2010 has offshore wind anomalies in Pine Island Bay and along the leading ice edge in the Amundsen Sea during MSA deposition in summer (Fig. 10D), which indicate that Pine Island Bay (and the polynyas) as well as the leading ice edge in the Amundsen Sea are source regions of marine biogenic aerosols to this site. THW2010 has offshore summer wind anomalies along the central Amundsen Coast during times of MSA deposition (Fig. 10G), and is situated geographically closest to the highly productive Amundsen Sea polynya. These results indicate that the Amundsen Sea polynya is a source region of marine biogenic aerosols to THW2010. The particularly high MSA concentrations at these two sites, situated near ice divides, could also be indicative of their receiving MSA from multiple nearby source regions. Of all four sites, PIG2010 is located the farthest east along the Amundsen Coast, and receives moisture both from the Amundsen-Bellingshausen Seas and the Weddell Sea (as has been previously shown by Kaspari et al. (2005) for a nearby site ITASE 01-3; Fig. 1). Similarly, THW2010 likely receives moisture from the Amundsen-Bellingshausen Seas and the Ross Sea due to its location between these two

415 catchments (similar to the findings by Kaspari et al. (2005) for the nearby ITASE 00-4
416 and 00-5 sites located on the Ross side of this divide; Fig. 1). Polynyas in the Weddell
417 and Ross Seas have been previously shown to contribute to marine aerosol records in
418 coastal Antarctic ice cores (Barber and Massom 2007, and references therein), and the
419 Bellingshausen Sea polynyas likely do as well.

420 DIV2010 has relatively high composite summer MSA concentrations (comparable
421 to THW2010; Fig. 3), and has offshore wind anomalies along the Amundsen Coast,
422 within Pine Island Bay, and near the leading ice edge in the Amundsen Sea during times
423 of MSA deposition (Fig. 10A). These results indicate that, likely due in part to its
424 location closest to Pine Island Bay, both near-shore regions such as the polynyas as well
425 as offshore regions near the leading ice edge in the Amundsen Sea are source regions of
426 MSA to DIV2010. In contrast to the other three sites, UPT2009 has both considerably
427 lower composite summer MSA concentrations and the least pronounced seasonal cycle of
428 all four core sites (Fig. 3). Results from this site show offshore summer wind anomalies
429 within Pine Island Bay, and easterly convergent wind anomalies along the Amundsen
430 Coast and near the leading ice edge in the Amundsen Sea during high MSA deposition
431 (Fig. 10J), and is located farthest inland and at a relatively high elevation. These results
432 show that UPT2009 is subject to both limited MSA source regions (primarily the leading
433 ice edge in the Amundsen Sea) and decreased transport of MSA, likely a result of its
434 location (farthest inland and at a relatively high elevation).

435

436 *b. Regional wind anomalies and sea-salt source and transport*

437 The annual cycle of Cl^- shown at all sites (Fig. 3) supports previous findings that
438 sea salts in cores from this region are derived largely from winter sea-ice formation,
439 though sea salts are deposited year-round. This sea-ice formation occurs within the
440 polynyas, across the Amundsen Coast continental shelf break, and in other regions in the
441 Amundsen Sea north of 70°S inferred to be the leading ice edge during the period of fall
442 sea-ice formation (Criscitiello et al. 2013). Akin to the discussion of MSA above, the
443 deposition of sea salts onto the ice sheet requires both conditions favorable for sea-ice
444 formation, as well as effective atmospheric transport of the resulting sea-salt aerosols to
445 the ice sheet.

446 Comparison of results from the four different core sites highlights the importance
447 of regional differences in sea-salt source and transport to any one specific ice-sheet
448 location. DIV2010 has the second highest composite winter Cl^- concentrations (Fig. 3),
449 and is the only site with offshore summer and winter wind anomalies associated with
450 enhanced sea-salt deposition (Figs. 10B&C). These results suggest polynyas and other
451 local near-shore areas in the Amundsen Sea sea-ice zone may be a larger source of Cl^- to
452 DIV2010 than at the other core sites, likely due to its proximity to Pine Island Bay.
453 PIG2010 and THW2010 have the lowest composite winter Cl^- concentrations (Fig. 3).
454 PIG2010 has winter onshore wind anomalies originating from the Amundsen Sea (strong
455 meridional winds) during times of winter Cl^- deposition, which may account for the low
456 wintertime Cl^- concentrations at this site. Previous work at the nearest ITASE site to
457 PIG2010 (ITASE 01-3; Fig. 1) suggests that blocking by katabatic winds and "blocking-
458 high effects" (Massom et al. 2004) may inhibit sea-salt deposition at this location
459 (Kaspari et al. 2005). THW2010 has onshore wind anomalies along the Amundsen Coast

460 in summer, and onshore wind anomalies near Pine Island Bay in winter which are part of
461 a low pressure system with an offshore limb over the Ross sector, during times of high
462 Cl^- deposition (Figs. 10H&I). As discussed above, this site has more than one moisture
463 source region. Previous evidence has shown that core sites in the Ross drainage have
464 particularly high sea-salt concentrations as a result of more efficient production of sea
465 salts in the Ross Sea (elevated production rate of highly saline frost flowers) as compared
466 to the Pine Island-Thwaites drainage system (Kaspari et al. 2005). For example, the
467 mean Na^+ concentration from 1922–1991 at ITASE 01-3 (nearest PIG2010) was 18.4
468 ppb, compared with ITASE 00-4 and 00-5 in the Ross sector (nearest THW2010) which
469 had mean Na^+ concentrations of 33.2 ppb and 38.3 ppb, respectively (Kaspari et al.
470 2005). The wind anomalies along the western Amundsen Coast (offshore during winter
471 and onshore during summer) during times of Cl^- deposition at THW2010 (Fig. 10H&I)
472 indicate that, similar to what we observe at PIG2010, sea salts from Ross Sea source
473 regions are not transported to THW2010. The fact that the Ross Sea is not a moisture
474 source region to THW2010 during times of Cl^- deposition may account for the relatively
475 low composite winter Cl^- concentrations at THW2010 (Fig. 3). Finally, UPT2009 has the
476 highest composite winter Cl^- concentration (Fig. 3), and the strongest onshore winter
477 wind anomalies of all four sites (Fig. 10L). While UPT2009 is farthest inland, the site's
478 relatively high elevation, and location within the Pine Island-Thwaites drainage system,
479 exposes it to strong onshore wind anomalies in winter. Enhanced onshore winds along
480 the Amundsen Coast and in particular from important sea-ice formation regions further
481 afield near the leading ice edge and continental shelf in the Amundsen Sea directly
482 increase the transport of sea salts from these source regions to UPT2009.

483

484 *c. SH teleconnection to the tropical Pacific*

485 Our regression analysis suggests that interannual variations in firn-core marine-
486 aerosol records from the Amundsen Coast region of West Antarctica are linked with
487 basin-scale SST variations particularly in the tropical Pacific that affect regional winds.
488 Other studies have also identified a teleconnection between the tropical Pacific Ocean
489 and aerosol deposition in Antarctica (Vance et al. 2012). Regressions of SST on
490 PIG2010 winter Cl^- anomalies (Fig. 5I), and THW2010 summer MSA and winter Cl^-
491 anomalies (Figs. 6G&I), are significant and negative in the eastern tropical Pacific. This
492 SST pattern indicates La Niña-like conditions, and combined with the SLP and 500 hPa
493 GH results, suggests that these sites may be more influenced by the tropical Pacific than
494 the DIV2010 and UPT2009 sites. The distinct SAM-like pattern of SLP and 500 hPa GH
495 seen with summer MSA at THW2010 suggests that the marine aerosols reaching this site
496 are influenced by internal atmospheric dynamics, in addition to large-scale atmospheric
497 dynamics. As discussed above, the proximity of DIV2010 to Pine Island Bay may result
498 in a larger contribution of local dynamics (i.e., polynya variability) to the ice-sheet
499 records (both marine biogenic and sea salt) at this most coastal site. The more inland
500 location of UPT2009, as well as its relatively high elevation, may account for its lower
501 overall summer MSA concentrations (as described above), and may also limit its
502 sensitivity to regional dynamics driven by large-scale variability as compared to PIG2010
503 and THW2010. Similarly, the weaker regressions of global winter atmospheric fields on
504 UPT2009 winter Cl^- indicate that the high Cl^- concentrations from offshore moisture
505 source regions may not be sensitive to tropical Pacific dynamics. We also note that the

506 well-studied, distinct changes between the 1980s and 1990s in the ENSO teleconnection
507 to the high-latitude South Pacific (e.g., Fogt and Bromwich 2006) would be captured by
508 the longer records in this study (DIV2010 and THW2010) but not the shorter records
509 (PIG2010 and UPT2009), which may account for some of the observations discussed in
510 this section.

511 The SIE results (Fig. 9), and to a lesser extent the TOWA results (Fig. 8), confirm
512 the relationship between remote atmospheric dynamics that affect regional winds and
513 Amundsen Sea sea-ice variability, which impact ice-sheet marine-aerosol records. The
514 regional SIE results also show the strong, well-established connection between
515 Amundsen Sea sea-ice variability and SAM (as has been previously shown, e.g.,
516 Lefebvre et al. 2004). The 500 hPa GH regression fields show similar results to the SLP
517 regression fields in terms of the teleconnection to the Antarctic. While the associated
518 SST regressions (Figs. 9E-F) in the eastern tropical Pacific are not as strong as the
519 regressions of pressure fields (which show a clear Rossby wave train connecting the
520 tropics to West Antarctica; Figs. 9A-D), there is relatively small amplitude of SST
521 variability in the tropics when compared to the high latitudes, so the patterns we do see
522 are both statistically and physically significant, and consistent with the other reanalysis
523 results. As mentioned previously, tropical Pacific SST variability influences the upper
524 troposphere, resulting in wave trains of alternating high and low pressure that emanate
525 both north and south (Trenberth et al. 1998), as seen in our results.

526 Our results highlight the importance of both seasonality and location on the
527 impact of atmospheric teleconnections on marine aerosol variability. The impact of
528 ENSO on SH atmospheric circulation is generally strongest in austral winter and spring

529 (e.g., Jin and Kirtman 2010). The wave train pattern therefore becomes prominent in
530 winter and spring, while a more annular pattern can be seen in summer. Our seasonal
531 results reflect these changes in strength and development of the teleconnection. This is
532 evident particularly at THW2010, where a SAM-like pattern is seen with summer
533 regressions of SLP and 500 hPa GH on summer MSA, and a more organized wave train
534 is seen with winter Cl^-. Since sea-salt aerosols are deposited year-round, but largely in
535 winter during sea-ice formation, it is expected that Cl^- would be more strongly influenced
536 by tropical forcing and atmospheric Rossby waves than biogenic aerosols, as we have
537 shown at THW2010 and PIG2010. Further, comparison of the summer and winter
538 regressions of SLP or 500 hPa GH on Cl^- show that the wave train becomes more
539 developed in winter, particularly at THW2010 (Fig. 6). Since marine biogenic aerosols
540 originate from biological productivity during spring and summer, it is also expected that
541 MSA may be more influenced by internal atmospheric variability than tropical forcing,
542 since it is deposited when the teleconnection to the tropics is generally weakest. While
543 the teleconnection may be weaker during times of MSA deposition, and there is certainly
544 variability from site to site, our results do show that summer regressions of SLP, 500 hPa
545 GH, and SST on summer MSA still reveal a significant link via a wave train to the
546 tropical Pacific.
547
548 **5. Conclusions**
549 This work investigates the influence of tropical Pacific dynamics on marine
550 aerosol transport to West Antarctica. We compare MSA and Cl^- concentrations from four
551 new West Antarctic firn cores with global reanalysis data of SLP, 500 hPa GH, SST, and

552 surface wind velocity. The use of multiple core sites enables us to assess spatial
553 variations in marine aerosol source and atmospheric transport as a function of distance
554 from the coast as well as location within the catchments. Our key findings are that: (1)
555 the tropical Pacific influences both the overall source and transport of marine aerosols to
556 the ice sheet through its remote control on regional winds, (2) weaker onshore winds
557 (which can enhance katabatic flow and favor polynya formation along the Amundsen
558 Coast) during times of MSA deposition suggest the polynyas are a major source region of
559 MSA to the Amundsen sector of WAIS, (3) stronger onshore winds during times of sea-
560 salt deposition at all but the most coastal core site suggest an offshore source region for
561 sea salts to most of the Amundsen sector of WAIS, while local dynamics (i.e., polynya
562 variability) may be more important nearer to the coast (i.e., at DIV2010), (4) regional
563 sea-ice behavior (SIE) is also strongly linked to the tropical Pacific via a Rossby wave
564 train, and (5) MSA variability may be more influenced by internal atmospheric variability
565 than Cl^- variability (since MSA is deposited predominantly in summer when the
566 teleconnection to the tropics is weakest), and Cl^- variability may be more influenced by
567 tropical forcing and atmospheric Rossby waves than biogenic aerosols (since Cl^- is
568 deposited largely in winter when the teleconnection to the tropics is strongest).

569 We show that both source and transport of marine aerosols to West Antarctica are
570 controlled by the dynamics of the response to remote atmospheric forcing. This study
571 provides a first assessment of remote atmospheric forcing on Amundsen Coast marine-
572 aerosol records, and benefits from the strength of having multiple coring sites that offer
573 seasonal resolution. Our results should aid future interpretations of ice-core marine-
574 aerosol records in West Antarctica, and provide additional evidence of the teleconnection

575 between the tropical Pacific and West Antarctica (previously shown using SST, SLP,
576 SIC) with independent ice-sheet variables.
577
578 *Acknowledgements*

579 Thanks to Lou Albershardt and RPSC support staff for assistance in the field.
580 Thanks to Luke Trusel, Twila Moon, and NICL staff for assistance processing the cores,
581 and DRI staff for continuous melter analyses. Thanks to Kevin Anchukaitis for
582 assistance with the Monte-Carlo simulations. This research was supported by an award
583 from the Department of Energy Office of Science Graduate Fellowship Program (DOE
584 SCGF) to ASC, a James E. and Barbara V. Moltz Research Fellowship to SBD, and by
585 grants from NSF-OPP (#ANT-0632031 & #ANT-0631973); NSF-MRI (#EAR-1126217);
586 NASA Cryosphere Program (#NNX10AP09G); and a WHOI Andrew W. Mellon
587 Foundation Award for Innovative Research.
588

589 **References**

590 Abram, N. J., R. Mulvaney, and C. Arrowsmith, 2011: Environmental signals in a highly
591 resolved ice core from James Ross Island, Antarctica. *J. Geophys. Res.*, **116**,
592 D20116.
593 Abram, N. J., R. Mulvaney, E. W. Wolff, and M. Mudelsee, 2007: Ice core records as sea
594 ice proxies: An evaluation from the Weddell Sea region of Antarctica. *J.*
595 *Geophys. Res.*, **112**, D15101.
596 Abram, N. J., E. W. Wolff, and M. A. J. Curran, 2013: A review of sea ice proxy
597 information from polar ice cores. *Quat. Sci. Rev.*, in press.
598 Arrigo, K. R., and G. L. van Dijken, 2003: Phytoplankton dynamics within 37 Antarctic
599 coastal polynya systems. *J. Geophys. Res.*, **108**, 3271.
600 Arrigo, K. R., K. E. Lowry, and G. L. van Dijken, 2012: Annual changes in sea ice and
601 phytoplankton in polynyas of the Amundsen Sea, Antarctica. *Deep Sea Res., Part*
602 *II*, **71–76**, 5-15.
603 Artaxo, P., M. L. C. Rabello, W. Maenhaut, and R. V. Grieken, 1992: Trace elements and
604 individual particle analysis of atmospheric aerosols from the Antarctic peninsula.
605 *Tellus B*, **44**, 318-334.
606 Ashok, K., S. K. Behera, S. A. Rao, H. Weng, and T. Yamagata, 2007: El Niño Modoki

607 and its possible teleconnection. *J. Geophys. Res.: Oceans*, **112**.
608 Barber, D. G., and R. A. Massom, 2007: The role of sea ice in Arctic and Antarctic
609 polynyas. *Polynyas: Windows to the World*, W. O. Smith and D. G. Barber,
610 Elsevier, 1-54.
611 Berrisford, P., D. Dee, K. Fielding, M. Fuentes, P. Kallberg, S. Kobayashi, and S.
612 Uppala, 2009: The ERA-Interim Archive. *European Centre for Medium-Range*
613 *Weather Forecasts*, 1-16.
614 Bracegirdle, T. J., 2012: Climatology and recent increase of westerly winds over the
615 Amundsen Sea derived from six reanalyses. *Int. J. Climatol.*,
616 doi:10.1002/joc.3473.
617 Bromwich, D. H., J. P. Nicolas, A. J. Monaghan, M. A. Lazzara, L. M. Keller, G. A.
618 Weidner, and A. B. Wilson, 2013: Central West Antarctica among the most
619 rapidly warming regions on Earth. *Nat. Geosci.*, **6**, 139-145.
620 Charlson, R. J., J. E. Lovelock, M. O. Andreae, and S. G. Warren, 1987: Oceanic
621 phytoplankton, atmospheric sulphur, cloud albedo and climate. *Nature*, **326**, 655-
622 661.
623 Criscitiello, A. S., and Coauthors, 2013: Ice sheet record of recent sea-ice behavior and
624 polynya variability in the Amundsen Sea, West Antarctica. *J. Geophys. Res.:*
625 *Oceans*, **118**, 1-13.
626 Cullather, R. I., D. H. Bromwich, and M. L. Van Woert, 1996: Interannual variations in
627 Antarctic precipitation related to El Nino-Southern Oscillation. *J. Geophys. Res.*,
628 **101**, 19109-19118.
629 Cunningham, W. C., and W. H. Zoller, 1981: The chemical composition of remote area
630 aerosols. *J. Aerosol Sci.*, **12**, 367-384.
631 Curran, M. A. J., and A. S. Palmer, 2001: Suppressed ion chromatography methods for
632 the routine determination of ultra low level anions and cations in ice cores. *J.*
633 *Chromatogr., A*, **919**, 107-113.
634 Dacey, J. W. H., and S. G. Wakeham, 1986: Oceanic dimethylsulfide: Production during
635 zooplankton grazing on phytoplankton. *Science*, **233**, 1314-1316.
636 Dee, D. P., and Coauthors, 2011: The ERA-Interim reanalysis: configuration and
637 performance of the data assimilation system. *Q.J.R. Meteorol. Soc.*, **137**, 553-597.
638 Ding, Q., E. J. Steig, D. S. Battisti, and M. Kuttel, 2011: Winter warming in West
639 Antarctica caused by central tropical Pacific warming. *Nat. Geosci.*, **4**, 398-403.
640 Ding, Q., E. J. Steig, D. S. Battisti, and J. M. Wallace, 2012: Influence of the tropics on
641 the Southern Annular Mode. *J. Climate,* **25**, 6330-6348.
642 Fischer, H., and Coauthors, 2007: Reconstruction of millennial changes in dust emission,
643 transport and regional sea ice coverage using the deep EPICA ice cores from the
644 Atlantic and Indian Ocean sector of Antarctica. *Earth Planet Sci. Lett.*, **260**, 340-
645 354.
646 Fitzgerald, J. W., 1991: Marine aerosols: A review. *Atmos. Environ., Part A.*, **25**, 533-
647 545.
648 Fogt, R. L., and D. H. Bromwich, 2006: Decadal variability of the ENSO teleconnection
649 to the high-latitude South Pacific governed by coupling with the Southern
650 Annular Mode. *J. Climate*, **19**, 979-997.
651 Fogt, R. L., D. H. Bromwich, and K. M. Hines, 2011: Understanding the SAM influence
652 on the South Pacific ENSO teleconnection. *Clim. Dyn.*, **36**, 1555-1576.

653 Fusco, G., G. Budillon, and G. Spezie, 2009: Surface heat fluxes and thermohaline
654 variability in the Ross Sea and in Terra Nova Bay polynya. *Cont. Shelf Res.*, **29**,
655 1887-1895.
656 Gill, A. E., 1980: Some simple solutions for heat-induced tropical circulation. *Q.J.R.*
657 *Meteorol. Soc.*, **106**, 447-462.
658 Hall, A., and M. Visbeck, 2002: Synchronous variability in the Southern Hemisphere
659 atmosphere, sea ice, and ocean resulting from the Annular Mode. *J. Climate*, **15**,
660 3043-3057.
661 Herron, M. M., 1982: Impurity sources of F^-, Cl^-, NO_3^- and SO_4^{2-} in Greenland and
662 Antarctic precipitation. *J. Geophys. Res.: Oceans*, **87**, 3052-3060.
663 Hezel, P. J., B. Alexander, C. M. Bitz, E. J. Steig, C. D. Holmes, X. Yang, and J. Sciare,
664 2011: Modeled methanesulfonic acid (MSA) deposition in Antarctica and its
665 relationship to sea ice. *J. Geophys. Res.*, **116**, D23214.
666 Hoskins, B. J., and D. J. Karoly, 1981: The steady linear response of a spherical
667 atmosphere to thermal and orographic forcing. *J. Atmos. Sci.*, **38**, 1179-1196.
668 Jacobs, S., A. Jenkins, C. F. Giulivi, and P. Dutrieux, 2011: Stronger ocean circulation
669 and increased melting under Pine Island Glacier ice shelf. *Nat. Geosci.*, **4**, 519-
670 523.
671 Jenkins, A., P. Dutrieux, S. S. Jacobs, S. D. McPhail, J. R. Perrett, A. T. Webb, and D.
672 White, 2010: Observations beneath Pine Island Glacier in West Antarctica and
673 implications for its retreat. *Nat. Geosci.*, **3**, 468-472.
674 Jin, F., and B. J. Hoskins, 1995: The direct response to tropical heating in a baroclinic
675 atmosphere. *J. Atmos. Sci.*, **52**, 3, 307-319.
676 Jin, D., and B. P. Kirtman, 2010: The impact of ENSO periodicity on North Pacific SST
677 variability. *Clim. Dyn.*, **34**, 1015-1039.
678 Joughin, I., E. Rignot, C. E. Rosanova, B. K. Lucchitta, and J. Bohlander, 2003: Timing
679 of recent accelerations of Pine Island Glacier, Antarctica. *Geophys. Res. Lett.*, **30**,
680 1706.
681 Kaleschke, L., and Coauthors, 2004: Frost flowers on sea ice as a source of sea salt and
682 their influence on tropospheric halogen chemistry. *Geophys. Res. Lett.*, **31**,
683 L16114.
684 Karoly, D. J., 1989: Southern hemisphere circulation features associated with El Nino-
685 Southern Oscillation events. *J. Climate*, **2**, 1239-1252.
686 Kaspari, S., D. A. Dixon, S. B. Sneed, and M. J. Handley, 2005: Sources and transport
687 pathways of marine aerosol species into West Antarctica. *Ann. Glaciol.*, **41**, 1-9.
688 Kinnard, C., C. M. Zdanowicz, D. A. Fisher, and C. P. Wake, 2006: Calibration of an ice-
689 core glaciochemical (sea-salt) record with sea-ice variability in the Canadian
690 Arctic. *Ann. Glaciol.*, **44**, 383-390.
691 Kreutz, K. J., and P. A. Mayewski, 1999: Spatial variability of Antarctic surface snow
692 glaciochemistry: implications for palaeoatmospheric circulation reconstructions.
693 *Antarct. Sci.*, **11**, 105-118.
694 Kwok, R., and J. C. Comiso, 2002: Southern Ocean climate and sea ice anomalies
695 associated with the Southern Oscillation. *J. Climate*, **15**, 487-501.
696 L'Heureux, M. L., and D. W. J. Thompson, 2006: Observed relationships between the El
697 Niño-Southern Oscillation and the extratropical zonal-mean circulation. *J.*
698 *Climate*, **19**, 276-287.

699 Lachlan-Cope, T., and W. Connolley, 2006: Teleconnections between the tropical Pacific
700 and the Amundsen-Bellinghausens Sea: Role of the El Nino/Southern Oscillation.
701 *J. Geophys. Res.*, **111**, D23101.
702 Lee, S., T. Gong, N. Johnson, S. B. Feldstein, and D. Pollard, 2011: On the possible link
703 between tropical convection and the northern hemisphere Arctic surface air
704 temperature change between 1958 and 2001. *J. Climate*, **24**, 4350-4367.
705 Lefebvre, W., H. Goosse, R. Timmermann, and T. Fichefet, 2004: Influence of the
706 Southern Annular Mode on the sea ice-ocean system. *J. Geophys. Res.*, **109**,
707 C09005.
708 Legrand, M., 1997: Ice-core records of atmospheric sulphur. *Philos. Trans. R. Soc., B*,
709 **352**, 241-250.
710 Liu, J., J. A. Curry, and D. G. Martinson, 2004: Interpretation of recent Antarctic sea ice
711 variability. *Geophys. Res. Lett.*, **31**, L02205.
712 Marshall, G. J., and J. Turner, 1997: Katabatic wind propagation over the western Ross
713 Sea observed using ERS-1 scatterometer data. *Antarct. Sci.*, **9**, 221-226.
714 Maselli, O., D. Fritzche, L. Layman, J. McConnell, and H. Meyer, 2013: Comparison of
715 water isotope ratio determinations using two cavity ring-down instruments and
716 classical mass spectrometry in continuous ice-core analysis. *Isot. Environ. Health*
717 *Stud.*, in press.
718 Massom, R. A., M. J. Pook, J. C. Comiso, N. Adams, J. Turner, T. Lachlan-Cope, and T.
719 T. Gibson, 2004: Precipitation over the interior East Antarctic Ice Sheet related to
720 midlatitude blocking-high activity. *J. Climate*, **17**, 1914-1928.
721 Matsuno, T., 1966: Quasi-geostrophic motions in the equatorial area. *J. Meteor. Soc.*
722 *Japan*, **44**, 25-43.
723 McConnell, J. R., G. W. Lamorey, S. W. Lambert, and K. C. Taylor, 2001: Continuous
724 ice-core chemical analyses using inductively coupled plasma mass spectrometry.
725 *Environ. Sci. Technol.*, **36**, 7-11.
726 Meskhidze, N., and A. Nenes, 2006: Phytoplankton and cloudiness in the Southern
727 Ocean. *Science*, **314**, 1419-1423.
728 Miles, G. M., G. J. Marshall, J. R. McConnell, and A. J. Aristarain, 2008: Recent
729 accumulation variability and change on the Antarctic Peninsula from the ERA40
730 reanalysis. *Int. J. Climatol.*, **28**, 1409-1422.
731 Morganti, A., S. Becagli, E. Castellano, M. Severi, R. Traversi, and R. Udisti, 2007: An
732 improved flow analysis-ion chromatography method for determination of cationic
733 and anionic species at trace levels in Antarctic ice cores. *Anal. Chim. Acta*, **603**,
734 190-198.
735 Nylen, T. H., A. G. Fountain, and P. T. Doran, 2004: Climatology of katabatic winds in
736 the McMurdo dry valleys, southern Victoria Land, Antarctica. *J. Geophys. Res.:*
737 *Atmos.*, **109**, D03114.
738 Okumura, Y. M., D. Schneider, C. Deser, and R. Wilson, 2012: Decadal–interdecadal
739 climate variability over Antarctica and linkages to the tropics: Analysis of ice
740 core, instrumental, and tropical proxy data. *J. Climate*, **25**, 7421-7441.
741 Orsi, A. J., B. D. Cornuelle, and J. P. Severinghaus, 2012: Little Ice Age cold interval in
742 West Antarctica: Evidence from borehole temperature at the West Antarctic Ice
743 Sheet (WAIS) Divide. *Geophys. Res. Lett.*, **39**, L09710.
744 Parish, T. R., and D. H. Bromwich, 1987: The surface windfield over the Antarctic ice

745 sheets. *Nature*, **328**, 51-54.
746 Pasteur, E. C., R. Mulvaney, D. A. Peel, E. S. Saltzman, and P.-Y. Whung, 1995: A 340
747 year record of biogenic sulphur from the Weddell Sea area, Antarctica. *Ann.*
748 *Glaciol.*, **21**, 169-174.
749 Pease, C. H., 1987: The size of wind-driven coastal polynyas. *J. Geophys. Res.: Oceans*,
750 **92**, 7049-7059.
751 Petit, J. R., and Coauthors, 1999: Climate and atmospheric history of the past 420,000
752 years from the Vostok ice core, Antarctica. *Nature*, **399**, 429-436.
753 Pszenny, A. A. P., A. J. Castelle, J. N. Galloway, and R. A. Duce, 1989: A study of the
754 sulfur cycle in the Antarctic marine boundary layer. *J. Geophys. Res.: Atmos.*, **94**,
755 9818-9830.
756 Rankin, A. M., E. W. Wolff, and S. Martin, 2002: Frost flowers: Implications for
757 tropospheric chemistry and ice core interpretation. *J. Geophys. Res.*, **107**, 4683.
758 Ravishankara, A. R., Y. Rudich, R. Talukdar, and S. B. Barone, 1997: Oxidation of
759 atmospheric reduced sulphur compounds: Perspective from laboratory studies.
760 *Philos. Trans. R. Soc., B*, **352**, 171-182.
761 Rhodes, R. H., N. A. N. Bertler, J. A. Baker, S. B. Sneed, H. Oerter, and K. R. Arrigo,
762 2009: Sea ice variability and primary productivity in the Ross Sea, Antarctica,
763 from methylsulphonate snow record. *Geophys. Res. Lett.*, **36**, L10704.
764 Rignot, E., D. G. Vaughan, M. Schmeltz, T. Dupont, and D. MacAyeal, 2002:
765 Acceleration of Pine Island and Thwaites Glaciers, West Antarctica. *Ann.*
766 *Glaciol.*, **34**, 189-194.
767 Roscoe, H. K., B. Brooks, A. V. Jackson, M. H. Smith, S. J. Walker, R. W. Obbard, and
768 E. W. Wolff, 2011: Frost flowers in the laboratory: Growth, characteristics,
769 aerosol, and the underlying sea ice. *J. Geophys. Res.*, **116**, D12301.
770 Schneider, D. P., and E. J. Steig, 2008: Ice cores record significant 1940s Antarctic
771 warmth related to tropical climate variability. *Proc. Natl. Acad. Sci.*, **105**, 12154-
772 12158.
773 Schneider, D. P., C. Deser, and Y. Okumura, 2011: An assessment and interpretation of
774 the observed warming of West Antarctica in the austral spring. *Clim. Dyn.*, **38**,
775 323-347.
776 Shepherd, A., D. J. Wingham, and J. A. D. Mansley, 2002: Inland thinning of the
777 Amundsen Sea sector, West Antarctica. *Geophys. Res. Lett.*, **29**, 1364.
778 Simpkins, G. R., L. M. Ciasto, D. W. J. Thompson, and M. H. England, 2012: Seasonal
779 relationships between large-scale climate variability and Antarctic sea ice
780 concentration. *J. Climate*, **25**, 5451-5469.
781 Smith Jr, W. O., J. Marra, M. R. Hiscock, and R. T. Barber, 2000: The seasonal cycle of
782 phytoplankton biomass and primary productivity in the Ross Sea, Antarctica.
783 *Deep Sea Res., Part II*, **47**, 3119-3140.
784 Smith, W. O., and L. I. Gordon, 1997: Hyperproductivity of the Ross Sea (Antarctica)
785 polynya during austral spring. *Geophys. Res. Lett.*, **24**, 233-236.
786 Stammerjohn, S. E., D. G. Martinson, R. C. Smith, X. Yuan, and D. Rind, 2008: Trends
787 in Antarctic annual sea ice retreat and advance and their relation to El Niño
788 Southern Oscillation and Southern Annular Mode variability. *J. Geophys. Res.*,
789 **113**, C03S90.
790 Steig, E. J., Q. Ding, D. S. Battisti, and A. Jenkins, 2012: Tropical forcing of circumpolar

deep water inflow and outlet glacier thinning in the Amundsen Sea Embayment, West Antarctica. *Ann. Glaciol.*, **53**, 19-28.

Steig, E. J., D. P. Schneider, S. D. Rutherford, M. E. Mann, J. C. Comiso, and D. T. Shindell, 2009: Warming of the Antarctic ice-sheet surface since the 1957 International Geophysical Year. *Nature*, **457**, 459-462.

Steig, E. J., and Coauthors, 2013: Assessing the significance of recent climate and ice sheet change in West Antarctica. *Nat. Geosci.*, in press.

Thomas, E. R., P. F. Dennis, T. J. Bracegirdle, and C. Franzke, 2009: Ice core evidence for significant 100-year regional warming on the Antarctic Peninsula. *Geophys. Res. Lett.*, **36**, L20704.

Trenberth, K. E., G. W. Branstator, D. Karoly, A. Kumar, N.-C. Lau, and C. Ropelewski, 1998: Progress during TOGA in understanding and modeling global teleconnections associated with tropical sea surface temperatures. *J. Geophys. Res.*, **103**, 14291-14324.

Trusel, L. D., K. E. Frey, and S. B. Das, 2012: Antarctic surface melting dynamics: Enhanced perspectives from radar scatterometer data. *J. Geophys. Res.: Earth Surf.*, **117**, F02023.

Turner, J., 2004: The El Niño–southern oscillation and Antarctica. *Int. J. Climatol*, **24**, 1-31.

Vance, T. R., T. D. van Ommen, M. A. J. Curran, C. T. Plummer, and A. D. Moy, 2012: A millennial proxy record of ENSO and eastern Australian rainfall from the Law Dome ice core, East Antarctica. *J. Climate*, doi:10.1175/JCLI-D-12-00003.1.

Weller, R., F. Traufetter, H. Fischer, H. Oerter, C. Piel, and H. Miller, 2004: Postdepositional losses of methane sulfonate, nitrate, and chloride at the European Project for Ice Coring in Antarctica deep-drilling site in Dronning Maud Land, Antarctica. *J. Geophys. Res.*, **109**, D07301.

Wolff, E. W., A. M. Rankin, and R. Röthlisberger, 2003: An ice core indicator of Antarctic sea ice production? *Geophys. Res. Lett.*, **30**, 2158.

Wolff, E. W., and Coauthors, 2006: Southern Ocean sea-ice extent, productivity and iron flux over the past eight glacial cycles. *Nature*, **440**, 491-496.

Yang, X., J. A. Pyle, and R. A. Cox, 2008: Sea salt aerosol production and bromine release: Role of snow on sea ice. *Geophys. Res. Lett.*, **35**, L16815.

Yuan, X., and D. G. Martinson, 2001: The Antarctic dipole and its predictability. *Geophys. Res. Lett.*, **28**, 3609-3612.

Yuan, X., and C. Li, 2008: Climate modes in southern high latitudes and their impacts on Antarctic sea ice. *J. Geophys. Res.*, **113**, C06S91.

Zhang, Y., J. M. Wallace, and D. S. Battisti, 1997: ENSO-like interdecadal variability: 1900–93. *J. Climate*, **10**, 1004-1020.

Figures

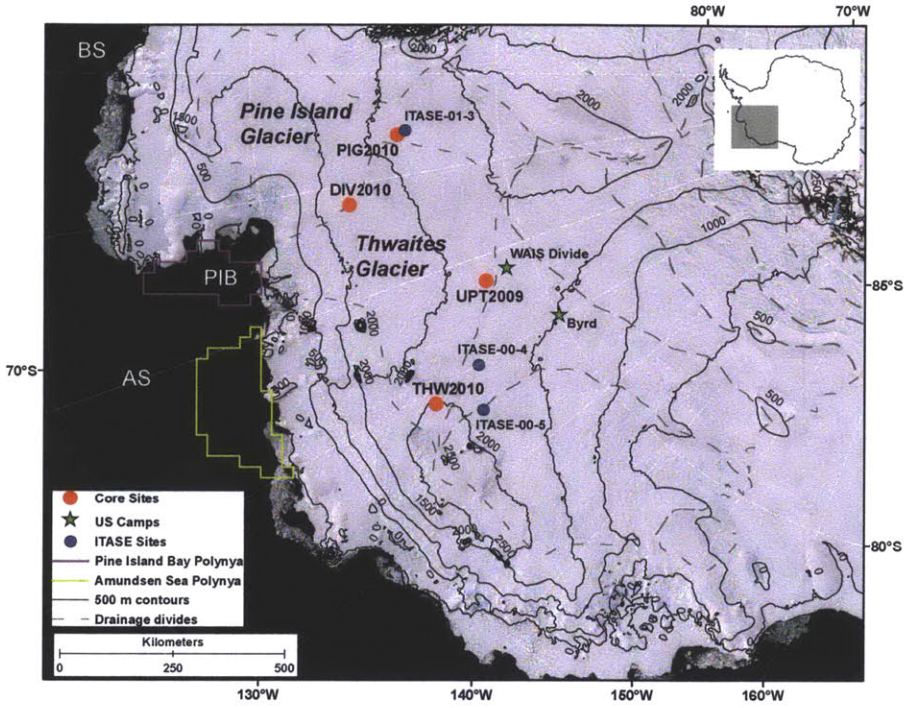

Figure 1. Regional setting of West Antarctica. Grey box in inset shows map location. Background MODIS mosaic of Antarctica is shown with 500 m contour intervals (black solid lines) and drainage divides (grey dashed lines). The DIV2010, PIG2010, THW2010, and UPT2009 drill sites are shown (red circles), as are Byrd and WAIS Divide (green stars), and relevant ITASE cores (blue circles). PIB=Pine Island Bay, AS=Amundsen Sea, BS=Bellingshausen Sea. The PIB polynya mask is shown in purple, and the AS polynya mask is shown in yellow (derived from SMMR- and SSM/I-based SIC).

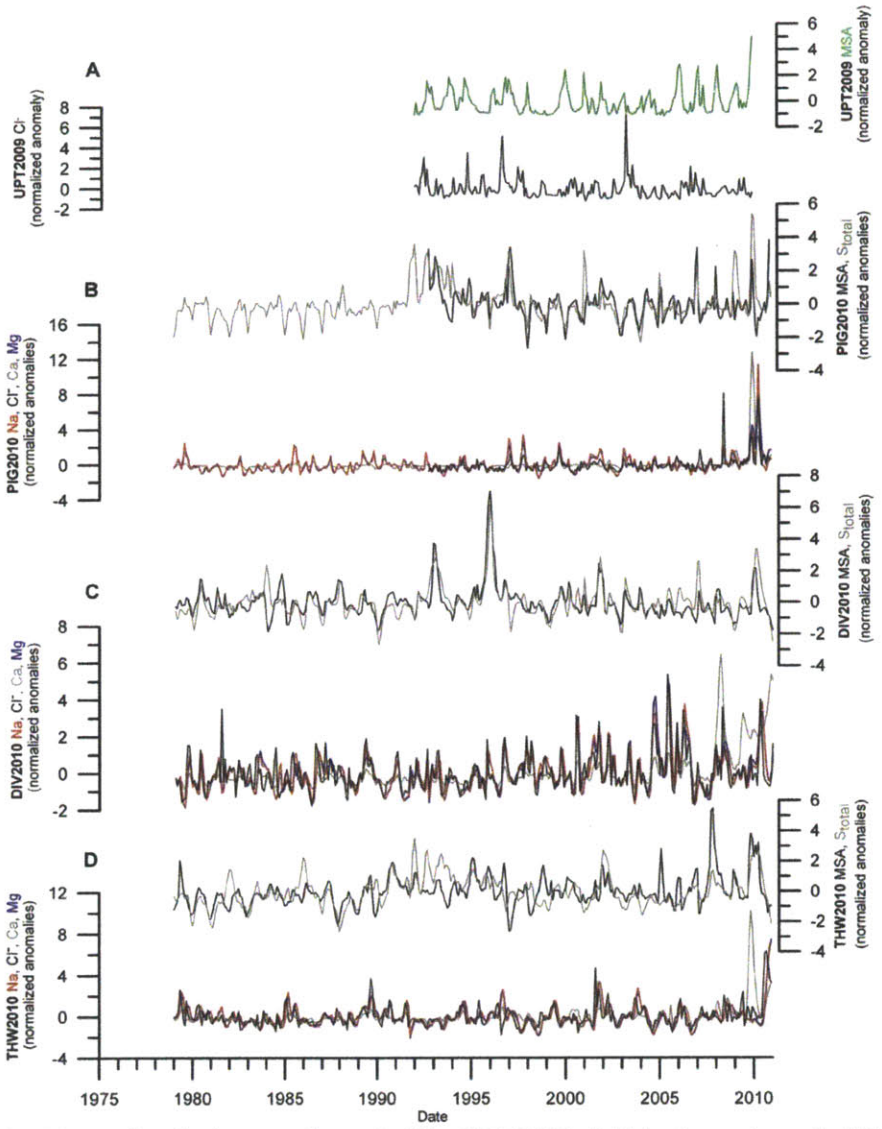

844
845 **Figure 2.** Normalized time series of (A) UPT2009 MSA (green) and Cl^- (black)
846 anomalies (only MSA and Cl^- data exist for UPT2009); normalized time series of Na
847 (red), Cl^- (black), Ca (grey), Mg (blue), MSA (black), and S_{total} (grey) anomalies for (B)
848 PIG2010, (C) DIV2010, and (D) THW2010. Sea-salt species at each site covary, and
849 marine biogenic species at each site covary.
850

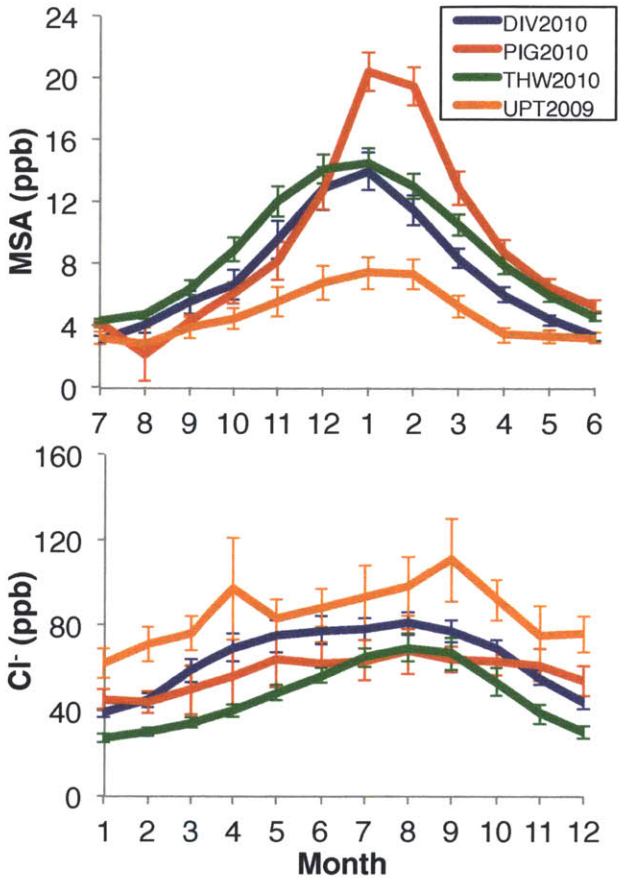

Figure 3. Seasonal cycle of MSA and Cl^- at DIV2010 (blue), PIG2010 (red), THW2010 (green), and UPT2009 (orange). Error bars indicate ±2 standard error. Annual MSA maxima occur in austral summer (DJF), and annual Cl^- maxima occur in austral winter (JJA). Note MSA and Cl^- are shown with different x-axes.

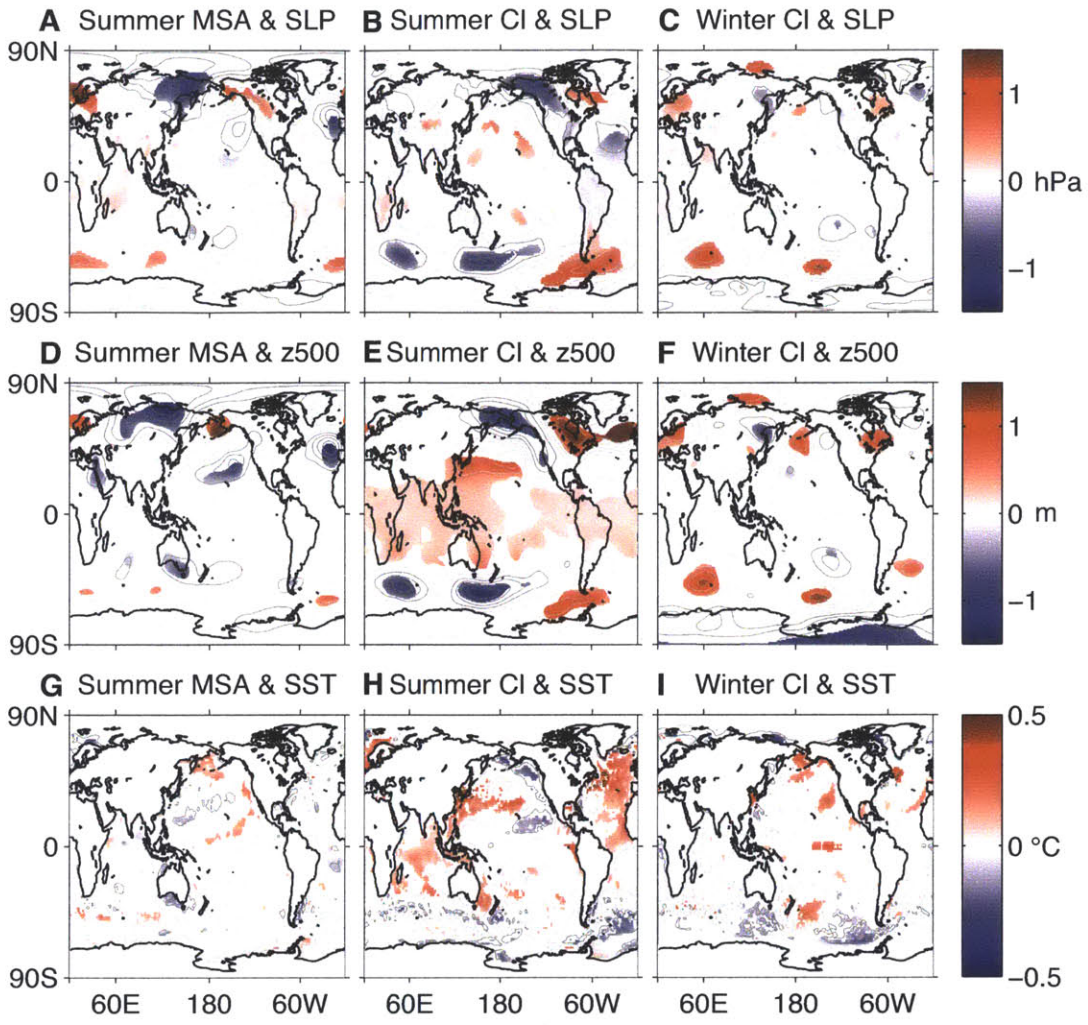

Figure 4. DIV2010 regression maps of summer (Nov–Mar) (A) SLP, (d) 500 hPa GH, and (G) SST on summer MSA; summer (B) SLP, (E) 500 hPa GH, and (H) SST on summer Cl^-; and winter (Jun–Oct) (C) SLP, (F) 500 hPa GH, and (I) SST on winter Cl^- (1979–2010). The SLP scale is -1.5–1.5 hPa (with 0.3 hPa contours), the 500 hPa GH scale is -1.5–1.5 m (with 0.3 m contours), and the SST scale is -0.5–0.5°C (with 0.4°C contours). Contours show all regression patterns (no threshold of statistical significance; positive contours light grey, negative contours dark grey), while shaded regions indicate >95% significance (determined using a two-tailed Student's *t*-test; positive shading red, negative shading blue).

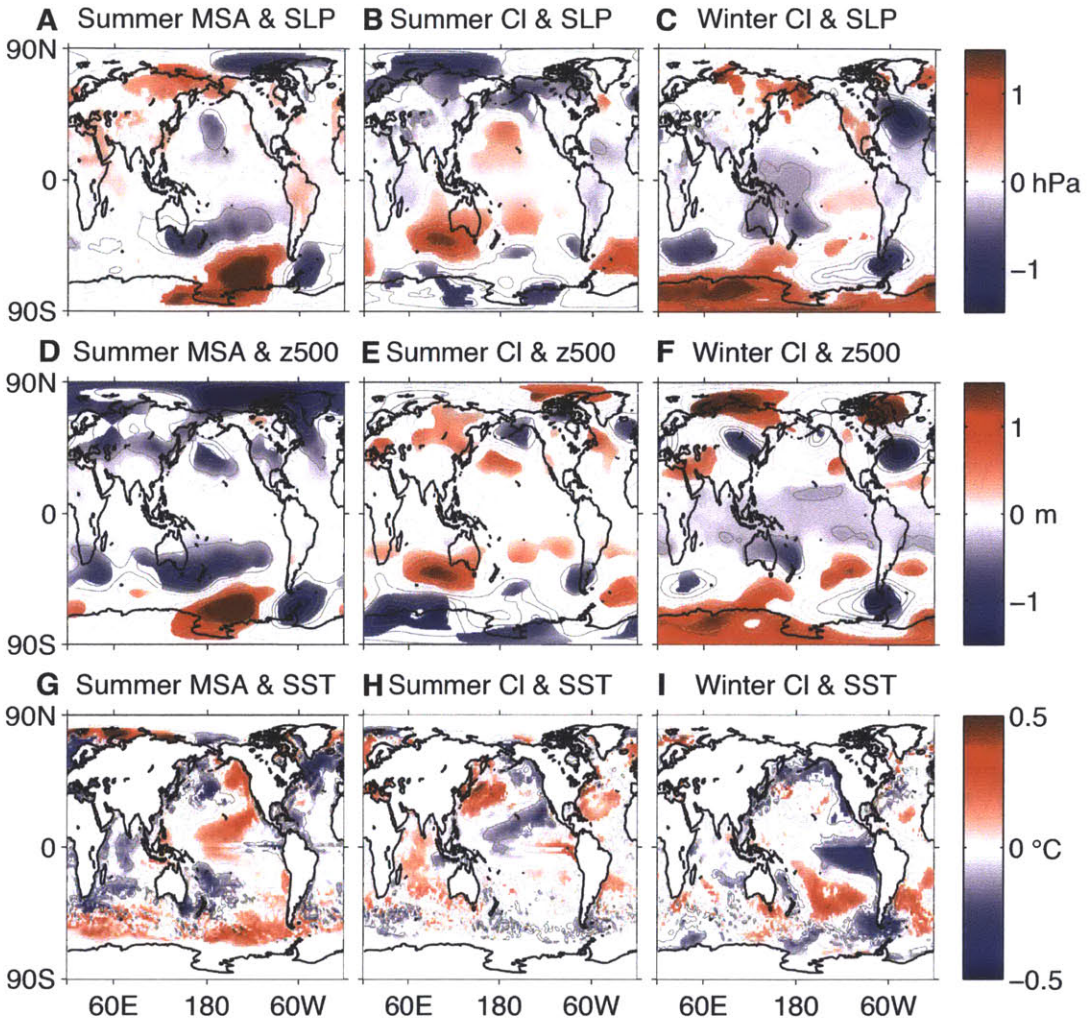

Figure 5. PIG2010 regression maps of summer (Nov–Mar) (A) SLP, (d) 500 hPa GH, and (G) SST on summer MSA; summer (B) SLP, (E) 500 hPa GH, and (H) SST on summer Cl^-; and winter (Jun–Oct) (C) SLP, (F) 500 hPa GH, and (I) SST on winter Cl^- (1992–2010). The SLP scale is -1.5–1.5 hPa (with 0.3 hPa contours), the 500 hPa GH scale is -1.5–1.5 m (with 0.3 m contours), and the SST scale is -0.5–0.5°C (with 0.4°C contours). Contours show all regression patterns (no threshold of statistical significance; positive contours light grey, negative contours dark grey), while shaded regions indicate >95% significance (determined using a two-tailed Student's *t*-test; positive shading red, negative shading blue).

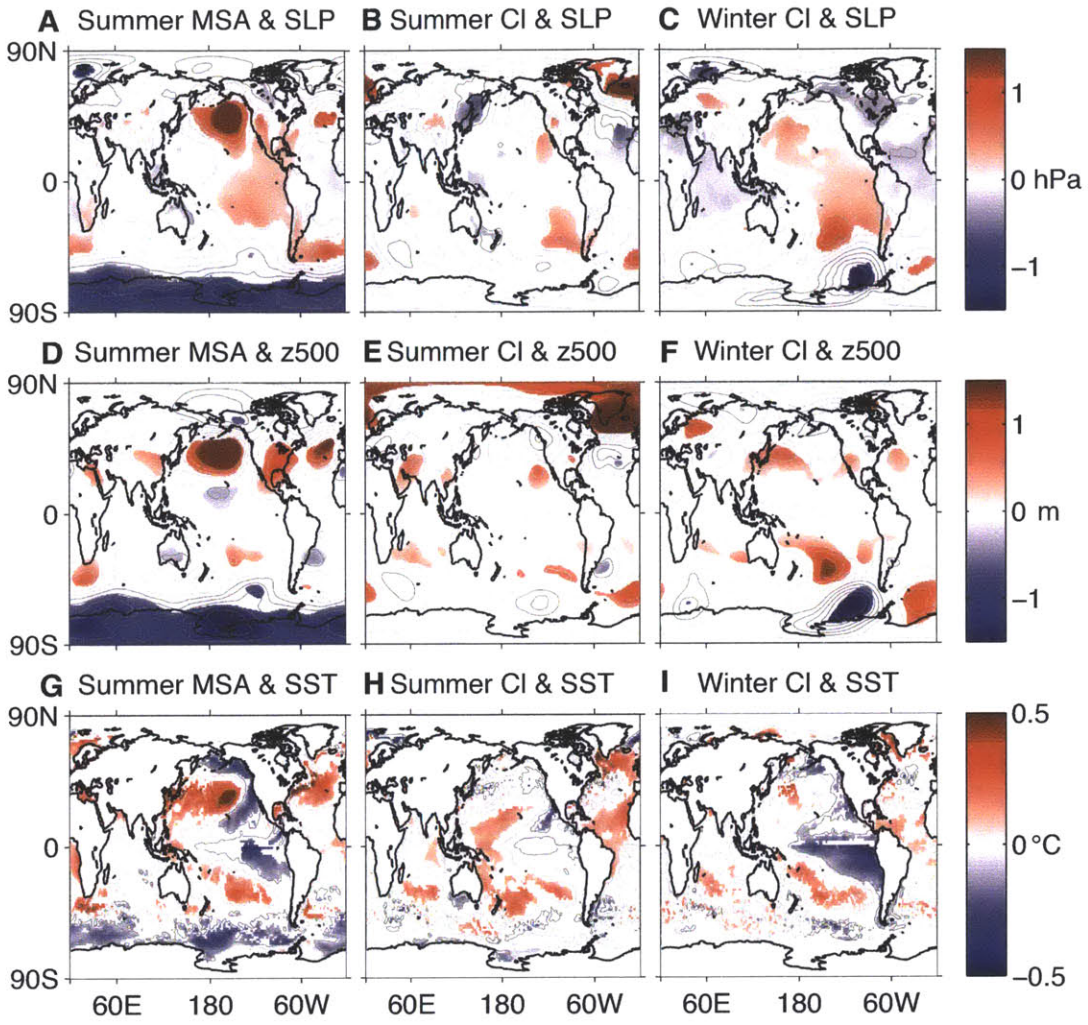

Figure 6. THW2010 regression maps of summer (Nov–Mar) (A) SLP, (d) 500 hPa GH, and (G) SST on summer MSA; summer (B) SLP, (E) 500 hPa GH, and (H) SST on summer Cl^-; and winter (Jun–Oct) (C) SLP, (F) 500 hPa GH, and (I) SST on winter Cl^- (1979–2010). The SLP scale is -1.5–1.5 hPa (with 0.3 hPa contours), the 500 hPa GH scale is -1.5–1.5 m (with 0.3 m contours), and the SST scale is -0.5–0.5°C (with 0.4°C contours). Contours show all regression patterns (no threshold of statistical significance; positive contours light grey, negative contours dark grey), while shaded regions indicate >95% significance (determined using a two-tailed Student's *t*-test; positive shading red, negative shading blue).

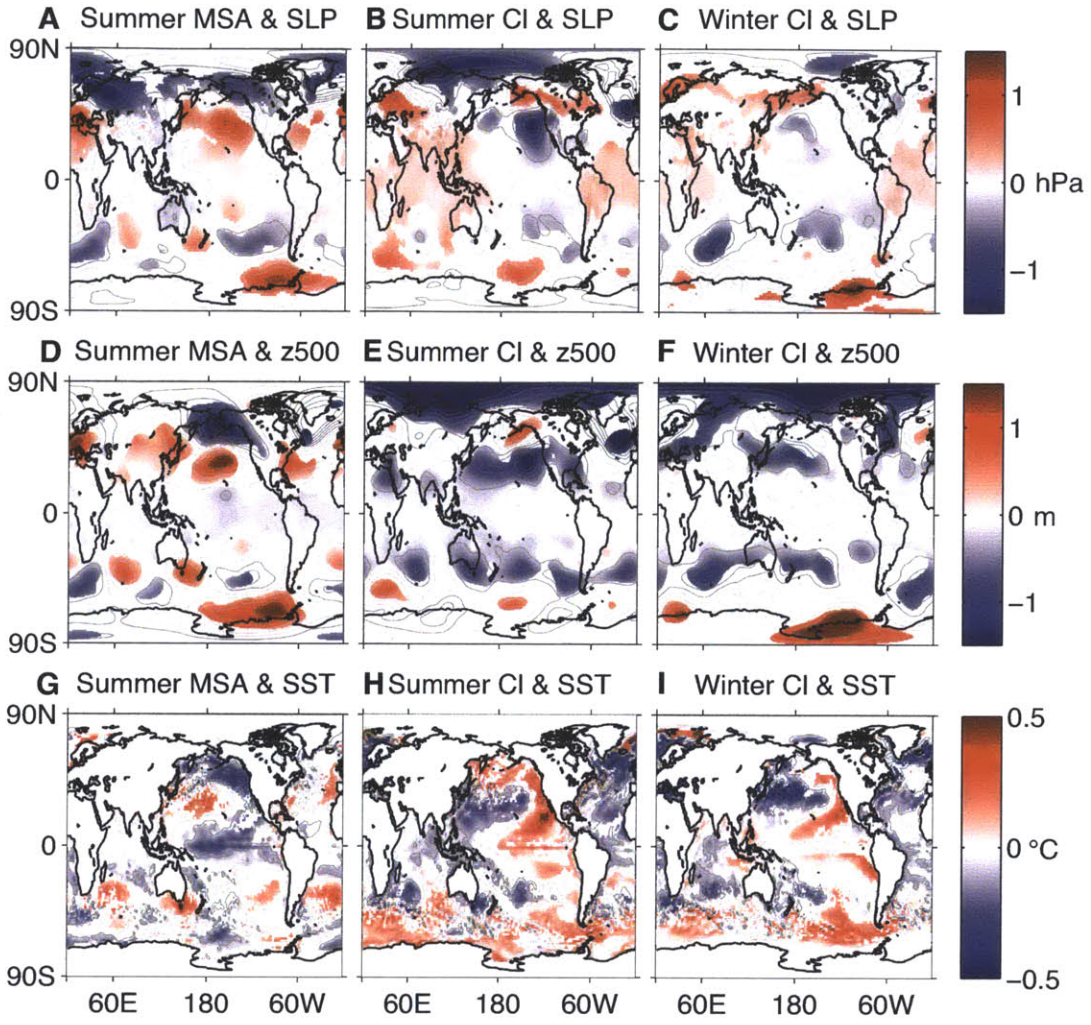

Figure 7. UPT2009 regression maps of summer (Nov–Mar) (A) SLP, (d) 500 hPa GH, and (G) SST on summer MSA; summer (B) SLP, (E) 500 hPa GH, and (H) SST on summer Cl^-; and winter (Jun–Oct) (C) SLP, (F) 500 hPa GH, and (I) SST on winter Cl^- (1992–2009). The SLP scale is -1.5–1.5 hPa (with 0.3 hPa contours), the 500 hPa GH scale is -1.5–1.5 m (with 0.3 m contours), and the SST scale is -0.5–0.5°C (with 0.4°C contours). Contours show all regression patterns (no threshold of statistical significance; positive contours light grey, negative contours dark grey), while shaded regions indicate >95% significance (determined using a two-tailed Student's *t*-test; positive shading red, negative shading blue).

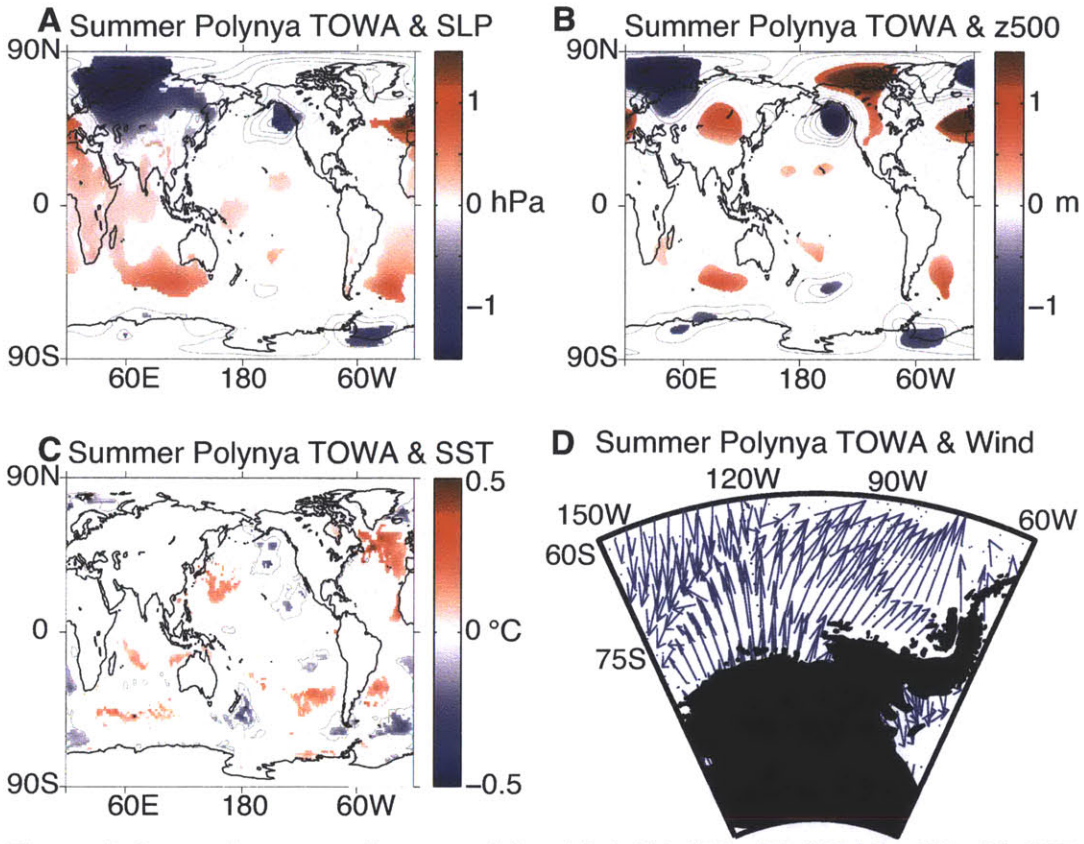

Figure 8. Regression maps of summer (Nov–Mar) (A) SLP, (B) 500 hPa GH, (C) SST, and (D) wind on regional summer polynya total open water area (TOWA). The SLP scale is -1.5–1.5 hPa (with 0.3 hPa contours), the 500 hPa GH scale is -1.5–1.5 m (with 0.3 m contours), and the SST scale is -0.5–0.5°C (with 0.4°C contours). Contours show all regression patterns (no threshold of statistical significance; positive contours light grey, negative contours dark grey), while shaded regions indicate >95% significance (determined using a two-tailed Student's *t*-test; positive shading red, negative shading blue). The average arrow length represents on the order of ~10 m/s.

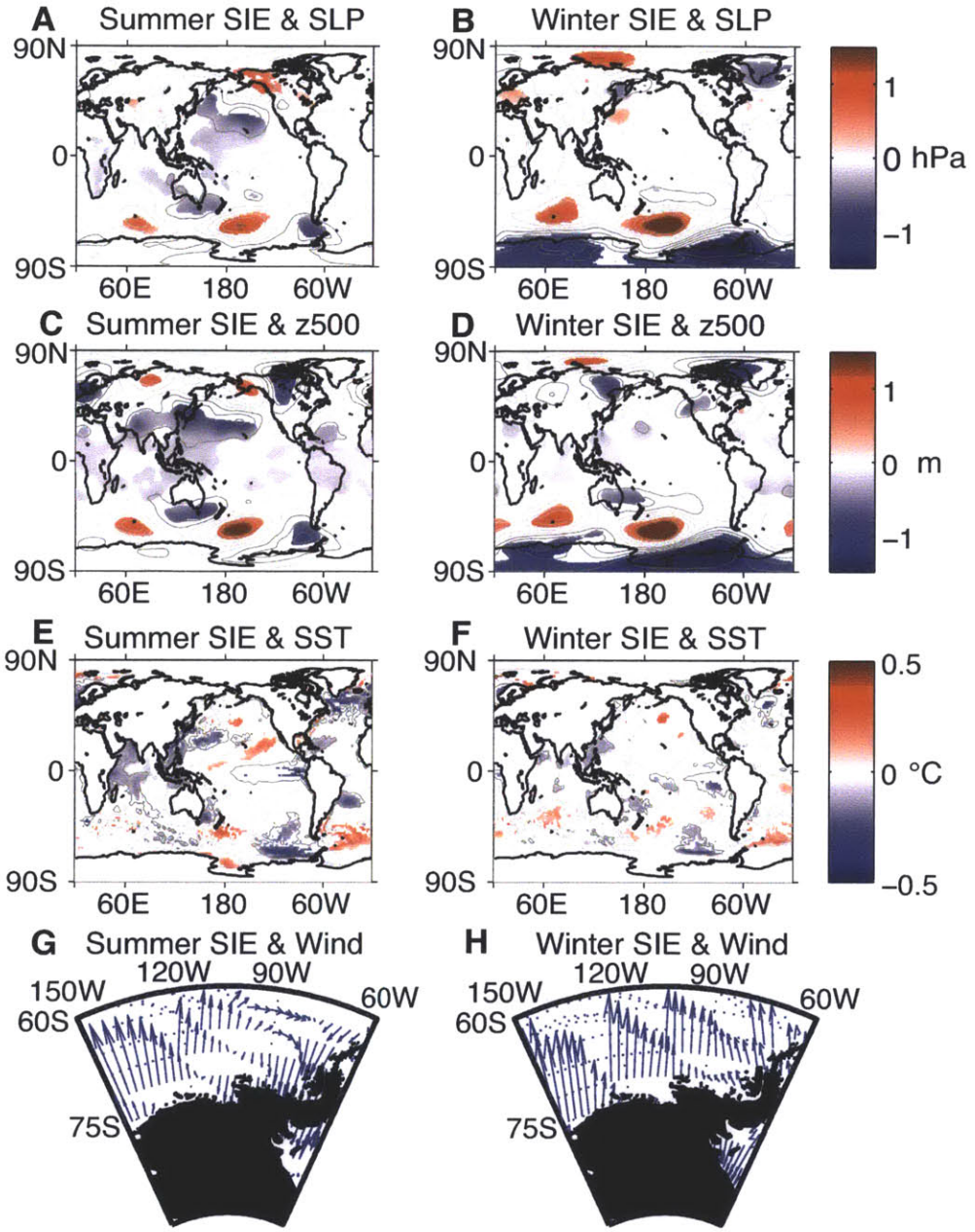

Figure 9. Regression maps of summer (Nov–Mar) (A) SLP, (C) 500 hPa GH, (E) SST, and (G) wind on regional summer sea-ice extent (SIE, for the region between 80°W–140°W and 60°S–71°S); and winter (Jun–Oct) (B) SLP, (D) 500 hPa GH, (F) SST, and (H) wind on winter SIE. The SLP scale is -2–2 hPa (with 0.3 hPa contours), the 500 hPa GH scale is -2–2 m (with 0.3 m contours), and the SST scale is -0.5–0.5°C (with 0.2°C contours). Contours show all regression patterns (no threshold of statistical significance; positive contours light grey, negative contours dark grey), while shaded regions indicate >95% significance (determined using a two-tailed Student's *t*-test; positive shading red, negative shading blue). The average arrow length represents on the order of ~10 m/s.

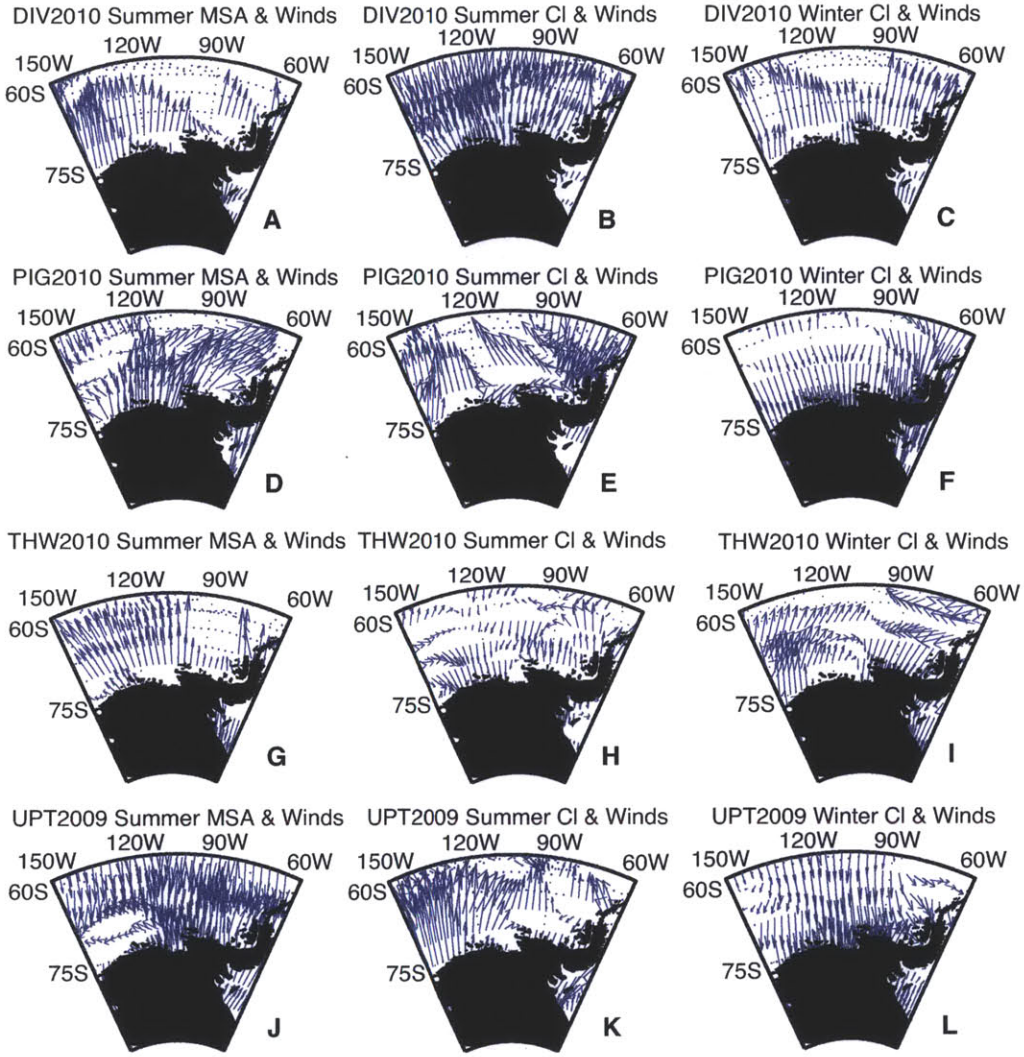

Figure 10. Regression of summer (Nov–Mar) wind on summer MSA at (A) DIV2010, (D) PIG2010, (G) THW2010, and (J) UPT2009; summer wind on summer Cl^- at (B) DIV2010, (E) PIG2010, (H) THW2010, and (K) UPT2009; and winter (Jun–Oct) wind on winter Cl^- at (C) DIV2010, (F) PIG2010, (I) THW2010, and (L) UPT2009. The average arrow length represents on the order of ~10 m/s.

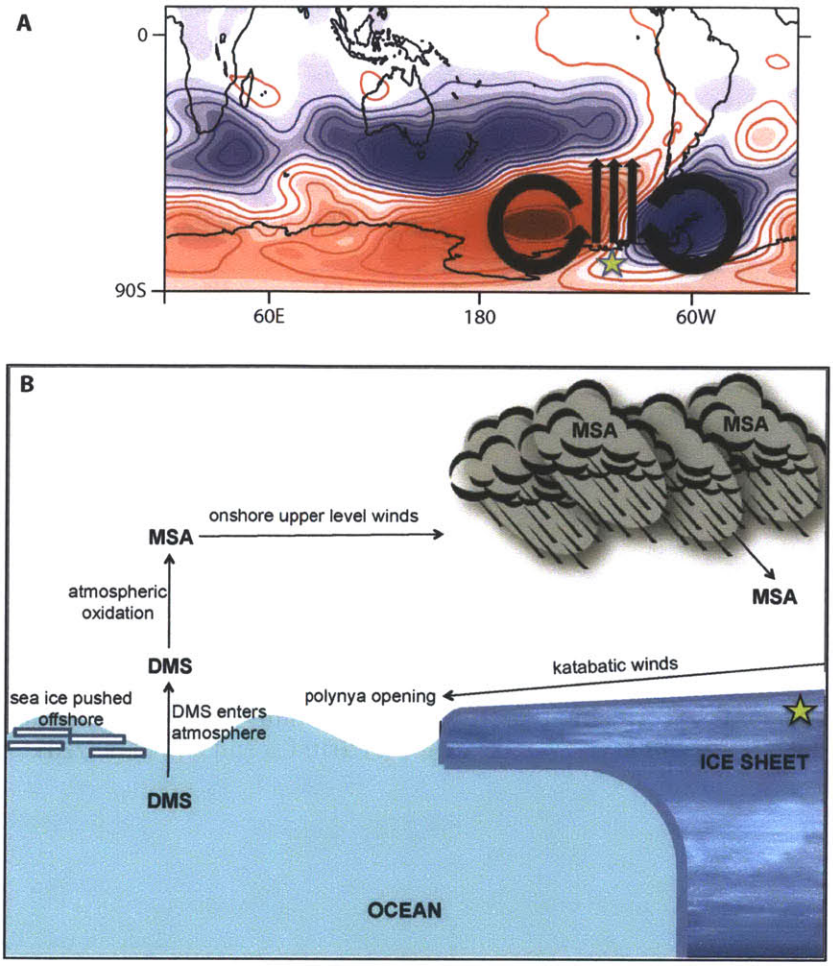

Figure 11. (A) Schematic map view of regional-scale circulation and winds during high summertime MSA deposition at DIV2010. Low pressure (cool colors) over the Antarctic Peninsula results in clockwise wind anomalies, while high pressure (warm colors) west of Pine Island Bay results in counter-clockwise wind anomalies. The result is strong offshore wind anomalies on the ice sheet near Pine Island Bay (indicated by yellow star). (B) Schematic side-view of the same ice-sheet location (yellow star), highlighting local dynamics associated with large-scale teleconnections. Katabatic winds flow off the ice sheet, opening the polynyas and allowing for DMS production. DMS is oxidized in the atmosphere to MSA, which is transported over the ice sheet by onshore upper level winds and precipitated on the ice sheet. While offshore wind anomalies are associated with MSA deposition at all sites, this schematic most directly represents dynamics at DIV2010, the most coastal site.

Tables

Name	Lat	Lon	Elevation (m)	Distance from coast (km)	Period	Mean Accumulation Rate (m·we·yr-1)	MSA range (ppb)	Cl- range (ppb)
DIV2010	-76.770	-101.738	1329	180	1979-2010	0.408	1.1 - 44.8	14.2 - 212.6
PIG2010	-77.957	-95.962	1593	350	1992-2010	0.424	2.6 - 31.7	19.0 - 282.7
THW2010	-76.952	-121.220	2020	340	1979-2010	0.281	2.0 - 31.3	12.2 - 244.6
UPT2009	-78.978	-112.616	1765	500	1992-2009	0.290	0.8 - 22.6	19.3 - 503.3

Table 1. List of four West Antarctic firn cores used in this study.

		Na	Cl-	Ca	Mg	S_{total}
DIV2010	**Na**	--	--	--	--	--
	Cl-	0.75	--	--	--	--
	Ca	0.39	0.31	--	--	--
	Mg	0.97	0.75	0.43	--	--
	MSA	--	--	--	--	0.71
PIG2010	**Na**	--	--	--	--	--
	Cl-	0.77	--	--	--	--
	Ca	0.44	*0.42*	--	--	--
	Mg	0.95	0.77	0.57	--	--
	MSA	--	--	--	--	0.55
THW2010	**Na**	--	--	--	--	--
	Cl-	0.60	--	--	--	--
	Ca	0.35	0.30	--	--	--
	Mg	0.99	0.63	0.36	--	--
	MSA	--	--	--	--	0.49

Table 2. Pearson's r correlation coefficients of monthly (unsmoothed) marine-aerosol anomalies (all significant at $p < 0.05$ except PIG2010 Ca and Cl^-, italicized). S_{total} = total soluble plus insoluble S.

Chapter 4

Regional and remote climatic influences on stable isotope records from high accumulation sites in West Antarctica

Abstract

Water isotope records from polar ice cores are a commonly used paleoclimate proxy, but they are influenced by many local, regional, and remote factors, thus their interpretation requires an understanding of these competing influences over space and time. In this paper we present three new high-resolution, stable water isotope records from ice cores collected along the Amundsen Coast of West Antarctica (DIV2010, PIG2010, and THW2010) to investigate the relationship between isotopic variations in the firn and ice-sheet temperature, precipitation origin, sea-ice variability, and large-scale atmospheric circulation over the satellite reanalysis era (1979–2010). We find the $\delta^{18}O$ records at all sites are only moderately correlated with reanalysis-based temperature reconstructions at the core locations, and are generally poorly correlated with temperature from a regional atmospheric climate model (RACMO2). DIV2010 shows a slight negative temperature trend (-0.1 °C/decade), in contrast to the slight positive temperature trend at the other two sites (+0.1 °C/decade), likely the result of the weaker link between DIV2010 and tropical Pacific forcing (note trends are based on annual 1979–2010 data). The deuterium excess (*d*) records offer additional insight into spatial and temporal moisture source variability. The DIV2010 core (our most coastal site) exhibits patterns in moisture source location distinct from the other two sites, and is also more strongly affected by polynya variability than the sites farther inland. Regressions of global atmospheric fields on firn-core isotope records, as well as analysis of temporal shifts in the $\delta^{18}O$-*d* lag, suggest that the tropical Pacific remotely influences the source and transport of the isotopic signal to the coastal ice sheet. While all isotope records are influenced by remote tropical climate variability, the more coastal isotope records better capture local dynamics (polynya variability).

1. Introduction

While the isotopic composition of polar precipitation provides one of the best known ice-sheet paleothermometers, these records are complicated by the influence of many factors other than air temperature such as variations in moisture source region, transport, seasonality of precipitation, sea-ice extent, and post-depositional alterations [*Bromwich and Weaver*, 1983; *Masson-Delmotte*, 2008; *Noone and Simmonds*, 2002; *Schlosser*, 1999; *Steig et al.*, 1994]. Such factors modify the relationship between $\delta^{18}O$ (and δD) and local temperature, resulting at times in correlations that may be low, or significantly variable over time [e.g., *Schneider and Noone*, 2007; *Sime et al.*, 2009]. In addition, remote atmospheric dynamics affect stable water isotopes at coastal Antarctic sites both directly by injection of enriched water vapor and indirectly by increasing the sensible heat flux during times of low sea-ice concentration (SIC) [*Bromwich and Weaver*, 1983; *Noone and Simmonds*, 2002; *Noone and Simmonds*, 2004; *Thomas and Bracegirdle*, 2009]. Interpretation of the isotopic composition of ice cores therefore requires investigation of these various influences.

Deuterium excess (*d*), calculated as $d = \delta D - 8*\delta^{18}O$ [*Dansgaard*, 1964], is another parameter that can help us separate the affects of temperature and moisture source location on isotope records [*Dansgaard*, 1964; *Merlivat and Jouzel*, 1979]. *d* can reflect changes in moisture transport and air mass trajectories [e.g., *Divine et al.*, 2011; *Kavanaugh and Cuffey*, 2003; *Stenni et al.*, 2010] and thus is often used as an integrated indicator of precipitation origin [e.g., *Ciais et al.*, 1995; *Delmotte et al.*, 2000]. In Antarctica, $\delta^{18}O$ and *d* records from coastal regions are more strongly affected by sea-ice variability than isotope records from the continent interior [*Noone and Simmonds*, 2004],

largely due to local deposition of the isotopic signal associated with water evaporated from the sea-ice zone [*Noone and Simmonds*, 2002]. This link between stable water isotopes and SIC may also allow us to investigate past polynya variability at coastal sites where polynya dynamics can have a large impact on ice-sheet records [e.g., *Criscitiello et al.*, 2013]. Using a suite of ice-core records, particularly in West Antarctica where drainage divides influence the distribution of precipitation [*Nicolas and Bromwich*, 2011], can allow for a more comprehensive representation of the isotopic variations and their relation to climate [e.g., *Küttel et al.*, 2012]. Additionally, comparison of firn-core records from coastal sites with those from farther inland can offer insight into the spatial variability of local (sea ice) and remote (tropical Pacific) impacts on oxygen isotope records.

Continental West Antarctica has experienced substantial, widespread warming in the past 50 years [*Bromwich et al.*, 2012; *Orsi et al.*, 2012; *Steig et al.*, 2009], which has been linked to sea surface temperature (SST) changes in the tropical Pacific [*Ding et al.*, 2011; *Ding et al.*, 2012; *Schneider et al.*, 2011; *Steig and Orsi*, 2013]. Several studies have shown the strong relationship between Antarctic isotopic variations and records of large-scale atmospheric circulation (El Niño Southern Oscillation (ENSO) and the Southern Annular Mode (SAM)) [e.g., *Divine et al.*, 2009; *Gregory and Noone*, 2008; *Schneider and Noone*, 2007; *Schneider and Steig*, 2008]. Variability of other marine-influenced glaciochemical records from East Antarctic [e.g., *Vance et al.*, 2012] and West Antarctic [e.g., *Criscitiello et al.*, 2013b; *Okumura et al.*, 2012] ice cores show a similar link to the tropical Pacific, in part because sea-ice variability is driven largely by remote atmospheric dynamics that control local winds [e.g., *Stammerjohn et al.*, 2008].

47 In this study, we present a set of three high-resolution firn-core records from West
48 Antarctica to investigate the relationship between isotopic variations in the firn and
49 temperature, precipitation origin, SIC and polynya variability, and large-scale
50 atmospheric circulation from 1979–2010. The relatively high accumulation rates at these
51 sites allows for precise dating, enabling us to examine the climate signal recorded in the
52 ice sheet on a seasonal timescale. Their spatial distribution allows us to establish how
53 this climatic signal varies spatially across the Amundsen sector of the West Antarctic Ice
54 Sheet (WAIS). We compared the mean annual and seasonal cycle in $\delta^{18}O$ in the firn
55 cores to the annual and seasonal temperature and precipitation cycles in the region using
56 observational and reanalysis data (ERA-Interim and Regional Atmospheric Climate
57 Model v.2.1 (RACMO2)). We also compared these $\delta^{18}O$ records to regional records of
58 sea-ice variability to investigate the effects of SIC and polynyas on the oxygen isotope
59 records at each site over the period of study. We additionally examined NOAA Hybrid
60 Single-Particle Lagrangian Integrated Trajectory (HySPLIT) model back-trajectory
61 results together with the *d* records to investigate temporal and spatial moisture source
62 variability. Finally, we analyzed the isotope records in conjunction with global reanalysis
63 fields of SST, sea level pressure (SLP), and 500 hPa geopotential height (GH) to explore
64 the local effects of remote atmospheric dynamics on these West Antarctic isotope
65 records. As climate data at high southern latitudes are most reliable from 1979 onwards,
66 we focus this study on stable water isotope firn-core records from 1979–2010.
67
68 **2. Data and Methods**
69 *2.1 Site descriptions*

70 In 2010-11, we used the US Eclipse drill to collect three firn cores from Pine
71 Island Glacier (PIG2010), Thwaites Glacier (THW2010), and the drainage divide
72 between Pine Island and Thwaites Glaciers (DIV2010; Fig. 1). As core was retrieved, we
73 measured temperature every ~0.5-1 m using a Fluke Type II thermistor probe (0.2°C
74 accuracy). The core sites range in elevation from 1329 to 2020 m, and range from 180 to
75 350 km in distance from the coast (Table 1). Annual accumulation rates at the sites are
76 relatively high (Table 1), with 1979–2010 averages of ~0.3 meters of water equivalent
77 per year ($m \cdot we \cdot yr^{-1}$; THW2010) and ~0.4 $m \cdot we \cdot yr^{-1}$ (DIV2010 and PIG2010). Annual
78 accumulation variability is also high at all sites, and shows no significant recent trend
79 [*Medley et al.*, 2013]. Ice velocities at the core locations are low (~10–20 $m \cdot yr^{-1}$)
80 [*Joughin et al.*, 2003].
81
82 *2.2 Glaciochemical records and dating*
83 Isotope values for the DIV2010, PIG2010, and THW2010 cores were measured
84 using a Picarro cavity ring-down spectroscopy analyzer linked directly with a continuous
85 ice-core melter system [*Maselli et al.*, 2013; *McConnell et al.*, 2001]. Sample isotope
86 ratios ($\delta^{18}O$ and δD) were standardized using three working standards calibrated against
87 the IAEA standards VSMOW and SLAP. Final values are reported on the
88 VSMOW/SLAP scale with a precision of <0.1‰ (for $\delta^{18}O$) and <0.5‰ (for δD).
89 We established age-depth relationships and determined accumulation rates by
90 identifying the midsummer maximum in three parameters (nssS/Na, H_2O_2, and $\delta^{18}O$) and
91 counting annual cycles. A volcanic time marker present in 1992 was also used to verify
92 the annual layer counting. As a result of the high accumulation rate and multiple dating

93 parameters, the standard error in the interannual dating is less than ±1 year [*Medley et al.*,
94 2013; *Pasteris et al.,* in review]. To allow for investigation of the isotope time series
95 alongside reanalysis records, we produced monthly-resolution isotope records by linear
96 interpolation between the midsummer annual picks. There is no systematic asymmetry in
97 the average annual cycle of H_2O_2 and $\delta^{18}O$, suggesting that errors in the subannual dating
98 from variations in snowfall distribution are minimal in the multiyear average annual
99 cycles [*Pasteris et al.,* in review]. Therefore we assume the average annual distribution
100 of snowfall is approximately uniform. Within the annual cycle, we estimate a maximum
101 possible error in the interpolated age scale of ±2 months, similar to others who utilize
102 comparable methods [e.g., *Abram et al.*, 2011]. To avoid errors in correlation with large-
103 scale reanalysis fields resulting from chronological uncertainty, we further applied a 3-
104 point running mean to all monthly isotope time series. At high accumulation rate sites,
105 the isotope signal on time scales longer than a few months is not appreciably influenced
106 by water vapor diffusion [*Küttel et al.*, 2012]. Thus, the amplitude of the seasonal cycle
107 is well preserved [*Masson-Delmotte*, 2008].
108 Finally, we created composite ("stacked") monthly and annual isotope records by
109 averaging the monthly and annual isotope data, respectively, from the three sites to
110 generate a multi-core average. The composite annual cycles of stacked $\delta^{18}O$ and d
111 presented in Fig. 2, for example, are monthly climatological means of each individual
112 month over the three records (1979–2010). The stacked records are presented in all time
113 series figures (Figs. 2-4), and are included in the discussion.
114
115 *2.3 Reanalysis climate datasets and temperature reconstructions*

116 We utilized ERA-Interim reanalysis products from the European Centre for
117 Medium-Range Weather Forecasts (ECMWF) [*Dee et al.*, 2011] to provide global
118 monthly SST, SLP, and 500 hPa GH over the study period. Recent assessments for the
119 Amundsen Sea region of Antarctica indicate that ERA-Interim is the most reliable
120 reanalysis product for this region of Antarctica that is currently available [*Bracegirdle*
121 *and Marshall*, 2012]. Our reanalysis results are presented as monthly anomalies
122 (monthly mean climatologies were removed), and to reduce subseasonal noise unrelated
123 to tropical forcing, we applied a 3-point running mean to all the monthly reanalysis data
124 as well (similar to the isotope records).

125 We conducted least-squares linear temporal regression analyses of atmospheric
126 fields on the anomalies of the firn-core isotope records (all time series 3-month
127 smoothed). Statistical significance for the regressions was determined using the two-
128 tailed Student's *t*-test ($p < 0.01$). In addition, we performed lag tests (0, 1 and 2-month)
129 between the isotope time series and reanalysis data. These did not strengthen regression
130 results; therefore only 0 lag results are presented.

131 We employed three separate methods to derive site-specific temperatures to
132 compare with firn-core isotope records. First, we used ERA-Interim 2 m reanalysis
133 temperature from ECMWF, which utilizes Special Sensor Microwave/Imager (SSM/I)
134 data [*Dee et al.*, 2011]. Second, we used temperature results from RACMO2 [*Lenaerts et*
135 *al.*, 2012], which has ~30 km resolution and is forced on its lateral boundary at 60°S by
136 observation-driven ERA-Interim reanalysis data. Finally, we used the new 52-year Byrd
137 temperature reconstruction, which is based on both observational (automatic weather
138 station) and global reanalysis data (ERA-Interim, where observational data are missing)

139 [*Bromwich et al.*, 2012]. Temperature variability at Byrd has been shown to be spatially
140 well correlated with temperature variability across much of West Antarctica [*Bromwich*
141 *et al.*, 2012].
142
143 *2.4 Regional sea-ice extent and total polynya open water area*
144 We created two time series to examine the link between $\delta^{18}O$ and *d*, and polynya
145 and sea-ice variability specifically relevant to this study. We created a polynya total open
146 water area time series (TOWA) for the sea surface within Pine Island Bay and Amundsen
147 Sea polynyas, as well as a regional sea-ice extent time series (SIE). Polynya masks were
148 defined by calculating spatial correlations between monthly DIV2010 methanesulfonic
149 acid (MSA) and Scanning Multichannel Microwave Radiometer (SMMR) and SSM/I
150 passive microwave data of SIC from 1979–2010, with a threshold value of $r > 0.4$ ($p <$
151 0.1). This method allows us to target areas of significant correlation between monthly
152 SIC and DIV2010 MSA as has been done previously [*Criscitiello et al.*, 2013;
153 *Criscitiello et al.*, 2013b], and results in polynya masks near-equivalent to those
154 generated by others [e.g., *Arrigo and van Dijken*, 2003]. Using these polynya masks, we
155 extracted daily open water areas (1979–2010) by summing the pixels (25 km x 25 km)
156 that had <15% SIC (our defined threshold value for open water). Next, we summed the
157 daily open-water areas of the Pine Island Bay and Amundsen Sea polynyas, and then
158 averaged these daily values to generate the TOWA monthly time series. Finally, we
159 smoothed the monthly TOWA anomalies with a 3-month running mean, as we did with
160 the reanalysis data and firn-core time series. The SIE time series also utilizes SMMR-
161 and SSM/I-based SIC, but in this case we created a monthly time series of SIE between

80°W and 140°W, and 60°S and 71°S (a large offshore region previously shown to be a source of marine aerosols to West Antarctica [*Criscitiello et al.*, 2013; *Dixon et al.*, 2004; *Kaspari et al.*, 2005]), where SIE is defined as the total area within this defined region with SIC > 15%.

2.5 HySPLIT back-trajectories

We used the HySPLIT model to compute air parcel back-trajectories, allowing us to examine air mass transport pathways into West Antarctica. The HySPLIT model has been used previously to assess the transport pathways of precipitation to ice-core sites along the Ross Sea [*Sinclair et al.*, 2010] and into West Antarctica [*Dixon et al.*, 2012]. The model is a hybrid between a Lagrangian approach (which utilizes a moving frame of reference for the advection and diffusion calculations as parcels travel from their starting location) and an Eulerian approach (which utilizes a fixed 3D grid) [*Draxler and Rolph*, 2003]. We calculated 3-day back-trajectories originating from the three core sites in conjunction with the National Centers for Environmental Protection and Atmospheric Research (NCEP/NCAR) global atmospheric reanalysis datasets [*Kalnay et al.*, 1996] archived on the NOAA READY website. The HySPLIT model control file included: (1) firn core start locations, (2) total run time, and (3) altitude of starting air parcel = 1500 m (agl). Following others [*Markle et al.*, 2012; *Sinclair et al.*, 2010], we tested initial starting heights of 500 m and 1000 m for trajectories arriving at the three core sites using a trajectory matrix. We ultimately chose the 1500 m altitude of the starting air parcels as it best captured synoptic-scale conditions, and avoided dynamics related to katabatic and surface winds, while additionally limiting the potential influence of underlying terrain

185 [*Markle et al.*, 2012]. We selected 3-day runs as we found that slightly longer runs (5
186 days) yielded similar trends but were computationally more expensive, and runs 7 days or
187 longer produced spurious results.

188 We investigate both mean annual conditions, as well as conditions during winter-
189 time polynya events. To assess mean annual conditions, we ran the model monthly at
190 each site (3-day runs; 12 back-trajectories per site) for the year that was most
191 representative of the mean precipitation at that location (mean calculated from 1979–
192 2010) which was 2008 (DIV2010), 1979 (PIG2010), and 2001 (THW2010). These
193 results are presented seasonally (winter = JJA, spring = SON, summer = DJF, fall =
194 MAM). We also ran 3-day back-trajectories at each site for the months with maximum
195 and minimum annual d values for every year from 1979–2010 (maxima = Mar
196 (DIV2010), Apr (PIG2010), Feb (THW2010)), minima = Oct (DIV2010), Nov
197 (PIG2010), Sep (THW2010)).

198 To investigate the potential influence of polynya variability on the isotope
199 records, we also ran 3-day back-trajectories for three individual months that had the
200 largest wintertime polynya events in the Amundsen Sea and Pine Island Bay (August
201 2002, July 2005, June 2007), events previously found to be coincident with the largest
202 winter MSA peaks at DIV2010 [*Criscitiello et al.*, 2013]. These HySPLIT runs were
203 compared with 3-day back-trajectories for three months that had the smallest or no
204 wintertime polynya events (July 2008, July 2009, July 2010) [*Criscitiello et al.*, 2013].
205

206 **3. Results**

207 ***3.1 Isotope records***

208 The climatology of the isotope records shows a summer maximum and winter
209 minimum in $\delta^{18}O$ and δD at all sites, as expected due to the primary temperature control
210 on these variables. $\delta^{18}O$ and δD are also highly correlated with each other at all sites ($r >$
211 0.99), with $\delta D/\delta^{18}O$ regression slopes of 7.86 (DIV2010), 7.95 (PIG2010), and 7.96
212 (THW2010), similar to the global meteoric water line of 8.0 [*Craig*, 1961]. *d* shows a
213 fall maximum and spring minimum at all sites (Fig. 2). The mean $\delta^{18}O$ values at
214 DIV2010, PIG2010, and THW2010 are -27.1, -32.2, and -33.1 ‰, respectively, and mean
215 *d* values are 1.75, 1.14, and 4.80, respectively (Table 1). The PIG2010, THW2010, and
216 stacked $\delta^{18}O$ records have a slight positive trend (~0.1 ‰/decade), and the DIV2010 $\delta^{18}O$
217 record has a slight negative trend (~-0.1 ‰/decade; note these trends are not statistically
218 significant due to the short length of the time series). The DIV2010, PIG2010, and
219 composite (stacked) *d* records have a slight positive trend (~0.25 decade^{-1}), and the
220 THW2010 *d* record has a slight negative trend (~-0.7 decade^{-1}). PIG2010 and THW2010
221 have similar $\delta^{18}O$ records ($r = 0.34$, $p < 0.1$), while DIV2010 $\delta^{18}O$ values remain lighter
222 than the other two sites for all years (Fig. 4). DIV2010 and PIG2010 have similar *d*
223 records ($r = 0.3$, $p < 0.1$), while THW2010 *d* values are higher than the other two sites for
224 all years except 2006 (Fig. 4). The stacked $\delta^{18}O$ record is most strongly correlated with
225 the PIG2010 $\delta^{18}O$ record ($r = 0.79$, $p < 0.1$), and the stacked *d* record is most strongly
226 correlated with the DIV2010 *d* record ($r = 0.69$, $p < 0.1$).
227 During the wintertime polynya events discussed, the corresponding increases in
228 MSA in a short core drilled at the DIV2010 site (DIV2010S, reported in Criscitiello et al.,
229 2013) are also expressed by a sharp increase in the DIV2010S oxygen isotope record (up
230 to 1.5‰ above background winter values), suggestive of temperature increases over the

231 coastal ice sheet during times of polynya formation (Fig. 5). We note that while the
232 uncertainty in the age scales for the cores in this study precludes us from confidently
233 identifying the timing of these brief (<1 month) events in these cores, the DIV2010 and
234 PIG2010 $\delta^{18}O$ records show mid-winter increases during many years. In contrast,
235 THW2010 does not show any mid-winter increase in $\delta^{18}O$ during polynya events,
236 although this could be due in part to the lower accumulation rate at this site (Table 1).
237 Monthly *d* variability is too high to detect a clear signal in the *d* records during polynya
238 events. Interannual correlations between all three firn-core $\delta^{18}O$ and *d* records and both
239 the TOWA and SIE time series are generally low to insignificant; the correlation between
240 THW2010 $\delta^{18}O$ and SIE yielded the only statistically significant value (r = -0.48, p <
241 0.01) (details presented in Table 4).

242 The number of months each year between the $\delta^{18}O$ and *d* maxima is presented as
243 the $\delta^{18}O$-*d* lag. There is both spatial and temporal variability in the $\delta^{18}O$-*d* lag. At
244 DIV2010, the most coastal site, the mean lag is two months, while the mean lag at
245 PIG2010 and THW2010 is three months (Fig. 6). A $\delta^{18}O$-*d* lag shift is defined as a rapid
246 increase in the number of months between $\delta^{18}O$ and *d* maxima, generally preceded and
247 followed by consistent lags. In all three records, there are significant $\delta^{18}O$-*d* lag shifts.
248 At DIV2010, the largest shift in $\delta^{18}O$-*d* lag (4 months) occurs in 1997/98; at PIG2010,
249 there are large shifts in 1988/89 and 1997/98; at THW2010, shifts in the $\delta^{18}O$-*d* lag occur
250 during 1988 and 1992 (Fig. 7).

251

252 *3.2 Site-specific temperature calibrations*

253 We first derive site-specific temperature-isotope gradients by evaluating the
254 relationship between our mean annual $\delta^{18}O$ records and mean annual temperature in three
255 independent surface temperature reconstructions from ERA-Interim, Byrd, and
256 RACMO2. Temperature-isotope gradients for DIV2010, PIG2010, and THW2010 of
257 0.68, 0.35, and 0.36 ‰/°C, respectively, were obtained using ERA-Interim temperatures.
258 Temperature-isotope gradients based on the Byrd temperature record were substantially
259 lower, yielding 0.22, 0.43, and 0.26 ‰/°C. Temperature-isotope gradients of 0.10, 0.17,
260 and 0.39 ‰/°C were obtained using RACMO2 temperatures. While the $\delta^{18}O$-ERA-
261 Interim temperature gradient at DIV2010 is comparable to what has been found at other
262 West Antarctic and full continent isotope-temperature gradients (0.6-0.8 ‰/°C) [*Masson*
263 *et al.*, 2000], all the other gradients are significantly lower (~0.3 ‰/°C).
264 Given that these site-specific calibrations do not enable us to derive realistic $\delta^{18}O$-
265 temperature slopes, we next evaluate an alternative method. We applied the commonly
266 used Antarctic $\delta^{18}O$-temperature slope of 0.8 ‰/°C [*Masson et al.*, 2000; *Masson-*
267 *Delmotte*, 2008], following the recent work of others in West Antarctica [e.g., *Fegyveresi*
268 *et al.*, 2011], to calculate mean annual temperature from our isotope records. We
269 determined intercepts by removing the mean ERA-Interim, Byrd, and RACMO2
270 temperatures over the 1979–2010 study period from the annual $\delta^{18}O$-derived temperature
271 records. Applying the commonly used Antarctic $\delta^{18}O$-temperature slope of 0.8 ‰/°C
272 results in reasonable temperature profiles at all three sites (both absolute values and
273 magnitude of interannual temperature variability; Fig. 3).
274 We next compared these $\delta^{18}O$-derived temperature records and the stacked
275 temperature record to available site-specific mean annual surface temperatures from

276 ERA-Interim, RACMO2, and Byrd over the 1979–2010 study period (Fig. 3). Across the
277 three sites, no one method out-performs the others. At DIV2010, ERA-Interim best
278 captures the absolute $\delta^{18}O$-derived temperature, as well as the amplitude of interannual
279 temperature variability (Table 2, Fig. 3); both Byrd and RACMO2 underestimate
280 temperatures (by 5.8°C and 4.4°C, respectively). At PIG2010, the Byrd temperature
281 reconstruction best captures the absolute $\delta^{18}O$-derived temperature, as well as the
282 amplitude of interannual temperature variability specifically prior to 1996 (Table 2, Fig.
283 3); neither ERA-Interim nor RACMO2 are significantly correlated. The amplitude of
284 interannual temperature variability is significantly underestimated by ERA-Interim (Fig.
285 3), and RACMO2 underestimates temperatures at PIG2010 by 4.6°C. The stacked
286 temperature record is most strongly correlated with the PIG2010 temperature record (r =
287 0.8); the aforementioned results for PIG2010 are therefore the same for the stacked
288 record. At THW2010, the ERA-Interim, Byrd, and RACMO2 temperature records are all
289 significantly correlated with $\delta^{18}O$-derived temperature; RACMO2 best captures the
290 absolute $\delta^{18}O$-derived temperature, although it still underestimates by 3.5°C (Table 2,
291 Fig. 3). The correlation between annual mean temperature at Byrd and the annual mean
292 temperature at the grid cell containing THW2010 (based on ERA-Interim 2-m
293 temperature) is r ~ 0.8 [*Bromwich et al.*, 2012], the highest correlation of the three sites
294 despite THW2010 being 335 km away from Byrd and 520 m higher.

295 Annual mean trends vary from site to site. The annual mean temperature trend
296 during the past 30 years at PIG2010 and THW2010 is +0.1°C/decade (Fig. 4), which is
297 the same as the decadal trend averaged over Antarctica from 1960–2010 [*Schneider et*
298 *al.*, 2011]. In contrast, the annual mean trend during the past 30 years at DIV2010 is -

299 0.1°C/decade (Fig. 4). There is no annual mean trend during the past 30 years in the
300 stacked record (linear fit slope = 0.0) in contrast to another stacked WAIS record over
301 this period which has a decadal trend of +0.1°C/decade for West Antarctica [*Steig et al.*,
302 2009]. Over the last 10 years (2000–2010), the temperature trends at DIV2010,
303 PIG2010, and THW2010 have been -0.3, 0.0, and -2.7°C/decade, respectively. Mean
304 $\delta^{18}O$-derived temperatures over the length of the records are similar at PIG2010 and
305 THW2010 (-26.0°C and -26.8°C, respectively), and are significantly warmer at DIV2010
306 (-20.7°C).
307
308 *3.3 Air-mass back-trajectory analyses*
309 In this subsection we present a series of back-trajectory analyses for times of
310 interest. First, we investigate times of maximum and minimum *d* for each year. Next, we
311 investigate seasonal results by selecting a single year that best represents mean
312 precipitation at each site. Finally, we investigate back-trajectory results during
313 contrasting polynya and non-polynya winters.
314 During the time of maximum *d* (fall), we find that the Amundsen-Bellingshausen
315 Sea is the predominant (>60%) moisture source region to all three sites, followed by
316 Weddell (<30%) and Ross Sea (<15%) inputs (Table 3). Site-specific back-trajectories
317 (Figs. 8–10) also suggest there may be different moisture sources within each of these
318 seas during this time. At DIV2010, the main cluster of back-trajectories in the
319 Amundsen-Bellingshausen Sea lies between 60-70°S, specifically in the sea-ice zone of
320 the Amundsen Sea; Weddell Sea inputs are largely along the Antarctic Peninsula and
321 within the sea-ice zone; Ross Sea inputs are largely between 140-180°W (Fig. 8; Table

3). At PIG2010, the Amundsen-Bellingshausen Sea inputs are spread more widely across the basin than at DIV2010, from the coast to ~50°S; the Weddell Sea inputs are similar to DIV2010, falling largely along the Antarctic Peninsula and within the Weddell Sea sea-ice zone (south of 70°S); there are no Ross Sea inputs in fall (Fig. 9; Table 3). At THW2010, the main cluster of back-trajectories in the Amundsen-Bellingshausen Sea spans the basin, between the coast and 55°S, similar to PIG2010; the Weddell and Ross Seas are shown to be secondary moisture source regions in fall, with Weddell Sea and Ross Sea inputs south of 70°S similar to DIV2010 and PIG2010 (Fig. 10; Table 3).

During the time of minimum *d* (spring), the Amundsen-Bellingshausen Sea is still the predominant (>50%) moisture source region to all sites, but there is an increase in Ross Sea inputs when compared with the fall (Table 3). Site-specific findings also exist during the spring. At DIV2010, the back-trajectories in the Amundsen-Bellingshausen Sea cluster largely between 50-70°S (Fig. 8), showing a northward shift in moisture source region when compared with the fall back-trajectories. At PIG2010, the inputs from the Amundsen-Bellingshausen Sea cluster largely between 80-120°W, showing a shift toward the central Amundsen Sea and Pine Island Bay in moisture source region when compared with the fall back-trajectories; the inputs from the Weddell Sea cluster largely in the central Weddell Sea, with a loss of input from regions along the Antarctic Peninsula; the inputs from the Ross Sea are predominantly in the sea-ice zone south of 70°S (Fig. 9). At THW2010, the inputs from the Amundsen-Bellingshausen Sea cluster largely in the eastern half of the basin (east of 100°W), showing an eastward shift in moisture source region when compared with the fall back-trajectories; Ross Sea inputs remain predominantly south of 70°S, similar to PIG2010 (Fig. 10).

345 The monthly runs for years of representative mean precipitation show the same
346 general shift at all sites from largely Amundsen-Bellingshausen and Weddell Sea
347 moisture source regions in summer/fall to Amundsen-Bellingshausen and Ross Sea
348 moisture source regions in winter/spring (Fig. 11; Table 3). There is, however, seasonal
349 site-specific variability in moisture source regions. Specifically, DIV2010 and PIG2010
350 show Amundsen-Bellingshausen and Weddell Sea moisture source regions in winter,
351 with a shift from the Weddell Sea input to a Ross Sea input in spring (Fig. 11). In
352 summer, the Amundsen-Bellingshausen Sea is the only moisture source region to both
353 sites, and the shift into fall adds the Weddell Sea as a moisture source region (Fig. 11).
354 Seasonal moisture source regions to THW2010 are distinct from the other two sites. In
355 winter, the Amundsen-Bellingshausen and Ross Seas are moisture source regions, and in
356 spring the Weddell is additionally a moisture source region to THW2010. In both
357 summer and fall, the Amundsen-Bellingshausen Sea is the only moisture source region to
358 THW2010.

359 Finally, we present results in which 3-day back-trajectories were run for the three
360 months over the 1979–2010 period that had the largest wintertime polynya events in the
361 Amundsen Sea and Pine Island Bay polynyas (August 2002, July 2005, June 2007), and
362 the three months that had the smallest or no wintertime polynya events (July 2008, July
363 2009, July 2010) [*Criscitiello et al.*, 2013]. The three back-trajectories at DIV2010
364 associated with polynya events have moisture source locations in the Amundsen Sea, and
365 all show back-trajectories that pass over the Amundsen Sea and/or Pine Island Bay
366 polynyas (Figs. 12A-C). The back-trajectories at DIV2010 associated with winters
367 lacking polynya events vary in moisture source location from the eastern Amundsen-

368 Bellingshausen Sea near the Antarctic Peninsula, the Weddell Sea, and the Ross Sea
369 (Figs. 12D-F). Two of the three back-trajectories at PIG2010 associated with polynya
370 events, similar to DIV2010, have moisture source locations in the Amundsen Sea, and
371 show back-trajectories that pass over the Amundsen Sea and/or Pine Island Bay polynyas
372 (Fig. 12A and 12B). The third back-trajectory (Fig. 12C) travels over the continent
373 interior from East Antarctica before reaching PIG2010. The back-trajectories at PIG2010
374 associated with winters lacking polynya events vary in moisture source location from the
375 eastern Amundsen-Bellingshausen Sea near the Antarctic Peninsula, the Weddell Sea,
376 and East Antarctica (Fig. 12D-F). Unlike the other two sites, the back-trajectories at
377 THW2010 associated with polynya events have moisture source locations in the western
378 Amundsen-Bellingshausen and Ross Seas, and do not pass over the polynya regions
379 (Figs. 12A-C). The back-trajectories at THW2010 associated with winters lacking
380 polynya events all have moisture source locations originating in the Ross Sea (Figs. 12D-
381 F).
382
383 *3.4 Global atmospheric anomalies*
384 Regressions of global SST on $\delta^{18}O$ reveal negative SST anomalies in the eastern
385 equatorial Pacific at all sites (Fig. 13). The largest cooling signature in the eastern
386 tropical Pacific is seen at PIG2010 (the site farthest inland); the weakest regressions in
387 the eastern tropical Pacific are seen with THW2010 (the highest elevation site; Fig. 13).
388 Such SST anomalies in the eastern tropical Pacific are in agreement with the initiation
389 and propagation of a Rossby wave train [*Hoskins and Karoly*, 1981; *Zhang et al.*, 1997]
390 as revealed by the SLP and 500 hPa GH analyses described below.

391 Regressions of SLP and 500 hPa GH on $\delta^{18}O$ at all sites reveal a low pressure
392 anomaly off the western Antarctic Peninsula, which alternates with a high pressure
393 anomaly in the central south Pacific and a low pressure anomaly in the western south
394 Pacific (Fig. 13). The alternating low and high pressure anomalies at both the surface as
395 well as throughout the atmospheric column confirm a barotropic response of the
396 atmosphere connecting the western tropical Pacific with the Antarctic Peninsula
397 [*Trenberth et al.*, 1998]. These global regressions of atmospheric variables on firn-core
398 $\delta^{18}O$ suggest, at all sites, a strong teleconnection between the tropical Pacific and
399 Antarctic via a Rossby wave train [e.g., *Ding et al.*, 2011].
400
401 **4. Discussion**
402 *4.1 Local influence on $\delta^{18}O$ and d*
403 Local variables (topography, elevation) influence our $\delta^{18}O$ and *d* records. While
404 moisture source and other variables can have an impact on isotope records, one of the
405 primary factors controlling the spatial distribution of Antarctic *d* is elevation [*Masson-*
406 *Delmotte*, 2008]. Our results show that DIV2010 and PIG2010 have both similar firn-
407 core temperatures (Fig. 14) and *d* records (Fig. 4), while the THW2010 firn-core
408 temperatures and *d* record are distinct from the other two sites. Additionally, the seasonal
409 back-trajectory analyses suggest that seasonal moisture source regions to THW2010 are
410 distinct from the other two sites (Figs. 10–11). The polynya results also indicate that
411 moisture source regions to THW2010 during wintertime polynya events are different
412 from the other two sites (Fig. 12). Together, these results indicate that the THW2010 *d*
413 record may be distinct from the other two sites as a result of its high elevation. *d* is

414 expected to increase inland as the temperature of condensation within clouds decreases
415 and the net kinetic fractionation increases [*Jouzel et al.*, 1987], as shown in model
416 simulations [*Noone and Simmonds*, 2004]. If distance from the coast had a stronger
417 control than elevation on the spatial distribution of *d* among our sites, we would expect
418 DIV2010 to have the lowest *d* values, and THW2010 and PIG2010 to have higher *d*
419 values comparable to one another (since PIG2010 and THW2010 are comparable
420 distances from the coast; Table 1). As this is not the case, our results point toward
421 elevation effects most strongly influencing the THW2010 *d* record. The similarity of
422 DIV2010 and PIG2010 *d* records especially in winter (Fig. 4) also indicates similar
423 moisture source regions to these two sites, confirmed by the back-trajectory results that
424 show THW2010 to have distinct moisture source regions from the other two sites,
425 particularly in winter (Fig. 12).

426 The influence of local variables such as topography and elevation ultimately
427 impacts the site-specific $\delta^{18}O$-derived temperature reconstructions. Our results show that
428 the strongest correlation to the firn-core $\delta^{18}O$-derived temperature record at DIV2010 is
429 with ERA-Interim, at PIG2010 is with the Byrd temperature reconstruction [*Bromwich et*
430 *al.*, 2012], and at THW2010 is with RACMO2 [*Lenaerts et al.*, 2012]. The inability of
431 the Byrd temperature reconstruction to robustly capture temperature variability at
432 DIV2010 is expected, as the DIV2010 core site is ~525 km from Byrd, only 180 km from
433 the coast, and ~200 m lower in elevation than Byrd. Additionally, a spatial correlation
434 map of annual mean temperature at Byrd and annual mean temperature at the grid cell
435 containing DIV2010 (based on ERA-Interim 2-m temperature) is $r \sim 0.6$ (the lowest
436 correlation of the three core sites) [*Bromwich et al.*, 2012]. While PIG2010 is the site

437 farthest from Byrd (540 km), it is the closest in elevation to Byrd (90 m higher), perhaps
438 accounting for the significant correlation between these two temperature time series.
439 This result highlights the importance of the isotopic altitude effect which results in -
440 0.2‰/100m [*Ambach et al.*, 1968], and should therefore result in a temperature
441 underestimation at PIG2010 of less than 0.2°C. The lack of correlation between
442 DIV2010 and THW2010 temperature records and the Byrd temperature reconstruction is
443 expected, as the spatial correlation map between Byrd temperature and West Antarctic
444 temperatures based on ERA-Interim shows stronger correlations near the Ross sector, and
445 weaker correlations in the Pine Island sector [*Bromwich et al.*, 2012].

446 Comparison of the $\delta^{18}O$-derived temperature records at the three core sites reveals
447 similar values in the PIG2010 and THW2010 $\delta^{18}O$ records (Fig. 4, Table 1). This is
448 consistent with ERA-Interim and RACMO2 temperature results that show comparable
449 mean temperatures between PIG2010 and THW2010 over the 1979–2010 study period
450 (mean temperatures at the two sites are within 0.7°C for ERA-Interim and 0.4°C for
451 RACMO2). In comparison, DIV2010 mean temperatures over the same period of study
452 are 5-6°C warmer than both PIG2010 and THW2010 (using ERA-Interim and RACMO2
453 temperatures). This is not, however, consistent with core temperatures measured in the
454 field, which show (for the overlapping upper 56 m of each core) DIV2010 and PIG2010
455 mean core temperatures within 2°C, and THW2010 mean core temperatures significantly
456 colder (7.5-9.5°C colder than the other two sites; Fig. 14). THW2010 is ~420 m higher
457 in elevation than PIG2010 (Table 1); the isotopic altitude effect [*Ambach et al.*, 1968]
458 previously discussed may account for the similar $\delta^{18}O$ values at these two sites despite
459 THW2010 firn-core temperatures being significantly colder (Fig. 14). While PIG2010 is

460 located closer to the Weddell sector and THW2010 is located closer to the Ross sector,
461 elevation profiles drawn from each site to the coast show a similar range in elevation
462 values. The existence of continental topography has a strong impact on the transport of
463 moist air over the ice sheet and, ultimately, the $\delta^{18}O$ signal [*Noone and Simmonds*, 2002],
464 so the similarity in elevation range between the two sites and the coastline may also
465 contribute to their similar $\delta^{18}O$ values. Additionally, the DIV2010 $\delta^{18}O$ values are likely
466 higher as a result of it being closest to the coast and Pine Island Bay, and most strongly
467 influenced by local dynamics such as polynya variability [*Criscitiello et al.*, 2013b].
468
469 *4.2 Regional influence on $\delta^{18}O$ and d*
470 Regional influences on $\delta^{18}O$ and *d* records include sea-ice and polynya variability,
471 as well as distance from the coast. Results from our back-trajectory analyses reveal
472 seasonal and site-to-site differences in the influence of SIC and polynya variability on
473 firn-core oxygen isotope records. Generally, the more coastal the ice-core site, the
474 stronger the dependence of the $\delta^{18}O$ and *d* records on changes in sea-ice state [*Noone and*
475 *Simmonds*, 2004]. Our results show that the back-trajectories at DIV2010 (the most
476 coastal site) associated with polynya events have transport pathways that travel over the
477 Pine Island Bay and Amundsen Sea polynya regions (Figs. 12A-C). This supports
478 previous work suggesting that MSA and sea salts at DIV2010 are significantly correlated
479 with polynya variability [*Criscitiello et al.*, 2013]. Seasonal back-trajectory results from
480 DIV2010 are consistent with the hypothesis that glaciochemical records from this site are
481 strongly influenced by Amundsen Sea sea-ice variability, and polynya dynamics in
482 particular. Air masses approaching DIV2010 in fall originate predominantly from the

region along and offshore of the continental shelf break that experiences intense sea-ice formation in winter associated with ice edge advance (Fig. 8); as a result, this region is a source area of sea salts in fall/winter to the DIV2010 site [*Criscitiello et al.*, 2013]. Our results confirm this is a primary region of moisture source to DIV2010 in fall. The Weddell Sea moisture source regions are also largely in the sea-ice zone in fall, providing further evidence that these areas of intense sea-ice formation provide moisture to the DIV2010 site. In spring (during sea-ice breakup), there is a shift in moisture source toward the western Amundsen Sea near the Ross Sea. This region of the Amundsen Sea (centered around 120°W) is a moisture source region of sea salts to DIV2010 in spring/summer [*Criscitiello et al.*, 2013]. Additionally, the moisture source region in the Amundsen-Bellingshausen Sea shifts northward, likely related to ice-edge advance. In fall, trajectories originating in the Amundsen-Bellingshausen Sea travel in cyclonic paths, often over the Amundsen Sea or Pine Island Bay polynyas, before reaching DIV2010 (Fig. 8). The polynya results show that DIV2010 is the only site that received moisture from the polynya regions during the three largest wintertime polynya events over the 1979–2010 record (Fig. 12), confirming that this site is most strongly impacted by polynya variability.

In contrast, transport pathways to THW2010 associated with polynya events travel over the Amundsen and Ross Seas, but not over the polynya regions. Likely due to its location farther west in the Amundsen sector on Thwaites Glacier (>150 km farther from Pine Island Bay than DIV2010), as well as its relatively high elevation and distance from the coast, the THW2010 isotope record is likely the least influenced by the polynyas, and more influenced by broader Amundsen Sea sea-ice variability. This is

506 supported by previous findings, that showed the region between 80°W and 140°W, and
507 60°S and 71°S (the SIE time series) is a significant source of sea-salt aerosols to
508 THW2010 [*Criscitiello et al.*, 2013b]. Further, the THW2010 $\delta^{18}O$ record is the only
509 isotope record with a significant correlation to this SIE time series (Table 4). This further
510 supports the argument that the THW2010 isotope record is less affected by polynya
511 variability and instead is influenced by broad offshore moisture source regions largely in
512 the Amundsen Sea.

513 Back-trajectory results from PIG2010 indicate sensitivity to the seasonality of
514 SAM and sea ice, and show air-mass trajectories most similar to DIV2010. The polynya
515 results show two of three back-trajectories during wintertime polynya events passing over
516 the polynya regions, similar to DIV2010 (Fig. 12). For the cases when no polynya events
517 occurred, two of the three back-trajectories closely track those of DIV2010 (Fig. 12).
518 PIG2010 is located farthest east (farthest from the Ross sector), accounting for the fact
519 that PIG2010 revieves the smallest percentage of moisture originating from the Ross Sea
520 (Table 3). The Amundsen-Bellingshausen Sea inputs are spread across the basin, and the
521 Weddell Sea inputs are largely along the Antarctic Peninsula and within the Weddell Sea
522 sea-ice zone (south of 70°S). As at DIV2010, this indicates that moisture source regions
523 to PIG2010 in fall may be located predominantly in regions of intense sea-ice formation.
524 In spring, there is a shift toward the Ross Sea sea-ice zone as a moisture source region,
525 and (as with DIV2010) the moisture source region in the Amundsen-Bellingshausen Sea
526 shifts northward (and along generally cyclonic transport pathways), likely related to ice-
527 edge retreat. The shift toward Ross Sea moisture sources in spring is likely related to the
528 seasonality of SAM, and the position of the Amundsen Sea low (ASL). Moisture into

529 West Antarctica increases when the ASL is displaced to the west of its long-term mean
530 position [*Barry*, 1980]. An eastward shift in the ASL in spring may account for more
531 frequent incursions of air masses from the Ross sector (and less frequent incursions of air
532 masses from the Amundsen sector), as our results show.

533 Results from THW2010 also indicate sensitivity to the position of the ASL, and
534 show back-trajectories that pass over regions of intense sea-ice formation in fall. Air
535 masses approaching the site in fall originate predominantly from areas of intense sea-ice
536 formation in the Amundsen-Bellingshausen Sea, between the coast and 55°S (Fig. 10).
537 Similar to DIV2010, regions of sea-ice formation (south of 70°S) in the Weddell and
538 Ross Seas are shown to a lesser extent to be moisture source regions in fall as well. In
539 spring, back-trajectories show a shift toward the Ross Sea as a moisture source region (as
540 seen at DIV2010 and PIG2010), and a shift toward predominantly cyclonic transport
541 pathways, again likely a result of the position of the ASL as discussed above.

542 Comparison of *d* values between sites offers additional insight into the interplay
543 of local and regional influences on the oxygen isotope records. If elevation is the primary
544 control on mean *d* values, we would expect PIG2010 *d* values to be significantly lower
545 than DIV2010 *d* values, but instead they are comparable. We propose that PIG2010 *d*
546 values may be depressed as a result of ice-edge extension effects. Previous work has
547 shown the importance of local water sources when SIC is reduced [*Noone and Simmonds*,
548 2004]. Since the $\delta^{18}O$ of evaporating ocean water is less depleted than the air advected
549 from farther north, reduced SIC allows local air to become relatively enriched. Exposure
550 to a cold ocean, then, would lower *d*. Similarly, sea ice-edge extension may lower *d*
551 values because of the greater contribution from kinetic effects along the distilling

552 transport path [*Noone and Simmonds*, 2004]. The back-trajectory results do show
553 moisture source regions largely within the sea-ice zone for PIG2010. This sea ice-edge
554 extension effect in particular, then, may contribute to depression of *d* values at PIG2010
555 from expected values if based solely on site elevation or distance from the coast. As
556 discussed previously in this section, the THW2010 *d* values are likely distinct from the
557 other two sites as a result of its high elevation.
558
559 *4.3 Remote influence on $\delta^{18}O$ and d*
560 The spatial regressions of global reanalysis fields of SST, SLP, and 500 hPa GH
561 on $\delta^{18}O$ are in agreement with a tropical Pacific influence on West Antarctic isotope
562 records via a Rossby wave train (Fig. 13). All sites reveal anomalous cooling in the
563 eastern tropical Pacific, and alternating low and high pressure anomalies both at the
564 surface as well as throughout the atmospheric column connecting the western tropical
565 Pacific with West Antarctica (Fig. 13). The HySPLIT back-trajectory results, which
566 generally show cyclonic air mass trajectories that are consistent with a pressure low over
567 the Antarctic Peninsula (Figs. 8-10), also suggest that atmospheric circulation is the
568 dominant factor affecting isotope concentrations at the three core sites. In agreement,
569 West Antarctic isotope records from cores collected during the International Trans-
570 Antarctic Scientific Expedition (ITASE) located on or west of the WAIS divide show
571 strong relationships in austral fall to pressure anomalies over West Antarctica, SIC in the
572 Ross and Amundsen Seas, and local temperatures [*Küttel et al.*, 2012]. These
573 correlations were attributed to pronounced meridional circulation that impacts sea-ice
574 variability in the Southern Ocean as well as local and regional temperatures [*Küttel et al.*,

575 2012]. Others have also shown that the seasonal isotopic cycle in the ITASE cores is
576 highly correlated with the local seasonal temperature cycle (minima in austral winter)
577 [*Schneider et al.*, 2005].

578 Variations in the $\delta^{18}O$-*d* lag confirm that major changes in interannual
579 atmospheric circulation over the 1979–2010 time period affect the oxygen isotope
580 records at our core sites. While some have found that *d* near the coast of Antarctica
581 varies in phase with $\delta^{18}O$ [e.g., *Ciais et al.*, 1995], others have found that *d* inland lags
582 $\delta^{18}O$ by ~4-6 months [e.g., *Delmotte et al.*, 2000]. There are many factors that can result
583 in a time lag between $\delta^{18}O$ and *d* in an ice core, including changes in precipitation
584 moisture source which are linked to systematic changes in atmospheric circulation
585 [*Schlosser et al.*, 2008]. A sudden temporal shift in the $\delta^{18}O$-*d* phase difference can be
586 generally interpreted as a change in atmospheric circulation, as atmospheric circulation
587 changes mean changes in moisture source and transport paths [*Schlosser et al.*, 2008].

588 Our results at all sites show shifts in the $\delta^{18}O$-*d* lag concurrent with shifts in large-
589 scale atmospheric circulation, in particular shifts from strong El Niño conditions to La
590 Niña conditions, or visa versa (Fig 7). At DIV2010, the largest shift in $\delta^{18}O$-*d* lag occurs
591 in 1997/98, concurrent with one of the strongest El Niño events over the length of our
592 records (Fig. 7). At PIG2010, the $\delta^{18}O$-*d* lag shifts are contemporaneous with a strong La
593 Niña (1988/89) and a strong El Niño (1997/98; Fig. 7). At THW2010, the largest $\delta^{18}O$-*d*
594 lag shifts occur during a strong La Niña (1988) and a strong El Niño (1992; Fig. 7).
595 These results suggest that major changes in interannual atmospheric circulation over the
596 1979–2010 time period affect the $\delta^{18}O$-*d* lag at our core sites.

597 Interestingly, the large 1982/83 El Niño does not show up in the $\delta^{18}O$-*d* lag
598 records. The phasing of this particular El Niño may have resulted in a weak
599 teleonnection with southern high latitudes. The 1982/83 El Niño peaked in austral
600 summer [*Karnauskas*, 2013], when the impact of ENSO on southern hemisphere
601 atmospheric circulation is generally weakest. In contrast, the 1997/98 El Niño (which
602 does show up in the $\delta^{18}O$-*d* lag records) developed in the austral winter [*Karnauskas*,
603 2013] when the telelconnection between the tropics and high southern latitudes is
604 strongest. This suggests that the timing of an El Niño event may determine the strength
605 of the teleconnection between the tropics and high southern latitudes.
606
607 **5. Conclusions**
608 This study provides a first assessment of three new stable isotope records from
609 West Antarctica, and focuses on relationships between $\delta^{18}O$ and *d* and: local temperature;
610 regional SIC; local polynya variability; and remote tropical Pacific forcing. We also use
611 back-trajectory analyses to provide additional insight into seasonal moisture source
612 regions to West Antarctica. Furthermore, by using an array of cores along the Amundsen
613 Coast, we are able to investigate the spatial variability in these relationships. Our most
614 significant findings are that: (1) the DIV2010 $\delta^{18}O$ record exhibits temporal patterns in
615 moisture source location distinct from the other two sites because it is closest to the coast
616 and Pine Island Bay, and is most strongly influenced by local dynamics such as polynya
617 variability, (2) sea ice-edge extension effects may contribute to depression of *d* values at
618 PIG2010 from expected values when based solely on site elevation or distance from the
619 coast, (3) THW2010 firn-core temperatures and *d* values are distinct from the other two

620 sites, owing largely to its higher elevation; the THW2010 isotope record is least affected
621 by polynya variability, and instead is strongly influenced by broad offshore moisture
622 source regions largely in the Amundsen Sea, (4) back-trajectories at all three sites show a
623 shift from predominantly Amundsen-Bellingshausen Sea moisture source regions in
624 spring toward Ross Sea moisture source regions in fall, concurrent with a shift toward
625 predominantly cyclonic transport pathways which is likely a result of the position of the
626 ASL, and (5) the source and transport of the isotopic signal to all sites, and ultimately
627 local winds, are remotely influenced by the tropical Pacific via large-scale atmospheric
628 teleconnections propagating through the extratropics. Major changes in interannual
629 atmospheric circulation over the 1979–2010 time period affect the δ^{18}O-*d* lag at our core
630 sites, and suggest that the δ^{18}O-*d* lag in future down-core work may be useful in
631 diagnosing the onset of major shifts in atmospheric circulation.
632
633 **Acknowledgements**
634 Thanks to Lou Albershardt, Howard Conway, and RPSC support staff for
635 assistance in the field. Thanks to Luke Trusel, Twila Moon, and NICL staff for assistance
636 processing the cores, and DRI staff for continuous melter analyses. This research was
637 supported by an award from the Department of Energy Office of Science Graduate
638 Fellowship Program (DOE SCGF) to ASC, and by grants from NSF-OPP (#ANT-
639 0632031 & #ANT-0631973); NSF-MRI (#EAR-1126217).
640
641 **References**
642 Abram, N. J., R. Mulvaney, and C. Arrowsmith (2011), Environmental signals in a highly
643 resolved ice core from James Ross Island, Antarctica, J. Geophys. Res.,
644 116(D20), D20116.

645 Ambach, W., W. Dansgaard, H. Eisner, and J. Møller (1968), The altitude effect on the
646 isotopic composition of precipitation and glacier ice in the Alps, Tellus, 20(4),
647 595-600.
648 Arrigo, K. R., and G. L. van Dijken (2003), Phytoplankton dynamics within 37 Antarctic
649 coastal polynya systems, J. Geophys. Res., 108(C8), 3271.
650 Barry, R. (1980), Synoptic and dynamic climatology, Progress in Physical geography,
651 4(1), 88-96.
652 Bracegirdle, T. J., and G. J. Marshall (2012), The reliability of Antarctic tropospheric
653 pressure and temperature in the latest global reanalyses, Journal of Climate,
654 25(20), 7138-7146.
655 Bromwich, D. H., and C. J. Weaver (1983), Latitudinal displacement from main moisture
656 source controls δ18O of snow in coastal Antarctica, Nature, 301(5896), 145-147.
657 Bromwich, D. H., J. P. Nicolas, A. J. Monaghan, M. A. Lazzara, L. M. Keller, G. A.
658 Weidner, and A. B. Wilson (2012), Central West Antarctica among the most
659 rapidly warming regions on Earth, Nature Geosci, 6, 139-145.
660 Ciais, P., J. W. C. White, J. Jouzel, and J. R. Petit (1995), The origin of present-day
661 Antarctic precipitation from surface snow deuterium excess data, J. Geophys.
662 Res., 100(D9), 18917-18927.
663 Craig, H. (1961), Isotopic variations in meteoric waters, Science, 133(3465), 1702-1703.
664 Criscitiello, A. S., S. B. Das, M. J. Evans, K. E. Frey, H. Conway, I. Joughin, B. Medley,
665 and E. J. Steig (2013), Ice sheet record of recent sea-ice behavior and polynya
666 variability in the Amundsen Sea, West Antarctica, Journal of Geophysical
667 Research: Oceans, 118(1), 118-130.
668 Criscitiello, A.S., S. B. Das, K. Karnauskas, M. J. Evans, K. E. Frey, I. Joughin, E. Steig,
669 J. McConnell, and B. Medley (2013b), Tropical Pacific influence on source and
670 transport of marine aerosols to West Antarctica, J. Clim., in press.
671 Dansgaard, W. (1964), Stable isotopes in precipitation, Tellus, 16(4), 436-468.
672 Dee, D. P., et al. (2011), The ERA-Interim reanalysis: configuration and performance of
673 the data assimilation system, Quarterly Journal of the Royal Meteorological
674 Society, 137(656), 553-597.
675 Delmotte, M., V. Masson, J. Jouzel, and V. I. Morgan (2000), A seasonal deuterium
676 excess signal at Law Dome, coastal eastern Antarctica: A Southern Ocean
677 signature, J. Geophys. Res., 105(D6), 7187-7197.
678 Ding, Q., E. J. Steig, D. S. Battisti, and M. Kuttel (2011), Winter warming in West
679 Antarctica caused by central tropical Pacific warming, Nature Geosci, 4(6), 398-
680 403.
681 Ding, Q., E. J. Steig, D. S. Battisti, and J. M. Wallace (2012), Influence of the tropics on
682 the Southern Annular Mode, Journal of Climate, 25(18), 6330-6348.
683 Divine, D., E. Isaksson, T. Martma, H. A. J. Meijer, J. Moore, V. Pohjola, R. S. W. van
684 de Wal, and F. Godtliebsen (2011), Thousand years of winter surface air
685 temperature variations in Svalbard and northern Norway reconstructed from ice
686 core data.
687 Divine, D. V., E. Isaksson, M. Kaczmarska, F. Godtliebsen, H. Oerter, E. Schlosser, S. J.
688 Johnsen, M. van den Broeke, and R. S. W. van de Wal (2009), Tropical Pacific–
689 high latitude south Atlantic teleconnections as seen in δ18O variability in

690 Antarctic coastal ice cores, Journal of Geophysical Research: Atmospheres,
691 114(D11).
692 Dixon, D., P. A. Mayewski, S. Kaspari, S. B. Sneed, and M. J. Handley (2004), A 200
693 year sub-annual record of sulfate in West Antarctica, from 16 ice cores, Annals of
694 Glaciology, 39, 545-556.
695 Dixon, D. A., P. A. Mayewski, I. D. Goodwin, G. J. Marshall, R. Freeman, K. A.
696 Maasch, and S. B. Sneed (2012), An ice-core proxy for northerly air mass
697 incursions into West Antarctica, International Journal of Climatology, 32(10),
698 1455-1465.
699 Draxler, R., and G. Rolph (2003), HYSPLIT (HYbrid Single-Particle Lagrangian
700 Integrated Trajectory) model, NOAA Air Resources Laboratory, Silver Spring,
701 MD.
702 Fegyveresi, J. M., R. B. Alley, M. K. Spencer, J. J. Fitzpatrick, E. J. Steig, J. W. C.
703 White, J. R. McConnell, and K. C. Taylor (2011), Late-Holocene climate
704 evolution at the WAIS Divide site, West Antarctica: bubble number-density
705 estimates, Journal of Glaciology, 57(204), 629-638.
706 Gregory, S., and D. Noone (2008), Variability in the teleconnection between the El Niño–
707 Southern Oscillation and West Antarctic climate deduced from West Antarctic ice
708 core isotope records, Journal of Geophysical Research: Atmospheres, 113(D17).
709 Hoskins, B. J., and D. J. Karoly (1981), The steady linear response of a spherical
710 atmosphere to thermal and orographic forcing, Journal of the Atmospheric
711 Sciences, 38(6), 1179-1196.
712 Joughin, I., E. Rignot, C. E. Rosanova, B. K. Lucchitta, and J. Bohlander (2003), Timing
713 of recent accelerations of Pine Island Glacier, Antarctica, Geophys. Res. Lett.,
714 30(13), 1706.
715 Jouzel, J., G. L. Russell, R. J. Suozzo, R. D. Koster, J. W. C. White, and W. S. Broecker
716 (1987), Simulations of the HDO and H218O atmospheric cycles using the NASA
717 GISS general circulation model: The seasonal cycle for present-day conditions,
718 Journal of Geophysical Research: Atmospheres, 92(D12), 14739-14760.
719 Kalnay, E., et al. (1996), The NCEP/NCAR 40-Year Reanalysis Project, Bulletin of the
720 American Meteorological Society, 77(3), 437-471.
721 Karnauskas, K. B. (2013), Can we distinguish canonical El Niño from Modoki?,
722 Geophys. Res. Lett., 40(19), 5246-5251.
723 Kaspari, S., D. A. Dixon, S. B. Sneed, and M. J. Handley (2005), Sources and transport
724 pathways of marine aerosol species into West Antarctica, Annals of Glaciology,
725 41(1), 1-9.
726 Kavanaugh, J. L., and K. M. Cuffey (2003), Space and time variation of d18O and dD in
727 Antarctic precipitation revisited, Global Biogeochem. Cycles, 17(1), 1017.
728 Küttel, M., E. Steig, Q. Ding, A. Monaghan, and D. Battisti (2012), Seasonal climate
729 information preserved in West Antarctic ice core water isotopes: relationships to
730 temperature, large-scale circulation, and sea ice, Climate Dynamics, 39(7-8),
731 1841-1857.
732 Lenaerts, J. T. M., M. R. van den Broeke, W. J. van de Berg, E. van Meijgaard, and P.
733 Kuipers Munneke (2012), A new, high-resolution surface mass balance map of
734 Antarctica (1979-2010) based on regional atmospheric climate modeling,
735 Geophys. Res. Lett., 39(4), L04501.

736 Markle, B. R., N. A. N. Bertler, K. E. Sinclair, and S. B. Sneed (2012), Synoptic
737 variability in the Ross Sea region, Antarctica, as seen from back-trajectory
738 modeling and ice core analysis, J. Geophys. Res., 117(D2), D02113.
739 Maselli, O., D. Fritzche, L. Layman, J. McConnell, and H. Meyer (2013), Comparison of
740 water isotope ratio determinations using two cavity ring-down instruments and
741 classical mass spectrometry in continuous ice-core analysis, Isotopes in
742 Environmental and Health Studies, in press.
743 Masson, V., et al. (2000), Holocene Climate Variability in Antarctica Based on 11 Ice-
744 Core Isotopic Records, Quaternary Research, 54(3), 348-358.
745 Masson-Delmotte, V. (2008), A review of Antarctic surface snow isotopic composition:
746 Observations, atmospheric circulation, and isotopic modeling, Journal of Climate,
747 21(13), 3359.
748 McConnell, J. R., G. W. Lamorey, S. W. Lambert, and K. C. Taylor (2001), Continuous
749 ice-core chemical analyses using inductively coupled plasma mass spectrometry,
750 Environmental Science & Technology, 36(1), 7-11.
751 Medley, B., et al. (2013), Airborne-radar and ice-core observations of annual snow
752 accumulation over Thwaites Glacier, West Antarctica confirm the spatiotemporal
753 variability of global and regional atmospheric models, Geophysical research
754 letters, 40(14), 3649-3654.
755 Merlivat, L., and J. Jouzel (1979), Global climatic interpretation of the deuterium-
756 oxygen18 relationship for precipitation, J. Geophys. Res., 84(C8), 5029-5033.
757 Nicolas, J. P., and D. H. Bromwich (2011), Climate of West Antarctica and influence of
758 marine air intrusions, Journal of Climate, 24(1), 49-67.
759 Noone, D., and I. Simmonds (2002), Annular variations in moisture transport
760 mechanisms and the abundance of δ18O in Antarctic snow, Journal of
761 Geophysical Research: Atmospheres, 107(D24), 4742.
762 Noone, D., and I. Simmonds (2002), Associations between δ18O of water and climate
763 parameters in a simulation of atmospheric circulation for 1979–95, Journal of
764 Climate, 15(22), 3150-3169.
765 Noone, D., and I. Simmonds (2004), Sea ice control of water isotope transport to
766 Antarctica and implications for ice core interpretation, Journal of Geophysical
767 Research: Atmospheres, 109(D7).
768 Orsi, A. J., B. D. Cornuelle, and J. P. Severinghaus (2012), Little Ice Age cold interval in
769 West Antarctica: Evidence from borehole temperature at the West Antarctic Ice
770 Sheet (WAIS) Divide, Geophysical research letters, 39(9).
771 Pasteris, D., J. McConnell, S. Das, A. Criscitiello, M. Evans, O. Maselli, M. Sigl, and L.
772 Layman (2013), Seasonal ice core records yield insight into past sea ice
773 conditions and sources of major ion species to West Antarctica, Journal of
774 Geophysical Research: Atmospheres, in review.
775 Schlosser, E. (1999), Effects of seasonal variability of accumulation on yearly mean
776 d18O values in Antarctic snow, International Glaciological Society, Cambridge,
777 ROYAUME-UNI.
778 Schlosser, E., H. Oerter, V. Masson-Delmotte, and C. Reijmer (2008), Atmospheric
779 influence on the deuterium excess signal in polar firn: Implications for ice-core
780 interpretation, Journal of Glaciology, 54, 117-124.

781 Schneider, D. P., and D. C. Noone (2007), Spatial covariance of water isotope records in
782 a global network of ice cores spanning twentieth-century climate change, Journal
783 of Geophysical Research: Atmospheres, 112(D18).
784 Schneider, D. P., and E. J. Steig (2008), Ice cores record significant 1940s Antarctic
785 warmth related to tropical climate variability, Proceedings of the National
786 Academy of Sciences, 105(34), 12154-12158.
787 Schneider, D. P., E. J. Steig, and T. Van Ommen (2005), High-resolution ice-core stable-
788 isotopic records from Antarctica: towards interannual climate reconstruction,
789 Annals of Glaciology, 41(1), 63-70.
790 Schneider, D. P., C. Deser, and Y. Okumura (2011), An assessment and interpretation of
791 the observed warming of West Antarctica in the austral spring, Climate
792 Dynamics, 38(1-2), 323-347.
793 Schneider, D. P., E. J. Steig, T. D. van Ommen, D. A. Dixon, P. A. Mayewski, J. M.
794 Jones, and C. M. Bitz (2006), Antarctic temperatures over the past two centuries
795 from ice cores, Geophys. Res. Lett., 33(16), L16707.
796 Sime, L. C., E. W. Wolff, K. I. C. Oliver, and J. C. Tindall (2009), Evidence for warmer
797 interglacials in East Antarctic ice cores, Nature, 462(7271), 342-345.
798 Sinclair, K. E., N. A. N. Bertler, and W. J. Trompetter (2010), Synoptic controls on
799 precipitation pathways and snow delivery to high-accumulation ice core sites in
800 the Ross Sea region, Antarctica, Journal of Geophysical Research: Atmospheres,
801 115(D22), D22112.
802 Stammerjohn, S. E., D. G. Martinson, R. C. Smith, X. Yuan, and D. Rind (2008), Trends
803 in Antarctic annual sea ice retreat and advance and their relation to El Niño
804 Southern Oscillation and Southern Annular Mode variability, J. Geophys. Res.,
805 113(C3), C03S90.
806 Steig, E. J., and A. J. Orsi (2013), Climate science: The heat is on in Antarctica, Nature
807 Geosci, 6(2), 87-88.
808 Steig, E. J., P. M. Grootes, and M. Stuiver (1994), Seasonal precipitation timing and ice
809 core records, Science, 266(5192), 1885-1886.
810 Steig, E. J., D. P. Schneider, S. D. Rutherford, M. E. Mann, J. C. Comiso, and D. T.
811 Shindell (2009), Warming of the Antarctic ice-sheet surface since the 1957
812 International Geophysical Year, Nature, 457(7228), 459-462.
813 Steig, E. J., et al. (2005), High-resolution ice cores from US ITASE (West Antarctica):
814 development and validation of chronologies and determination of precision and
815 accuracy, Annals of Glaciology, 41(1), 77-84.
816 Stenni, B., et al. (2010), The deuterium excess records of EPICA Dome C and Dronning
817 Maud Land ice cores (East Antarctica), Quaternary Science Reviews, 29(1–2),
818 146-159.
819 Thomas, E. R., and T. J. Bracegirdle (2009), Improving ice core interpretation using in
820 situ and reanalysis data, Journal of Geophysical Research: Atmospheres,
821 114(D20).
822 Trenberth, K. E., G. W. Branstator, D. Karoly, A. Kumar, N.-C. Lau, and C. Ropelewski
823 (1998), Progress during TOGA in understanding and modeling global
824 teleconnections associated with tropical sea surface temperatures, J. Geophys.
825 Res., 103(C7), 14291-14324.

826 Vance, T. R., T. D. van Ommen, M. A. J. Curran, C. T. Plummer, and A. D. Moy (2012),
827 A millennial proxy record of ENSO and eastern Australian rainfall from the Law
828 Dome ice core, East Antarctica, Journal of Climate(2012).
829 Zhang, Y., J. M. Wallace, and D. S. Battisti (1997), ENSO-like interdecadal variability:
830 1900–93, Journal of Climate, 10(5), 1004-1020.
831
832 **Figures**
833

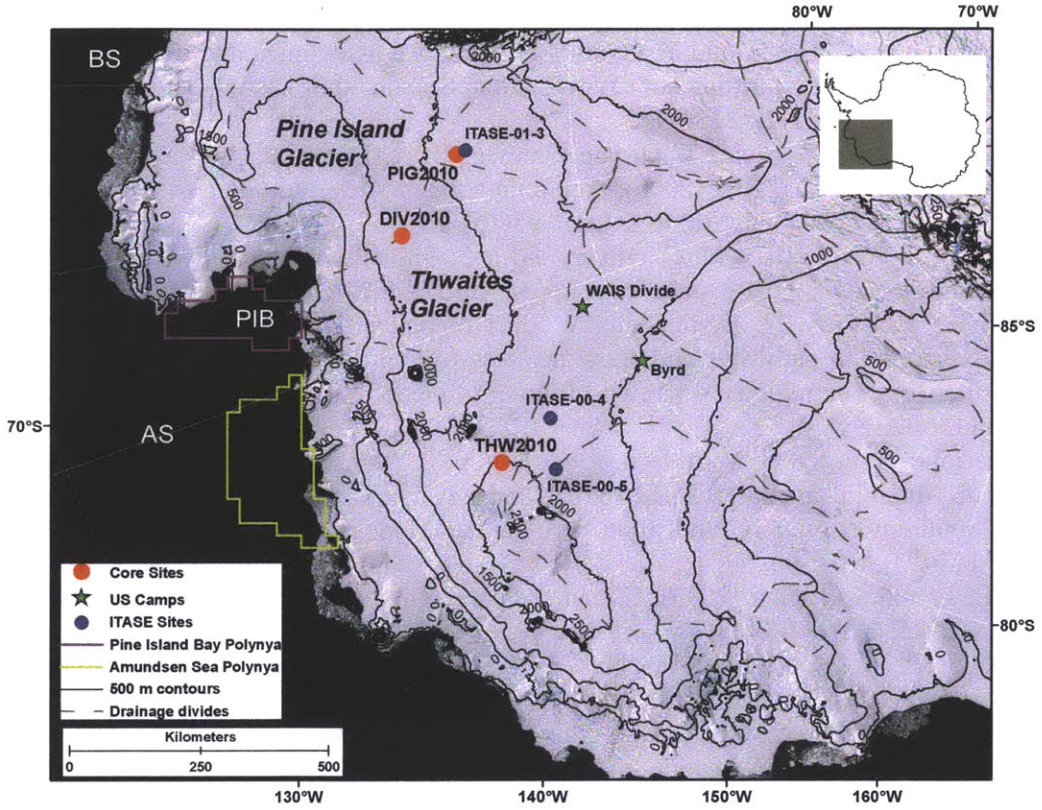

834
835 **Figure 1.** Regional setting of West Antarctica. Grey box in inset shows map location.
836 Background MODIS mosaic of Antarctica is shown with 500 m contour intervals (black
837 solid lines) and drainage divides (grey dashed lines). The DIV2010, PIG2010, and
838 THW2010 drill sites are shown (red circles), as are Byrd and WAIS Divide (green stars),
839 and relevant ITASE cores (blue circles). PIB=Pine Island Bay, AS=Amundsen Sea,
840 BS=Bellingshausen Sea. The PIB polynya mask is shown in purple, and the AS polynya
841 mask is shown in yellow (derived from SMMR- and SSM/I-based SIC).
842

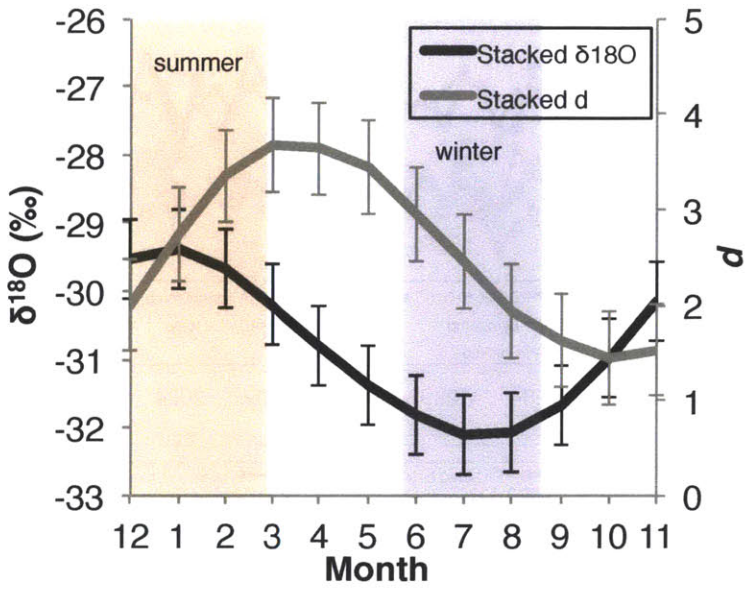

Figure 2. Seasonal cycle of $\delta^{18}O$ and d for the stacked mean monthly records (climatology averaged across the three sites). Pink shading indicates summer months, blue shading indicates winter months. Error bars indicate ±2 standard error.

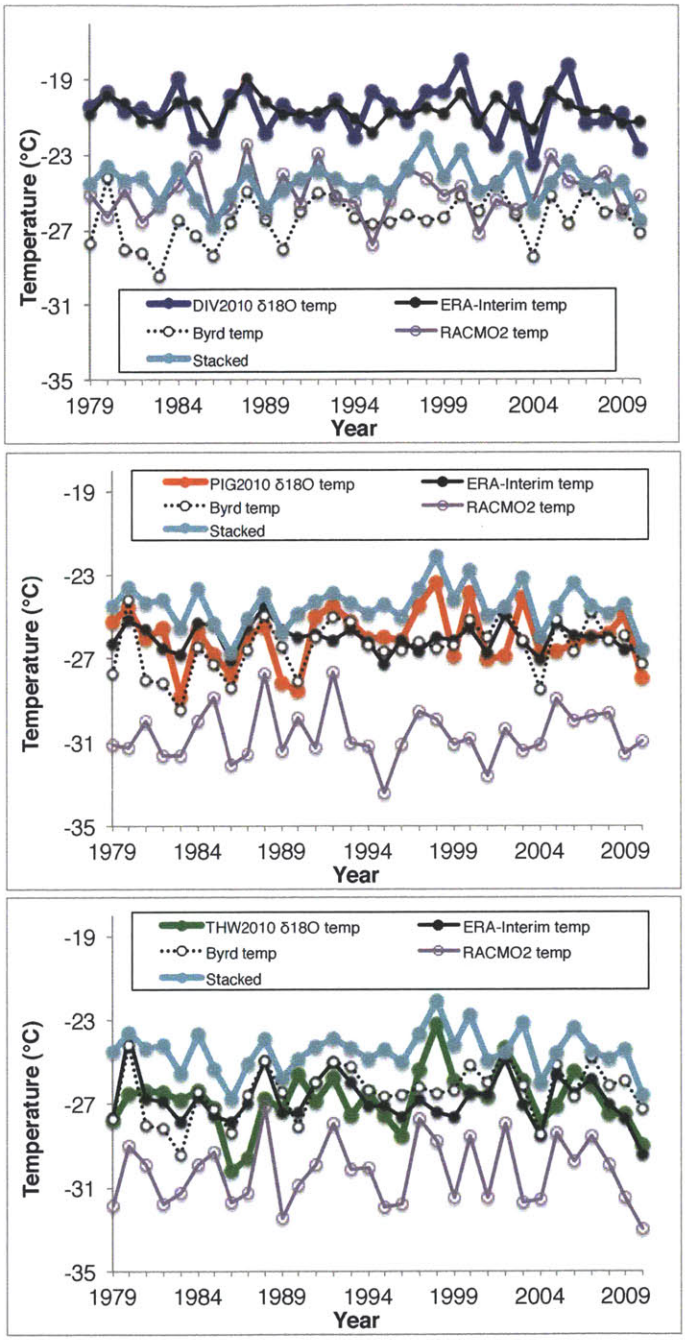

848
849 **Figure 3.** Monthly temperature reconstructions (1979–2010) at (A) DIV2010, (B)
850 PIG2010, and (C) THW2010. $\delta^{18}O$-derived temperatures (bright blue, red, and green,
851 respectively) are based on a temperature slope of 0.8 ‰/°C, and are shown with the
852 stacked temperature record (aqua), Byrd temperature reconstruction (black dashed),
853 ERA-Interim temperature (black solid), and RACMO2 temperature (light purple solid)
854 interpolated to each ice-core location.
855

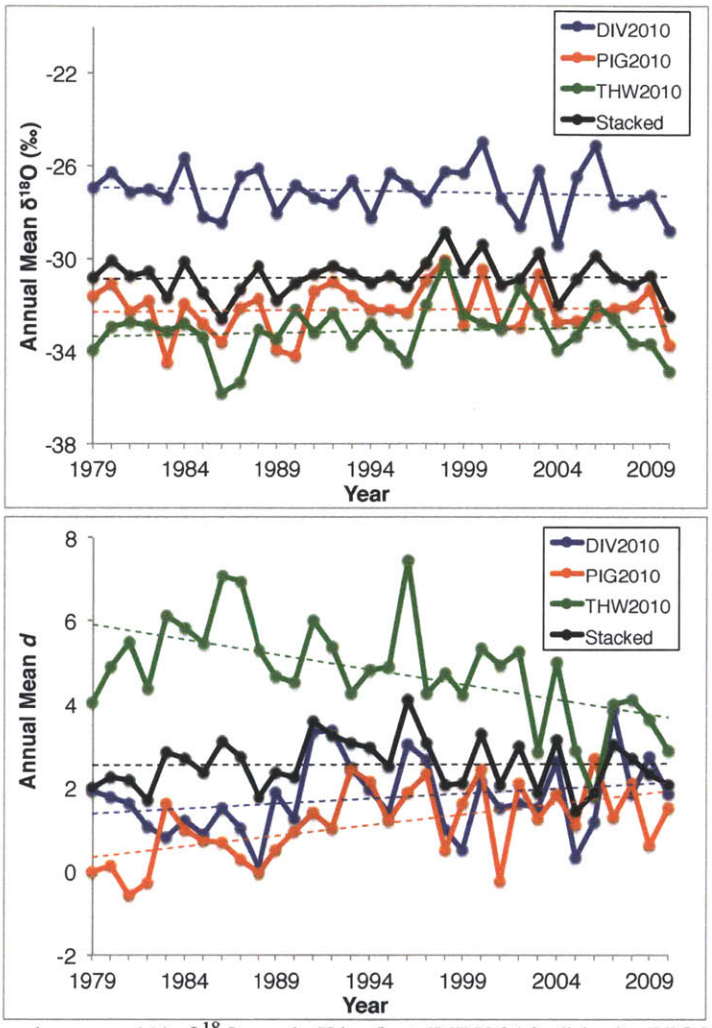

Figure 4. Annual mean (A) $\delta^{18}O$ and (B) *d* at DIV2010 (blue), PIG2010 (red), and THW2010 (green), 1979–2010. The stacked $\delta^{18}O$ and *d* records are included (black). Linear fits are shown (dashed lines).

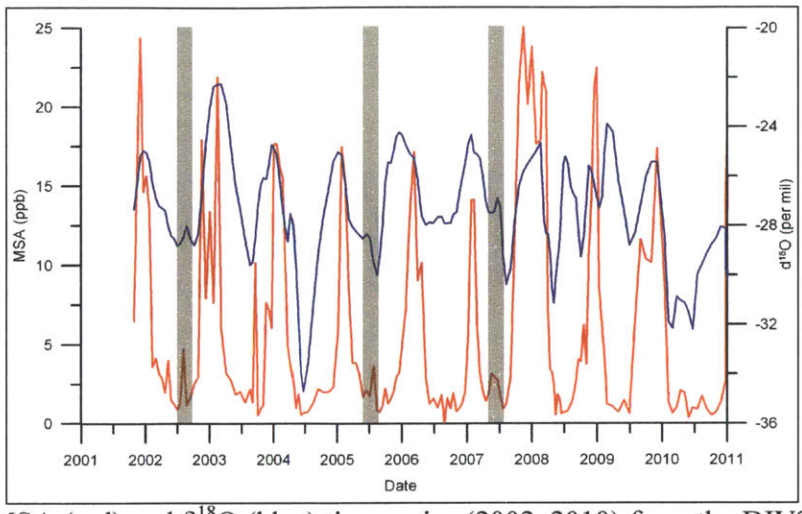

Figure 5. MSA (red) and $\delta^{18}O$ (blue) time series (2002–2010) from the DIV2010S short core drilled within ~3 meters of the DIV2010 core. Winter polynya events discussed (August 2002, July 2005, June 2007) show concurrent increases in MSA and $\delta^{18}O$ in DIV2010S, and are highlighted by grey shading. Highlighted peaks lie above the MSA detection limit of 2.5 ppb. X-axis years indicate start (January) of a year.

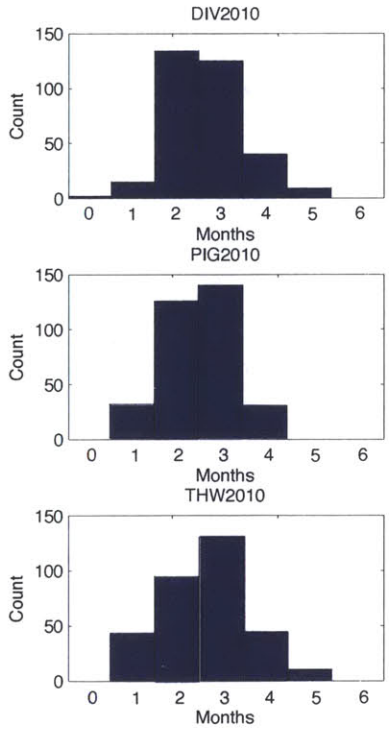

Figure 6. Histograms of the $\delta^{18}O$-*d* lags (in months) at (A) DIV2010, (B) PIG2010, and (C) THW2010, 1979–2010.

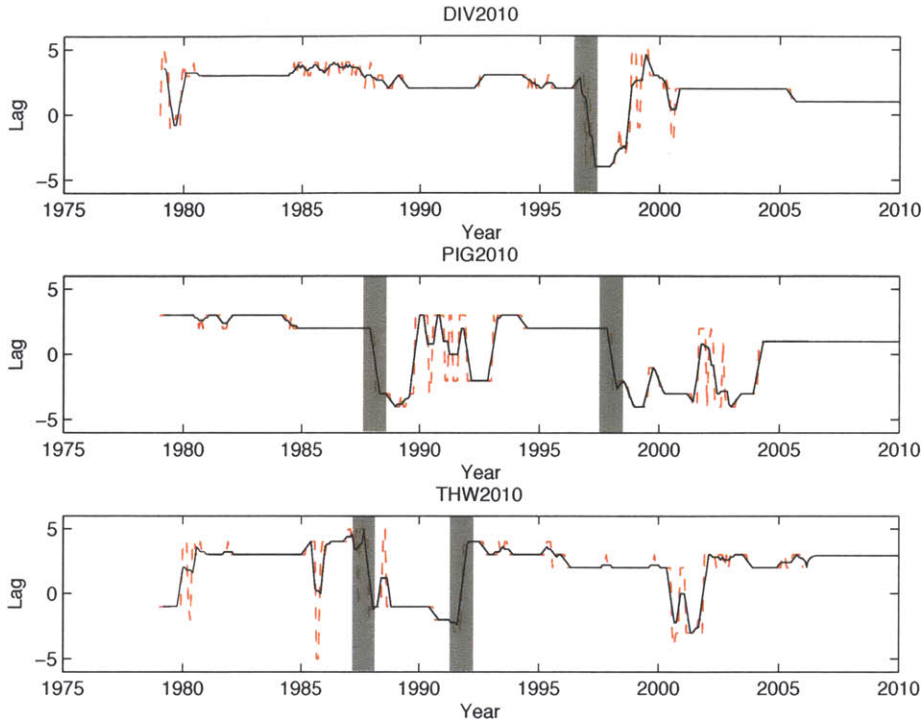

872
873 **Figure 7.** Annual lags (in months) between *d* and $\delta^{18}O$ at (A) DIV2010, (B) PIG2010,
874 and (C) THW2010, 1979–2010. Monthly data (red dashed) and 5-point running means
875 (black) are shown. Grey shaded bars indicate large shifts in the $\delta^{18}O$-*d* lag that are
876 concurrent with shifts in large-scale atmospheric circulation (e.g., shifts from strong El
877 Niño conditions to La Niña conditions, or visa versa).
878

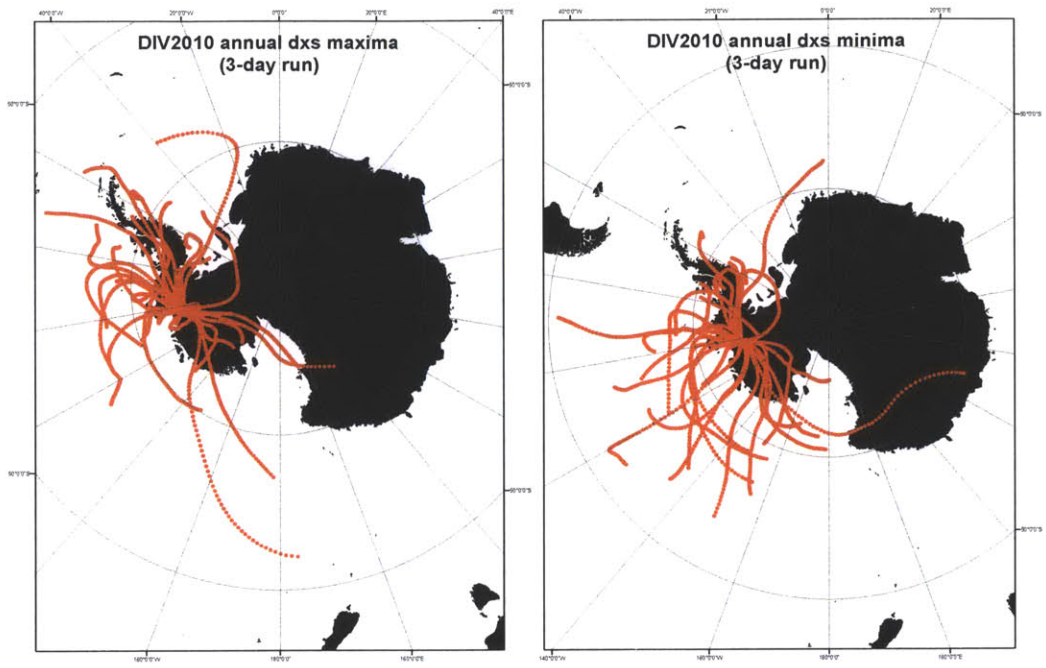

879
880 **Figure 8.** 3-day HySPLIT back-trajectories at DIV2010 for (A) annual *d* maxima (fall),
881 and (B) annual *d* minima (spring), 1979–2010.
882
883
884

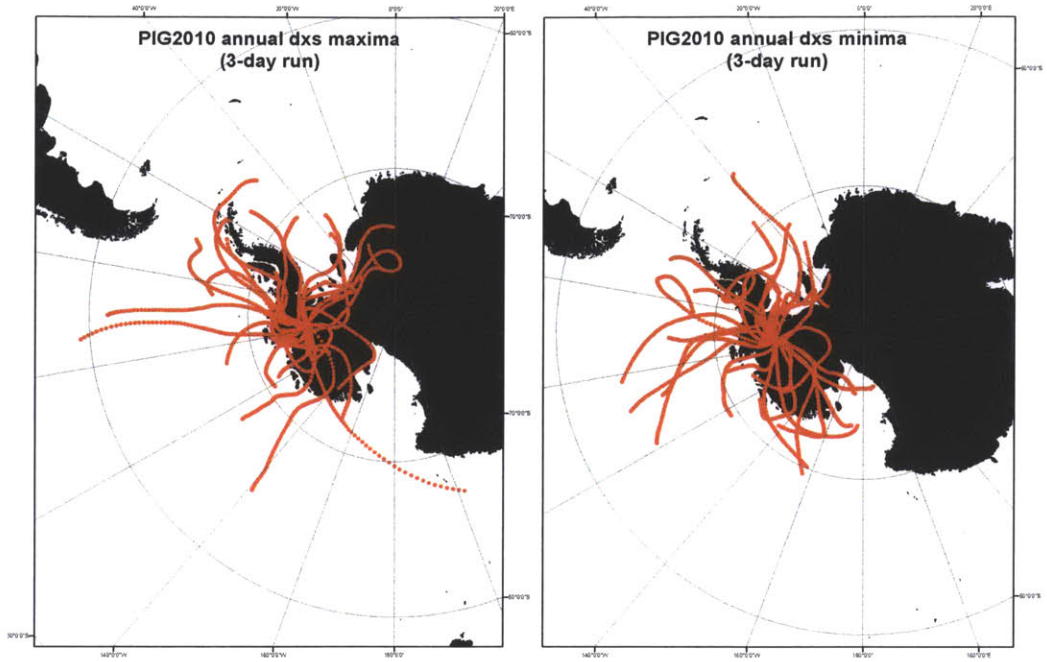

885
886 **Figure 9.** 3-day HySPLIT back-trajectories at PIG2010 for (A) annual *d* maxima (fall),
887 and (B) annual *d* minima (spring), 1979–2010.
888
889
890

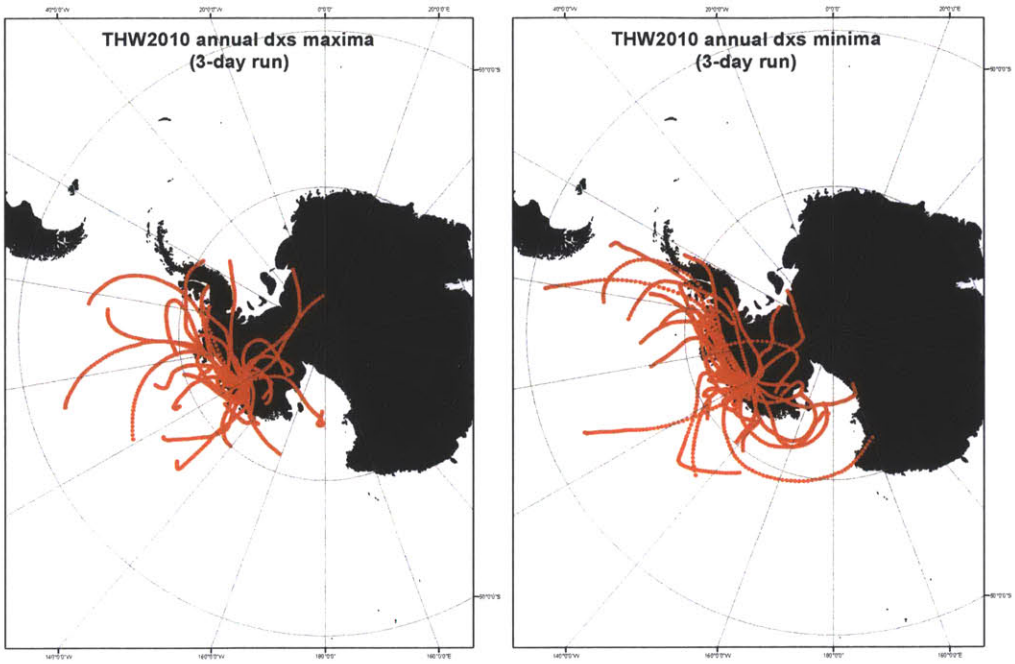

Figure 10. 3-day HySPLIT back-trajectories at THW2010 for (A) annual *d* maxima (fall), and (B) annual *d* minima (spring), 1979–2010.

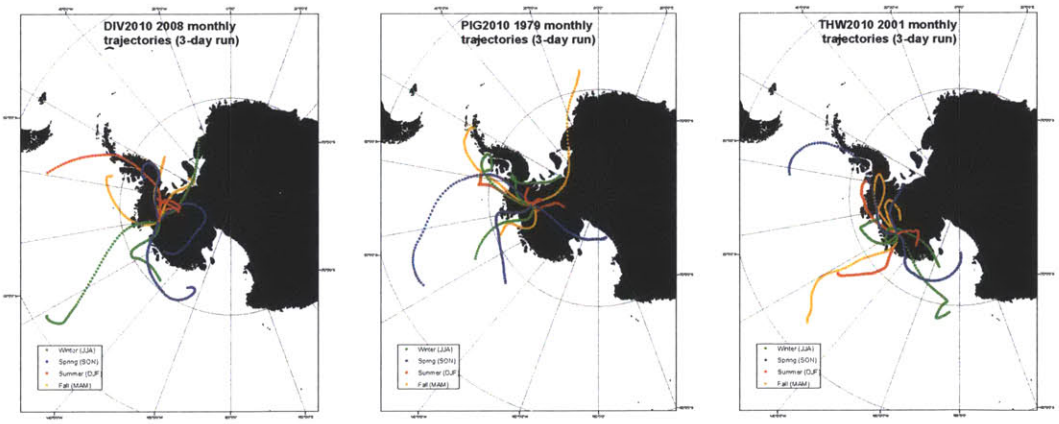

Figure 11. Monthly HySPLIT back-trajectory runs (3-day) for years of mean accumulation and precipitation at each site over 1979–2010; (A) 2008 for DIV2010, (B) 1979 for PIG2010, and (C) 2001 for THW2010. Results are presented seasonally (winter = JJA/blue, spring = SON/green, summer = DJF/red, fall = MAM/orange).

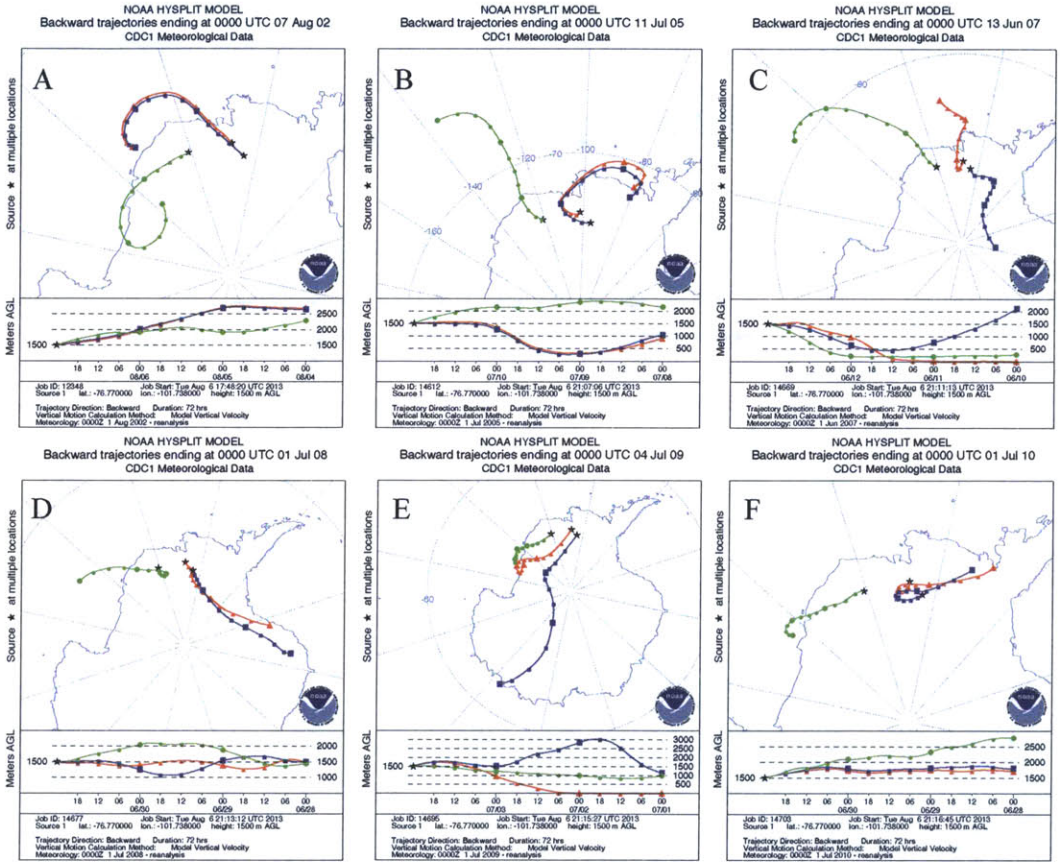

Figure 12. Case studies at DIV2010 (red), PIG2010 (blue), and THW2010 (green) of 3-day back-trajectories for the three months over the 1979–2010 period that had the largest wintertime polynya events in the Amundsen Sea and Pine Island Bay polynyas that correspond to elevated wintertime MSA concentrations and $\delta^{18}O$ values at DIV2010S ((A) August 2002, (B) July 2005, (C) June 2007), as well as for three months over the 1979–2010 period that had the smallest or no wintertime polynya events, and winter MSA concentrations in DIV2010S below the detection limit ((D) July 2008, (E) July 2009, (F) July 2010).

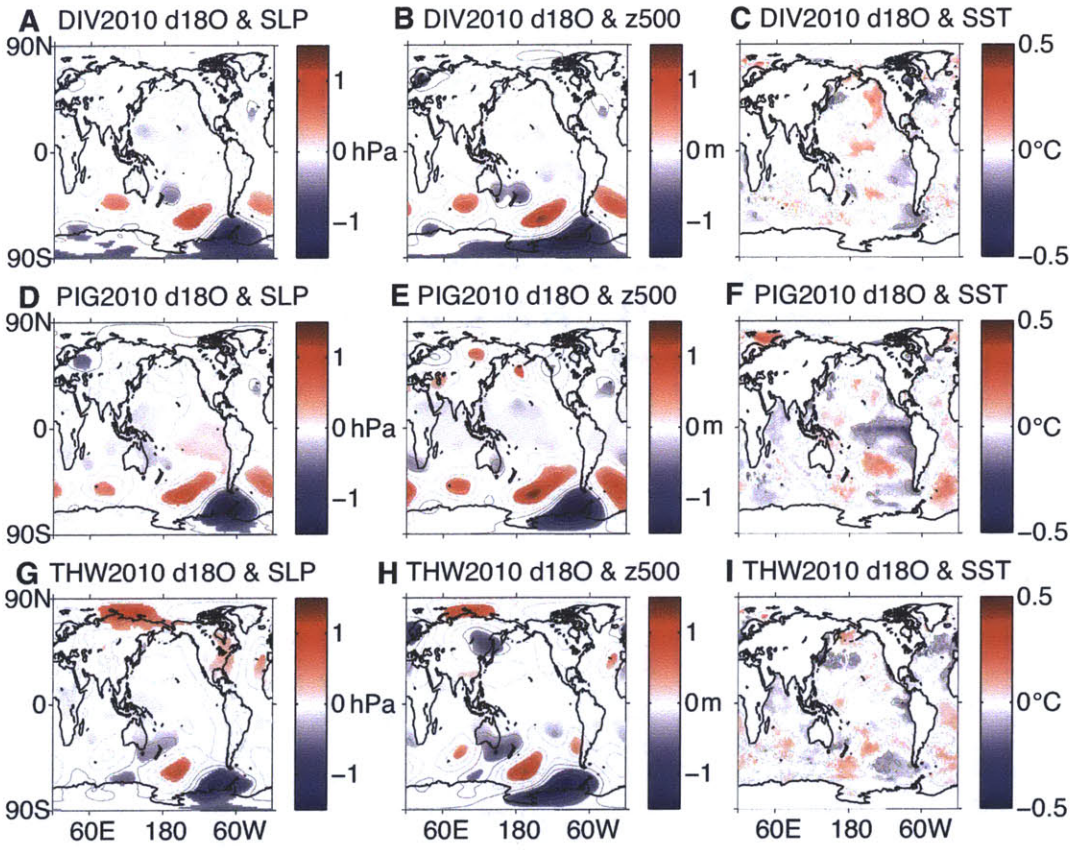

Figure 13. Regression maps of DIV2010 $\delta^{18}O$ anomalies and (A) SLP, (B) 500 hPa GH, and (C) SST anomalies; PIG2010 $\delta^{18}O$ anomalies and (D) SLP, (E) 500 hPa GH, and (F) SST anomalies; THW2010 $\delta^{18}O$ anomalies and (G) SLP, (H) 500 hPa GH, and (I) SST anomalies. The SLP scale is -1.5–1.5 hPa (with 0.2 hPa contours), the 500 hPa GH scale is -1.5–1.5 m (with 0.2 m contours), and the SST scale is -0.5–0.5°C (with 0.2°C contours). Contours show all regression patterns (no threshold of statistical significance), while shaded regions indicate >99% significance (determined using a two-tailed Student's *t*-test).

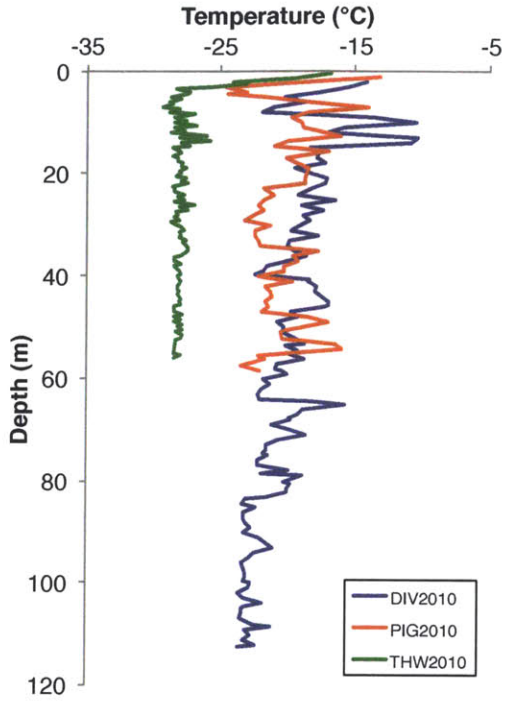

Figure 14. Firn-core temperature profiles with depth measured in the field for DIV2010 (blue), PIG2010 (red), and THW2010 (green).

Tables

Name	Lat	Lon	Elevation (m)	Distance from coast (km)	Period	Mean accumulation rate (m·we·yr-1)	Mean δ18O (‰)	Mean *d*	Mean ERA-Interim temp (°C)	Mean RACMO2 temp (°C)
DIV2010	-76.77	-101.74	1329	180	1979-2010	0.408	-27.10	1.75	-20.7	-25.1
PIG2010	-77.96	-95.96	1593	350	1979-2010	0.424	-32.21	1.14	-26.0	-30.6
THW2010	-76.95	-121.22	2020	340	1979-2010	0.281	-33.14	4.80	-26.8	-30.3

Table 1. Location and annual mean values (accumulation, $\delta^{18}O$, *d*, temperature) of three West Antarctic firn cores used in this study.

		Byrd temp	ERA-Int temp	RACMO2 temp	RACMO2 SMB	ERA-Int precip
DIV2010	**δ18O**	*0.28*	0.44	*0.09*	--	--
	accumulation	--	--	--	0.46	0.61
PIG2010	**δ18O**	0.50	*0.21*	*0.20*	--	--
	accumulation	--	--	--	0.52	0.76
THW2010	**δ18O**	0.30	0.38	0.55	--	--
	accumulation	--	--	--	0.51	0.56

Table 2. Pearson's *r* correlation coefficients of mean annual $\delta^{18}O$ at the three core sites and Byrd, ERA-Interim, and RACMO2 temperature (1979–2010); mean annual accumulation at the three core sites and ERA-Interim and RACMO2 precipitation (1979–2010). Italicized/grey numbers indicate *r*-values not significant at $p < 0.01$.

	max *d*	min *d*	summer/fall	winter/spring
DIV2010	**60% AB**, W 20%, R 15%	**50% AB**, 15% W, 30% R	AB, W	AB, R
PIG2010	**60% AB**, W 30%	**50% AB**, 25% W, 20% R	AB, W	AB, R
THW2010	**70% AB**, W 10%, R 10%	**65% AB**, 10% W, 25% R	AB	AB, R

Table 3. Overview of moisture source regions to the three core sites during times of maximum and minimum *d* (shown in map form in Figs. 5-7), and during summer/fall versus winter/spring for years of average precipitation (shown in map form in Fig. 8). AB=Amundsen-Bellingshausen Sea, W=Weddell Sea, R=Ross Sea. Primary moisture source regions are in bold.

Annual

	TOWA & δ18O	SIE & δ18O	TOWA & *d*	SIE & *d*
DIV2010	*-0.09*	*-0.12*	*0.32*	*-0.14*
PIG2010	*0.24*	*-0.34*	*0.21*	*-0.09*
THW2010	*0.07*	-0.48	*-0.15*	*0.25*

Monthly

	TOWA & δ18O	SIE & δ18O	TOWA & *d*	SIE & *d*
DIV2010	0.29	-0.37	*0.13*	-0.38
PIG2010	0.39	-0.56	*-0.11*	-0.30
THW2010	0.30	-0.15	0.23	-0.43

Table 4. Pearson's *r* correlation coefficients of mean annual $\delta^{18}O$ and *d* at the three core sites and TOWA and SIE (1979–2010). Italicized/grey numbers indicate *r*-values not significant at $p < 0.01$.

Chapter 5

Decadal climate and sea-ice variability from ice-core marine aerosol records, West Antarctica

Abstract

We investigate coastal Antarctic climate, sea-ice, and polynya variability using three new annually-resolved marine aerosol and isotopic records from ice cores from Pine Island and Thwaites Glaciers in West Antarctica. Methanesulfonic acid (MSA), non sea-salt sulfate (nssS), sodium (Na), and $\delta^{18}O$ were compared with anomalies of global atmospheric fields and show a remote tropical Pacific influence on West Antarctic climate over the past 200 years. Moreover, we find these remote atmospheric dynamics, well known to drive local fluctuations in winds and Circumpolar Deep Water influx to the Amundsen Coast today, also result in strong decadal variability in coastal West Antarctic marine aerosol records over longer time-scales. Na and $\delta^{18}O$ records are more influenced by remote atmospheric dynamics than records of marine biogenic compounds, which are more influenced by local dynamics (e.g., sea-ice and polynya variability), and the highest elevation site is most strongly influenced by remote tropical Pacific dynamics. Our results indicate that the 1870's, 1930/40's, and 1990's were likely some of the regionally warmest years over the length of our records, with low sea-ice concentration (SIC) in the Amundsen Sea, and the 1920's and 1960/70's were likely some of the regionally coldest years over the length of our records, with high SIC in the Amundsen Sea. MSA and nssS records indicate that 1877, 1910, 1950, 1976, 1993, 1995, and 2010 were likely years of unusually enhanced polynya activity.

1. Introduction

Climate trends over the past 200 years at high southern latitudes are marked by warming of the Antarctic troposphere [*Turner et al.*, 2006] and the upper km of the circumpolar Southern Ocean [*Gille*, 2008], warming of the dense bottom water in the Weddell Sea [*Robertson et al.*, 2002], and freshening of Antarctic Bottom Water [*Jacobs*, 2006; *Jacobs et al.*, 2011; *Rintoul*, 2007]. These Antarctic climate changes are due to a combination of multidecadal variability and anthropogenic effects, and multidecadal- to millennial-scale natural variability forced by changes in orbital insolation, greenhouse gases, solar variability, ice dynamics, and aerosols [*Mayewski et al.*, 2009]. Surface trends in West Antarctica have been unique over the past half-century; the region has experienced widespread warming in the past 50 years [e.g., *Bromwich et al.*, 2012], in particular over the interior of the West Antarctic Ice Sheet (WAIS), which has been linked to sea surface temperature (SST) increase in the tropical Pacific [e.g., *Ding et al.*, 2011]. Climate records from coastal West Antarctica are scarce, although show strong links between stable isotope records and tropical Pacific SST and atmospheric pressure, as well as local sea-ice conditions (1700's–2000) [*Okumura et al.*, 2012; *Thomas et al.*, 2013]. Much recent attention is focused on glacier behavior along the Amundsen Coast of West Antarctica, where ice mass loss is accelerating and is presently the largest Antarctic contributor to sea level rise. Recent work has concentrated on constraining grounding-line retreat and melting rates under Pine Island Glacier [e.g., *Stanton et al.*, 2013; *Park et al.*, 2013], largely because Pine Island Glacier has accelerated exponentially over the last 30 years [*Rignot et al.*, 2008] and has been thinning at unprecedented rates since the early 1990's [*Wingham et al.*, 2009]. Thwaites Glacier is

similarly unstable [*Parizek et al.*, 2013]. Dynamic losses are expected to persist and penetrate farther inland in this key region that has potential for catastrophic ice-sheet collapse [e.g., *Rignot et al.*, 2011], and longer-term studies of Pine Island and Thwaites Glacier retreat indicate that today's rapid retreat is exceptional during the Holocene, and may be the result of recent changes in regional climate, ocean circulation, and ice-sheet dynamics [*Hillenbrand et al.*, 2013]. It is critical that we continue focusing efforts on understanding regional interactions between sea ice, the ocean, and the ice sheet, particularly in the Pine Island Bay region.

In order to assess such interactions between the marine environment and West Antarctica, long-term records of sea-ice concentration (SIC) off the Antarctic coast are needed. Sea ice is a key component of the southern high latitude climate system; an increase in sea-ice extent increases the albedo of the ocean, reduces ocean-atmosphere gas exchange, and decreases ocean mixing. Sea ice plays a major role in the formation of deep waters in the ocean, and therefore in global ocean circulation and the carbon cycle [e.g., *Dieckmann and Hellmer*, 2010]. Over the satellite era (1970's to present), total Arctic sea ice has diminished at a rapid pace [*Comiso*, 2008] while total Antarctic sea ice has increased [*Turner et al.*, 2009]. However, regional Antarctic trends vary. In contrast to the Weddell and Ross Sea regions of Antarctica, which have shown a recent increase in sea-ice extent [*Jacobs*, 2006], the Amundsen Sea has shown a decline in sea-ice extent over the last quarter century [*Turner et al.*, 2009].

Marine aerosol records, most notably methanesulfonic acid (MSA) and sea salt (Na), obtained from ice cores are one of the most useful methods to reconstruct long-term sea-ice variability, and assess the changing marine influence on the ice sheet prior to the

47 satellite era [see *Abram et al.*, 2013 for a recent review]. During sea-ice breakup,
48 phytoplankton blooms release dimethylsulfoniopropionate (DMSP), which degrades to
49 dimethyl sulfide (DMS) [*Dacey and Wakeham*, 1986]. DMS is oxidized in the
50 atmosphere to MSA, which is deposited onto the ice sheet in snow [*Gibson et al.*, 1990].
51 The duration and spatial extent of sea-ice breakup therefore exert a control on the timing
52 and amount of DMSP produced and, subsequently, MSA precipitated on the ice sheet. In
53 contrast to sea-ice break-up described above, sea-ice formation processes (frost flower
54 formation, brine production, release of blowing snow from sea-ice surfaces) are often the
55 dominant source of sea-salt aerosols to Antarctica [*Rankin et al.*, 2002; *Wolff et al.*,
56 2003]. Sea-ice proxies require regional validation, as previous studies have shown both
57 strong negative and strong positive correlations between sea-ice proxies and SIC. In a
58 previous study using records from a WAIS site adjacent to Pine Island Bay we found that
59 MSA maxima occur in summer corresponding to sea-ice breakup and phytoplankton
60 blooms, while sea salt maxima occur in winter corresponding to formation of new sea-ice
61 surfaces [*Criscitiello et al.*, 2013a]. In addition, stable oxygen isotopes ($\delta^{18}O$) can
62 provide information on temperature, precipitation origin, sea-ice variability, and large-
63 scale atmospheric circulation.

64 In this study we use a multi-core, multi-proxy approach. We utilize MSA, non
65 sea-salt sulfate (nssS), Na, and $\delta^{18}O$ from three sites (DIV2010, PIG2010, and
66 THW2010) across the Amundsen Coast to investigate Amundsen Sea sea-ice and
67 polynya variability over longer time-scales, as well as decadal changes in atmospheric
68 transport from 1786–2010. As MSA is known to be subject to post-depositional
69 processes within the firn (in contrast to sea salts), we investigate MSA migration and loss

70 at DIV2010, our most coastal site, where we have a long MSA record. At PIG2010 and
71 THW2010, where only short MSA records are available, we further assess the use of nssS
72 as a proxy for MSA. This work builds on our previous studies that focused on linked
73 ocean and ice-sheet changes during the satellite era [*Criscitiello et al.*, 2013a; *Criscitiello*
74 *et al.*, 2013b; *Criscitiello et al.*, in prep]. We accomplish these goals in four main
75 sections: (1) analysis of MSA migration in the longest core (1801–2010), (2)
76 reconstruction of long-term temperature records using oxygen isotopes, (3) reconstruction
77 of records of sea-ice and polynya variability using glaciochemical sea-ice proxies, and (4)
78 investigation of the influence of the tropical Pacific on atmospheric transport of marine
79 aerosols to the Amundsen Coast of West Antarctica on decadal timescales.
80
81 **2. Data and Methods**
82 *2.1 Site descriptions*
83 In 2010-11, we collected three firn cores using the US Eclipse drill from Pine
84 Island Glacier (PIG2010), Thwaites Glacier (THW2010), and the drainage divide
85 between Pine Island and Thwaites Glaciers (DIV2010; Fig. 1). These are among the
86 most coastal, highest resolution cores drilled in West Antarctica to date. The core sites
87 range in elevation from 1329 to 2020 m, and range from 180 to 350 km in distance from
88 the coast (Table 1). Annual accumulation variability is also high at all sites, and shows
89 no significant trend over 1980–2009 [*Medley et al.*, 2013]. Ice velocities at the core
90 locations are low (~10–20 $m \cdot yr^{-1}$) [*Joughin et al.*, 2003].
91
92 *2.2 Glaciochemical records and dating*

93 Data for the DIV2010, PIG2010, and THW2010 cores include $\delta^{18}O$, δD, nssS,
94 total soluble plus insoluble S (S_{total}), Na, Ca, Mg, and MSA. nssS is calculated as: nssS =
95 S_{total}-Na*(905/10770). We performed analyses of S_{total}, Na, Ca, and Mg on an
96 inductively coupled plasma mass spectrometer (ICP-MS) linked directly with a
97 continuous ice-core melter system (detection limits ~500 ppq for elements in this study)
98 [*Maselli et al.*, 2013; *McConnell et al.*, 2001]. Isotope data for the cores were collected
99 on a Picarro cavity ring-down spectroscopy analyzer, also linked directly with the
100 continuous ice-core melter system. The Picarro oxygen isotope analyzer produces high-
101 precision, simultaneous measurements of $\delta^{18}O$ (<0.1‰) and δD (<0.5‰) for liquid water
102 samples. We performed MSA analyses using suppressed ion chromatography on discrete
103 samples [*Curran and Palmer*, 2001]. The detection limit for MSA is 0.4 ppb, with
104 analytical precision of <5%.
105 We established age-depth relationships and determined accumulation rates by
106 identifying the midsummer maximum in three parameters (nssS/Na, H_2O_2, and $\delta^{18}O$) and
107 counting annual cycles. Volcanic time markers present in 1810, 1816, 1885, 1928, 1964,
108 and 1992 were also used to verify the annual layer counting. As a result of the high
109 accumulation rate and multiple dating parameters, the standard error in the interannual
110 dating is ±1 year [*Medley et al.*, 2013; *Pasteris et al.*, in revision]. To allow for
111 investigation of the marine aerosol and isotope time series alongside reanalysis records,
112 we produced annual resolution glaciochemical records by annually averaging monthly
113 records. Spectral analysis of marine biogenic and sea-salt species indicates strong
114 decadal variability; we therefore applied a low-pass filter to all annual glaciochemical
115 time series, removing interannual variability.

116

117 *2.3 Global instrumental datasets*

118 We utilized the Hadley Center Sea Ice and SST (HadISST1) [*Rayner et al.*, 2003]
119 and Hadley Center SLP version 2 (HadSLP2r) [*Allan and Ansell*, 2006] instrumental
120 datasets to provide global monthly SST and sea level pressure (SLP). These datasets
121 were used to analyze decadal patterns of large-scale climate variability associated with
122 marine aerosol and oxygen isotope anomalies in our West Antarctic firn cores.
123 HadISST1 data are available 1870–present on a 1° latitude-longitude grid, and are based
124 on historical in situ ship and buoy observations as well as satellite data post-1982 [*Rayner*
125 *et al.*, 2003]. HadSLP2r data are available 1850–present on a 5° latitude-longitude grid,
126 and are based on terrestrial station records and marine observations, as well as
127 NCEP/NCAR reanalysis data post-2004 [*Allan and Ansell*, 2006]. HadISST1 and
128 HadSLP2r are spatially smoothed using a low-pass filter to reduce sub-annual and
129 interannual noise. We conducted linear temporal regression analysis to explore the
130 relationships between firn-core records and global climate fields. Statistical significance
131 was determined using the 2-tailed Student's *t*-test. In addition to this significance test, we
132 rely on physical consistencies among global climate variables and the robustness of
133 results (both site to site and glaciochemical species to species) to additionally validate
134 results.

135 We additionally created an SST time series from the HadISST1 dataset from a
136 region that shows significant regressions of SST on many of the glaciochemical time
137 series (10°N to 10°S, 140°W to 80°W; Figs. 12-14). This SST time series was then
138 correlated with the firn-core glaciochemical records.

139

140 **3. Results**

141 *3.1 Glaciochemical records*

142 The highest measured Na, Mg, and nssS concentrations (73.9 ppb, 8.5 ppb, and
143 56.1 ppb, respectively), and the highest $\delta^{18}O$ values (-24.7 ‰), occur in the DIV2010
144 core (the site closest to Pine Island Bay; Table 1). The highest measured Ca
145 concentrations (41.8 ppb) occur in the PIG2010 core (the site farthest inland). MSA
146 concentrations range from 3.6–18.4 ppb at DIV2010 (1801–2010), 6.7–12.1 ppb at
147 PIG2010 (1993–2010), and 5.7–13.5 ppb at THW2010 (1945–2010), comparable to
148 similar studies in Antarctic coastal regions [e.g., *Abram et al.*, 2011]. We present these
149 new glaciochemical time series in Figs. 2-4, and note that none of the records show
150 statistically significant trends over the full length of each record. The monthly MSA
151 concentrations show a distinct shift around 1977 (Fig. 5A). Post-1977, MSA shows
152 distinct summertime peaks, mainly in January; prior to 1977, annual peaks are both more
153 variable in timing and show a migration from summer toward winter layers (Fig. 6).
154 There is also a concurrent decrease in seasonality prior to 1977 (Fig. 7). Climatological
155 means remain the same before and after 1977 (8 ppb) suggesting MSA migration is
156 confined to within the annual layers and does not result in overall loss of the MSA signal;
157 therefore we assume that MSA migration does not degrade the interannual or longer-term
158 signal. In contrast to MSA, Na shows no such shift in seasonality in 1977 (Figure 7B),
159 nor any abrupt shift in the month of maximum Na at any point over the length of the time
160 series.

161 Correlations between log transformed MSA (log(MSA)) and nssS are generally
162 significant for all three records, though there is variability over time (Fig. 8). MSA and
163 nssS both have marine biogenic sources, and correlations over the time period of
164 overlapping data are significant at $p < 0.05$, as has been shown previously at these core
165 sites for years 1979–2010 [*Pasteris et al.*, in revision]. Years of overlapping MSA and
166 nssS data for DIV2010, PIG2010, and THW2010 in this study are 1801–2010, 1993–
167 2010, and 1945–2010, respectively. These full records have *r*-values of 0.28, 0.35, and
168 0.51 (significant at $p < 0.05$). There are, however, periods of exceptionally high
169 correlation between MSA and nssS at all sites (Fig. 8). At DIV2010, only the earliest 10-
170 year part of the record has insignificant correlations between MSA and nssS; the
171 correlation between MSA and nssS for 1820–2010 has an *r*-value of 0.63. At PIG2010,
172 the correlation between MSA and nssS for 2004–2010 has an *r*-value of 0.83. At
173 THW2010, the entire lengths of the MSA and nssS records are highly correlated.
174 At each site, the $\delta^{18}O$ and δD records are highly correlated ($r > 0.98$); therefore
175 we present only the $\delta^{18}O$ records. Similarly, the sea salt records at each site are highly
176 correlated (Table 2), therefore we present Na as the representative sea-salt species.
177 Significant correlations between sea-salt species have been found at many other Antarctic
178 sites [e.g., *Abram et al.*, 2011; *Artaxo et al.*, 1992], and in this study are generally
179 weakest at PIG2010 (Table 2). Correlations between Na and Mg (r = 0.65–0.97) are
180 stronger than correlations between Ca and any other sea-salt species (r = 0.37–0.64), as
181 has been previously found at these three sites over the 1979–2010 period [*Criscitiello et*
182 *al.*, 2013b]. This is likely the result of the large aerosol size of Ca which can result in
183 dilution effects at high accumulation sites [e.g., *Kreutz and Mayewski*, 1999]. Similarly

184 for marine biogenic compounds, S_{total} and nssS at all sites are highly correlated ($r > 0.96$;
185 Table 2); therefore we present only the nssS records along with MSA. Decadal records
186 of $\delta^{18}O$ and Na at DIV2010 and THW2010 are significantly correlated as well ($r = -0.4$).
187
188 *3.2 Interannual and decadal variability*
189 In this section we present years and decades of maxima and minima in the various
190 glaciochemical records, which are used to reconstruct long-term record of regional
191 climate and Amundsen Sea sea-ice and polynya variability. While we primarily use
192 decadal records for such reconstructions, interannual data are useful for investigating
193 short-lived, anomalous events. At DIV2010, the highest $\delta^{18}O$ values occur in 1931 (the
194 1930's having the highest decadal average as well), coincident with lower than average
195 decadal Na concentrations, and marine biogenic concentrations approximately at the full-
196 record mean (Fig. 2). The highest Na concentrations in the DIV2010 core occur in 1950,
197 a period marked by a rise in marine biogenic compounds. The highest nssS
198 concentrations in the DIV2010 core occur in 1810, 1816, and 1951 (Fig. 2). The highest
199 MSA concentrations in the DIV2010 core occur in 1877, 1910, and 1995 (Fig. 2). At
200 PIG2010, the highest $\delta^{18}O$ values occur in 1941 and 1998, years with lower than average
201 decadal Na and nssS concentrations (Fig. 3). The highest Na concentrations in the
202 PIG2010 core occur in 1920, 1933, 1950, 1968, and 2010. The highest nssS
203 concentrations in the PIG2010 core occur in 1964 and 1992, years with known volcanic
204 horizons, and coincident with lower than decadal average Na concentrations and elevated
205 $\delta^{18}O$ values (Fig. 3). The PIG2010 MSA time series is the shortest of the three (1993–
206 2010), with the highest values occurring in 1993 and 2010. At THW2010, the highest

207 $\delta^{18}O$ values occur in 1878, 1941, and 1998 (similar to PIG2010; Fig. 4). The highest Na
208 concentrations in the THW2010 core occur in 1921, 1943, and 1975, corresponding to
209 lower than decadal average $\delta^{18}O$ values. The highest nssS concentrations in the
210 THW2010 core occur in 1885, 1928, 1964, and 1992, also years with known volcanic
211 horizons, and corresponding to years with generally lower than average $\delta^{18}O$ and Na
212 concentrations, similar to PIG2010 (Fig. 4). The highest MSA concentrations at
213 THW2010 occur in 1976 and 1995 (Fig. 4).

214 Low-pass filtered time series reveal significant decadal variability in both the
215 marine aerosols and oxygen isotopes (Figs. 2-4). This is confirmed by spectral analysis
216 of the annual time series anomalies, which show significant power (at $p < 0.05$) in
217 decadal time periods for almost all species at all sites (Figs. 9-11). Decadal maxima and
218 minima of the glaciochemical species often occur over the decades that include the
219 interannual minima and maxima. At DIV2010, the decadal average in $\delta^{18}O$ is highest in
220 the 1920/30's, and lowest in the 1950/60's (Fig. 2). The decadal average in Na is highest
221 in the 1850's, though decadal Na variability is fairly uniform over the length of the
222 record. The decadal average in nssS is highest in the 1810's and 1930's due to
223 significant volcanic activity during these decades. The decadal average in MSA is
224 highest in the 1990's (Fig. 2). At PIG2010, the decadal average in $\delta^{18}O$ is highest in the
225 1930/40's and 1990's (Fig. 3). The decadal average in Na is highest in the 1920/30's
226 (Fig. 3). The decadal average in nssS is highest in the 1960's and 1990's due to
227 significant volcanic activity during these decades. The MSA record at PIG2010 is not
228 sufficiently long to investigate decadal variability. At THW2010, the decadal average in
229 $\delta^{18}O$ is highest in the 1870/80's, 1940's, and 1990's (Fig. 4). The decadal average in Na

230 is highest in the 1970's; from 1880–1980 there is a steady increase in the amplitude of the
231 decadal signal of Na. The decadal average in nssS is highest in the 1880's, 1920's, and
232 1990's due to significant volcanic activity during these decades (Fig. 4). Though short,
233 the MSA record at PIG2010 reveals an increase in the amplitude of the decadal signal
234 from the 1960's through the 2000's (Fig. 4).
235
236 *3.3 Global atmospheric anomalies*
237 At all sites, regression analysis of low-pass filtered SLP and SST on low-pass
238 filtered Na and $\delta^{18}O$ reveal a low pressure anomaly over the Antarctic Peninsula which
239 alternates with a high pressure anomaly in the central south Pacific and a low pressure
240 anomaly in the western tropical or western south Pacific (Figs. 12-14). This decadal
241 pattern in SLP anomalies corresponds to anomalous cooling in the eastern tropical Pacific
242 (Figs. 12-14). The SST regressions are in agreement with initiation and propagation of a
243 Rossby wave train [*Hoskins and Karoly*, 1981]. There is symmetry in the northern
244 hemisphere SLP and SST regression patterns in many cases (additional evidence of the
245 influence of the tropics on both hemispheres [*Lee et al.*, 2011; *Trenberth et al.*, 1998]).
246 Regressions of SLP and SST on MSA and nssS (the biogenic species) do not as clearly
247 show this Rossby wave train (Figs. 12-14). There are no significant correlations ($p <$
248 0.05) between the annual or decadal SST time series (10°N to 10°S, 140°W to 80°W) and
249 any annual or decadal glaciochemical record from the three core sites. Though not
250 significant at $p < 0.05$, the highest correlation between the SST time series and a
251 glaciochemical record is with the THW2010 Na record (r = -0.24). At all sites,

252 correlations of the SST time series with Na and $\delta^{18}O$ are higher than correlations with
253 MSA or nssS.

254 Global regression fields also reveal spatial variability. Regressions of SLP on
255 PIG2010 and THW2010 nssS and $\delta^{18}O$ reveal a Southern Annular Mode (SAM) -like
256 pattern (Figs. 13-14), as shown in previous work using the same core records from 1979–
257 2010 [*Criscitiello et al.*, 2013b]. In contrast, regression of SLP on DIV2010
258 glaciochemical records shows an organized wave train but no SAM signature (Fig. 12).
259 Regressions of SST on DIV2010 and PIG2010 $\delta^{18}O$ and Na, and THW2010 Na, most
260 clearly show the associated La Niña-like conditions consistent with propagation of a
261 Rossby wave train (anomalous cooling in the eastern tropical Pacific). We note that
262 regressions of SLP on MSA and nssS at DIV2010 appear visually distinct (Figs. 12E &
263 12G) due to masking of regressions with $p < 0.05$; however, non-masked maps reveal
264 markedly similar results between biogenic species (as expected due to the high
265 correlations between log(MSA) and nssS at all sites).
266

267 **4. Discussion**

268 *4.1 MSA migration in the DIV2010 long core*

269 At low accumulation sites (<100 kg m^{-2}·yr^{-1}, or 10 cm water-equivalent), post-
270 depositional loss of MSA (increasing with depth) is significant [*Weller et al.*, 2004]. It is
271 not presently known if such post-depositional loss is due to photochemical destruction of
272 MSA in the snow and/or re-emission of MSA to the atmosphere [*Abram et al.*, 2013].
273 However, it is known that the presence of salt and dust can act to stabilize MSA in
274 Antarctic snow [*Legrand and Saigne*, 1991]. At such sites, MSA migrates within the ice

275 from summer layers towards winter layers, where it becomes chemically stabilized by
276 reactions with salt and dust impurities [*Curran et al.*, 2002; *Mulvaney et al.*, 1992;
277 *Pasteur and Mulvaney*, 2000]. The MSA peak, once it has migrated to the winter layer,
278 can sharpen with depth [*Pasteur and Mulvaney*, 2000], though our data do not show this.
279 Model predictions have shown that the bulk concentrations of different species adjust so
280 that their ratios become spatially uniform [*Rempel et al.*, 2002]. This behavior helps to
281 explain the migration of MSA, whereby the MSA peaks adjust post-depositionally to
282 coincide with the sea-salt peaks that were originally deposited at maximal concentrations
283 during winter months [*Pasteur and Mulvaney*, 2000; *Rempel et al.*, 2002].

284 At high accumulation sites, MSA migration is confined to within the annual
285 layers and therefore it is generally assumed that this process should not degrade the
286 interannual or longer-term signals related to sea-ice variability [*Abram et al.*, 2013].
287 Post-depositional loss of MSA has previously been shown to not be a significant factor at
288 high accumulation coastal core sites [*Abram et al.*, 2013]. A study that utilized the James
289 Ross Island core (a high accumulation site off the Antarctic Peninsula) found no evidence
290 for MSA migration in the 1967–2008 monthly data [*Abram et al.*, 2011]. Similarly, our
291 prior studies across this region of monthly-resolved MSA records over the satellite era
292 showed no evidence of MSA migration in monthly data [*Criscitiello et al.*, 2013a;
293 2013b], likely due to a combination of the high accumulation rate and short length of the
294 time series.

295 Our data for the full DIV2010 record clearly show MSA migration from summer
296 to winter layers as well as decreased seasonality, with an abrupt shift occurring over the
297 period of a few years prior to 1977 (Figs. 5-7). This finding is in agreement with

298 previous studies that have shown post-depositional flattening of the annual signal, and
299 migration of MSA such that peaks in bulk MSA concentration adjust to coincide with
300 bulk concentrations of sea salt that were originally deposited at maximal concentrations
301 during winter months [*Pasteur and Mulvaney*, 2000; *Rempel et al.*, 2002]. MSA peaks in
302 summer from 1977–2010, but generally peaks in winter prior to 1977 in addition to
303 showing a flattening over the older part of the record (Fig. 7). This indicates that over the
304 earlier part of the record (prior to 1977) there is MSA loss, the seasonality is weaker, or a
305 combination of these two factors accounts for the observed shifts. As the climatological
306 mean remains constant before and after 1977, it is likely that MSA loss has not occurred
307 and that migration of MSA from summer towards winter layers accounts for the
308 flattening of the MSA curve prior to 1977 (Fig. 7). In contrast, the Na record reveals
309 consistent wintertime peaks with similar amplitudes for the duration of the record (Fig.
310 7).

311 We suggest the reason MSA migration occurs at 1977 likely is related to a change
312 in the physical properties of the firn at this depth (23 m), where it passes a density
313 threshold (~0.65 $g \cdot cm^{-3}$) indicative of a transition from convective layer to diffusive layer
314 [*Bender et al.*, 1997]. MSA migration results from intergranular diffusion between ice
315 grain surfaces, and is thus density dependent [*Rempel et al.*, 2002]; therefore this depth
316 and density in the DIV2010 core mark where grain boundary migration can begin to
317 occur.

318

319 *4.2 Long-term record of regional climate and Amundsen Sea sea-ice and polynya*
320 *variability*

321 In this section, we utilize glaciochemical proxies to reconstruct long-term records
322 of temperature, sea-ice, and polynya variability. As described above we use nssS (during
323 years with no significant global volcanic activity) as a proxy for MSA at THW2010 and
324 PIG2010, where MSA data are not available for the full record. We extrapolate previous
325 relationships observed over the satellite era between MSA and sea salts and SIC (both
326 general Amundsen Sea SIC and polynya variability) to infer meaning from long-term
327 glaciochemical records. In particular, monthly and summer MSA concentrations at
328 DIV2010 are significantly negatively correlated over the satellite era with monthly and
329 summer polynya SIC [*Criscitiello et al.*, 2013a]; we assume this relationship holds over
330 time, and that interannual and decadal maxima in DIV2010 MSA similarly indicate
331 Amundsen Sea and/or Pine Island Bay polynya opening. Also, monthly and winter
332 DIV2010 sea-salt concentrations are significantly positively correlated with monthly and
333 winter polynya SIC (indicative of sea-ice formation largely within the Amundsen Sea
334 polynya), and summer DIV2010 sea-salt concentrations are negatively correlated with
335 SIC in the coastal Amundsen Sea along 70°S, reflecting sea-ice production associated
336 with ice-edge advance [*Criscitiello et al.*, 2013a]; we likewise assume that these
337 relationships hold over time, and interannual to decadal maxima in DIV2010 Na indicate
338 increased polynya SIC and/or ice-edge advance along 70°S. PIG2010 and THW2010
339 interannual and decadal maxima in MSA and Na can be used to infer past Amundsen Sea
340 SIC and polynya variability, as the source and transport of marine aerosols to all sites
341 over the satellite era have been constrained [*Criscitiello et al.*, 2013b].
342 At DIV2010, the combined use of MSA, nssS, Na, and $\delta^{18}O$ records illuminate
343 several time periods of interest with respect to Amundsen Sea SIC and Amundsen Sea

344 and Pine Island Bay polynya variability. (A) Exceptionally high Na concentrations in the
345 1950's (Fig. 2) suggest that the 1950's were a decade marked by significant Amundsen
346 Sea polynya activity, and/or ice-edge advance in the Amundsen Sea along 70°S. (B)
347 Decadal records of $\delta^{18}O$ and Na at DIV2010 are significantly correlated (r = -0.4). The
348 highest $\delta^{18}O$ values coincident with low Na concentrations and average MSA and nssS
349 concentrations in the 1930's (Fig. 2) suggest that this time period was particularly warm
350 and SIC was low in the Amundsen Sea. (C) The highest DIV2010 MSA concentrations
351 occur in 1877, 1910, and 1995 (years with average nssS, Na, and $\delta^{18}O$ values; Fig. 2).
352 An increase in transport would have also increased the Na values during these time
353 periods. This suggests that while the 1877 elevated MSA values may indicate anomalous
354 events (e.g., years of enhanced polynya activity, substantial phytoplankton blooms), the
355 1990's MSA values may be indicative of a more global shift. The elevated MSA
356 concentrations in 1877 are coincident with a significant 50-year warming trend (1839–
357 1888) in Ellsworth Land, West Antarctica [*Thomas et al.*, 2013], supporting the
358 conclusion that this time period may have been one of enhanced polynya activity and
359 substantial phytoplankton blooms in the Amundsen Sea. Over the 1990s there was a
360 strengthening of the El Niño Southern Oscillation (ENSO) teleconnection to the high-
361 latitude South Pacific [*Fogt and Bromwich*, 2006]. The decadal glaciochemical results
362 from DIV2010 appear to capture this global shift.

363 The combined use of the glaciochemical records at PIG2010 highlights other
364 years of potentially significant SIC. (A) One of the highest Na concentrations over the
365 length of the record occurs in 1968, coincident with low $\delta^{18}O$ values and low MSA
366 concentrations (Fig. 3), indicative of cooler regional temperatures and high SIC in the

367 Amundsen Sea and near the leading ice edge (this relationship has been shown over the
368 satellite era [*Criscitiello et al.*, 2013b]). The amplitude of the decadal signal in nssS is
369 particularly high in the 1960's (Fig. 3) due to volcanic activity, which suggests that this
370 was a decade of cooling and above average Amundsen Sea SIC. 1950 also had high Na
371 concentrations concurrent with elevated nssS concentrations (Fig. 3), also seen at
372 DIV2010, indicative of significant winter sea-ice formation and polynya activity. The
373 1950's are discussed in Section 5.4 below in the context of global shifts. (C) Na and nssS
374 concentrations were particularly low in 1941 and 1998, coincident with the highest $\delta^{18}O$
375 values over the interannual record and highest decadal $\delta^{18}O$ averages (Fig. 3). The
376 decadal imprint on the PIG2010 $\delta^{18}O$ record is indicative of warmer temperatures and
377 low SIC likely linked to large-scale atmospheric variability. (D) While the MSA record
378 is short (1993–2010), particularly high MSA concentrations in 1993 and 2010 suggest
379 that during these years the polynyas may have been particularly active. A recent study
380 over 2002–2010 confirms that 2010 was a year with particularly low SIC and high
381 polynya activity [*Criscitiello et al.*, 2013]. However, the DIV2010 MSA record does not
382 show elevated concentrations in 1993 or 2010, so it is likely that polynya activity cannot
383 be deduced from the PIG2010 MSA record due to its short length. We are also cautious
384 about using the PIG2010 MSA data as a proxy for Amundsen Sea polynya variability as
385 the Weddell Sea also influences PIG2010 records [*Criscitiello et al.*, 2013b].

386 Finally, the glaciochemical records at THW2010 highlight several periods of
387 interest with respect to SIC. (A) The years with the highest interannual and decadal Na
388 values have below average interannual $\delta^{18}O$ values (1921, 1943, and 1975), and below
389 average decadal $\delta^{18}O$ values except for the 1940's (Fig. 4). Decadal records of $\delta^{18}O$ and

390 Na at THW2010 are significantly correlated (r = -0.4). These results indicate that the
391 1921 and 1975 $\delta^{18}O$ anomalies may have been the result of local variability (e.g., cooler
392 temperatures and intense sea-ice formation within the polynyas and/or in the Amundsen
393 Sea along 70°S), however the 1943 Na spike may be somewhat anomalous (related to a
394 short-term shift in transport or moisture source), as the 1940's were a warm decade. (B)
395 The highest interannual and decadal $\delta^{18}O$ values at THW2010 occur in 1878, 1941, and
396 1998, concurrent with low interannual and decadal Na values (Fig. 4). These are the
397 same decades that PIG2010 had the highest $\delta^{18}O$ values, and as noted above, the high
398 1878 $\delta^{18}O$ values are coincident with some of the highest $\delta^{18}O$ values from a 308-year
399 record at Ellsworth Land (1702–2009; *Thomas et al.*, 2013). This result indicates that the
400 1870's, 1940's, and 1990's were particularly warm years with lower than average
401 Amundsen Sea SIC, likely driven by large-scale atmospheric variability. (C) The highest
402 MSA concentrations occur in 1976 and 1995; MSA concentrations at DIV2010 were also
403 particularly high in 1995. The amplitude of the decadal Na signal was high in the 1970's,
404 and the amplitude of the decadal $\delta^{18}O$ signal was high in the 1990's. These years likely
405 experienced enhanced Amundsen Sea and Pine Island Bay polynya activity accounting
406 for the elevated MSA concentrations; the 1970's may additionally have been a period of
407 change in predominant moisture source region to THW2010, accounting for the high
408 decadal Na values (Fig. 4).

409 MSA and nssS records at all sites together indicate an increase in polynya activity
410 over the past ~ 200 years (1877, 1910, 1950, 1976, 1993, 1995, and 2010 are indicated as
411 years of unusually enhanced polynya activity). Enhanced polynya activity is driven in
412 part by wind forcing that is controlled primarily by the position of the Amundsen Sea

413 Low (ASL), thus increased polynya activity is consistent with an intensification of the
414 ASL over this time period. The intensification of the ASL has been linked to observed
415 Amundsen Sea sea-ice decline and warming SSTs over recent decades [*Kwok and*
416 *Comiso*, 2002], as well as proposed as a mechanism to explain longer-term decline in
417 Bellingshausen Sea sea ice over the 20th century [*Abram et al.*, 2010]. A strengthening of
418 meridional winds (onshore northerlies; 50–70°S, 100–140°W) during warmer periods
419 since the early 1700s [*Thomas et al.*, 2013] suggest that meridional winds in the
420 Amundsen Sea may strongly influence interannual temperature variability across West
421 Antarctica. In agreement, seasonal analysis of $\delta^{18}O$ records from the ITASE ice cores in
422 West Antarctica has shown that for all seasons, elevated $\delta^{18}O$ values are related to
423 enhanced meridional (onshore) flow [*Kuttel et al.*, 2012]. Intensification of the ASL and
424 increases in meridional winds, therefore, would be consistent with an increase in polynya
425 activity over the past ~200 years. This increase in polynya activity may have critical
426 implications for outlet glacier thinning and speeds, as recent model-based results have
427 shown a negative correlation between polynya area and ice-shelf melting [*Khazendar et*
428 *al.*, 2013].
429
430 *4.3 Southern hemisphere teleconnection to the tropical Pacific*
431 At all three sites, regression analysis of low-pass filtered SLP and SST (from
432 HadISST1 and HadSLP2r data) on low-pass filtered Na and $\delta^{18}O$ reveal a decadal
433 teleconnection between West Antarctica and the tropical Pacific via a Rossby wave train.
434 The impact of tropical Pacific dynamics on West Antarctic climate resulting from a
435 Rossby wave teleconnection has been well studied on seasonal to interannual timescales

436 [*Ding et al.*, 2011; *Criscitiello et al.*, 2013b]; this is one of the first studies to show that
437 such a teleconnection exists on decadal timescales. Comparison of a δD record from
438 Ellsworth Land with several proxy records from the central and west Pacific suggests that
439 the tropical teleconnection has persisted over longer (several hundred year) timescales
440 [*Thomas et al.*, 2013]. Further, recent model ensembles of high latitude climate
441 variability have shown that the mechanisms linking climate in the Pacific with that of
442 coastal West Antarctica have remained stable during the past 500 years [*Wilmes et al.*,
443 2012].

444 Regression of SST on Na at DIV2010 reveals a horseshoe pattern in both
445 hemispheres; the northern hemisphere horseshoe pattern is likely associated with the
446 Pacific Decadal Oscillation (PDO) [*Mantua et al.*, 1997], which has been previously
447 shown with regressions of SST on oxygen isotope records from West Antarctica
448 [*Okumura et al.*, 2012]. PIG2010 and THW2010 regressions of SLP on all
449 glaciochemical records except Na reveal a SAM-like pattern. These regression analyses
450 suggest that decadal variability in marine aerosol and oxygen isotope records from the
451 Amundsen Coast are linked with tropical Pacific SST anomalies. Interestingly, there are
452 no significant correlations between the annual SST time series (10°N to 10°S, 140°W to
453 80°W) and any annual glaciochemical record from the three core sites. Though not
454 significant at $p < 0.05$, the highest correlation between the SST time series and any
455 glaciochemical record is with the THW2010 Na record (r = -0.24). At all sites,
456 correlation of the SST time series with Na and $\delta^{18}O$ are much higher than correlations
457 with MSA or nssS. These results confirm what the spatial regression maps suggest (Figs.
458 12-14); Na and $\delta^{18}O$ are more influenced by remote atmospheric dynamics than marine

biogenic compounds, which are more influenced by local dynamics (e.g., polynya variability). The SST time series results also indicate that THW2010 is most strongly influenced by tropical Pacific dynamics.

The presence or absence of volcanic markers in our cores may offer additional insight into spatial variability of atmospheric transport. The nssS record at DIV2010 stands out, as it is the only record that shows nssS peaks concurrent with volcanic eruptions in 1810 and 1816, but no nssS peaks during volcanic activity since then. These are two of the largest volcanic eruptions in recorded history. Ice cores from both poles show evidence of a large volcanic eruption in 1810 (unknown source), with a magnitude roughly half the magnitude of Mt. Tambora [*D'Arrigo et al.*, 2009]. This contributed to the 1810's being the coldest decade in ~500 years [*D'Arrigo et al.*, 2009]. The eruption of Mt. Tambora (Indonesia) in 1816 was the largest volcanic eruption in recorded history [*Oppenheimer*, 2003]. The presence of nssS peaks in the DIV2010 record only during these very large volcanic events, and the lack of nssS peaks in the DIV2010 record during the more recent smaller volcanic events, suggests that the DIV2010 site may be more affected by local dynamics than the other two sites, as a previous study focusing on the 1979–2010 part of this record has shown [*Criscitiello et al.*, 2013b].

The PIG2010 and THW2010 cores have nssS peaks coincident with the more recent volcanic eruptions: 1885 (Krakatoa, Indonesia), 1928 (Hokkaido Komagatake, Japan), 1964 (Mt. Agung, Indonesia), and 1992 (Mt. Spurr, AK). The 1964 and 1992 volcanic events show up in both records, while the 1928 eruption of Hokkaido Komagatake only shows up in the THW2010 nssS record. These results suggest that of the three sites, THW2010 may be most influenced by remote atmospheric dynamics.

482 This is in agreement with previous work that has shown over the 1979–2010 time period
483 that the THW2010 isotope record is least affected by local polynya variability, and
484 instead is strongly influenced by broad offshore moisture source regions largely in the
485 Amundsen Sea, and remote atmospheric dynamics [*Criscitiello et al.*, 2013b; *Criscitiello*
486 *et al.*, in prep].
487
488 *4.4 Decadal atmospheric transport, sea-ice, and polynya variability and relation to*
489 *recently observed changes in ice-sheet behavior*
490 Decadal variability in sea-ice and polynya activity is directly related to changes in
491 ocean heat transport and Southern Ocean dynamics. The oceanic influence on the Pine
492 Island Glacier ice shelf is determined by the properties and circulation of Circumpolar
493 Deep Water (CDW) on the continental shelf [*Walker et al.*, 2007]. Interannual changes
494 in regional winds, which are controlled by the position of the ASL, lead to decadal
495 variability in the influx of CDW to the Amundsen Coast [*Thoma et al.*, 2008]. This wind
496 forcing also exerts a primary control on polynya variability over the satellite era
497 [*Criscitiello et al.*, 2013b], and thus wind variability should also impact polynya activity
498 over longer timescales. This is evident in our results, which show strong decadal
499 variability in MSA due to polynya variability, and strong decadal variability in Na which
500 is linked to both general Amundsen Sea sea-ice formation and sea-ice formation within
501 the polynyas [*Criscitiello et al.*, 2013a]. Recent model-based work has illustrated a
502 negative correlation between polynya size and ice-shelf melting rates at Totten Glacier,
503 Antarctica, as a result of enhanced basal melting caused by a decrease in cold polynya
504 water reaching the ice-shelf cavity when polynya size in reduced [*Khazendar et al.*,

505 2013]. This mechanism may contribute significantly to ice-shelf instability, and is
506 therefore crucial in regions such as Pine Island and Thwaites Glaciers.

507 There are two decades in which the multi-site, multi-record decadal anomalies
508 shed additional insight into regional climate. (1) The 1950's include some of the highest
509 interannual and decadal Na values at both DIV2010 and PIG2010, during times of
510 relatively low $\delta^{18}O$ values, suggesting that the 1950's were a decade marked by cooling
511 temperatures, ice-edge advance in the Amundsen Sea along 70°S and/or enhanced
512 wintertime Amundsen Sea polynya activity. In contrast, the THW2010 record in the
513 1950's shows no Na maxima. This is consistent with previous results that have shown
514 THW2010 sea-salt source regions may differ from DIV2010 and PIG2010 on seasonal to
515 interannual timescales [*Criscitiello et al.*, 2013b]. (2) The 1990's contain some of the
516 highest interannual and decadal $\delta^{18}O$ values at PIG2010 and THW2010, elevated $\delta^{18}O$
517 values at DIV2010 (though not the highest of record) and the highest interannual and
518 decadal MSA values at DIV2010 and THW2010 (PIG2010 MSA record is not
519 sufficiently long to compare here). These records suggest the 1990s were a decade
520 marked by warmer temperatures, increased polynya activity, and low SIC in the
521 Amundsen Sea.

522 The 1990's are of particular interest, as previous work has shown rapid melting of
523 the buttressing ice shelves of Pine Island Glacier and rapid acceleration of Pine Island
524 Glacier over this decade. This behavior is thought to be due to increased sub-ice-shelf
525 circulation and warming of CDW on the Amundsen Sea continental shelf [*Jacobs et al.*,
526 2011; *Jenkins et al.*, 2010]. This time period was preceded by a period of near-steady ice
527 flow [*Joughin et al.*, 2003], which corresponded to the weakest inflow of CDW to the

528 shelf and lowest water column heat content [*Thoma et al.*, 2008]. Increases in CDW
529 input to Pine Island Bay are thought to drive the observed glaciological changes over the
530 satellite era; for example, dynamically induced ice thickness changes have been shown to
531 propagate inland on decadal timescales [*Payne et al.*, 2004]. These fluctuations in CDW
532 input are in turn driven by decadal variability in large-scale atmospheric circulation (e.g.,
533 phasing of ENSO and SAM) [*Fogt and Bromwich*, 2006]. While increases in CDW input
534 to Pine Island Bay are an important driver of observed glaciological changes over the
535 satellite era, polynya varaiability in this region may also directly influence Pine Island
536 and Thwaites Glacier thinning and acceleration rates (as recently shown for Totten
537 Glacier in Khazendar et al. [2013]). The trends observed in our records over the 1990's
538 (warming temperatures, increased polynya activity, low SIC in the Amundsen Sea) are
539 consistent with dynamical ice-sheet changes observed over this same time period driven
540 by increased sub-ice-shelf circulation and warming of CDW on the Amundsen Sea
541 continental shelf.
542
543 **5. Conclusions**
544 In this study we used MSA, nssS, Na, and $\delta^{18}O$ records from three new coastal,
545 high-resolution firn cores from the Amundsen Coast of West Antarctica to investigate
546 decadal climate variability from 1786–2010. These glaciochemical records were also
547 used to investigate long-term changes in sea-ice and polynya variability in the Amundsen
548 Sea. Our key findings are that: (1) Na and $\delta^{18}O$ records at all sites are more influenced
549 by remote atmospheric dynamics than records of marine biogenic compounds, which are
550 more influenced by local dynamics (e.g., sea-ice and polynya variability), (2) of all three

551 sites, THW2010 is most strongly influenced by remote, tropical Pacific dynamics, (3) the
552 1870's, 1930/40's, and 1990's were likely some of the regionally warmest years over the
553 length of our records, with low SIC in the Amundsen Sea, (4) the 1920's and 1960/70's
554 were likely some of the regionally coldest years over the length of our records, with high
555 SIC in the Amundsen Sea, (5) MSA and nssS records indicate that 1877, 1910, 1950,
556 1976, 1993, 1995, and 2010 were likely years of unusually enhanced polynya activity.
557 Remote atmospheric dynamics drive local fluctuations in winds and CDW influx to the
558 Amundsen Coast, which in turn lead to strong decadal variability in coastal West
559 Antarctic marine aerosol records.
560
561 **Acknowledgements**
562 Thanks to Lou Albershardt, Howard Conway, and RPSC support staff for
563 assistance in the field. Thanks to Luke Trusel, Twila Moon, and NICL staff for
564 assistance processing the cores, and DRI staff for continuous melter analyses. This
565 research was supported by an award from the Department of Energy Office of Science
566 Graduate Fellowship Program (DOE SCGF) to ASC, and by grants from NSF-OPP
567 (#ANT-0632031 & #ANT-0631973); NSF-MRI (#EAR-1126217); NASA Cryosphere
568 Program (#NNX10AP09G); and a WHOI Andrew W. Mellon Foundation Award for
569 Innovative Research.
570
571 **References**
572 Abram, N. J., E. R. Thomas, J. R. McConnell, R. Mulvaney, T. J. Bracegirdle, L. C.
573 Sime, and A. J. Aristarain (2010), Ice core evidence for a 20th century decline of
574 sea ice in the Bellingshausen Sea, Antarctica, J. Geophys. Res., 115(D23),
575 D23101.

576 Abram, N. J., R. Mulvaney, and C. Arrowsmith (2011), Environmental signals in a highly
577 resolved ice core from James Ross Island, Antarctica, J. Geophys. Res.,
578 *116*(D20), D20116.
579 Abram, N. J., E. W. Wolff, and M. A. J. Curran (2013), A review of sea ice proxy
580 information from polar ice cores, Quaternary Science Reviews.
581 Allan, R., and T. Ansell (2006), A new globally complete monthly historical gridded
582 mean sea level pressure dataset (HadSLP2): 1850–2004, Journal of Climate,
583 19(22), 5816-5842.
584 Artaxo, P., M. L. C. Rabello, W. Maenhaut, and R. V. Grieken (1992), Trace elements
585 and individual particle analysis of atmospheric aerosols from the Antarctic
586 peninsula, Tellus B, 44(4), 318-334.
587 Bender, M., T. Sowers, and E. Brook (1997), Gases in ice cores, Proceedings of the
588 National Academy of Sciences, 94(16), 8343-8349.
589 Bromwich, D. H., J. P. Nicolas, A. J. Monaghan, M. A. Lazzara, L. M. Keller, G. A.
590 Weidner, and A. B. Wilson (2012), Central West Antarctica among the most
591 rapidly warming regions on Earth, Nature Geosci, 6, 139-145.
592 Comiso, J. C. (2008), Accelerated decline in the Arctic sea ice cover, Geophysical
593 research letters, 35(1), L01703.
594 Criscitiello, A. S., S. B. Das, M. J. Evans, K. E. Frey, H. Conway, I. Joughin, B. Medley,
595 and E. J. Steig (2013a), Ice sheet record of recent sea-ice behavior and polynya
596 variability in the Amundsen Sea, West Antarctica, Journal of Geophysical
597 Research: Oceans, 118(1), 118-130.
598 Criscitiello, A.S., S. B. Das, K. Karnauskas, M. J. Evans, K. E. Frey, I. Joughin, E. Steig,
599 J. McConnell, and B. Medley (2013b), Tropical Pacific influence on source and
600 transport of marine aerosols to West Antarctica, J. Clim., in press.
601 Criscitiello, A.S., S. B. Das, I. Joughin, E. J. Steig, M. R. van den Broeke, J. T. M.
602 Lenaerts, and J. McConnell (in prep), Regional and remote climatic influences on
603 stable isotope records from high accumulation sites in West Antarctica.
604 Curran, M. A. J., and A. S. Palmer (2001), Suppressed ion chromatography methods for
605 the routine determination of ultra low level anions and cations in ice cores,
606 Journal of Chromatography A, 919(1), 107-113.
607 Curran, M. A. J., A. S. Palmer, T. D. Van Ommen, V. I. Morgan, K. L. Phillips, A. J.
608 McMorrow, and P. A. Mayewski (2002), Post-depositional movement of
609 methanesulphonic acid at Law Dome, Antarctica, and the influence of
610 accumulation rate, Annals of Glaciology, 35(1), 333-339.
611 D'Arrigo, R., R. Wilson, and A. Tudhope (2009), The impact of volcanic forcing on
612 tropical temperatures during the past four centuries, Nature Geosci, 2(1), 51-56.
613 Dacey, J. W. H., and S. G. Wakeham (1986), Oceanic dimethylsulfide: Production during
614 zooplankton grazing on phytoplankton, Science, 233(4770), 1314-1316.
615 Dieckmann, G. S., and H. H. Hellmer (2010), The importance of sea ice: an overview,
616 Sea Ice, 2, 1-22.
617 Ding, Q., E. J. Steig, D. S. Battisti, and M. Kuttel (2011), Winter warming in West
618 Antarctica caused by central tropical Pacific warming, Nature Geosci, 4(6), 398-
619 403.

620 Fogt, R. L., and D. H. Bromwich (2006), Decadal variability of the ENSO teleconnection
621 to the high-latitude South Pacific governed by coupling with the Southern
622 Annular Mode, Journal of Climate, 19(6), 979-997.
623 Gibson, J. A. E., R. C. Garrick, H. R. Burton, and A. R. McTaggart (1990),
624 Dimethylsulfide and the alga Phaeocystis pouchetii in Antarctic coastal waters,
625 Marine Biology, 104(2), 339-346.
626 Gille, S. T. (2008), Decadal-scale temperature trends in the southern hemisphere ocean,
627 Journal of Climate, 21(18), 4749-4765.
628 Hillenbrand, C.-D., et al. (2013), Grounding-line retreat of the West Antarctic Ice Sheet
629 from inner Pine Island Bay, Geology, 41(1), 35-38.
630 Hoskins, B. J., and D. J. Karoly (1981), The steady linear response of a spherical
631 atmosphere to thermal and orographic forcing, Journal of the Atmospheric
632 Sciences, 38(6), 1179-1196.
633 Jacobs, S. (2006), Observations of change in the Southern Ocean, Philosophical
634 Transactions of the Royal Society A, 364(1844), 1657-1681.
635 Jacobs, S., A. Jenkins, C. F. Giulivi, and P. Dutrieux (2011), Stronger ocean circulation
636 and increased melting under Pine Island Glacier ice shelf, Nature Geosci, 4(8),
637 519-523.
638 Jenkins, A., P. Dutrieux, S. S. Jacobs, S. D. McPhail, J. R. Perrett, A. T. Webb, and D.
639 White (2010), Observations beneath Pine Island Glacier in West Antarctica and
640 implications for its retreat, Nature Geosciences, 3(7), 468-472.
641 Joughin, I., B. E. Smith, and D. M. Holland (2010), Sensitivity of 21st century sea level
642 to ocean-induced thinning of Pine Island Glacier, Antarctica, Geophys. Res. Lett.,
643 37(20), L20502.
644 Joughin, I., E. Rignot, C. E. Rosanova, B. K. Lucchitta, and J. Bohlander (2003), Timing
645 of recent accelerations of Pine Island Glacier, Antarctica, Geophys. Res. Lett.,
646 30(13), 1706.
647 Khazendar, A., M. P. Schodlok, I. Fenty, S. R. M. Ligtenberg, E. Rignot, and M. R. van
648 den Broeke (2013), Observed thinning of Totten Glacier is linked to coastal
649 polynya variability, Nat Commun, 4.
650 Kreutz, K. J., and P. A. Mayewski (1999), Spatial variability of Antarctic surface snow
651 glaciochemistry: implications for palaeoatmospheric circulation reconstructions,
652 Antarctic Science, 11(01), 105-118.
653 Küttel, M., E. Steig, Q. Ding, A. Monaghan, and D. Battisti (2012), Seasonal climate
654 information preserved in West Antarctic ice core water isotopes: relationships to
655 temperature, large-scale circulation, and sea ice, Climate Dynamics, 39(7-8),
656 1841-1857.
657 Kwok, R., and J. C. Comiso (2002), Southern Ocean climate and sea ice anomalies
658 associated with the Southern Oscillation, Journal of Climate, 15(5), 487-501.
659 Lee, S., T. Gong, N. Johnson, S. B. Feldstein, and D. Pollard (2011), On the possible link
660 between tropical convection and the northern hemisphere Arctic surface air
661 temperature change between 1958 and 2001, Journal of Climate, 24(16), 4350-
662 4367.
663 Legrand, M., and C. F. Saigne (1991), Methanesulfonic acid in south polar snow layers:
664 A record of strong El Nino?, Geophysical research letters, 18(2), 187-190.

665 Lythe, M. B., and D. G. Vaughan (2001), BEDMAP: A new ice thickness and subglacial
666 topographic model of Antarctica, Journal of Geophysical Research: Solid Earth,
667 106(B6), 11335-11351.
668 Mantua, N. J., S. R. Hare, Y. Zhang, J. M. Wallace, and R. C. Francis (1997), A Pacific
669 interdecadal climate oscillation with impacts on salmon production, Bulletin of
670 the American Meteorological Society, 78(6), 1069-1079.
671 Maselli, O., D. Fritzche, L. Layman, J. McConnell, and H. Meyer (2013), Comparison of
672 water isotope ratio determinations using two cavity ring-down instruments and
673 classical mass spectrometry in continuous ice-core analysis, Isotopes in
674 Environmental and Health Studies, in press.
675 Mayewski, P. A., et al. (2009), State of the Antarctic and Southern Ocean climate system,
676 Rev. Geophys., 47(1), RG1003.
677 McConnell, J. R., G. W. Lamorey, S. W. Lambert, and K. C. Taylor (2001), Continuous
678 ice-core chemical analyses using inductively coupled plasma mass spectrometry,
679 Environmental Science & Technology, 36(1), 7-11.
680 Medley, B., et al. (2013), Airborne-radar and ice-core observations of annual snow
681 accumulation over Thwaites Glacier, West Antarctica confirm the spatiotemporal
682 variability of global and regional atmospheric models, Geophysical research
683 letters, 40(14), 3649-3654.
684 Mulvaney, R., E. C. Pasteur, D. A. Peel, E. S. Saltzman, and P.-Y. Whung (1992), The
685 ratio of MSA to non-sea-salt sulphate in Antarctic Peninsula ice cores, Tellus B,
686 44(4), 295-303.
687 Okumura, Y. M., D. Schneider, C. Deser, and R. Wilson (2012), Decadal–interdecadal
688 climate variability over Antarctica and linkages to the tropics: Analysis of ice
689 core, instrumental, and tropical proxy data, Journal of Climate, 25(21), 7421-
690 7441.
691 Oppenheimer, C. (2003), Climatic, environmental and human consequences of the largest
692 known historic eruption: Tambora volcano (Indonesia) 1815, Progress in Physical
693 geography, 27(2), 230-259.
694 Parish, T. R., and D. H. Bromwich (1987), The surface windfield over the Antarctic ice
695 sheets, Nature, 328(6125), 51-54.
696 Parizek, B. R., et al. (2013), Dynamic (in)stability of Thwaites Glacier, West Antarctica,
697 Journal of Geophysical Research: Earth Surface, 118(2), 638-655.
698 Park, J. W., N. Gourmelen, A. Shepherd, S. W. Kim, D. G. Vaughan, and D. J. Wingham
699 (2013), Sustained retreat of the Pine Island Glacier, Geophysical research letters,
700 40(10), 2137-2142.
701 Pasteris, D., J. McConnell, S. B. Das, A. S. Criscitiello, M. J. Evans, O. Maselli, M. Sigl,
702 and L. Layman (in revision), Seasonal ice core records yield insight into past sea
703 ice conditions and sources of major ion species to West Antarctica, Journal of
704 Geophysical Research: Atmospheres.
705 Pasteur, E. C., and R. Mulvaney (2000), Migration of methane sulphonate in Antarctic
706 firn and ice, J. Geophys. Res., 105(D9), 11525-11534.
707 Payne, A. J., A. Vieli, A. P. Shepherd, D. J. Wingham, and E. Rignot (2004), Recent
708 dramatic thinning of largest West Antarctic ice stream triggered by oceans,
709 Geophysical research letters, 31(23), L23401.

710 Rankin, A. M., E. W. Wolff, and S. Martin (2002), Frost flowers: Implications for
711 tropospheric chemistry and ice core interpretation, J. Geophys. Res., 107(D23),
712 4683.
713 Rayner, N. A., D. E. Parker, E. B. Horton, C. K. Folland, L. V. Alexander, D. P. Rowell,
714 E. C. Kent, and A. Kaplan (2003), Global analyses of sea surface temperature, sea
715 ice, and night marine air temperature since the late nineteenth century, Journal of
716 Geophysical Research: Atmospheres, 108(D14), 4407.
717 Rempel, A. W., J. S. Wettlaufer, and E. D. Waddington (2002), Anomalous diffusion of
718 multiple impurity species: Predicted implications for the ice core climate records,
719 Journal of Geophysical Research: Solid Earth, 107(B12), 2330.
720 Rignot, E. (2001), Evidence for rapid retreat and mass loss of Thwaites Glacier, West
721 Antarctica, Journal of Glaciology, 47(157), 213-222.
722 Rignot, E., I. Velicogna, M. R. van den Broeke, A. Monaghan, and J. Lenaerts (2011),
723 Acceleration of the contribution of the Greenland and Antarctic ice sheets to sea
724 level rise, Geophys. Res. Lett., 38(5), L05503.
725 Rignot, E., J. L. Bamber, M. R. van den Broeke, C. Davis, Y. Li, W. J. van de Berg, and
726 E. van Meijgaard (2008), Recent Antarctic ice mass loss from radar
727 interferometry and regional climate modelling, Nature Geosciences, 1(2), 106-
728 110.
729 Rintoul, S. R. (2007), Rapid freshening of Antarctic Bottom Water formed in the Indian
730 and Pacific Oceans, Geophys. Res. Lett., 34(6), L06606.
731 Robertson, R., M. Visbeck, A. L. Gordon, and E. Fahrbach (2002), Long-term
732 temperature trends in the deep waters of the Weddell Sea, Deep Sea Research Part
733 II: Topical Studies in Oceanography, 49(21), 4791-4806.
734 Stanton, T. P., W. J. Shaw, M. Truffer, H. F. J. Corr, L. E. Peters, K. L. Riverman, R.
735 Bindschadler, D. M. Holland, and S. Anandakrishnan (2013), Channelized ice
736 melting in the ocean boundary layer beneath Pine Island Glacier, Antarctica,
737 Science, 341(6151), 1236-1239.
738 Thoma, M., A. Jenkins, D. Holland, and S. Jacobs (2008), Modelling Circumpolar Deep
739 Water intrusions on the Amundsen Sea continental shelf, Antarctica, Geophysical
740 research letters, 35(18), L18602.
741 Thomas, E. R., T. J. Bracegirdle, J. Turner, and E. W. Wolff (2013), A 308 year record of
742 climate variability in West Antarctica, Geophysical research letters, 40(20),
743 L057782.
744 Trenberth, K. E., G. W. Branstator, D. Karoly, A. Kumar, N.-C. Lau, and C. Ropelewski
745 (1998), Progress during TOGA in understanding and modeling global
746 teleconnections associated with tropical sea surface temperatures, J. Geophys.
747 Res., 103(C7), 14291-14324.
748 Turner, J., T. A. Lachlan-Cope, S. Colwell, G. J. Marshall, and W. M. Connolley (2006),
749 Significant warming of the Antarctic winter troposphere, Science, 311(5769),
750 1914-1917.
751 Turner, J., J. C. Comiso, G. J. Marshall, Lachlan, T. A. Cope, T. Bracegirdle, T. Maksym,
752 M. P. Meredith, Z. Wang, and A. Orr (2009), Non-annular atmospheric
753 circulation change induced by stratospheric ozone depletion and its role in the
754 recent increase of Antarctic sea ice extent, Geophys. Res. Lett., 36(8), L08502.

Walker, D. P., M. A. Brandon, A. Jenkins, J. T. Allen, J. A. Dowdeswell, and J. Evans (2007), Oceanic heat transport onto the Amundsen Sea shelf through a submarine glacial trough, Geophysical research letters, 34(2), L02602.

Weller, R., F. Traufetter, H. Fischer, H. Oerter, C. Piel, and H. Miller (2004), Postdepositional losses of methane sulfonate, nitrate, and chloride at the European Project for Ice Coring in Antarctica deep-drilling site in Dronning Maud Land, Antarctica, J. Geophys. Res., 109(D7), D07301.

Wilmes, S. B., C. C. Raible, and T. F. Stocker (2012), Climate variability of the mid- and high-latitudes of the Southern Hemisphere in ensemble simulations from 1500 to 2000 AD, Clim. Past, 8(1), 373-390.

Wingham, D. J., D. W. Wallis, and A. Shepherd (2009), Spatial and temporal evolution of Pine Island Glacier thinning, 1995-2006, Geophys. Res. Lett., 36(17), L17501.

Wolff, E. W., A. M. Rankin, and R. Röthlisberger (2003), An ice core indicator of Antarctic sea ice production?, Geophys. Res. Lett., 30(22), 2158.

771 **Figures**
772

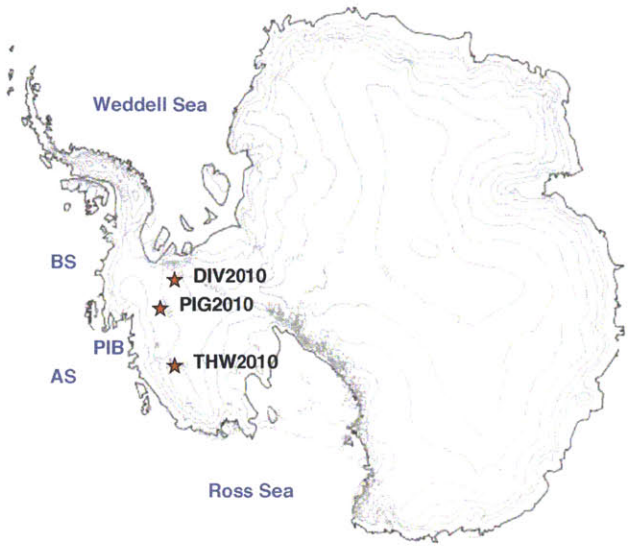

773
774 **Figure 1.** Location of our three firn-core sites (red stars). 500 m contour intervals shown
775 in grey. Blue words indicate important regions discussed (AS = Amundsen Sea, BS =
776 Bellingshausen Sea, PIB = Pine Island Bay).
777

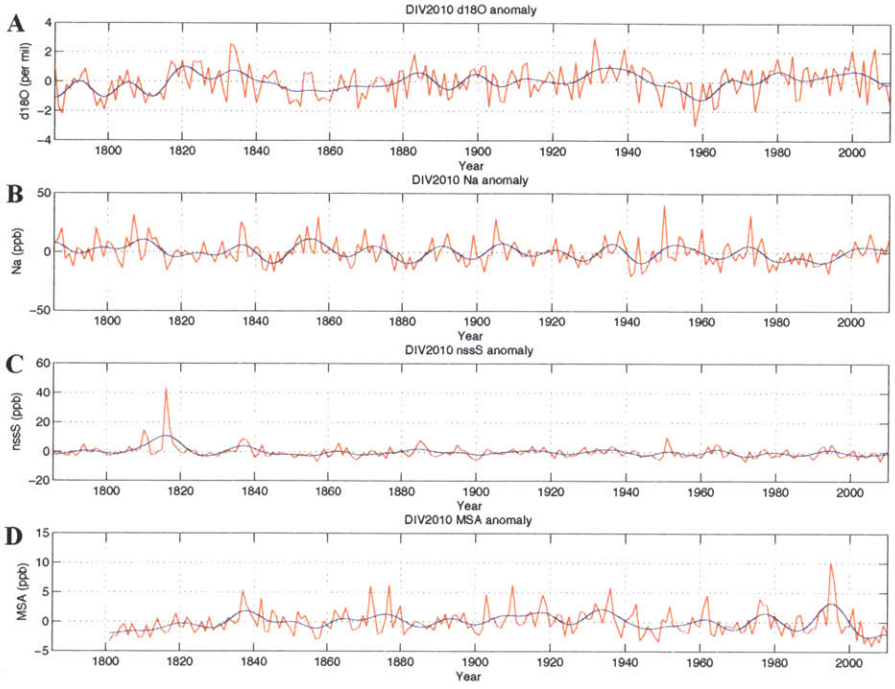

Figure 2. DIV2010 annual anomalies of (A) $\delta^{18}O$, (B) Na, (C) nssS, and (D) MSA (red). Low-pass filtered time series are shown in blue. $\delta^{18}O$, Na, and nssS data are from 1786–2010, and MSA data are from 1801–2010. All data are presented on the DIV2010 timescale (1786–2010).

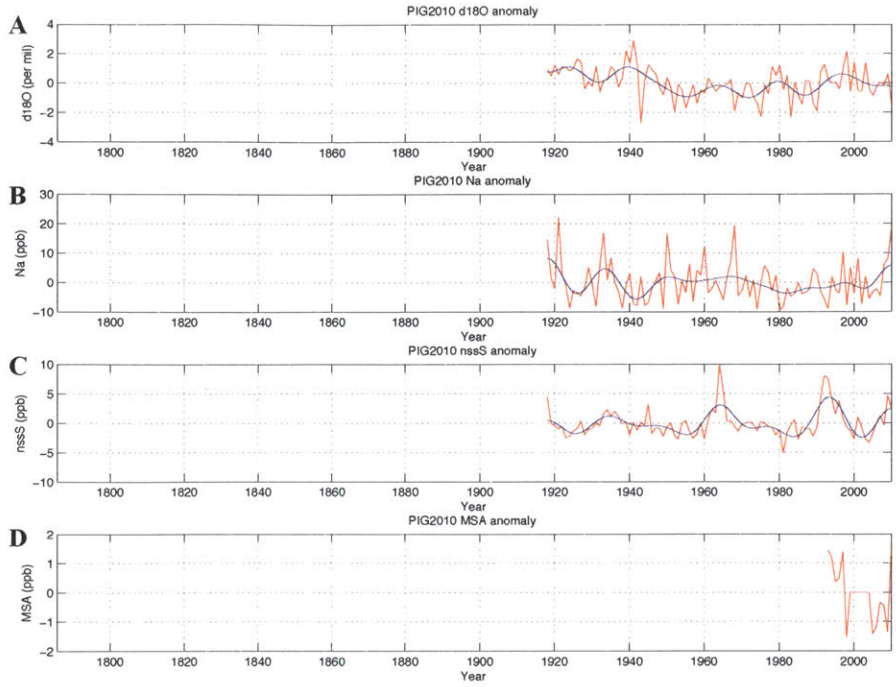

786
787 **Figure 3.** PIG2010 annual anomalies of (A) $\delta^{18}O$, (B) Na, (C) nssS, and (D) MSA (red).
788 Low-pass filtered time series are shown in blue. $\delta^{18}O$, Na, and nssS data are from 1918–
789 2010, and MSA data are from 1993–2010. All data are presented on the DIV2010
790 timescale (1786–2010).
791

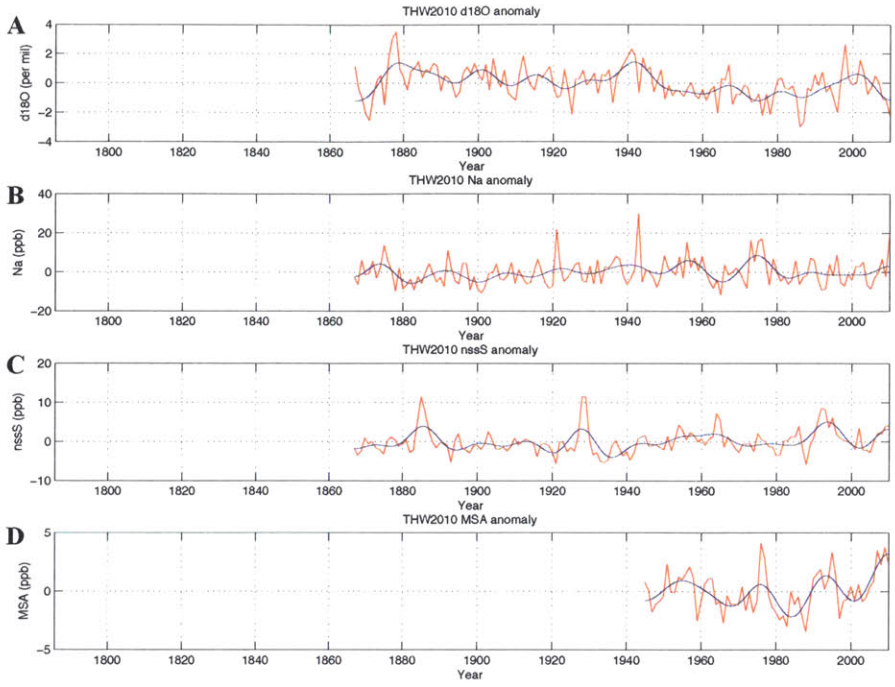

792
793 **Figure 4.** THW2010 annual anomalies of (A) $\delta^{18}O$, (B) Na, (C) nssS, and (D) MSA
794 (red). Low-pass filtered time series are shown in blue. $\delta^{18}O$, Na, and nssS data are from
795 1867–2010, and MSA data are from 1945–2010. All data are presented on the DIV2010
796 timescale (1786–2010).
797

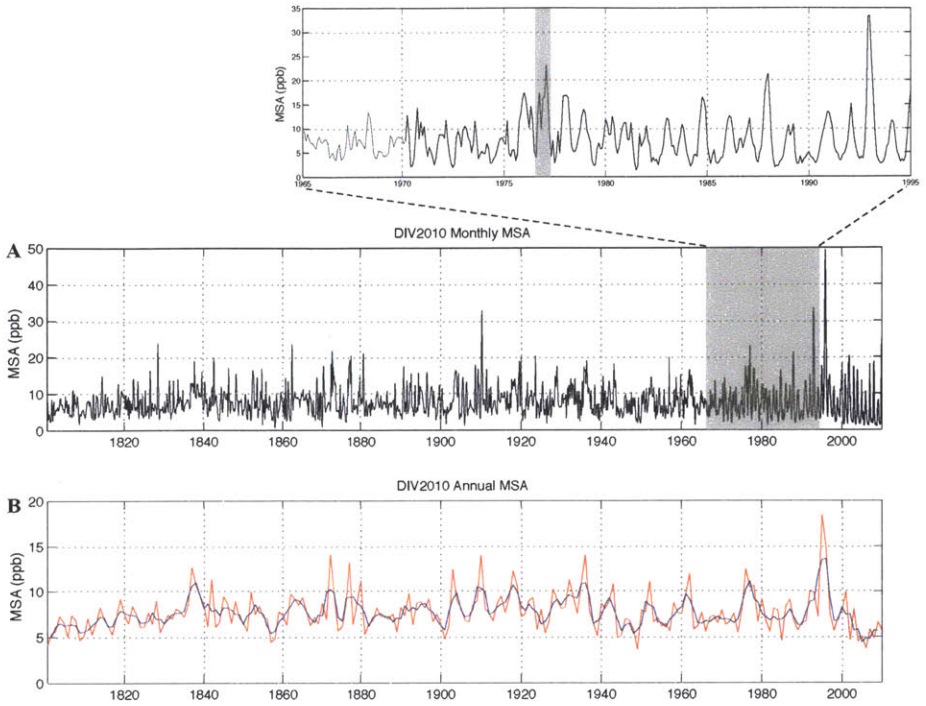

798
799 **Figure 5.** (A) DIV2010 monthly MSA concentrations 1801–2010 (black solid line), with
800 the time period of transition to MSA migration centered around 1977 shown by grey
801 shading and enlarged in the panel above (1965–1995 shown in enlarged upper panel). (B)
802 DIV2010 annual MSA concentrations (red) shown with a 3-year running mean (blue).
803

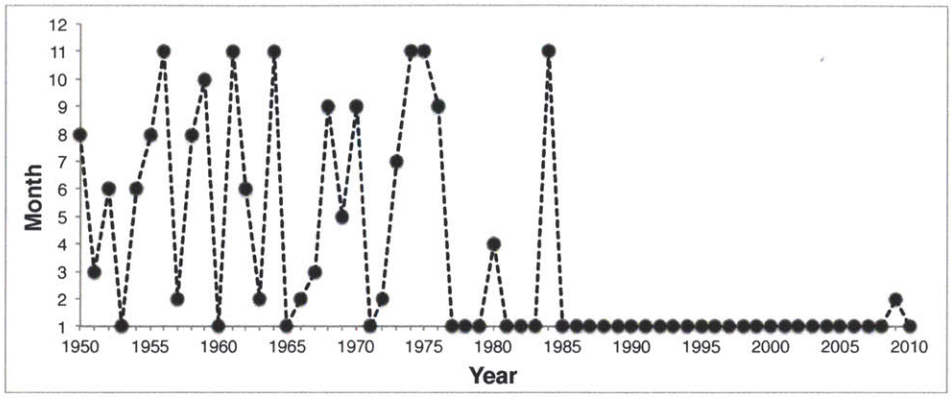

Figure 6. Annual time series of the month of maximum MSA at DIV2010, 1950–2010. An abrupt shift in month of maximum MSA is seen at 1977. Before 1977, MSA consistently peaks in January (austral summer); after 1977 the MSA peak generally migrates toward winter months, and peak timing becomes more variable.

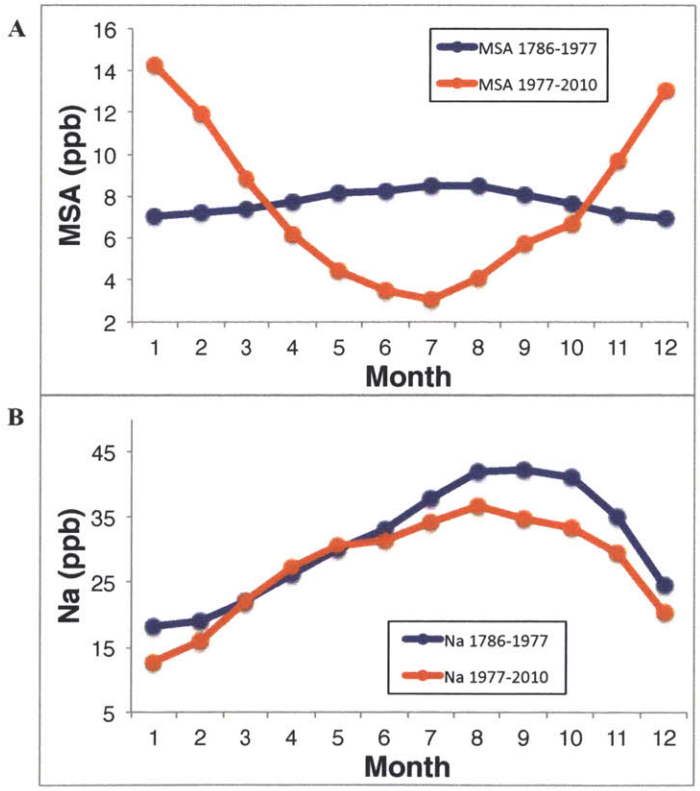

Figure 7. DIV2010 composite monthly (A) MSA and (B) Na concentrations for 1786–1977 (blue) and 1977–2010 (red).

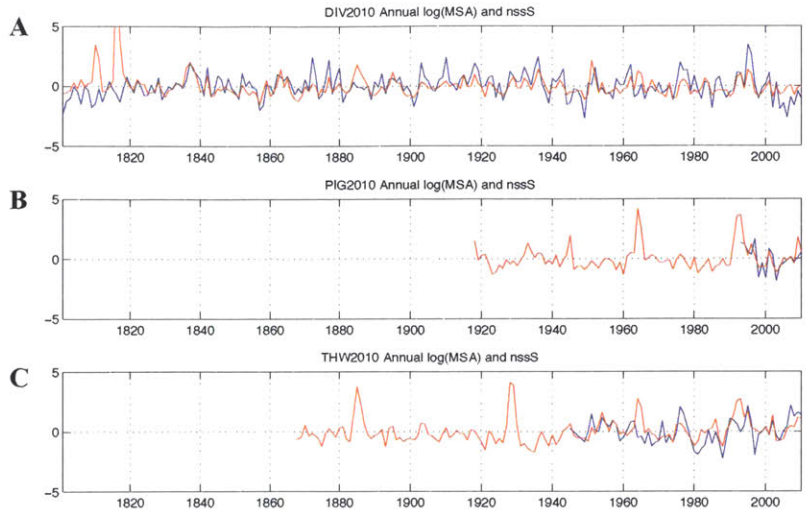

816
817 **Figure 8.** Normalized time series of annual log transformed MSA (blue) and annual nssS
818 (red) for (A) DIV2010, (B) PIG2010, and (C) THW2010. All data are presented on the
819 DIV2010 MSA timescale (1801–2010), and the same y-axis.
820

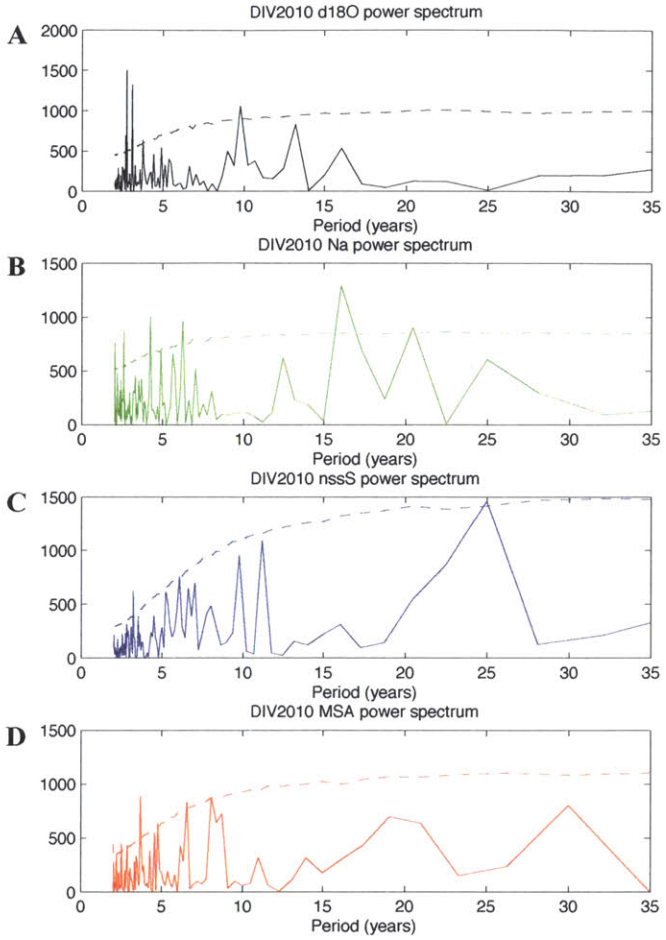

821
822 **Figure 9.** DIV2010 power spectra for (A) $\delta^{18}O$, (B) Na, (C) nssS, and (D) MSA (in
823 years). Dashed lines indicate 95% confidence.
824

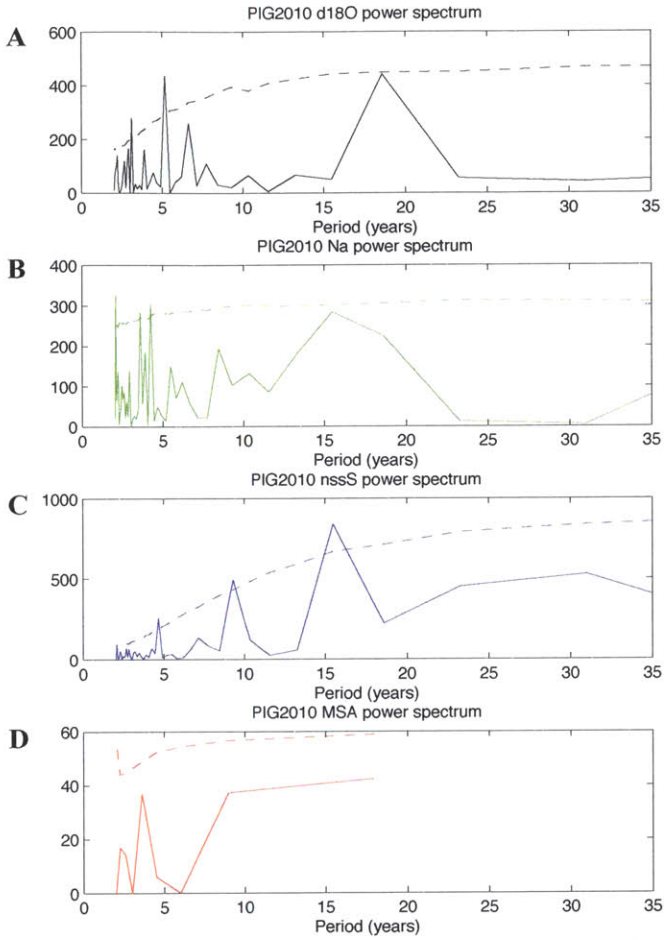

Figure 10. PIG2010 power spectra for (A) $\delta^{18}O$, (B) Na, (C) nssS, and (D) MSA (in years). Dashed lines indicate 95% confidence.

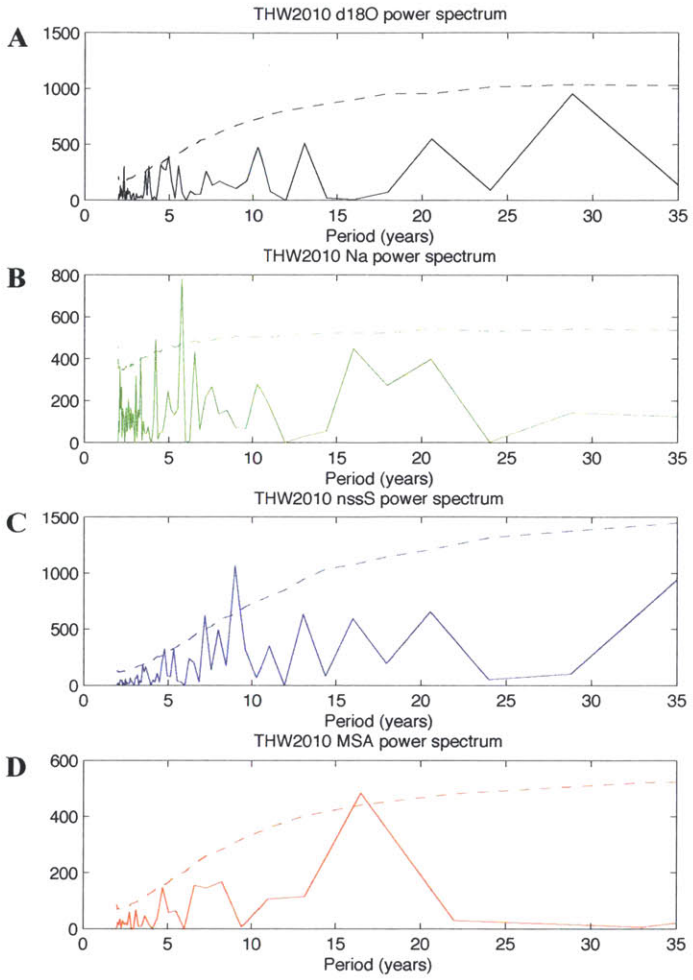

829
830 **Figure 11.** THW2010 power spectra for (A) $\delta^{18}O$, (B) Na, (C) nssS, and (D) MSA (in
831 years). Dashed lines indicate 95% confidence.
832

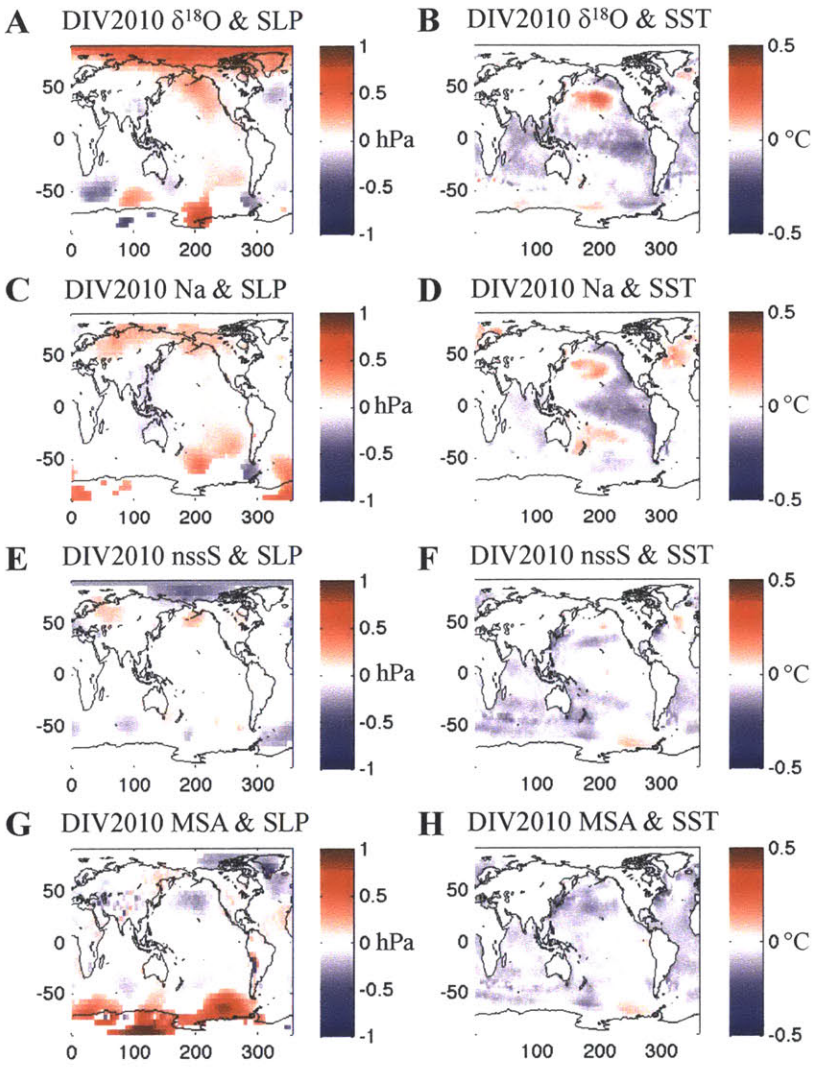

Figure 12. DIV2010 regression maps of annual low-pass filtered (A) $\delta^{18}O$ on SLP, (B) $\delta^{18}O$ on SST, (C) Na on SLP, (D) Na on SST, (E) nssS on SLP, (F) nssS on SST, (G) MSA on SLP, and (H) MSA on SST (1870–2010). The SLP scale is -1–1 hPa, and the SST scale is -0.5–0.5°C. Shaded regions indicate >95% significance (determined using a two-tailed Student's *t*-test; positive shading red, negative shading blue).

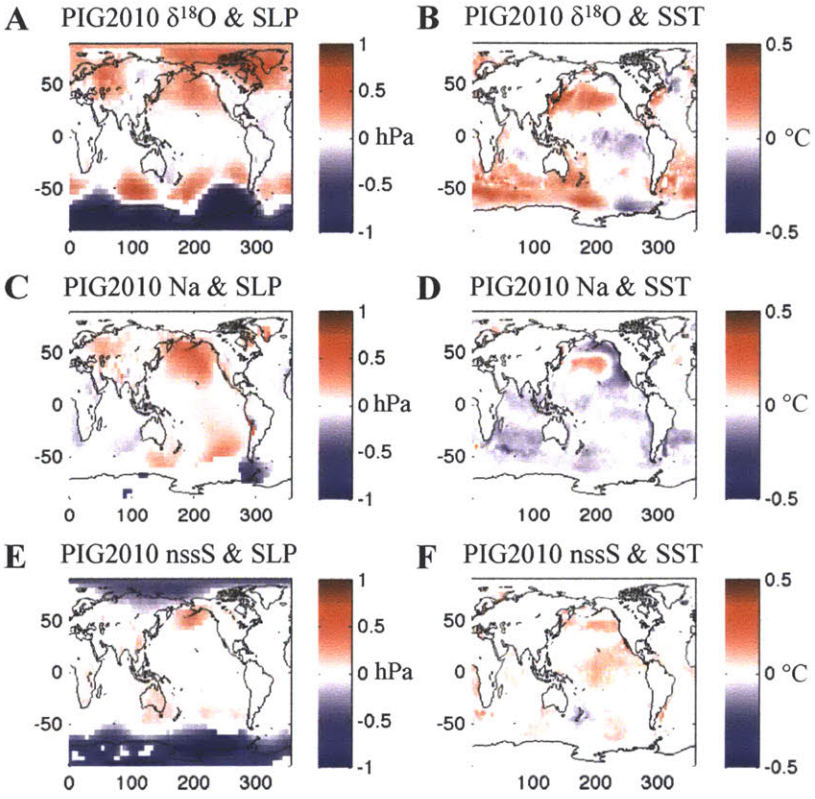

840
841 **Figure 13.** PIG2010 regression maps of annual low-pass filtered (A) $\delta^{18}O$ on SLP, (B)
842 $\delta^{18}O$ on SST, (C) Na on SLP, (D) Na on SST, (E) nssS on SLP, and (F) nssS on SST
843 (1918–2010). The SLP scale is -1–1 hPa, and the SST scale is -0.5–0.5°C. Shaded
844 regions indicate >95% significance (determined using a two-tailed Student's *t*-test;
845 positive shading red, negative shading blue).
846

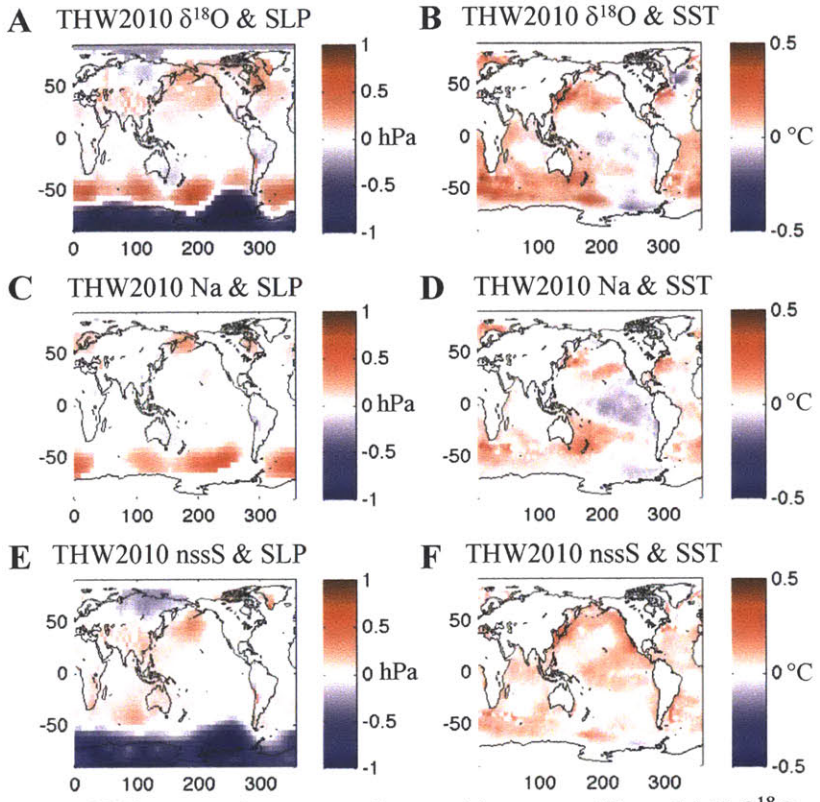

Figure 14. THW2010 regression maps of annual low-pass filtered (A) $\delta^{18}O$ on SLP, (B) $\delta^{18}O$ on SST, (C) Na on SLP, (D) Na on SST, (E) nssS on SLP, and (F) nssS on SST (1867–2010). The SLP scale is -1–1 hPa, and the SST scale is -0.5–0.5°C. Shaded regions indicate >95% significance (determined using a two-tailed Student's *t*-test; positive shading red, negative shading blue).

Tables

Name	Lat	Lon	Elevation (m)	Distance from coast (km)	Period	Mean Accumulation (m·we·yr-1)
DIV2010	-76.77	-101.74	1329	180	1786-2010	0.408
PIG2010	-77.96	-95.96	1593	350	1918-2010	0.424
THW2010	-76.95	-121.22	2020	340	1867-2010	0.281
	MSA range (ppb)	**Na range (ppb)**	**Ca range (ppb)**	**Mg range (ppb)**	**nssS range (ppb)**	**d18O range (per mil)**
DIV2010	3.6 - 18.4	11.3 - 73.9	0.4 - 7.4	1.4 - 8.5	4.1 - 56.1	-30.4 to -24.7
PIG2010	6.7 - 12.1	7.7 - 41.1	0.1 - 41.8	0.6 - 7.5	7.9 - 22.2	-34.8 to -29.6
THW2010	5.7 - 13.5	8.9 - 51.2	0.3 - 3.9	1.2 -6.8	5.9 - 24.6	-35.8 to -29.4

Table 1. Location, mean annual accumulation rate, and mean annual concentration ranges (MSA, Na, Ca, Mg, nssS, $\delta^{18}O$) of three West Antarctic firn cores used in this study.

DIV2010	**Ca**	**Mg**			**nssS**	**Stot**
Na	0.59	0.95		**MSA**	0.30	0.35
Ca	-	0.61		**nssS**	-	0.96
PIG2010	**Ca**	**Mg**			**nssS**	**Stot**
Na	0.37	0.65		**MSA**	-	-
Ca	-	0.63		**nssS**	-	0.96
THW2010	**Ca**	**Mg**			**nssS**	**Stot**
Na	0.64	0.97		**MSA**	-	-
Ca	-	0.64		**nssS**	-	0.97

Table 2. Pearson's *r* correlation coefficients of mean annual sea-salt species and mean annual marine biogenic species (all *r*-values significant at $p < 0.01$).

Appendix A1
Data Tables

Table A1. Chemistry for DIV2010S (short Pico core drilled at the same location as the deep DIV2010 core). Chemistry includes methanesulfonic acid (MSA), chloride (Cl^-), $\delta^{18}O$ (‰), and δD (‰). Sample depth (cm) and density (g/cm^3) are given as well, along with a pinned age-depth scale that was primarily established by matching the $\delta^{18}O$ firn-core record with regional surface temperature data.

Table A2. Monthly MSA for DIV2010S (short Pico core located at the deep DIV2010 site), and monthly total water area (in km^2) for the area within the Pine Island Bay and Amundsen Sea polynyas (TWA; reported in Criscitiello et al., 2013), calculated from AMSR-E values of sea-ice concentration.

Table A3. Monthly chemistry for DIV2010, PIG2010, and THW2010 cores (1979-2010). Latitude, longitude, and elevation of the drill sites are given. Data include bromine (BrO), iodine (IO), calcium (Ca), magnesium (Mg), sodium (Na), total sulfur (S_{tot}), chloride (Cl^-), $\delta^{18}O$ (‰), δD (‰), methanesulfonic acid (MSA), and non sea-salt sulfur (nssS).

Table A4. Monthly SMMR- and SSM/I-based polynya total open water area (TOWA) for the Pine Island Bay and Amundsen Sea polynas combined, and sea-ice extent (SIE) time series for the region between 80°W and 140°W, and 60°S and 71°S (as reported in Criscitiello et al., 2013b), 1979-2010.

Table A5. Annual chemistry for the DIV2010 (1786–2010), PIG2010 (1918–2010), and THW2010 (1867–2010) long cores. Data include calcium (Ca), magnesium (Mg), sodium (Na), total sulfur (S_{tot}), non sea-salt sulfur (nssS), $\delta^{18}O$ (‰), and δD (‰). DIV2010 data additionally include methanesulfonic acid (MSA).

Table A1: Chemistry for DIV2010S (short Pico core located at the deep DIV2010 site), pinned dates

DIV2010S		Lat: -76.76807	Lon: -101.73545		Elevation: 1292m	
Date	MSA (ppb)	Cl^- (ppb)	δ18O (‰)	δD (‰)	Ave Depth (cm)	Density (g/cm^3)
10/26/01	6.474	87.651	-27.314	-215.464	791.500	0.537
11/12/01	16.244	85.903	-26.300	-206.248	787.500	0.537
11/30/01	24.393	65.872	-25.156	-197.442	783.500	0.537
12/18/01	14.651	59.953	-24.941	-192.177	779.500	0.536
1/5/02	15.663	112.388	-25.020	-192.800	775.500	0.536
1/22/02	13.437	115.323	-25.384	-199.285	771.000	0.536
2/9/02	3.566	95.735	-26.266	-206.431	766.500	0.535
2/26/02	4.136	104.665	-26.839	-211.032	762.000	0.535
3/16/02	3.176	163.892	-27.153	-213.579	757.500	0.535
4/3/02	2.849	90.518	-27.249	-213.254	753.500	0.535
4/20/02	1.943	118.799	-27.337	-213.303	749.500	0.534
5/8/02	3.998	91.197	-27.968	-217.388	745.500	0.534
5/25/02	1.486	142.213	-28.367	-221.906	741.500	0.534
6/12/02	1.211	173.440	-28.482	-224.751	737.000	0.533
6/30/02	0.872	273.972	-28.778	-226.475	732.500	0.533
7/17/02	1.349	146.063	-28.657	-227.644	728.750	0.533
8/4/02	4.714	121.625	-28.409	-222.400	725.250	0.533
8/22/02	1.169	53.854	-27.959	-218.186	721.500	0.532
9/13/02	1.682	52.373	-28.521	-222.494	717.000	0.532
10/5/02	2.518	84.764	-28.755	-226.738	712.500	0.532
10/27/02	2.916	64.807	-28.294	-223.291	708.500	0.531
11/18/02	17.975	89.826	-26.678	-209.568	704.500	0.531
12/10/02	7.920	121.307	-24.613	-191.981	700.000	0.531
1/1/03	13.427	108.762	-23.169	-179.293	695.500	0.530
1/23/03	7.659	52.231	-22.323	-173.626	691.250	0.530
2/14/03	21.951	310.011	-22.235	-172.508	686.500	0.530
3/8/03	5.984	71.044	-22.241	-172.411	682.000	0.529
4/4/03	3.165	59.139	-23.026	-176.018	678.000	0.529
5/1/03	2.780	215.580	-24.686	-189.988	674.000	0.529
5/28/03	1.836	366.151	-26.370	-205.758	669.500	0.528
6/24/03	2.023	110.926	-27.337	-214.765	665.000	0.528
7/21/03	1.330	184.231	-28.517	-222.756	661.000	0.528
8/18/03	2.166	91.528	-29.558	-234.492	657.000	0.527
9/2/03	1.326	118.112	-29.442	-232.847	652.500	0.527
9/17/03	10.183	51.869	-28.429	-223.296	648.000	0.527
10/3/03	0.519	50.972	-27.156	-215.552	643.500	0.526
10/18/03	0.944	54.651	-26.283	-206.432	639.000	0.526
11/2/03	1.144	35.477	-26.025	-205.836	634.500	0.525

11/18/03	7.656	130.278	-26.079	-205.698	630.000	0.525
12/3/03	7.166	46.136	-25.476	-200.789	626.000	0.525
12/18/03	6.020	163.550	-24.683	-194.538	621.500	0.524
1/3/04	17.701	102.945	-24.848	-193.779	616.500	0.524
1/18/04	17.711	92.765	-25.104	-196.422	611.500	0.523
2/2/04	16.256	189.717	-26.070	-202.116	606.750	0.523
2/18/04	15.578	190.563	-27.281	-211.500	602.750	0.523
3/4/04	10.856	66.061	-27.984	-217.654	599.250	0.522
3/19/04	4.898	146.736	-28.608	-222.480	595.000	0.522
4/4/04	3.665	130.173	-27.466	-211.742	590.250	0.522
4/19/04	2.781	121.002	-27.924	-215.789	585.500	0.521
5/4/04	0.952	142.577	-29.704	-230.949	581.000	0.521
5/20/04	1.857	146.338	-31.740	-249.350	576.500	0.520
6/4/04	0.530	226.301	-33.938	-267.541	572.000	0.520
6/20/04	0.655	201.060	-34.694	-274.035	567.500	0.520
7/18/04	0.733	159.596	-33.576	-263.320	563.000	0.519
8/16/04	1.272	214.610	-31.214	-247.176	558.500	0.519
9/13/04	2.178	229.733	-29.127	-229.268	554.000	0.518
10/12/04	1.979	172.063	-27.672	-216.561	549.500	0.518
11/9/04	1.963	265.897	-26.610	-209.533	545.000	0.517
12/8/04	2.286	43.823	-25.364	-199.986	540.500	0.517
1/6/05	5.984	160.292	-24.976	-196.395	535.500	0.516
1/25/05	17.508	157.466	-25.122	-196.390	530.500	0.516
2/14/05	15.224	129.601	-26.325	-205.024	525.500	0.515
3/6/05	8.412	44.910	-27.724	-215.824	521.000	0.515
3/26/05	3.822	116.469	-28.025	-219.184	516.500	0.515
4/15/05	3.832	87.210	-28.196	-219.094	512.000	0.514
5/5/05	3.129	152.342	-28.342	-221.285	507.500	0.514
5/25/05	1.659	230.662	-28.507	-223.895	503.000	0.513
6/14/05	2.130	427.879	-28.299	-220.632	498.500	0.513
7/4/05	1.706	80.451	-28.477	-223.835	494.000	0.512
7/24/05	3.649	61.486	-29.472	-232.865	489.500	0.512
8/13/05	0.840	177.268	-29.976	-237.635	485.000	0.511
8/28/05	0.714	134.841	-29.187	-232.572	480.500	0.511
9/13/05	1.135	148.868	-27.950	-219.894	476.000	0.510
9/29/05	2.225	62.366	-26.219	-205.511	471.500	0.510
10/14/05	1.223	84.803	-25.398	-199.441	467.000	0.509
10/30/05	1.563	234.382	-25.434	-201.304	462.500	0.509
11/15/05	1.977	100.824	-24.969	-196.583	458.000	0.508
11/30/05	2.933	213.618	-24.365	-191.311	453.500	0.508
12/16/05	3.186	167.356	-24.202	-190.567	449.000	0.507
1/1/06	4.855	47.301	-24.293	-193.547	445.000	0.507
1/23/06	7.170	46.344	-24.710	-194.969	441.000	0.506

2/14/06	13.325	35.231	-25.051	-195.732	436.500	0.506
3/8/06	17.186	31.792	-25.211	-194.808	432.000	0.505
3/30/06	9.035	74.750	-26.115	-204.021	427.500	0.504
4/22/06	10.180	104.055	-27.575	-215.764	423.000	0.504
5/14/06	2.975	102.384	-27.931	-218.731	418.500	0.503
6/5/06	1.222	144.529	-27.842	-217.188	414.000	0.503
6/27/06	1.584	178.475	-27.863	-218.011	409.500	0.502
7/19/06	0.974	177.422	-27.626	-216.725	405.000	0.502
8/11/06	1.793	133.967	-27.608	-215.829	400.500	0.501
8/27/06	0.004	253.928	-27.882	-218.175	396.000	0.500
9/13/06	1.592	370.259	-27.880	-219.045	391.500	0.500
9/29/06	0.912	47.474	-27.869	-219.154	387.000	0.499
10/16/06	1.916	30.700	-27.514	-216.686	383.500	0.499
11/1/06	0.745	76.530	-27.442	-216.246	380.500	0.498
11/18/06	0.936	32.477	-26.681	-211.445	377.000	0.498
12/4/06	1.306	50.595	-25.985	-204.850	373.000	0.497
12/21/06	2.054	29.453	-25.433	-199.777	369.000	0.497
1/6/07	5.483	49.892	-24.687	-194.276	364.500	0.496
1/23/07	14.131	75.007	-24.298	-189.614	359.500	0.495
2/8/07	14.149	136.457	-25.020	-194.256	355.000	0.495
2/25/07	6.244	49.191	-25.091	-196.528	351.000	0.494
3/13/07	3.179	31.728	-25.253	-194.624	346.500	0.493
3/30/07	2.080	30.444	-25.951	-201.612	342.000	0.493
4/15/07	1.409	45.479	-26.994	-209.628	337.750	0.492
5/2/07	1.841	64.302	-27.425	-211.596	333.750	0.491
5/18/07	3.158	56.467	-27.458	-212.329	330.250	0.491
6/4/07	2.954	52.888	-27.409	-213.181	326.000	0.490
6/20/07	2.718	55.832	-26.872	-209.298	321.000	0.489
7/7/07	1.737	193.098	-27.243	-212.645	316.500	0.489
7/23/07	0.914	287.319	-29.282	-230.571	312.500	0.488
8/9/07	1.204	92.974	-30.356	-239.927	308.000	0.487
9/2/07	2.915	153.249	-29.712	-233.037	303.500	0.486
9/26/07	11.865	107.120	-27.772	-218.362	299.250	0.486
10/20/07	21.519	99.984	-26.343	-206.149	294.500	0.485
11/13/07	25.050	64.190	-25.789	-202.149	290.000	0.484
12/7/07	20.160	78.554	-25.477	-201.521	285.500	0.483
12/31/07	23.837	46.003	-25.226	-198.482	280.500	0.482
1/24/08	17.667	58.877	-24.964	-196.314	276.000	0.481
2/17/08	17.904	97.188	-24.622	-192.262	271.500	0.480
2/27/08	22.214	78.660	-26.236	-205.158	266.500	0.479
3/9/08	21.431	168.836	-27.832	-220.140	262.000	0.479
3/20/08	21.008	1009.120	-28.296	-220.766	257.500	0.478
3/31/08	7.041	111.996	-28.317	-222.656	252.500	0.477

4/11/08	3.415	104.995	-29.086	-226.661	248.250	0.476
4/22/08	3.208	176.510	-30.520	-239.545	244.750	0.475
5/2/08	2.495	130.017	-31.128	-245.067	240.500	0.474
5/13/08	0.496	136.391	-30.102	-236.831	235.500	0.473
5/24/08	1.824	111.678	-29.376	-231.079	230.500	0.472
6/4/08	1.514	158.592	-28.552	-225.680	225.500	0.471
6/15/08	0.574	169.403	-26.953	-210.598	221.000	0.469
6/26/08	0.692	242.462	-25.476	-199.175	216.500	0.468
7/7/08	0.693	262.335	-25.185	-196.479	211.500	0.467
7/21/08	0.786	83.761	-25.472	-201.365	207.000	0.466
8/5/08	1.143	36.469	-26.396	-209.541	203.000	0.465
8/19/08	1.613	41.723	-26.686	-211.385	198.500	0.464
9/3/08	2.633	82.903	-26.876	-214.413	194.000	0.463
9/17/08	4.047	50.201	-28.197	-223.259	189.500	0.461
10/2/08	3.911	61.721	-29.256	-233.295	185.000	0.460
10/16/08	6.221	98.911	-28.434	-226.828	181.000	0.459
10/31/08	3.733	57.210	-27.010	-213.613	176.500	0.458
11/15/08	10.699	28.346	-25.555	-202.249	171.500	0.456
11/29/08	14.055	29.664	-25.753	-201.249	166.750	0.455
12/14/08	21.195	34.283	-26.313	-207.270	162.000	0.453
12/28/08	22.502	55.404	-26.809	-209.658	157.000	0.451
1/12/09	8.497	42.584	-27.261	-212.259	152.000	0.450
1/26/09	6.118	58.440	-26.828	-208.490	147.000	0.448
2/10/09	4.187	53.059	-25.011	-194.911	142.000	0.446
2/25/09	1.214	191.120	-23.863	-186.297	137.000	0.444
3/28/09	1.057	142.779	-24.180	-188.916	132.000	0.442
4/28/09	0.684	154.985	-26.177	-203.366	127.000	0.440
5/29/09	1.453	130.882	-27.409	-215.017	122.000	0.438
6/29/09	0.608	101.868	-28.782	-225.921	117.000	0.436
7/30/09	6.492	49.609	-28.285	-222.890	112.000	0.433
8/30/09	11.622	41.225	-27.127	-213.026	107.000	0.431
9/30/09	10.385	68.417	-26.012	-204.652	102.000	0.428
10/31/09	10.158	72.498	-25.399	-201.200	97.000	0.426
12/1/09	17.392	50.550	-25.420	-199.219	92.000	0.423
1/12/10	8.945	247.759	-28.400	-223.182	87.000	0.420
2/4/10	1.317	339.573	-31.884	-251.223	82.000	0.417
2/27/10	0.620	514.678	-32.148	-252.595	77.000	0.414
3/22/10	0.991	106.310	-30.866	-241.106	72.750	0.411
4/13/10	2.065	156.854	-31.017	-240.167	68.750	0.408
5/6/10	1.933	104.295	-31.108	-242.281	64.000	0.404
5/29/10	0.363	118.536	-31.515	-247.312	59.000	0.399
6/21/10	0.968	350.190	-32.191	-254.536	54.000	0.395
7/17/10	0.890	295.929	-29.954	-238.082	49.000	0.390

8/12/10	1.709	65.781	-29.546	-231.865	44.000	0.384
9/7/10	0.909	81.250	-29.115	-228.342	39.000	0.377
10/3/10	0.482	101.292	-28.763	-225.211	34.000	0.370
10/29/10	0.691	183.277	-28.515	-223.573	28.000	0.360
11/24/10	1.289	191.537	-28.041	-220.111	22.000	0.347
12/21/10	2.594	120.110	-28.104	-223.000	17.000	0.333
12/25/10	15.192	69.830	-29.753	-233.953	12.000	0.315
12/29/10	17.815	113.370	-30.222	-239.058	7.250	0.288

Table A2: Monthly MSA and TWA for DIV2010S (short Pico core located at the deep DIV2010 site)

DIV2010S

Year	Month	TWA (km^2)	MSA (ppb)
2002	Jul	3135.1	1.3
	Aug	228.1	2.9
	Sep	2227.9	1.7
	Oct	4669.9	2.7
	Nov	35849.0	18.0
	Dec	52075.4	7.9
2003	Jan	54366.2	10.5
	Feb	58775.1	22.0
	Mar	31493.2	6.0
	Apr	2966.1	3.2
	May	1142.9	2.3
	Jun	1259.1	2.0
	Jul	2283.3	1.3
	Aug	1515.9	2.2
	Sep	1875.0	5.8
	Oct	1780.5	0.7
	Nov	20569.0	1.1
	Dec	36672.1	7.4
2004	Jan	42725.6	12.7
	Feb	49885.5	1.7
	Mar	15223.0	1.2
	Apr	2016.9	0.7
	May	1049.6	1.3
	Jun	2246.1	1.7
	Jul	365.4	2.2
	Aug	964.0	2.0
	Sep	3464.8	2.0
	Oct	6073.6	2.0
	Nov	12339.8	2.3
	Dec	34337.2	7.0
2005	Jan	47613.4	11.7
	Feb	51868.0	15.2
	Mar	11242.4	6.1
	Apr	2295.6	3.8
	May	667.8	2.4
	Jun	850.3	2.1
	Jul	1048.4	2.7
	Aug	1199.6	0.8

	Sep	963.5	1.7
	Oct	5734.6	1.4
	Nov	12119.8	2.5
	Dec	27621.0	3.2
2006	Jan	39366.2	6.0
	Feb	32742.7	13.3
	Mar	19060.0	13.1
	Apr	3535.2	10.2
	May	2056.5	3.0
	Jun	1842.4	1.4
	Jul	465.0	1.0
	Aug	1919.1	0.9
	Sep	1263.0	1.3
	Oct	5645.2	1.9
	Nov	16897.1	0.8
	Dec	45482.6	1.7
2007	Jan	46314.3	9.8
	Feb	43391.5	10.2
	Mar	16077.4	2.6
	Apr	1462.2	1.4
	May	2047.6	2.5
	Jun	1078.1	2.8
	Jul	578.4	1.3
	Aug	1568.8	1.2
	Sep	2911.5	7.4
	Oct	6227.3	21.5
	Nov	18945.3	25.1
	Dec	37958.7	22.0
2008	Jan	54516.1	17.7
	Feb	58713.6	20.1
	Mar	35562.0	16.5
	Apr	1778.6	3.3
	May	1420.1	1.6
	Jun	1480.5	0.9
	Jul	774.9	0.7
	Aug	868.2	1.4
	Sep	2543.0	3.3
	Oct	7278.2	4.6
	Nov	25815.1	12.4
	Dec	47619.7	21.8
2009	Jan	56673.4	7.3
	Feb	48406.8	2.7
	Mar	23816.8	1.1

	Apr	3312.5	0.7
	May	3860.9	1.5
	Jun	1406.3	0.6
	Jul	1014.4	6.5
	Aug	1783.0	11.6
	Sep	1628.9	10.4
	Oct	4152.0	10.2
	Nov	11644.5	13.8
	Dec	41596.5	17.4
2010	Jan	58591.2	8.9
	Feb	58438.9	1.0
	Mar	37440.8	1.0
	Apr	4856.8	2.1
	May	1514.6	1.1
	Jun	1212.2	1.0
	Jul	249.5	0.9
	Aug	933.7	1.7
	Sep	2914.1	0.9
	Oct	6873.7	0.6
	Nov	17554.7	1.3
	Dec	39596.8	11.9

Table A3: Monthly chemistry for DIV2010, PIG2010, and THW2010 cores (1979-2010)

DIV 2010	Lat: -76.77		Lon: -101.74		Elevation: 1329m						
Date	BrO (ppb)	Ca (ppb)	IO (ppb)	Mg (ppb)	Na (ppb)	S_{tot} (ppb)	Cl^- (ppb)	δ18O (‰)	δD (‰)	MSA (ppb)	nssS (ppb)
Jan-79	0.4	0.3	9.5	1.2	9.3	18.5	19.6	-24.7	-194.2	12.8	17.7
Feb-79	0.4	0.4	9.5	1.4	11.3	13.0	28.2	-25.1	-197.3	10.3	12.0
Mar-79	0.3	0.6	13.8	1.8	16.6	9.4	37.6	-25.5	-200.8	8.4	8.0
Apr-79	0.2	0.7	17.9	2.1	19.0	7.3	36.9	-26.0	-204.9	6.3	5.8
May-79	0.2	0.6	17.0	1.8	16.0	5.7	28.0	-26.3	-207.9	4.3	4.4
Jun-79	0.2	0.3	11.7	1.2	10.1	4.2	21.5	-26.7	-211.3	2.8	3.4
Jul-79	0.2	0.3	9.5	1.4	11.0	3.7	45.4	-27.3	-216.7	3.6	2.8
Aug-79	0.3	0.8	18.2	2.6	22.6	4.8	86.6	-28.2	-225.0	5.0	2.9
Sep-79	0.5	1.3	31.9	4.2	36.2	6.9	119.6	-28.9	-231.7	6.1	3.9
Oct-79	0.7	1.5	40.6	4.7	41.6	10.7	108.7	-28.9	-232.0	6.2	7.2
Nov-79	0.7	1.1	34.7	3.8	30.7	13.1	68.5	-28.1	-224.1	6.7	10.5
Dec-79	0.6	0.6	20.7	2.2	16.1	14.0	32.0	-27.0	-213.3	8.6	12.7
Jan-80	0.5	0.3	9.0	1.0	6.1	12.7	19.7	-26.1	-205.3	10.3	12.2
Feb-80	0.4	0.2	4.9	0.7	4.7	11.6	21.1	-25.7	-201.8	10.5	11.0
Mar-80	0.4	0.2	5.6	1.1	6.5	11.1	35.5	-25.8	-202.9	9.6	10.4
Apr-80	0.5	0.5	12.1	2.1	16.1	11.3	71.2	-26.1	-206.1	10.1	9.8
May-80	0.6	0.9	25.6	3.5	31.0	11.8	88.3	-26.4	-210.1	10.7	9.2
Jun-80	0.8	1.2	37.0	4.1	39.9	11.1	84.7	-26.8	-213.4	10.0	7.7
Jul-80	0.8	1.1	37.3	3.7	35.1	9.3	52.4	-26.8	-214.6	7.6	6.3
Aug-80	0.8	0.8	26.9	2.8	22.9	7.5	37.9	-26.8	-213.8	6.0	5.6
Sep-80	0.6	0.7	17.9	2.2	16.0	7.6	39.7	-26.5	-212.0	6.5	6.2
Oct-80	0.5	0.7	15.6	2.1	15.6	9.3	40.6	-26.4	-209.7	8.2	8.0
Nov-80	0.4	0.7	16.0	2.0	15.8	12.3	37.9	-26.1	-207.3	9.9	11.0
Dec-80	0.5	0.6	14.5	1.8	13.9	14.9	28.2	-25.8	-204.7	10.7	13.7

Jan-81	0.5	0.5	12.6	1.6	13.2	14.8	29.7	-25.5	-202.4	10.0	13.7
Feb-81	0.5	0.5	12.9	1.8	14.2	12.7	38.9	-25.5	-202.0	8.9	11.5
Mar-81	0.6	0.9	18.0	2.7	21.9	9.8	61.5	-25.9	-205.1	9.0	8.0
Apr-81	0.8	1.2	28.1	3.8	31.7	8.3	83.3	-26.5	-210.2	8.7	5.6
May-81	0.8	1.3	35.6	4.3	36.3	6.8	84.3	-27.2	-215.6	7.1	3.7
Jun-81	0.6	1.2	34.6	3.8	31.4	5.8	124.8	-27.8	-221.1	3.9	3.2
Jul-81	0.4	1.0	27.1	3.2	24.0	5.6	111.1	-28.5	-227.0	2.3	3.6
Aug-81	0.3	1.1	24.8	3.5	26.2	6.8	130.2	-28.9	-230.1	4.1	4.6
Sep-81	0.4	1.3	29.0	4.0	30.1	8.3	74.9	-28.5	-227.2	5.7	5.7
Oct-81	0.5	1.3	30.5	4.1	31.5	11.2	73.6	-27.6	-220.2	7.3	8.6
Nov-81	0.6	1.1	28.8	3.6	28.2	15.1	54.2	-26.9	-213.2	7.1	12.7
Dec-81	0.7	0.8	22.2	2.9	22.8	18.1	50.0	-26.6	-209.9	8.5	16.1
Jan-82	0.6	0.5	18.9	2.4	20.0	18.4	50.1	-26.7	-210.9	8.7	16.7
Feb-82	0.6	0.5	17.3	2.3	19.3	15.4	54.1	-27.1	-214.1	8.2	13.7
Mar-82	0.4	0.7	19.0	2.5	21.4	11.5	49.9	-27.5	-217.5	5.7	9.7
Apr-82	0.4	0.9	20.4	2.8	23.3	8.0	54.6	-27.8	-220.5	4.5	6.1
May-82	0.4	1.1	24.0	3.4	28.2	6.7	66.1	-28.1	-223.3	3.4	4.3
Jun-82	0.4	1.3	29.9	4.2	34.7	6.7	86.9	-28.2	-225.0	3.6	3.8
Jul-82	0.3	1.4	35.2	4.8	39.6	7.5	85.3	-28.1	-223.9	3.1	4.2
Aug-82	0.2	1.4	37.3	4.9	39.8	8.5	81.1	-27.5	-219.3	3.4	5.1
Sep-82	0.3	1.2	35.7	4.5	36.1	10.6	66.5	-26.6	-212.7	3.9	7.6
Oct-82	0.6	1.0	31.5	3.7	29.8	14.1	58.2	-25.8	-206.0	5.3	11.6
Nov-82	0.8	0.8	24.0	2.5	21.0	17.8	45.7	-25.1	-202.3	7.2	16.0
Dec-82	0.7	0.6	16.3	1.7	14.7	20.5	49.0	-25.0	-200.5	9.6	19.3
Jan-83	0.6	0.5	12.3	1.2	11.1	20.7	46.1	-25.3	-202.0	11.3	19.8
Feb-83	0.5	0.5	9.8	1.1	9.7	19.3	37.3	-25.9	-205.4	11.0	18.5
Mar-83	0.5	0.5	9.6	1.1	9.9	16.0	33.6	-26.6	-211.1	9.0	15.2

Apr-83	0.5	0.4	10.7	1.4	11.3	12.3	59.9	-27.3	-217.2	7.3	11.3
May-83	0.6	0.7	15.9	2.3	17.8	9.5	89.5	-28.0	-222.7	5.9	8.0
Jun-83	0.7	1.2	27.8	3.8	30.2	8.8	103.1	-28.5	-227.4	5.3	6.3
Jul-83	0.7	1.6	41.5	5.3	43.5	9.6	95.2	-28.9	-229.9	5.3	5.9
Aug-83	0.5	1.7	49.0	6.0	47.8	10.4	74.7	-28.8	-230.0	6.5	6.4
Sep-83	0.4	1.6	48.0	5.8	45.1	12.3	57.9	-28.5	-227.0	8.6	8.5
Oct-83	0.5	1.5	42.8	5.1	39.0	17.1	39.7	-27.8	-222.2	9.6	13.8
Nov-83	0.6	1.3	36.3	4.2	33.0	24.3	36.6	-26.9	-215.1	9.1	21.5
Dec-83	0.6	1.0	28.2	3.2	25.7	29.3	37.2	-25.9	-206.9	7.2	27.1
Jan-84	0.5	0.7	20.4	2.3	18.8	28.0	36.1	-25.2	-199.3	5.1	26.5
Feb-84	0.5	0.5	16.1	2.0	16.5	21.3	30.5	-24.9	-196.5	3.5	19.9
Mar-84	0.6	0.5	15.5	1.9	16.3	14.2	34.6	-25.2	-198.8	2.8	12.8
Apr-84	0.7	0.3	15.0	1.8	15.6	9.3	59.2	-25.7	-203.5	3.1	8.0
May-84	0.6	0.3	13.1	1.6	13.4	7.5	93.3	-26.1	-206.9	3.9	6.3
Jun-84	0.4	0.4	11.5	1.7	13.4	6.8	92.5	-26.7	-213.0	4.3	5.7
Jul-84	0.3	0.8	16.9	2.7	22.7	7.3	67.6	-27.7	-221.5	6.0	5.4
Aug-84	0.3	1.1	28.8	3.8	33.8	8.4	39.6	-28.0	-224.1	8.8	5.6
Sep-84	0.4	1.1	33.8	3.8	34.5	9.8	36.8	-26.8	-214.9	12.9	7.0
Oct-84	0.5	0.9	29.1	3.0	26.6	12.9	35.2	-24.8	-198.1	15.0	10.6
Nov-84	0.5	0.6	18.7	2.0	16.7	15.8	32.7	-23.5	-187.7	15.1	14.4
Dec-84	0.6	0.5	12.9	1.5	13.0	18.1	33.8	-23.6	-187.0	12.0	17.1
Jan-85	0.6	0.3	10.5	1.2	10.8	17.0	34.4	-24.7	-196.4	8.2	16.1
Feb-85	0.6	0.2	10.1	1.2	10.8	13.8	28.6	-26.1	-207.6	4.7	12.9
Mar-85	0.6	0.3	11.2	1.4	11.6	9.7	50.0	-27.4	-217.2	3.8	8.8
Apr-85	0.5	0.5	12.7	1.8	13.8	6.9	81.9	-28.3	-223.9	4.1	5.8
May-85	0.4	0.9	20.0	2.8	25.1	6.2	105.6	-29.2	-230.6	4.3	4.1
Jun-85	0.4	1.3	33.2	4.0	39.4	6.8	96.8	-30.1	-238.1	3.7	3.5

Jul-85	0.3	1.5	43.5	4.7	46.7	7.6	82.2	-30.7	-244.3	3.0	3.7
Aug-85	0.2	1.5	44.7	4.4	43.3	7.5	87.8	-30.8	-246.3	3.2	3.8
Sep-85	0.2	1.4	40.0	3.7	37.9	7.5	80.2	-30.1	-242.1	3.6	4.2
Oct-85	0.2	1.3	34.7	3.0	32.5	8.0	61.3	-28.7	-231.1	4.6	5.2
Nov-85	0.4	1.0	25.9	2.3	23.7	9.7	39.1	-27.0	-216.7	6.3	7.7
Dec-85	0.5	0.7	17.0	1.8	15.8	12.1	32.7	-25.5	-204.7	8.7	10.8
Jan-86	0.7	0.6	12.1	1.6	12.9	14.5	34.8	-24.8	-198.1	10.9	13.4
Feb-86	0.7	0.7	12.1	1.5	13.6	15.6	31.8	-24.9	-198.1	11.9	14.5
Mar-86	0.7	0.6	12.1	1.4	13.3	14.9	27.6	-25.7	-203.4	11.3	13.8
Apr-86	0.6	0.4	10.7	1.3	11.4	12.6	21.6	-26.8	-212.3	9.5	11.7
May-86	0.5	0.2	8.7	1.1	9.2	9.9	19.1	-28.2	-223.7	7.1	9.1
Jun-86	0.5	0.3	9.4	1.5	10.3	7.8	36.3	-29.6	-235.0	5.8	6.9
Jul-86	0.4	0.8	16.3	2.6	18.5	6.7	80.2	-30.8	-244.5	6.1	5.2
Aug-86	0.4	1.5	29.7	4.1	32.6	7.0	115.9	-31.5	-250.0	7.1	4.3
Sep-86	0.5	1.7	42.3	5.3	44.9	8.0	121.0	-31.4	-249.8	7.1	4.2
Oct-86	0.7	1.6	46.1	5.6	47.4	9.4	86.5	-30.6	-243.8	7.0	5.4
Nov-86	0.8	1.2	39.0	4.9	39.4	11.1	50.9	-29.3	-233.8	7.3	7.8
Dec-86	0.8	0.9	27.2	3.6	26.4	12.8	27.0	-28.2	-223.1	8.7	10.6
Jan-87	0.7	0.7	18.5	2.6	17.7	13.9	51.3	-27.3	-216.0	10.3	12.5
Feb-87	0.6	0.7	19.0	2.4	19.0	13.9	67.5	-27.1	-213.8	10.3	12.3
Mar-87	0.6	0.9	25.7	3.0	27.6	12.6	81.7	-27.2	-215.8	9.2	10.3
Apr-87	0.6	1.3	33.0	3.8	36.4	10.6	81.0	-27.5	-218.7	7.1	7.5
May-87	0.5	1.5	36.5	4.5	40.7	8.3	89.3	-27.6	-219.5	5.4	4.9
Jun-87	0.4	1.5	37.7	4.9	41.5	6.9	97.2	-27.3	-217.4	4.1	3.4
Jul-87	0.3	1.5	39.4	5.0	41.5	6.5	93.0	-26.7	-213.6	3.8	3.1
Aug-87	0.3	1.3	40.2	4.7	40.0	7.2	79.3	-26.2	-209.7	4.7	3.8
Sep-87	0.5	1.1	37.6	4.4	37.0	8.9	70.2	-25.8	-206.3	7.4	5.8
Oct87	0.7	1.0	33.1	4.1	34.1	12.4	61.8	-25.3	-202.3	11.5	9.5

Nov-87	0.8	1.0	29.4	3.8	30.4	18.6	62.1	-24.7	-197.5	16.0	16.0
Dec-87	0.8	1.0	25.8	3.2	25.7	23.9	51.7	-24.4	-194.6	19.3	21.7
Jan-88	0.8	0.7	22.4	2.6	21.1	24.3	41.7	-24.8	-197.5	18.7	22.6
Feb-88	0.9	0.5	18.7	2.1	18.3	18.2	35.6	-25.6	-204.7	14.8	16.6
Mar-88	0.8	0.4	16.5	1.8	16.9	10.7	35.4	-26.6	-213.1	9.1	9.3
Apr-88	0.7	0.5	15.3	1.8	16.0	5.6	29.1	-27.3	-218.6	4.7	4.3
May-88	0.4	0.6	17.2	2.1	18.6	4.2	44.4	-27.8	-221.9	2.7	2.7
Jun-88	0.2	0.7	21.6	2.8	24.0	4.4	53.3	-27.8	-222.7	2.2	2.4
Jul-88	0.2	0.9	26.1	3.3	28.2	5.0	66.2	-27.3	-219.6	2.5	2.7
Aug-88	0.4	0.9	26.6	3.2	26.7	6.1	56.6	-26.6	-213.8	2.9	3.9
Sep-88	0.8	0.8	23.3	2.8	21.6	7.6	49.8	-25.8	-206.2	3.6	5.8
Oct-88	1.3	0.7	18.6	2.3	16.8	10.1	38.5	-25.1	-199.8	4.9	8.7
Nov-88	1.3	0.6	14.8	1.9	14.0	13.8	30.9	-24.5	-195.2	6.7	12.6
Dec-88	1.0	0.6	12.7	1.7	12.7	18.2	31.5	-24.5	-194.3	8.7	17.2
Jan-89	0.7	0.6	11.7	1.6	11.8	20.6	31.9	-25.0	-197.5	9.3	19.6
Feb-89	0.5	0.7	12.1	1.8	13.5	19.5	42.0	-26.1	-205.6	9.5	18.4
Mar-89	0.4	1.0	19.4	2.7	23.5	15.2	74.4	-27.5	-217.8	9.5	13.2
Apr-89	0.5	1.5	33.3	3.9	37.2	11.2	115.4	-29.0	-230.6	8.3	8.0
May-89	0.5	1.8	46.3	4.8	47.9	8.4	123.9	-30.0	-239.2	6.0	4.3
Jun-89	0.5	1.8	51.4	5.2	50.2	7.2	112.5	-30.4	-242.1	3.4	3.0
Jul-89	0.4	1.7	50.3	5.3	48.8	7.1	99.7	-30.2	-239.4	3.2	3.0
Aug-89	0.3	1.6	48.1	5.4	46.2	7.9	100.0	-29.4	-234.0	3.2	4.0
Sep-89	0.3	1.4	44.8	5.0	41.4	9.5	86.9	-28.5	-226.6	3.5	6.0
Oct-89	0.3	1.1	37.0	4.2	32.8	11.4	64.1	-27.6	-218.6	3.4	8.7
Nov-89	0.3	0.7	26.2	3.0	22.9	12.1	43.7	-26.7	-212.1	4.0	10.2
Dec-89	0.4	0.5	16.4	1.9	14.5	10.8	31.1	-26.3	-208.0	4.5	9.6
Jan-90	0.4	0.4	10.2	1.2	9.3	8.4	22.2	-26.2	-206.9	4.6	7.6

Feb-90	0.3	0.4	7.4	0.9	7.2	6.5	19.4	-26.5	-208.6	4.3	5.9
Mar-90	0.3	0.4	6.9	0.8	7.2	5.7	21.2	-27.0	-212.0	3.8	5.1
Apr-90	0.3	0.4	7.5	0.9	8.2	5.4	26.3	-27.5	-216.7	3.3	4.7
May-90	0.3	0.4	9.6	1.2	10.4	5.4	38.2	-28.0	-220.8	3.2	4.5
Jun-90	0.4	0.5	13.2	1.7	14.5	5.6	51.0	-28.1	-223.8	3.8	4.3
Jul-90	0.5	0.6	17.8	2.3	19.4	5.9	61.0	-27.9	-224.0	5.2	4.3
Aug-90	0.5	0.8	22.1	2.9	24.2	7.0	66.0	-27.5	-221.2	7.0	5.0
Sep-90	0.6	1.0	25.0	3.3	26.8	8.8	65.1	-26.9	-216.5	8.7	6.5
Oct-90	0.6	1.1	25.9	3.4	27.4	11.3	62.9	-26.2	-210.3	10.2	9.0
Nov-90	0.6	1.0	25.1	3.3	26.4	13.9	63.7	-25.4	-204.2	11.6	11.6
Dec-90	0.5	0.9	23.7	3.1	25.0	15.4	69.4	-24.8	-197.9	12.5	13.3
Jan-91	0.5	0.7	21.9	2.7	22.2	14.5	68.2	-24.3	-193.7	12.5	12.7
Feb-91	0.4	0.6	18.2	2.1	17.3	12.2	51.6	-24.3	-192.3	11.4	10.8
Mar-91	0.4	0.6	12.9	1.5	11.7	9.8	33.8	-24.7	-194.7	9.2	8.8
Apr-91	0.3	0.8	8.6	1.1	8.4	8.2	27.4	-25.6	-201.5	7.1	7.5
May-91	0.4	1.0	7.7	1.1	8.8	7.4	31.7	-27.0	-211.1	5.4	6.6
Jun-91	0.4	1.1	9.7	1.4	11.6	6.6	37.6	-28.3	-222.5	4.4	5.6
Jul-91	0.4	1.1	12.9	1.8	15.1	6.3	39.2	-29.5	-231.7	3.9	5.0
Aug-91	0.4	1.1	17.2	2.5	20.0	6.6	59.8	-30.0	-236.3	3.8	4.9
Sep-91	0.5	1.2	23.2	3.4	26.2	8.2	69.0	-29.8	-233.7	4.2	6.0
Oct-91	0.6	1.1	27.5	3.7	28.6	10.4	63.1	-28.9	-227.5	5.0	8.0
Nov-91	0.6	0.9	26.2	3.4	26.0	12.8	38.7	-28.1	-221.7	6.0	10.6
Dec-91	0.5	0.8	20.2	2.7	19.9	15.0	37.0	-27.7	-219.8	8.1	13.3
Jan-92	0.3	0.8	17.2	2.5	20.0	17.7	42.7	-27.7	-220.5	11.2	16.0
Feb-92	0.2	0.7	17.9	2.4	19.9	17.9	52.0	-27.3	-217.1	12.3	16.3
Mar-92	0.2	0.6	20.4	2.5	21.8	15.5	47.0	-26.6	-209.5	11.1	13.7
Apr-92	0.3	0.5	20.6	2.3	20.0	11.4	48.7	-26.2	-204.8	8.0	9.7

May-92	0.3	0.5	19.9	2.2	19.6	8.7	43.3	-27.0	-209.5	5.9	7.0
Jun-92	0.3	0.7	19.3	2.5	19.8	8.0	53.9	-28.2	-220.3	4.5	6.4
Jul-92	0.3	0.9	25.2	3.5	29.7	8.3	82.7	-30.2	-235.3	3.9	5.8
Aug-92	0.3	1.0	23.8	3.3	28.5	10.2	85.6	-30.0	-235.0	3.8	7.8
Sep-92	0.4	1.0	24.1	3.3	29.0	14.3	80.3	-29.3	-230.6	4.8	11.9
Oct-92	0.5	0.9	21.2	2.9	23.8	20.4	61.1	-27.4	-217.3	8.4	18.4
Nov-92	0.7	0.9	26.3	3.2	26.7	27.0	56.5	-26.4	-210.7	18.0	24.7
Dec-92	0.8	0.5	24.3	2.7	22.1	31.9	44.7	-25.4	-202.6	26.7	30.0
Jan-93	0.8	0.4	18.1	1.9	14.8	32.5	50.9	-24.3	-193.1	30.0	31.2
Feb-93	0.5	0.5	17.6	2.2	18.7	29.3	74.7	-23.8	-187.9	25.0	27.7
Mar-93	0.4	0.8	26.5	3.1	28.2	24.1	82.1	-24.2	-190.5	17.3	21.7
Apr-93	0.3	0.9	32.3	3.4	31.5	19.2	62.0	-25.3	-198.9	10.5	16.5
May-93	0.4	0.8	27.9	2.7	24.1	14.9	36.5	-26.4	-207.2	5.9	12.9
Jun-93	0.5	0.7	18.4	2.0	15.5	11.4	33.5	-27.1	-212.7	3.5	10.1
Jul-93	0.5	0.6	14.9	2.0	15.1	9.5	48.1	-27.6	-217.8	3.0	8.2
Aug-93	0.6	0.7	19.0	2.6	20.6	9.5	59.5	-28.2	-223.6	2.9	7.7
Sep-93	0.8	0.8	24.5	3.2	26.8	10.4	72.8	-28.5	-227.6	3.3	8.2
Oct-93	0.9	0.8	28.4	3.4	28.9	12.4	66.8	-28.5	-226.9	4.4	10.0
Nov-93	1.0	0.7	26.6	3.0	24.7	15.0	56.1	-28.3	-223.7	5.7	12.9
Dec-93	0.8	0.4	21.0	2.3	17.8	17.3	36.6	-27.8	-219.8	7.7	15.8
Jan-94	0.6	0.3	15.1	1.7	12.7	17.7	29.9	-27.5	-216.8	9.5	16.7
Feb-94	0.4	0.4	12.9	1.5	12.2	15.9	31.2	-27.3	-215.5	10.9	14.9
Mar-94	0.4	0.5	13.7	1.5	13.5	13.4	35.0	-27.5	-216.3	10.2	12.2
Apr-94	0.4	0.5	13.8	1.4	13.4	10.9	32.1	-27.6	-218.0	8.1	9.8
May-94	0.3	0.5	13.4	1.5	13.4	9.0	33.6	-27.8	-220.1	5.9	7.9
Jun-94	0.3	0.5	14.3	1.8	14.7	7.3	37.4	-28.2	-223.5	4.3	6.1
Jul-94	0.4	0.6	17.1	2.3	18.1	6.6	49.4	-29.0	-229.5	3.6	5.0
Aug94	0.5	0.8	21.0	2.8	21.1	6.6	58.4	-29.9	-236.6	3.2	4.8

Sep-94	0.6	0.8	23.0	3.0	22.1	7.2	54.8	-30.2	-240.4	3.6	5.3
Oct-94	0.7	0.9	21.3	2.6	19.3	8.6	42.0	-29.7	-237.2	5.3	7.0
Nov-94	0.6	1.0	16.9	2.1	15.4	11.9	32.7	-28.2	-225.9	8.8	10.6
Dec-94	0.5	1.3	13.2	1.6	12.3	16.6	30.0	-26.2	-209.2	13.2	15.6
Jan-95	0.4	1.3	12.1	1.6	12.4	19.7	43.2	-24.6	-195.5	15.8	18.6
Feb-95	0.3	1.2	14.6	2.0	16.4	18.7	53.8	-24.2	-191.7	14.4	17.3
Mar-95	0.3	1.1	20.1	2.8	22.8	14.5	74.7	-25.3	-199.7	12.6	12.6
Apr-95	0.3	1.0	25.4	3.4	26.8	10.2	68.5	-26.9	-212.8	8.8	8.0
May-95	0.4	0.9	26.4	3.5	25.5	7.6	62.2	-28.1	-223.2	7.2	5.4
Jun-95	0.5	1.0	26.3	3.5	25.4	7.2	55.7	-28.5	-227.1	5.5	5.1
Jul-95	0.5	1.1	27.9	3.5	27.1	9.2	54.9	-28.2	-224.9	7.5	6.9
Aug-95	0.4	1.1	28.0	3.4	27.2	12.5	46.9	-27.3	-217.7	11.9	10.2
Sep-95	0.3	1.2	27.5	3.5	28.2	16.9	70.7	-26.1	-208.4	19.3	14.6
Oct-95	0.2	1.4	31.0	4.0	33.5	24.8	71.8	-25.3	-201.2	29.8	22.0
Nov-95	0.3	1.5	35.5	4.2	36.6	36.6	73.2	-25.3	-200.7	40.3	33.6
Dec-95	0.3	1.2	33.2	3.6	31.2	44.8	35.3	-25.9	-206.7	44.8	42.2
Jan-96	0.3	0.7	23.4	2.4	19.8	42.2	30.5	-26.9	-213.4	40.4	40.5
Feb-96	0.3	0.5	15.9	1.8	14.5	31.4	31.9	-27.3	-215.7	31.4	30.2
Mar-96	0.4	0.3	14.2	1.5	13.5	20.3	39.9	-27.1	-212.4	20.8	19.2
Apr-96	0.5	0.3	14.5	1.5	13.7	14.1	39.2	-26.6	-208.2	13.4	13.0
May-96	0.5	0.4	14.5	1.5	14.1	10.5	39.8	-26.5	-208.1	7.4	9.3
Jun-96	0.5	0.6	15.8	1.9	17.1	8.5	42.0	-27.0	-213.4	5.0	7.1
Jul-96	0.4	1.2	23.2	3.1	28.4	8.2	74.7	-27.7	-219.0	4.8	5.8
Aug-96	0.3	1.8	38.0	5.0	45.4	10.2	114.7	-27.7	-219.0	7.7	6.4
Sep-96	0.5	2.2	51.4	6.2	55.5	13.9	130.1	-27.1	-213.9	10.6	9.2
Oct-96	0.7	2.0	52.6	5.9	50.7	17.2	108.5	-26.4	-208.3	12.7	12.9
Nov-96	0.9	1.3	40.3	4.2	34.2	17.5	68.6	-26.1	-206.1	13.3	14.7

Dec-96	0.8	0.6	24.3	2.5	19.5	15.4	41.1	-26.3	-205.9	14.2	13.8
Jan-97	0.6	0.3	13.9	1.5	11.7	12.7	27.4	-26.7	-207.7	14.2	11.8
Feb-97	0.5	0.2	10.7	1.3	10.6	10.9	27.6	-27.4	-212.7	12.5	10.1
Mar-97	0.4	0.3	12.8	1.8	14.0	10.0	36.6	-28.0	-218.8	10.5	8.8
Apr-97	0.4	0.5	19.0	2.6	20.6	8.8	52.1	-28.4	-222.8	8.5	7.0
May-97	0.5	0.9	26.6	3.5	27.8	7.7	67.4	-28.4	-223.9	6.8	5.4
Jun-97	0.5	1.1	33.7	4.1	35.0	7.0	83.6	-28.5	-226.1	5.2	4.1
Jul-97	0.5	1.3	38.9	4.5	39.7	7.2	94.1	-28.8	-228.9	4.2	3.8
Aug-97	0.5	1.7	41.3	4.9	43.2	8.9	90.0	-28.6	-228.1	3.8	5.3
Sep-97	0.7	1.8	41.9	5.1	43.8	11.1	89.3	-27.9	-222.2	3.8	7.4
Oct-97	0.8	2.0	43.7	5.4	45.9	13.4	99.6	-26.8	-214.1	4.7	9.5
Nov-97	0.9	1.5	44.6	5.3	43.9	15.2	93.1	-25.9	-206.4	7.1	11.5
Dec-97	0.8	1.2	39.5	4.5	35.9	16.7	71.6	-25.2	-200.6	9.3	13.7
Jan-98	0.6	0.9	31.0	3.6	28.1	16.3	65.3	-24.9	-198.5	11.1	14.0
Feb-98	0.4	0.9	28.3	3.4	27.8	13.7	80.2	-25.3	-202.0	10.3	11.4
Mar-98	0.4	1.0	30.5	3.5	30.7	9.9	87.1	-25.8	-205.8	8.0	7.3
Apr-98	0.4	0.9	29.9	3.1	28.3	6.8	61.0	-26.0	-206.0	5.0	4.4
May-98	0.4	0.8	25.0	2.5	24.1	5.4	37.8	-26.0	-204.8	2.9	3.4
Jun-98	0.5	0.9	25.4	2.7	27.5	5.6	45.7	-26.5	-209.0	2.4	3.3
Jul-98	0.6	1.2	32.6	3.5	36.4	6.9	61.3	-27.4	-216.9	2.5	3.8
Aug-98	0.7	1.3	38.7	4.2	40.6	8.0	76.9	-27.9	-222.2	2.6	4.6
Sep-98	0.7	1.3	40.3	4.7	41.6	9.0	84.4	-27.5	-219.4	3.5	5.5
Oct-98	0.6	1.4	40.2	4.9	41.0	10.2	86.8	-26.5	-212.3	4.7	6.7
Nov-98	0.6	1.4	39.1	4.7	39.5	11.8	76.2	-25.6	-206.0	6.7	8.5
Dec-98	0.5	1.0	34.1	3.8	31.9	13.2	54.0	-26.1	-208.6	7.4	10.5
Jan-99	0.4	0.8	25.3	2.8	23.2	12.4	37.7	-27.7	-219.7	7.1	10.4
Feb-99	0.3	0.7	20.0	2.4	20.4	9.9	47.0	-29.2	-230.6	6.0	8.2

Mar-99	0.3	0.9	20.9	2.6	23.4	7.2	55.5	-29.2	-231.6	5.0	5.2
Apr-99	0.3	0.8	23.3	2.8	25.0	5.7	56.9	-28.2	-223.8	4.5	3.6
May-99	0.4	0.8	23.4	2.7	24.5	5.2	51.7	-26.8	-214.0	4.1	3.1
Jun-99	0.5	0.8	23.0	2.9	24.6	5.4	51.2	-25.8	-206.2	3.9	3.4
Jul-99	0.4	1.0	25.6	3.2	28.6	6.9	59.1	-25.1	-201.8	4.6	4.5
Aug-99	0.5	1.3	30.7	4.1	35.3	9.5	86.4	-24.8	-199.5	6.8	6.5
Sep-99	0.6	1.5	38.4	4.9	43.8	12.7	99.2	-24.8	-199.0	9.3	9.0
Oct-99	0.7	1.4	41.7	5.0	43.7	16.0	84.8	-24.8	-198.5	10.7	12.4
Nov-99	0.7	1.0	35.7	3.9	34.1	17.8	49.2	-24.8	-198.6	11.5	15.0
Dec-99	0.6	0.5	23.0	2.4	19.4	17.9	25.0	-24.9	-198.6	12.9	16.2
Jan-00	0.5	0.5	13.0	1.6	12.6	16.5	29.5	-24.7	-196.7	15.5	15.4
Feb-00	0.4	0.5	12.9	1.7	14.9	15.7	40.0	-24.4	-193.2	15.6	14.4
Mar-00	0.3	0.6	16.2	2.0	17.2	13.5	43.2	-24.6	-194.2	12.5	12.1
Apr-00	0.3	0.4	16.7	2.0	16.5	10.7	41.9	-24.9	-197.2	7.6	9.3
May-00	0.3	0.6	14.7	2.2	16.4	7.0	31.2	-25.1	-198.6	3.8	5.6
Jun-00	0.4	1.4	22.2	4.3	34.2	6.7	88.5	-25.0	-197.8	2.2	3.9
Jul-00	0.5	2.3	44.9	7.1	57.2	8.6	126.7	-25.2	-200.1	1.7	3.8
Aug-00	0.5	2.5	57.3	7.7	60.9	10.1	131.5	-25.6	-203.5	1.6	5.0
Sep-00	0.5	2.2	49.9	5.6	42.8	10.1	78.2	-25.3	-200.4	2.4	6.5
Oct-00	0.5	1.5	27.6	2.9	20.5	11.2	48.3	-24.8	-195.4	5.8	9.5
Nov-00	0.4	1.2	16.6	2.0	15.6	17.6	55.0	-25.0	-196.5	10.3	16.3
Dec-00	0.4	0.8	14.9	1.7	13.9	22.1	48.9	-25.4	-200.0	12.8	20.9
Jan-01	0.4	0.6	14.1	1.6	12.9	22.0	48.9	-25.5	-200.5	11.2	20.9
Feb-01	0.4	0.5	14.9	1.9	14.8	16.3	57.2	-25.1	-197.9	8.1	15.1
Mar-01	0.5	0.7	21.7	2.9	24.7	11.9	84.1	-25.5	-200.6	5.8	9.8
Apr-01	0.6	1.2	34.5	4.3	39.3	9.8	104.8	-26.6	-210.5	4.6	6.5
May-01	0.8	1.8	48.1	5.7	53.2	9.0	113.6	-28.0	-222.6	3.4	4.5

Jun-01	0.7	2.2	55.6	6.3	59.2	8.7	108.5	-29.2	-233.0	2.3	3.8
Jul-01	0.6	2.3	57.4	6.6	61.0	9.7	107.5	-29.7	-237.2	4.1	4.6
Aug-01	0.4	2.4	58.9	7.0	64.3	13.1	132.5	-29.6	-236.3	9.5	7.7
Sep-01	0.4	2.5	61.3	7.2	66.3	18.8	137.7	-29.0	-231.8	14.4	13.3
Oct-01	0.4	2.1	56.1	6.3	56.7	23.9	109.5	-28.0	-224.4	18.3	19.1
Nov-01	0.4	1.4	40.1	4.2	35.9	25.4	53.6	-26.9	-214.5	18.8	22.4
Dec-01	0.4	1.0	21.2	2.2	16.8	23.0	25.6	-25.9	-205.1	17.0	21.6
Jan-02	0.4	1.0	12.1	1.9	13.8	18.5	31.3	-25.7	-203.2	12.7	17.4
Feb-02	0.4	1.5	20.4	3.3	28.5	14.8	69.5	-26.2	-208.3	9.1	12.4
Mar-02	0.3	1.9	37.6	5.2	46.0	12.8	102.5	-27.2	-217.1	7.0	9.0
Apr-02	0.4	1.9	48.2	5.7	49.9	11.5	103.1	-28.2	-225.3	5.6	7.3
May-02	0.5	1.6	43.6	5.2	42.6	9.5	94.4	-29.0	-231.1	3.6	5.9
Jun-02	0.5	1.3	38.6	4.9	39.6	7.5	85.0	-29.4	-234.4	2.7	4.2
Jul-02	0.5	1.2	35.4	4.7	37.0	5.9	85.0	-29.7	-235.8	2.4	2.8
Aug-02	0.5	1.0	34.0	4.5	34.4	5.3	69.3	-29.8	-236.9	2.2	2.4
Sep-02	0.5	0.9	27.3	3.7	26.6	4.9	58.8	-30.1	-238.7	2.1	2.6
Oct-02	0.5	0.8	22.6	3.3	24.0	5.8	50.0	-30.1	-238.4	2.1	3.8
Nov-02	0.6	0.8	18.8	2.5	18.9	7.8	38.8	-29.4	-233.3	3.7	6.2
Dec-02	0.5	0.5	13.8	1.8	13.0	12.5	26.0	-28.0	-221.1	8.7	11.5
Jan-03	0.4	0.4	10.5	1.5	11.4	18.6	34.0	-26.1	-206.6	13.1	17.6
Feb-03	0.3	0.4	12.0	1.9	15.2	20.9	34.7	-24.6	-194.2	14.1	19.6
Mar-03	0.3	0.9	21.0	3.4	28.8	18.5	72.1	-23.8	-188.4	10.5	16.1
Apr-03	0.4	1.4	34.8	5.0	42.5	13.1	87.8	-24.0	-190.3	6.5	9.5
May-03	0.5	1.5	42.8	5.5	46.0	9.1	94.6	-25.0	-197.2	3.8	5.2
Jun-03	0.6	1.2	37.8	4.3	34.7	6.3	61.7	-26.1	-206.7	2.1	3.3
Jul-03	0.5	0.7	24.6	2.6	20.1	4.8	36.6	-26.9	-213.2	1.6	3.1
Aug-03	0.2	0.6	15.7	2.2	15.4	5.1	43.3	-27.6	-220.1	2.1	3.8
Sep03	0.2	0.9	19.8	3.1	23.6	7.3	63.9	-28.3	-225.8	3.1	5.3

Oct-03	0.3	1.3	29.8	4.1	33.8	10.9	75.2	-28.2	-225.7	7.3	8.1
Nov-03	0.6	1.2	34.1	4.0	33.2	15.3	57.8	-27.2	-217.6	11.6	12.5
Dec-03	0.8	0.9	26.4	2.7	22.0	18.9	35.9	-26.2	-209.2	14.8	17.0
Jan-04	0.7	0.6	14.8	1.5	11.2	18.7	29.3	-26.1	-207.5	12.8	17.8
Feb-04	0.6	0.6	8.9	1.1	8.6	14.7	31.6	-26.5	-209.6	8.5	13.9
Mar-04	0.7	0.5	8.6	1.0	9.4	9.5	30.1	-26.7	-210.9	4.9	8.7
Apr-04	0.7	0.4	8.9	1.0	9.8	6.3	34.8	-27.1	-212.7	3.0	5.5
May-04	0.6	0.7	10.4	1.6	13.2	5.5	43.4	-28.7	-225.6	2.3	4.4
Jun-04	0.4	1.4	19.7	3.8	29.1	5.6	86.2	-31.5	-247.7	1.9	3.2
Jul-04	0.4	2.3	40.9	7.1	54.5	6.1	130.4	-34.2	-270.2	1.8	1.6
Aug-04	0.5	3.0	65.4	10.1	76.8	6.9	173.8	-35.4	-279.9	1.8	0.4
Sep-04	0.6	3.0	77.2	10.6	78.8	8.4	157.7	-33.4	-265.7	2.3	1.8
Oct-04	0.6	2.5	70.2	9.1	65.8	11.9	131.7	-30.2	-240.3	3.3	6.4
Nov-04	0.5	1.7	54.8	6.5	48.4	15.8	83.7	-27.0	-214.6	5.3	11.7
Dec-04	0.4	1.1	39.1	4.4	35.2	18.4	68.6	-26.1	-206.8	8.5	15.4
Jan-05	0.5	0.8	28.7	3.0	26.0	17.5	45.6	-27.3	-215.1	9.5	15.3
Feb-05	0.5	0.7	21.1	2.4	21.5	14.3	49.4	-29.4	-231.5	8.3	12.5
Mar-05	0.5	0.9	21.2	3.3	25.1	10.7	54.5	-30.7	-242.4	4.8	8.6
Apr-05	0.4	1.9	36.8	6.5	51.1	9.6	137.2	-30.3	-240.7	3.8	5.3
May-05	0.4	2.8	65.1	9.7	78.4	10.2	197.2	-28.8	-230.3	4.0	3.6
Jun-05	0.4	3.3	80.3	11.0	89.9	10.7	212.6	-27.1	-218.4	3.9	3.1
Jul-05	0.4	2.6	74.0	8.9	72.3	9.4	132.4	-25.6	-206.2	2.7	3.4
Aug-05	0.6	1.8	48.4	5.9	45.2	7.6	68.7	-24.4	-195.9	1.7	3.8
Sep-05	0.8	1.3	31.1	4.1	30.5	7.2	57.5	-23.7	-189.8	1.9	4.6
Oct-05	0.9	1.4	28.4	4.2	33.4	10.1	95.9	-23.5	-189.3	3.6	7.3
Nov-05	0.8	1.6	34.9	4.6	39.2	16.4	96.9	-23.5	-189.8	6.3	13.1
Dec-05	0.7	1.2	35.7	4.2	36.6	22.1	76.8	-23.5	-189.6	8.6	19.0

Jan-06	0.5	1.0	30.0	3.4	29.1	23.1	51.7	-23.5	-188.9	8.6	20.7
Feb-06	0.4	1.3	30.7	4.0	37.6	19.3	100.2	-23.7	-189.9	7.1	16.2
Mar-06	0.3	2.1	46.8	5.7	60.5	14.3	150.3	-24.4	-194.0	4.7	9.2
Apr-06	0.2	2.5	61.8	6.9	74.4	10.8	157.6	-25.4	-201.2	3.5	4.5
May-06	0.2	2.6	66.0	7.2	75.4	8.9	138.9	-26.1	-207.6	2.5	2.6
Jun-06	0.2	2.5	62.1	7.0	67.8	8.1	126.1	-26.3	-208.6	1.9	2.4
Jul-06	0.3	2.6	54.3	6.2	56.5	7.4	115.9	-26.1	-205.5	1.5	2.7
Aug-06	0.4	2.1	41.9	4.9	40.3	7.0	77.9	-25.6	-201.9	1.3	3.6
Sep-06	0.5	1.3	25.5	3.1	21.3	7.6	33.1	-25.5	-201.9	1.2	5.8
Oct-06	0.7	0.8	12.2	1.8	10.1	11.3	14.2	-25.3	-202.1	1.8	10.4
Nov-06	0.8	0.7	7.2	1.2	6.8	20.0	29.8	-25.0	-199.8	4.2	19.4
Dec-06	0.7	0.8	6.8	1.1	7.5	28.3	35.3	-24.7	-197.2	9.7	27.6
Jan-07	0.6	0.7	7.0	1.0	7.5	29.5	36.7	-25.0	-198.2	12.7	28.9
Feb-07	0.4	0.7	7.0	0.9	7.7	23.3	27.5	-25.5	-201.0	11.7	22.7
Mar-07	0.5	0.7	8.4	1.1	9.6	14.5	31.2	-25.9	-203.6	6.7	13.7
Apr-07	0.6	0.8	10.8	1.3	11.8	8.7	32.6	-26.3	-205.7	3.4	7.7
May-07	0.7	0.9	12.8	1.4	13.4	5.4	36.9	-27.1	-211.2	2.2	4.3
Jun-07	0.7	1.0	13.6	1.5	14.0	4.5	36.0	-28.0	-217.9	2.3	3.4
Jul-07	0.6	1.0	14.2	1.7	15.5	4.8	41.2	-28.7	-223.7	2.3	3.5
Aug-07	0.6	0.9	17.7	2.3	20.6	5.3	51.6	-29.2	-228.3	2.3	3.6
Sep-07	0.6	1.1	22.1	3.1	24.4	6.4	62.4	-29.6	-232.4	1.9	4.3
Oct-07	0.6	2.0	25.6	4.2	28.5	10.5	78.2	-29.8	-235.3	2.1	8.1
Nov-07	0.6	3.6	28.6	4.7	30.8	16.3	85.0	-28.9	-228.9	6.7	13.7
Dec-07	0.5	5.5	29.3	4.4	31.0	20.5	72.2	-28.1	-223.5	12.2	17.9
Jan-08	0.5	8.2	29.0	3.6	30.3	20.7	66.0	-27.7	-219.2	16.5	18.2
Feb-08	0.4	10.7	26.4	2.9	27.7	17.9	46.3	-28.2	-222.3	12.8	15.6
Mar-08	0.3	11.8	26.4	3.6	30.5	14.6	107.7	-28.5	-224.1	7.7	12.1

Apr-08	0.4	10.1	33.0	4.9	38.2	10.8	129.6	-28.3	-223.4	3.0	7.5
May-08	0.5	7.4	41.7	6.1	46.2	7.6	151.5	-28.0	-221.7	1.9	3.8
Jun-08	0.6	5.3	48.0	6.6	51.2	6.3	115.8	-27.6	-219.7	1.4	2.0
Jul-08	0.6	4.4	47.5	6.2	48.9	6.5	90.2	-27.3	-218.5	1.4	2.4
Aug-08	0.6	3.7	41.2	5.5	42.8	6.9	70.9	-27.3	-218.4	1.3	3.3
Sep-08	0.6	3.2	33.1	4.4	34.3	6.8	52.7	-27.5	-219.0	1.1	4.0
Oct-08	0.6	2.6	25.2	3.4	26.1	6.9	50.2	-27.5	-218.6	1.5	4.7
Nov-08	0.5	2.1	19.4	2.6	19.9	8.5	45.3	-27.1	-215.0	3.2	6.8
Dec-08	0.4	1.9	15.5	2.1	16.1	11.4	39.9	-26.1	-207.5	5.3	10.0
Jan-09	0.4	1.8	13.2	1.9	14.3	13.7	40.3	-25.5	-201.3	7.2	12.5
Feb-09	0.3	2.2	12.8	1.9	14.4	14.4	43.8	-25.5	-200.2	7.7	13.2
Mar-09	0.3	3.6	14.8	2.3	17.3	13.2	55.5	-26.0	-203.9	6.8	11.8
Apr-09		5.5	20.5	3.1	23.9	11.5	68.8	-26.5	-208.4	4.8	9.5
May-09		6.8	27.9	3.9	31.2	9.4	76.9	-26.9	-211.8	2.7	6.8
Jun-09		6.9	31.9	4.1	33.5	7.6	70.3	-27.0	-213.6	1.7	4.8
Jul-09		6.3	29.9	3.9	30.5	6.4	66.1	-27.6	-218.2	1.4	3.8
Aug-09		5.8	26.2	3.9	28.4	6.2	78.9	-28.8	-227.2	1.4	3.8
Sep-09		5.4	26.9	4.4	31.0	7.7	98.8	-29.7	-235.0	1.9	5.1
Oct-09		5.5	31.0	4.9	34.5	12.1	84.9	-29.4	-233.3	6.8	9.2
Nov-09		5.6	33.5	4.7	32.8	20.0	61.8	-27.9	-221.2	14.3	17.2
Dec-09		5.6	29.5	3.7	25.9	29.0	36.0	-26.5	-209.4	21.8	26.9
Jan-10		5.1	24.1	3.2	22.2	34.1	29.3	-26.2	-207.5	21.7	32.2
Feb-10		4.8	25.8	3.9	29.5	32.5	48.4	-27.1	-215.0	16.5	30.0
Mar-10		5.0	40.8	5.9	50.1	26.1	114.1	-28.3	-224.9	9.0	21.9
Apr-10		5.4	60.7	7.8	72.2	18.7	158.2	-29.2	-230.7	4.4	12.7
May-10		5.8	72.7	8.6	80.7	13.0	149.0	-29.3	-231.7	2.0	6.2
Jun-10		6.4	69.7	8.0	73.0	9.1	95.3	-29.2	-230.9	1.4	3.0

Jul-10		6.9	56.6	6.5	56.0	7.2	64.5	-29.1	-230.4	1.2	2.4
Aug-10		7.8	42.0	5.1	41.5	6.1	60.6	-29.4	-233.3	1.2	2.7
Sep-10		9.0	31.9	4.1	31.9	6.0	52.6	-30.0	-237.8	1.5	3.3
Oct-10		10.4	27.4	3.7	27.3	6.4	48.6	-30.3	-240.2	1.9	4.1
Nov-10		11.0	27.6	3.9	28.1	7.3	63.9	-29.5	-235.1	2.7	4.9
Dec-10		10.7	30.8	4.4	31.8	8.2	100.6	-27.9	-224.0	3.8	5.5
PIG2010		**Lat: -77.96**		**Lon: -95.96**		**Elevation: 1593m**					
Date	**BrO (ppb)**	**Ca (ppb)**	**IO (ppb)**	**Mg (ppb)**	**Na (ppb)**	**S_{tot} (ppb)**	**Cl^- (ppb)**	**δ18O (‰)**	**δD (‰)**	**MSA (ppb)**	**nssS (ppb)**
Jan-79	0.2	0.3	6.5	0.9	5.6	16.6		-29.4	-234.9		16.2
Feb-79	0.2	0.5	7.4	1.3	9.9	13.3		-28.7	-228.4		12.5
Mar-79	0.3	1.1	10.3	1.9	16.5	10.4		-28.6	-227.2		9.0
Apr-79	0.4	1.4	12.7	2.3	20.5	8.2		-29.4	-232.6		6.5
May-79	0.5	1.3	12.4	2.4	19.5	6.6		-30.6	-243.1		5.0
Jun-79	0.6	1.0	10.8	2.9	20.1	6.2		-32.0	-255.7		4.5
Jul-79	0.6	1.4	11.4	4.6	32.9	7.7		-33.4	-268.0		4.9
Aug-79	0.6	1.9	14.9	5.6	40.0	9.1		-34.4	-277.4		5.7
Sep-79	0.6	1.9	16.4	5.7	42.1	10.4		-34.8	-280.9		6.8
Oct-79	0.5	1.3	13.3	4.1	29.3	11.2		-34.0	-274.3		8.7
Nov-79	0.4	0.8	7.6	2.8	20.8	14.0		-32.4	-259.9		12.3
Dec-79	0.3	0.5	3.7	1.7	12.0	17.7		-30.8	-245.9		16.7
Jan-80	0.3	0.3	3.7	1.2	7.5	19.4		-30.1	-239.8		18.8
Feb-80	0.4	0.3	6.4	1.1	6.7	18.0		-30.4	-242.2		17.4
Mar-80	0.4	0.5	11.1	1.3	8.7	14.0		-31.0	-246.4		13.3
Apr-80	0.5	0.6	15.6	1.5	12.0	10.6		-31.5	-249.3		9.6
May-80	0.6	0.7	18.0	1.6	13.0	8.6		-31.7	-250.5		7.5
Jun-80	0.6	0.7	16.7	1.5	11.5	8.2		-31.8	-251.7		7.1
Jul-80	0.6	0.7	12.6	1.4	10.4	8.2		-31.8	-253.7		7.3
Aug80	0.5	0.8	8.6	1.7	13.2	9.0		-31.9	-255.5		7.8

Sep-80	0.4	0.9	7.4	2.0	16.6	10.8	-31.6	-255.0	9.4
Oct-80	0.5	0.9	9.2	2.0	15.9	12.7	-31.1	-251.5	11.4
Nov-80	0.6	0.7	10.5	1.5	10.9	14.4	-30.3	-245.6	13.5
Dec-80	0.5	0.4	9.8	0.9	5.4	15.6	-29.6	-238.8	15.2
Jan-81	0.3	0.4	8.2	0.5	3.2	15.6	-29.3	-234.7	15.3
Feb-81	0.3	0.5	7.2	0.7	4.9	13.5	-29.6	-236.4	13.1
Mar-81	0.3	0.6	8.7	1.1	8.7	10.2	-30.4	-243.1	9.5
Apr-81	0.5	0.6	10.6	1.7	13.7	7.9	-31.2	-250.3	6.7
May-81	0.6	0.6	15.4	2.0	17.2	7.0	-31.8	-254.2	5.5
Jun-81	0.6	0.6	22.5	2.1	18.1	6.7	-32.1	-256.5	5.1
Jul-81	0.4	0.6	29.7	1.8	14.7	6.1	-32.7	-260.9	4.8
Aug-81	0.4	0.5	26.9	1.4	10.2	5.8	-33.5	-268.2	4.9
Sep-81	0.4	0.4	17.4	1.1	7.3	5.8	-34.3	-276.0	5.2
Oct-81	0.4	0.4	6.6	1.2	8.0	7.1	-34.7	-279.1	6.4
Nov-81	0.4	0.4	3.1	1.3	10.2	9.8	-34.2	-275.8	9.0
Dec-81	0.3	0.4	2.9	1.3	10.3	13.2	-33.3	-268.6	12.4
Jan-82	0.2	0.2	3.8	1.1	9.0	14.3	-33.0	-264.8	13.6
Feb-82	0.2	0.2	4.1	0.9	7.2	12.5	-33.4	-266.7	11.9
Mar-82	0.2	0.3	3.9	1.0	7.6	9.1	-34.2	-271.8	8.5
Apr-82	0.3	0.5	5.0	1.2	9.6	7.1	-34.5	-273.9	6.3
May-82	0.4	0.6	10.0	1.6	12.5	6.3	-34.0	-270.7	5.3
Jun-82	0.4	0.9	17.5	2.3	18.7	7.0	-32.9	-263.2	5.5
Jul-82	0.4	1.3	21.8	3.3	27.3	8.3	-31.4	-251.8	6.0
Aug-82	0.4	1.3	20.3	3.6	29.9	8.8	-30.0	-241.0	6.3
Sep-82	0.4	1.0	16.8	2.9	22.9	9.4	-29.1	-234.0	7.5
Oct-82	0.5	0.5	16.0	1.6	10.8	10.7	-29.0	-233.7	9.8
Nov-82	0.5	0.3	16.0	0.8	3.8	13.5	-29.7	-238.8	13.2

Dec-82	0.4	0.2	12.8	0.5	2.8	16.0	-30.7	-247.0	15.7
Jan-83	0.3	0.2	8.1	0.4	3.3	16.3	-31.7	-254.4	16.0
Feb-83	0.2	0.2	5.8	0.5	3.9	14.6	-32.4	-259.2	14.3
Mar-83	0.3	0.2	5.8	0.5	3.8	11.3	-32.8	-260.3	11.0
Apr-83	0.5	0.2	6.0	0.5	3.9	8.5	-33.1	-260.9	8.2
May-83	0.7	0.2	10.0	0.8	7.0	7.3	-33.7	-265.3	6.7
Jun-83	0.8	0.4	16.2	1.6	14.1	7.5	-34.8	-274.3	6.2
Jul-83	0.7	0.6	23.6	2.4	21.1	8.0	-36.0	-285.2	6.2
Aug-83	0.7	0.8	25.6	2.5	22.0	8.4	-36.9	-292.5	6.6
Sep-83	0.7	0.7	21.1	2.2	18.3	9.1	-36.9	-293.9	7.6
Oct-83	0.6	0.7	13.8	2.0	15.8	10.8	-36.3	-290.2	9.5
Nov-83	0.5	0.7	6.6	2.1	16.3	14.2	-35.2	-282.3	12.8
Dec-83	0.4	0.8	5.2	2.0	15.1	18.2	-33.9	-271.4	16.9
Jan-84	0.4	0.6	6.6	1.4	10.3	19.8	-32.5	-257.9	18.9
Feb-84	0.4	0.4	9.3	0.9	6.5	17.8	-31.2	-246.9	17.3
Mar-84	0.5	0.2	10.2	0.7	5.5	13.8	-30.6	-241.0	13.3
Apr-84	0.7	0.1	9.8	0.7	6.0	10.3	-30.6	-241.5	9.8
May-84	0.8	0.2	18.7	1.0	7.5	8.0	-31.2	-246.8	7.4
Jun-84	0.7	0.4	34.9	1.8	13.5	7.1	-32.3	-256.4	6.0
Jul-84	0.7	0.6	43.8	2.7	19.9	7.2	-33.6	-268.8	5.6
Aug-84	0.8	1.0	39.4	3.4	26.6	9.3	-34.4	-276.3	7.0
Sep-84	0.8	0.9	24.9	3.2	24.2	11.2	-33.9	-273.2	9.1
Oct-84	0.7	0.9	14.7	2.4	18.4	13.0	-32.3	-259.4	11.4
Nov-84	0.6	0.5	8.3	1.3	9.3	13.9	-30.7	-246.0	13.1
Dec-84	0.5	0.4	6.2	0.7	5.2	15.2	-30.2	-241.7	14.8
Jan-85	0.4	0.3	10.1	0.6	5.4	15.6	-31.0	-247.5	15.2
Feb-85	0.3	0.7	12.6	0.9	8.4	14.2	-31.9	-254.5	13.5

Mar-85	0.4	1.3	12.0	1.1	9.7	11.4	-32.2	-256.5	10.6
Apr-85	0.4	1.4	10.0	1.2	9.2	8.5	-32.5	-258.1	7.7
May-85	0.5	1.5	14.6	2.1	14.9	7.1	-33.0	-261.5	5.8
Jun-85	0.4	1.3	25.0	4.0	29.6	6.9	-34.4	-273.2	4.4
Jul-85	0.5	2.0	30.3	5.9	44.1	8.1	-35.6	-283.8	4.4
Aug-85	0.6	2.0	26.5	5.8	42.4	8.3	-35.7	-286.5	4.8
Sep-85	0.7	1.7	18.3	4.8	34.0	8.6	-34.5	-277.7	5.7
Oct-85	0.6	1.3	12.8	2.7	18.9	8.9	-32.3	-258.4	7.3
Nov-85	0.5	1.4	9.0	1.7	12.7	10.6	-30.7	-245.5	9.5
Dec-85	0.4	1.5	6.4	0.7	5.5	13.0	-29.8	-237.9	12.5
Jan-86	0.3	1.3	5.3	0.9	7.8	14.5	-29.9	-238.9	13.9
Feb-86	0.2	1.0	6.5	1.3	11.5	14.3	-30.4	-242.7	13.4
Mar-86	0.3	0.7	9.9	1.5	12.8	12.4	-31.1	-248.5	11.3
Apr-86	0.3	0.4	14.8	1.3	10.4	9.7	-32.2	-257.5	8.8
May-86	0.2	0.5	21.6	1.5	10.8	8.4	-33.7	-267.4	7.5
Jun-86	0.2	1.6	25.4	2.6	19.9	8.0	-35.2	-279.1	6.3
Jul-86	0.3	2.5	23.2	3.8	29.9	8.4	-36.4	-288.9	5.8
Aug-86	0.5	2.5	16.6	3.9	30.6	8.5	-36.3	-288.9	5.9
Sep-86	0.6	1.5	12.1	3.1	23.0	8.8	-36.1	-288.9	6.8
Oct-86	0.6	0.7	12.8	2.1	15.1	10.3	-35.2	-282.8	9.0
Nov-86	0.6	0.4	14.3	1.5	10.7	12.7	-34.4	-275.6	11.8
Dec-86	0.6	0.4	12.4	1.1	7.4	15.4	-32.3	-258.4	14.8
Jan-87	0.4	0.3	9.1	0.8	5.5	16.1	-30.7	-245.0	15.7
Feb-87	0.3	0.4	6.8	0.7	5.3	15.3	-30.4	-241.1	14.9
Mar-87	0.3	0.4	5.9	1.0	7.7	13.1	-31.2	-247.2	12.5
Apr-87	0.3	0.5	5.6	1.4	12.1	11.1	-32.3	-255.7	10.1
May-87	0.4	0.7	6.8	2.3	17.8	9.4	-33.0	-262.3	7.9

Jun-87	0.5	0.9	14.6	3.4	24.9	8.2	-33.2	-265.3	6.1
Jul-87	0.4	0.9	20.0	3.7	25.3	7.0	-33.2	-265.4	4.9
Aug-87	0.4	0.7	19.6	3.2	20.9	6.2	-32.9	-264.1	4.4
Sep-87	0.5	0.5	15.0	2.1	13.4	6.0	-32.8	-263.1	4.9
Oct-87	0.6	0.6	14.8	1.7	11.9	8.3	-32.7	-262.8	7.3
Nov-87	0.6	0.7	15.9	1.9	13.9	13.6	-32.2	-259.7	12.4
Dec-87	0.5	0.7	14.1	1.9	14.1	19.6	-31.0	-250.1	18.4
Jan-88	0.4	0.5	10.2	1.5	10.6	23.1	-29.4	-236.0	22.2
Feb-88	0.4	0.3	14.5	1.0	7.8	22.4	-28.7	-229.0	21.7
Mar-88	0.6	0.2	23.6	0.7	6.1	18.1	-29.3	-232.7	17.6
Apr-88	0.8	0.3	28.9	0.7	6.0	12.4	-30.6	-243.5	11.9
May-88	1.0	0.2	28.7	0.6	5.0	7.5	-31.8	-252.8	7.1
Jun-88	0.9	0.4	25.0	1.2	9.7	5.5	-32.6	-259.6	4.7
Jul-88	0.8	0.7	25.9	2.3	18.5	6.0	-33.2	-264.2	4.4
Aug-88	0.7	0.9	26.1	2.8	21.0	6.9	-33.3	-266.1	5.1
Sep-88	0.7	0.8	29.8	2.4	17.5	7.8	-33.1	-266.0	6.4
Oct-88	0.7	0.7	31.3	2.0	14.0	9.0	-33.1	-266.7	7.8
Nov-88	0.7	0.7	26.0	2.1	15.8	12.4	-33.1	-267.2	11.1
Dec-88	0.7	0.7	15.7	2.1	15.7	17.4	-32.6	-263.3	16.1
Jan-89	0.5	0.6	6.1	1.5	11.8	19.9	-32.1	-257.8	18.9
Feb-89	0.4	0.7	5.6	1.4	10.5	17.5	-32.1	-256.5	16.6
Mar-89	0.4	0.9	11.7	2.3	20.2	12.4	-33.1	-262.8	10.7
Apr-89	0.5	1.1	21.8	3.1	27.3	8.8	-34.2	-271.8	6.4
May-89	0.5	1.2	29.3	3.6	31.3	7.6	-35.0	-278.0	4.9
Jun-89	0.5	1.1	30.3	3.4	26.5	6.7	-35.2	-280.5	4.5
Jul-89	0.5	1.1	27.8	3.4	25.1	7.0	-35.2	-279.7	5.0
Aug-89	0.5	1.1	25.0	3.5	25.2	8.5	-34.9	-277.8	6.4
Sep89	0.6	1.2	22.5	3.7	26.4	10.2	-34.7	-276.8	8.1

Oct-89	0.7	1.3	19.7	4.2	31.6	11.9	-34.3	-275.4	9.2
Nov-89	0.7	1.2	16.6	3.8	28.8	13.8	-33.5	-270.9	11.4
Dec-89	0.6	0.9	13.1	2.7	21.3	16.4	-32.7	-263.6	14.6
Jan-90	0.5	0.5	8.9	1.3	9.0	17.4	-32.3	-259.3	16.6
Feb-90	0.4	0.3	6.6	0.7	4.6	15.8	-32.8	-260.8	15.4
Mar-90	0.4	0.4	7.4	1.0	7.4	12.4	-33.7	-266.5	11.7
Apr-90	0.4	0.7	12.7	1.9	16.3	9.5	-34.7	-274.0	8.2
May-90	0.5	1.1	20.6	2.9	26.1	7.9	-35.7	-282.0	5.8
Jun-90	0.6	1.5	25.8	3.5	30.6	7.3	-36.3	-288.1	4.8
Jul-90	0.5	1.6	25.1	3.6	28.8	7.5	-36.4	-289.6	5.2
Aug-90	0.5	1.7	22.0	3.5	26.0	8.1	-35.9	-286.9	5.9
Sep-90	0.7	1.5	21.8	3.3	23.4	8.7	-35.0	-281.0	6.7
Oct-90	0.8	1.3	21.8	2.9	21.1	9.6	-34.0	-273.3	7.8
Nov-90	0.7	1.0	17.8	2.4	17.9	13.8	-32.7	-262.7	12.3
Dec-90	0.5	0.9	11.1	2.0	14.7	19.2	-31.1	-249.5	18.0
Jan-91	0.3	0.7	6.1	1.5	10.6	22.6	-29.5	-236.4	21.7
Feb-91	0.2	0.5	5.0	1.0	7.2	19.8	-28.4	-228.1	19.2
Mar-91	0.2	0.4	6.5	0.8	6.4	14.7	-28.5	-226.9	14.1
Apr-91	0.3	0.4	9.1	1.1	9.2	10.3	-29.2	-232.2	9.5
May-91	0.5	0.5	11.8	2.0	16.7	8.7	-30.5	-241.4	7.3
Jun-91	0.6	0.8	18.8	3.0	24.1	8.1	-32.1	-253.7	6.1
Jul-91	0.6	1.0	28.1	3.5	26.4	8.0	-33.6	-266.5	5.8
Aug-91	0.6	1.2	31.7	3.4	23.4	9.6	-34.7	-275.5	7.7
Sep-91	0.6	1.1	28.2	3.1	21.4	14.7	-34.7	-275.5	12.9
Oct-91	0.6	1.1	16.9	3.1	22.5	21.2	-33.5	-266.8	19.3
Nov-91	0.5	1.1	9.6	2.8	20.4	28.3	-31.7	-252.5	26.6
Dec-91	0.5	0.9	5.5	2.1	14.5	35.4	-30.2	-240.4	34.2

Jan-92	0.4	0.8	7.7	1.3	7.8	36.6		-29.5	-235.3		36.0
Feb-92	0.2	0.5	9.1	0.9	5.1	30.0		-29.4	-235.4		29.6
Mar-92	0.2	0.4	9.1	0.7	5.4	18.5		-29.6	-236.1		18.1
Apr-92	0.3	0.2	8.0	0.9	7.9	11.8		-29.9	-236.5		11.1
May-92	0.4	0.3	7.8	1.2	10.3	10.6		-30.6	-241.4		9.7
Jun-92	0.4	0.5	7.6	1.7	13.4	13.1		-31.9	-251.7		12.0
Jul-92	0.4	1.0	7.8	3.1	24.0	17.1		-33.3	-264.6		15.0
Aug-92	0.5	1.3	11.3	3.9	29.2	21.7	244.4	-34.0	-271.3		19.3
Sep-92	0.6	1.4	15.2	4.1	32.0	24.3	124.6	-33.4	-267.7		21.6
Oct-92	0.6	0.9	14.5	2.7	21.6	24.1	59.4	-31.6	-254.1	12.9	22.2
Nov-92	0.5	0.7	11.6	1.6	13.3	25.1	30.0	-29.8	-238.6	17.1	24.0
Dec-92	0.4	0.6	8.3	0.9	6.4	28.9	33.2	-28.7	-229.1	18.9	28.4
Jan-93	0.3	0.7	8.3	0.9	6.1	31.6	25.0	-28.7	-226.6	25.7	31.0
Feb-93	0.3	0.8	7.4	1.0	7.9	30.2	35.5	-29.5	-231.8	28.1	29.6
Mar-93	0.3	0.7	7.5	1.0	8.6	24.7	33.0	-31.0	-243.3	25.4	24.0
Apr-93	0.3	0.7	13.3	0.9	7.9	21.2	42.2	-32.6	-256.5	18.4	20.5
May-93	0.5	0.5	21.2	0.9	7.7	19.2	34.5	-33.3	-263.5	12.9	18.6
Jun-93	0.6	0.5	27.4	0.9	7.7	17.4	36.0	-32.8	-260.3	8.3	16.8
Jul-93	0.5	0.4	32.7	0.9	7.2	15.3	27.4	-31.9	-252.4	5.6	14.7
Aug-93	0.4	0.5	31.6	1.2	9.2	14.2	33.3	-31.7	-251.3	4.2	13.5
Sep-93	0.5	0.7	27.4	1.7	13.8	17.0	42.0	-32.5	-258.5	4.1	15.8
Oct-93	0.6	0.7	16.2	1.9	15.8	20.2	48.7	-33.1	-264.7	4.4	18.8
Nov-93	0.5	0.7	8.6	1.7	14.0	22.6	54.1	-32.7	-261.4	5.7	21.2
Dec-93	0.4	0.7	5.4	1.2	10.2	27.9	49.2	-31.6	-251.7	9.6	26.9
Jan-94	0.3	0.6	5.8	1.0	8.4	29.5	47.4	-30.9	-245.0	15.4	28.7
Feb-94	0.3	0.5	8.6	0.9	7.8	27.8	36.8	-30.6	-242.5	18.1	27.2
Mar-94	0.4	0.3	11.4	0.7	6.9	19.4	33.7	-30.6	-241.8	16.7	18.8

Apr-94	0.5	0.4	13.7	1.1	8.9	14.1	35.8	-30.6	-240.9	12.1	13.4
May-94	0.5	0.6	16.0	2.0	17.6	11.9	51.5	-30.8	-241.8	8.5	10.5
Jun-94	0.5	0.7	20.2	2.8	24.0	10.6	57.8	-31.1	-244.5	6.0	8.6
Jul-94	0.6	1.0	24.9	3.7	31.2	10.3	76.8	-32.0	-252.5	5.6	7.7
Aug-94	0.7	1.1	26.5	4.0	32.5	10.6	64.6	-33.6	-266.3	5.3	7.9
Sep-94	0.7	1.1	21.7	3.9	30.1	11.0	60.0	-35.2	-281.2	5.9	8.5
Oct-94	0.7	0.8	13.3	2.9	22.0	12.1	33.0	-35.6	-285.5	7.8	10.2
Nov-94	0.6	0.6	6.8	1.7	11.3	15.1	26.3	-34.2	-274.5	12.8	14.1
Dec-94	0.5	0.5	4.6	1.0	6.5	20.8	22.1	-31.9	-255.9	19.3	20.3
Jan-95	0.4	0.5	5.2	0.7	4.9	22.8	26.4	-30.2	-241.6	20.6	22.4
Feb-95	0.3	0.4	5.9	0.9	7.0	19.5	30.0	-29.9	-237.4	17.0	18.9
Mar-95	0.3	0.6	6.7	1.2	10.1	13.0	33.8	-30.4	-240.7	10.6	12.2
Apr-95	0.4	0.6	8.5	1.5	12.6	8.7	51.6	-31.5	-248.8	7.7	7.7
May-95	0.6	0.7	11.6	1.8	14.7	7.7	56.5	-32.9	-259.5	6.6	6.4
Jun-95	0.7	0.8	14.8	2.3	17.7	7.3	66.1	-34.2	-270.3	6.1	5.9
Jul-95	0.9	0.9	15.6	2.9	22.6	8.1	59.1	-34.8	-276.8	5.5	6.2
Aug-95	0.9	1.1	14.5	3.2	26.8	9.4	65.2	-34.5	-276.1	5.4	7.2
Sep-95	0.9	1.0	14.5	3.0	25.1	11.5	59.1	-33.6	-270.0	6.3	9.4
Oct-95	0.7	0.7	16.9	2.2	17.7	13.8	45.1	-32.4	-259.9	8.2	12.3
Nov-95	0.5	0.4	25.4	1.2	9.2	16.1	34.2	-31.3	-250.6	11.7	15.4
Dec-95	0.4	0.2	35.8	0.7	5.1	17.8	28.0	-30.7	-245.0	14.8	17.4
Jan-96	0.3	0.2	37.0	0.6	4.7	18.7	25.6	-30.6	-244.3	16.9	18.3
Feb-96	0.3	0.2	28.8	0.6	5.6	17.6	22.9	-30.9	-244.6	16.4	17.2
Mar-96	0.3	0.2	17.3	0.6	6.1	15.3	22.1	-31.0	-245.0	14.2	14.7
Apr-96	0.4	0.3	13.4	0.8	7.4	12.2	27.5	-31.4	-247.3	10.5	11.6
May-96	0.5	0.4	12.6	1.2	9.9	10.7	31.9	-32.2	-253.8	7.1	9.9
Jun-96	0.6	0.5	12.8	1.7	13.4	10.3	37.1	-33.2	-261.3	4.8	9.1

Jul-96	0.7	0.6	17.9	2.0	15.6	10.7	38.9	-33.7	-266.8	3.7	9.4
Aug-96	0.6	0.7	32.6	1.9	15.1	11.4	38.4	-34.0	-269.9	3.7	10.1
Sep-96	0.5	0.7	48.3	1.8	13.7	12.6	36.6	-33.9	-269.5	5.0	11.5
Oct-96	0.5	0.7	48.5	1.9	15.1	15.5	43.2	-33.3	-266.2	9.0	14.2
Nov-96	0.6	0.8	34.1	2.6	19.9	22.1	52.3	-32.3	-259.4	12.0	20.4
Dec-96	0.7	1.1	15.1	3.7	32.3	30.0	62.2	-31.4	-252.1	21.2	27.3
Jan-97	0.6	1.3	6.9	4.2	38.7	32.9	78.1	-31.0	-246.3	27.8	29.6
Feb-97	0.4	1.3	5.3	3.8	35.2	27.7	75.5	-31.1	-245.0	31.7	24.7
Mar-97	0.3	1.0	7.6	2.6	22.7	18.1	65.4	-31.6	-247.8	24.9	16.2
Apr-97	0.3	0.7	13.7	1.8	14.3	11.2	45.1	-31.9	-251.2	15.5	10.0
May-97	0.3	0.4	16.1	1.6	12.9	7.9	38.7	-31.8	-251.0	8.6	6.8
Jun-97	0.3	0.4	14.4	1.5	12.2	6.8	36.6	-31.4	-247.3	4.8	5.9
Jul-97	0.3	0.6	8.3	1.8	14.1	6.8	36.3	-31.0	-244.5	3.5	5.7
Aug-97	0.4	1.0	7.6	3.1	23.8	7.8	51.7	-31.0	-244.8	3.4	5.9
Sep-97	0.4	1.4	11.2	5.1	42.5	10.0	80.3	-31.0	-246.5	3.7	6.4
Oct-97	0.6	1.6	18.8	5.9	51.6	12.0	102.1	-30.7	-245.2	4.4	7.7
Nov-97	0.7	1.3	20.7	5.0	44.0	14.1	82.9	-30.0	-240.7	4.9	10.4
Dec-97	0.7	0.9	17.3	2.9	24.3	16.4	55.5	-29.2	-234.7	6.5	14.3
Jan-98	0.5	0.4	10.1	1.4	9.4	17.7	25.1	-28.4	-228.7	8.9	16.9
Feb-98	0.3	0.1	7.0	0.7	5.5	17.6	25.7	-27.8	-222.8	11.2	17.1
Mar-98	0.3	0.1	9.4	0.6	5.5	14.5	22.8	-27.6	-220.6	11.7	14.0
Apr-98	0.3	0.3	15.8	1.1	10.5	11.4	31.8	-27.8	-221.9	10.0	10.5
May-98	0.5	0.4	20.9	1.5	14.9	8.1	42.3	-27.9	-223.6	7.9	6.8
Jun-98	0.7	0.5	25.6	1.6	15.6	6.4	57.2	-28.2	-224.4	5.6	5.1
Jul-98	0.8	0.4	32.1	1.2	11.0	5.2	52.2	-29.2	-231.9	3.9	4.4
Aug-98	0.8	0.4	42.1	0.9	7.1	4.9	41.5	-31.1	-246.2	2.9	4.4
Sep-98	0.7	0.4	42.8	1.0	8.9	5.3	29.3	-33.2	-262.9	3.2	4.6
Oct98	0.7	0.6	34.5	1.7	14.8	7.2	29.1	-34.1	-271.4	4.1	6.0

Nov-98	0.7	0.9	20.4	2.4	20.6	11.3	46.2	-33.5	-268.2	5.9	9.6
Dec-98	0.6	1.0	11.9	2.4	19.1	16.1	51.5	-32.3	-259.7	8.9	14.5
Jan-99	0.4	0.8	10.9	1.7	13.7	18.6	51.9	-31.7	-253.4	12.6	17.5
Feb-99	0.2	0.5	11.6	1.0	7.4	16.8	33.3	-32.2	-255.3	14.6	16.2
Mar-99	0.2	0.4	11.7	0.9	7.5	12.7	26.6	-33.2	-262.8	13.6	12.0
Apr-99	0.2	0.6	7.9	1.5	11.9	9.0	27.5	-34.0	-268.4	10.5	8.0
May-99	0.3	0.9	5.9	2.2	18.9	7.9	41.7	-34.3	-270.5	7.8	6.4
Jun-99	0.4	1.2	7.4	2.7	22.3	7.2	50.7	-34.3	-270.6	6.4	5.4
Jul-99	0.5	1.8	11.6	3.4	28.1	7.8	72.2	-34.2	-269.7	5.8	5.4
Aug-99	0.6	4.1	14.5	4.8	37.5	8.8	105.2	-33.9	-268.9	5.9	5.6
Sep-99	0.6	7.0	15.4	5.8	45.2	10.7	121.6	-33.2	-264.8	6.0	6.9
Oct-99	0.6	7.2	14.4	5.3	40.4	11.7	107.2	-32.4	-260.0	6.2	8.3
Nov-99	0.6	4.8	13.6	3.6	27.0	12.5	76.4	-31.2	-251.4	6.3	10.2
Dec-99	0.4	1.6	13.1	2.0	14.9	15.2	52.5	-30.0	-241.5	8.0	14.0
Jan-00	0.3	0.6	10.6	1.3	9.6	16.2	41.7	-29.2	-232.8	10.6	15.4
Feb-00	0.3	0.6	10.9	1.2	11.0	15.7	34.5	-28.8	-227.5	11.8	14.8
Mar-00	0.3	0.6	16.1	1.2	11.2	12.1	32.3	-28.9	-227.6	11.0	11.2
Apr-00	0.4	0.6	25.1	1.1	10.5	9.6	30.9	-29.4	-231.8	8.7	8.7
May-00	0.5	0.6	31.6	0.7	5.9	7.7	21.7	-30.3	-239.4	7.0	7.2
Jun-00	0.5	0.8	34.8	0.7	6.1	7.1	22.0	-30.9	-244.0	5.9	6.6
Jul-00	0.5	1.1	34.1	1.0	8.8	6.8	26.0	-30.7	-241.7	4.9	6.0
Aug-00	0.6	1.1	33.4	1.5	13.4	6.7	35.6	-31.5	-247.7	3.9	5.6
Sep-00	0.7	1.0	34.8	1.8	14.7	6.5	36.2	-32.3	-255.6	3.3	5.3
Oct-00	0.7	1.0	37.7	2.0	15.7	7.4	52.5	-32.8	-260.4	3.3	6.1
Nov-00	0.6	1.1	36.0	1.8	13.2	11.4	51.6	-31.2	-249.4	5.3	10.3
Dec-00	0.5	1.1	25.3	1.8	14.2	23.4	58.2	-29.8	-238.4	9.1	22.2
Jan-01	0.3	0.8	12.8	1.6	11.4	30.9	41.2	-29.6	-236.8	14.7	29.9

Feb-01	0.2	0.5	5.2	1.4	10.5	29.6	34.1	-30.5	-243.1	17.2	28.7
Mar-01	0.1	0.5	4.7	1.5	12.2	18.7	31.6	-31.3	-249.1	15.1	17.6
Apr-01	0.1	0.7	9.1	2.3	20.4	10.8	42.6	-32.0	-254.8	10.8	9.1
May-01	0.2	1.0	12.4	3.1	28.5	8.6	58.3	-32.9	-262.4	7.2	6.2
Jun-01	0.3	1.2	14.5	3.8	33.7	7.8	68.9	-34.0	-272.5	5.7	4.9
Jul-01	0.5	1.4	12.2	4.3	34.6	8.0	75.0	-34.8	-279.8	4.9	5.1
Aug-01	0.5	1.2	9.0	4.4	33.4	8.1	70.8	-34.9	-280.8	4.5	5.3
Sep-01	0.4	1.2	5.8	4.6	33.7	9.1	71.7	-34.5	-277.0	5.0	6.3
Oct-01	0.3	1.1	4.5	4.7	36.4	10.4	76.2	-34.1	-273.7	7.7	7.4
Nov-01	0.3	1.5	4.5	4.8	38.3	15.1	82.0	-34.0	-273.3	13.0	11.9
Dec-01	0.3	1.9	9.1	3.9	31.6	21.9	71.0	-33.8	-271.1	19.4	19.2
Jan-02	0.3	1.8	19.2	2.3	18.5	23.8	43.6	-33.0	-263.7	22.5	22.3
Feb-02	0.3	1.3	26.3	1.1	7.8	20.8	24.5	-32.1	-253.8	20.9	20.1
Mar-02	0.3	1.5	28.1	0.5	3.7	13.7	21.3	-31.8	-249.9	15.8	13.4
Apr-02	0.4	2.5	27.1	0.7	6.4	10.2	36.8	-32.3	-254.8	11.3	9.7
May-02	0.5	2.6	28.6	1.2	10.8	8.3	47.3	-33.2	-262.5	9.3	7.4
Jun-02	0.7	1.9	28.6	1.6	13.4	7.3	48.9	-33.8	-267.8	8.3	6.2
Jul-02	0.8	0.8	26.5	1.7	14.1	6.8	43.1	-34.0	-269.8	6.7	5.6
Aug-02	0.8	0.6	24.9	1.4	10.3	6.0	34.7	-34.0	-270.0	4.9	5.1
Sep-02	0.8	0.5	21.2	1.1	7.5	5.7	28.1	-33.8	-268.8	3.8	5.0
Oct-02	0.6	0.4	14.7	0.7	4.5	6.1	21.9	-33.3	-264.5	3.4	5.8
Nov-02	0.5	0.5	8.4	0.6	4.3	8.6	20.8	-32.5	-259.2	3.7	8.3
Dec-02	0.4	0.5	5.6	0.6	4.6	13.5	23.3	-31.2	-249.5	6.5	13.2
Jan-03	0.3	0.7	3.9	1.6	14.1	16.3	39.8	-29.4	-236.0	10.4	15.1
Feb-03	0.2	0.9	3.4	2.6	23.3	16.1	54.9	-27.4	-218.2	11.9	14.2
Mar-03	0.2	0.9	5.9	3.2	28.6	12.2	60.7	-26.4	-209.7	9.7	9.8
Apr-03	0.3	0.8	12.1	3.2	26.5	9.6	57.6	-27.4	-216.7	7.2	7.3

May-03	0.5	0.9	17.7	3.4	26.9	8.1	58.1	-29.3	-232.6	6.4	5.9
Jun-03	0.7	1.0	19.0	3.5	28.9	8.2	66.3	-31.5	-249.7	6.2	5.8
Jul-03	0.8	1.1	18.1	3.3	27.4	8.4	62.2	-32.9	-260.9	5.2	6.1
Aug-03	0.7	1.0	22.1	3.0	26.3	8.2	62.3	-33.2	-263.4	4.5	6.0
Sep-03	0.6	0.9	25.9	2.8	23.3	7.4	54.7	-32.8	-260.1	3.8	5.4
Oct-03	0.6	0.7	24.2	2.2	18.6	7.1	48.8	-32.4	-258.1	3.6	5.5
Nov-03	0.5	1.1	15.9	1.5	11.0	8.1	38.3	-32.9	-264.1	3.9	7.2
Dec-03	0.4	1.2	9.4	0.9	6.7	11.1	43.6	-32.6	-261.5	7.9	10.5
Jan-04	0.3	1.1	8.2	0.6	4.8	12.7	38.7	-31.5	-251.1	12.3	12.3
Feb-04	0.3	0.4	9.7	0.3	3.1	12.6	31.5	-30.7	-242.2	14.3	12.3
Mar-04	0.3	0.1	12.5	0.4	4.2	11.2	19.0	-30.8	-242.3	13.2	10.8
Apr-04	0.4	0.2	14.4	1.0	8.4	10.3	24.2	-30.8	-243.5	11.4	9.6
May-04	0.5	0.5	18.9	1.8	15.5	9.4	35.1	-30.8	-243.9	9.8	8.1
Jun-04	0.5	0.6	23.1	2.3	18.7	8.3	42.2	-31.6	-250.3	7.5	6.7
Jul-04	0.4	0.7	22.1	2.3	18.1	7.3	42.4	-33.6	-266.0	5.1	5.8
Aug-04	0.4	0.9	19.8	2.7	20.0	7.9	49.8	-35.9	-284.7	4.2	6.2
Sep-04	0.4	1.1	18.7	3.4	25.4	8.7	66.1	-36.9	-293.1	4.1	6.5
Oct-04	0.4	1.3	18.6	3.6	26.6	9.8	73.1	-35.6	-284.2	4.0	7.6
Nov-04	0.3	1.1	13.6	2.8	20.5	12.4	61.9	-33.3	-267.4	4.8	10.7
Dec-04	0.3	0.7	9.0	1.6	11.2	21.0	43.1	-31.5	-252.9	10.6	20.0
Jan-05	0.3	0.5	9.7	1.1	8.5	24.7	31.8	-31.8	-253.8	17.5	24.0
Feb-05	0.4	0.3	13.0	1.0	8.2	21.7	29.4	-33.3	-263.9	18.0	21.0
Mar-05	0.7	0.6	14.4	1.3	11.3	12.3	31.8	-36.0	-284.4	12.2	11.3
Apr-05	0.9	0.8	15.2	1.7	13.9	7.4	38.5	-37.7	-297.9	5.5	6.2
May-05	0.9	1.1	16.2	2.0	16.2	6.7	53.0	-37.0	-292.6	4.1	5.4
Jun-05	0.8	1.2	18.5	2.8	22.5	6.7	60.8	-34.8	-276.4	3.7	4.8
Jul-05	0.6	1.1	17.0	2.9	22.9	6.7	63.3	-32.4	-258.6	3.5	4.8
Aug05	0.6	0.9	14.2	2.7	22.1	7.4	56.4	-31.2	-249.9	4.4	5.6

Sep-05	0.6	0.8	12.0	2.2	18.6	9.1	57.1	-30.5	-244.6	6.0	7.6
Oct-05	0.7	0.8	10.1	2.3	20.1	12.1	65.1	-29.8	-239.4	6.4	10.4
Nov-05	0.6	0.8	8.2	1.9	16.5	15.2	81.7	-29.1	-234.4	8.3	13.9
Dec-05	0.4	0.5	5.4	1.3	11.1	18.8	76.9	-28.9	-230.1	12.6	17.9
Jan-06	0.2	0.4	5.0	1.0	8.1	19.3	71.1	-29.6	-234.3	17.6	18.7
Feb-06	0.2	0.4	6.2	1.3	11.6	16.7	55.8	-31.0	-243.5	16.1	15.7
Mar-06	0.2	0.4	7.3	1.5	14.1	11.4	55.6	-32.3	-254.2	10.4	10.2
Apr-06	0.4	0.5	7.6	1.7	14.9	7.8	53.6	-33.0	-260.3	5.0	6.5
May-06	0.6	0.4	7.4	1.7	15.5	6.1	50.4	-33.4	-265.2	3.3	4.8
Jun-06	0.7	0.5	10.0	2.1	17.4	5.6	53.8	-33.7	-268.4	3.1	4.2
Jul-06	0.6	0.6	17.1	2.3	18.8	6.3	53.0	-34.0	-270.2	3.4	4.8
Aug-06	0.5	0.5	24.8	1.9	15.2	7.8	43.9	-34.0	-269.2	4.4	6.5
Sep-06	0.6	0.4	25.5	1.6	13.7	10.1	43.8	-33.6	-265.0	5.3	8.9
Oct-06	0.7	0.3	19.4	1.3	10.8	11.7	41.8	-33.0	-261.0	5.8	10.8
Nov-06	0.7	0.4	10.8	1.1	10.0	17.5	43.3	-31.6	-251.5	11.5	16.6
Dec-06	0.5	0.4	6.3	0.8	6.7	25.5	34.1	-30.5	-242.9	21.4	24.9
Jan-07	0.2	0.5	5.5	0.6	4.9	28.6	37.3	-29.8	-236.5	25.5	28.1
Feb-07	0.2	0.6	7.6	0.6	5.5	22.5	74.2	-29.8	-236.4	20.6	22.0
Mar-07	0.4	1.0	10.1	0.6	6.9	12.4	86.9	-30.3	-240.3	10.1	11.8
Apr-07	0.6	1.1	19.1	0.7	7.6	7.2	79.9	-31.2	-247.6	5.5	6.6
May-07	0.9	0.9	28.1	0.8	7.5	6.3	44.9	-32.6	-258.2	3.9	5.7
Jun-07	0.9	0.5	32.9	1.0	7.9	6.0	34.1	-33.4	-264.2	3.6	5.4
Jul-07	0.9	0.5	30.3	1.6	12.7	6.3	40.4	-33.5	-266.1	3.2	5.3
Aug-07	0.8	0.9	25.0	2.6	20.9	6.9	54.7	-33.4	-266.7	3.7	5.2
Sep-07	0.8	1.1	27.0	3.3	27.1	8.4	69.1	-33.6	-269.0	4.4	6.1
Oct-07	0.7	0.8	32.2	2.9	23.3	11.0	66.6	-33.6	-269.7	6.9	9.1
Nov-07	0.7	0.5	33.6	2.0	15.6	15.2	59.4	-32.8	-262.6	9.1	13.9

Dec-07	0.7	0.3	29.2	1.0	7.0	20.2	41.4	-31.9	-254.1	17.6	19.6
Jan-08	0.6	0.3	19.4	0.6	5.5	22.2	37.7	-30.9	-244.5	20.3	21.7
Feb-08	0.4	0.2	13.1	0.6	6.2	19.3	35.1	-31.3	-246.9	19.9	18.8
Mar-08	0.3	0.2	10.7	0.9	8.7	13.7	40.1	-32.1	-253.3	11.2	13.0
Apr-08	0.4	0.4	13.9	1.3	12.0	8.6	52.2	-32.9	-260.0	6.0	7.6
May-08	0.5	1.0	19.9	2.7	24.4	6.7	198.0	-32.7	-259.0	4.0	4.6
Jun-08	0.5	1.3	24.7	3.6	29.8	6.0	202.1	-31.9	-253.4	3.3	3.5
Jul-08	0.5	1.4	27.0	4.1	33.6	6.3	202.9	-32.4	-256.6	3.5	3.4
Aug-08	0.5	1.0	27.9	3.4	25.6	6.8	57.6	-32.7	-259.0	3.2	4.7
Sep-08	0.5	0.9	31.0	3.2	25.0	7.2	59.1	-32.7	-260.0	3.3	5.1
Oct-08	0.7	1.0	42.8	3.5	29.3	8.3	68.2	-31.9	-254.0	3.8	5.9
Nov-08	0.8	2.0	50.1	4.0	33.4	15.7	73.3	-31.7	-253.0	8.2	12.9
Dec-08	0.8	5.5	49.4	3.9	32.1	27.4	74.1	-31.5	-252.4	12.6	24.7
Jan-09	0.6	8.3	33.9	3.1	24.2	35.4	57.8	-30.7	-246.8	17.0	33.4
Feb-09	0.6	8.9	17.5	2.0	15.7	32.3	52.1	-29.1	-233.8	16.4	30.9
Mar-09		6.3		1.5	10.9	22.1	44.9	-28.4	-226.9	13.9	21.1
Apr-09		3.5		1.5	11.5	13.0	51.9	-28.9	-229.7	9.4	12.1
May-09		2.0		2.0	16.8	8.6	59.6	-30.2	-240.9	5.9	7.2
Jun-09		1.3		2.7	22.8	7.0	72.6	-31.2	-249.5	4.2	5.2
Jul-09		1.2		3.2	26.0	6.7	77.4	-32.0	-255.5	3.6	4.6
Aug-09		1.4		3.5	27.6	6.4	87.5	-32.6	-258.9	3.5	4.1
Sep-09		3.5		3.8	28.0	6.7	87.8	-33.3	-264.1	3.3	4.3
Oct-09		19.6		5.4	35.7	11.7	127.4	-33.8	-268.7	4.5	8.7
Nov-09		44.4		7.4	47.0	25.4	166.8	-33.6	-268.0	11.7	21.5
Dec-09		60.9		8.6	49.7	40.1	155.6	-32.1	-256.7	18.1	35.9
Jan-10		50.0		7.1	35.1	41.8	100.5	-30.2	-240.7	20.0	38.8
Feb-10		30.1		7.3	32.7	31.0	106.9	-30.1	-238.7	13.1	28.2

Mar-10		17.7		11.2	75.9	17.4	238.4	-32.1	-253.6	7.3	11.0
Apr-10		15.4		13.4	92.7	11.0	282.7	-34.4	-272.4	3.8	3.2
May-10		12.5		11.9	80.4	8.0	227.5	-35.6	-281.3	3.4	1.3
Jun-10		7.7		7.0	32.3	6.6	114.7	-35.4	-281.3	2.6	3.9
Jul-10		5.8		5.0	20.0	6.4	98.7	-34.5	-274.8	2.8	4.8
Aug-10		4.5		4.3	17.6	6.6	94.5	-33.5	-268.2	2.7	5.3
Sep-10		4.1		4.2	18.7	8.3	97.8	-33.9	-271.0	4.7	6.8
Oct-10		4.6		4.5	21.4	12.8	86.9	-34.9	-279.0	12.4	11.0
Nov-10		6.6		5.0	24.8	18.2	87.9	-35.6	-284.1	25.8	16.1
Dec-10		9.7		4.8	21.9	22.5		-34.8	-276.4		20.7
THW2010		**Lat: -76.95**		**Lon: -121.22**		**Elevation: 2020m**					
Date	**BrO (ppb)**	**Ca (ppb)**	**IO (ppb)**	**Mg (ppb)**	**Na (ppb)**	**S_{tot} (ppb)**	**Cl^- (ppb)**	**δ18O (‰)**	**δD (‰)**	**MSA (ppb)**	**nssS (ppb)**
Jan-79	0.6	0.5	5.2	1.4	8.3	21.3	24.2	-33.2	-261.0	10.5	20.6
Feb-79	0.6	0.5	6.8	1.3	9.3	17.8	29.9	-33.4	-261.1	9.2	17.0
Mar-79	0.6	0.6	11.3	1.5	12.1	14.2	42.1	-33.8	-264.5	7.9	13.2
Apr-79	0.5	0.9	19.4	2.3	19.7	11.3	75.5	-34.6	-271.7	9.5	9.6
May-79	0.3	1.3	27.9	3.6	32.8	9.5	95.1	-35.5	-280.8	10.1	6.7
Jun-79	0.2	1.7	32.8	4.7	43.6	8.8	94.0	-36.2	-287.1	9.5	5.1
Jul-79	0.3	1.8	33.7	5.1	44.6	8.2	68.1	-36.3	-288.4	5.9	4.4
Aug-79	0.4	1.6	32.5	5.0	39.2	8.3	75.4	-35.5	-282.8	4.4	5.0
Sep-79	0.6	1.4	30.6	4.9	37.1	9.7	78.9	-34.2	-271.5	4.8	6.6
Oct-79	0.8	1.2	28.3	4.7	37.1	11.3	72.1	-32.6	-257.3	6.1	8.2
Nov-79	0.9	1.1	24.8	3.9	31.2	12.1	38.9	-31.2	-244.5	7.4	9.5
Dec-79	0.9	0.7	19.0	2.5	19.0	12.1	23.0	-30.5	-237.7	8.4	10.5
Jan-80	0.7	0.4	12.2	1.4	9.1	12.0	19.7	-30.6	-237.5	8.7	11.2
Feb-80	0.5	0.3	8.3	1.0	5.9	12.0	25.7	-31.3	-243.8	8.4	11.5
Mar-80	0.4	0.3	9.4	1.1	7.6	11.1	42.2	-32.2	-252.4	7.9	10.4

Apr-80	0.4	0.5	14.3	1.7	13.5	9.8	63.7	-33.1	-260.4	7.4	8.7
May-80	0.4	0.7	21.3	2.6	22.8	8.6	71.6	-33.7	-265.5	6.5	6.7
Jun-80	0.4	1.0	28.3	3.3	30.9	7.5	61.2	-34.0	-267.4	5.1	4.9
Jul-80	0.4	1.1	33.1	3.6	33.6	6.8	63.1	-33.9	-267.8	4.2	4.0
Aug-80	0.5	1.1	30.9	3.8	33.0	6.7	65.7	-33.8	-266.8	4.0	3.9
Sep-80	0.7	1.2	23.6	3.8	32.2	7.6	68.6	-33.6	-265.6	4.6	4.9
Oct-80	1.0	1.3	14.8	3.7	31.3	8.8	57.0	-33.4	-262.8	5.4	6.2
Nov-80	0.9	1.2	8.7	3.3	28.0	10.3	43.0	-32.9	-258.5	6.4	8.0
Dec-80	0.8	1.1	6.0	2.7	22.1	11.3	31.4	-32.5	-253.3	7.3	9.5
Jan-81	0.6	0.8	6.9	1.9	15.0	11.4	17.3	-32.1	-248.7	7.8	10.1
Feb-81	0.5	0.4	11.4	1.3	9.2	9.9	15.7	-31.9	-246.0	7.6	9.2
Mar-81	0.6	0.3	15.3	1.0	7.8	8.0	24.8	-31.9	-247.0	6.9	7.3
Apr-81	0.6	0.5	16.6	1.4	11.2	6.7	34.0	-32.2	-250.8	6.1	5.7
May-81	0.5	0.7	17.9	2.1	17.6	6.3	42.0	-32.9	-256.7	5.0	4.7
Jun-81	0.4	0.9	22.5	3.0	24.5	5.8	48.3	-33.7	-263.4	4.2	3.7
Jul-81	0.3	1.2	26.9	4.0	32.7	6.0	61.6	-34.5	-270.3	3.8	3.3
Aug-81	0.3	1.3	26.5	4.3	35.4	6.5	64.9	-34.8	-274.1	3.8	3.5
Sep-81	0.5	1.2	21.2	3.9	31.0	8.7	57.4	-34.1	-270.7	4.4	6.1
Oct-81	0.6	0.9	15.1	2.9	20.9	12.5	40.7	-32.8	-260.7	5.6	10.7
Nov-81	0.6	0.6	10.0	1.8	12.0	18.1	27.5	-31.5	-248.8	7.6	17.1
Dec-81	0.5	0.4	6.3	1.1	7.4	23.9	23.2	-30.9	-243.0	9.3	23.3
Jan-82	0.4	0.3	4.6	0.9	6.2	26.9	24.6	-31.2	-244.5	9.9	26.4
Feb-82	0.4	0.5	5.6	1.1	9.6	25.7	34.8	-31.9	-250.7	9.7	24.9
Mar-82	0.3	0.7	8.5	1.6	14.7	20.8	37.1	-32.4	-255.5	8.8	19.5
Apr-82	0.3	0.7	11.3	1.8	17.3	14.8	36.1	-32.8	-257.6	7.3	13.3
May-82	0.2	0.7	13.3	1.9	17.4	9.9	38.9	-32.9	-258.3	5.8	8.5
Jun-82	0.3	0.7	15.0	2.3	19.3	7.0	55.0	-33.1	-260.0	4.9	5.4

Jul-82	0.3	0.8	16.5	2.8	24.5	6.1	57.1	-33.3	-262.5	4.3	4.0
Aug-82	0.4	0.9	17.0	3.1	27.4	6.0	49.6	-33.5	-264.7	4.2	3.7
Sep-82	0.5	1.0	17.3	2.9	24.8	7.0	32.4	-33.5	-265.2	4.4	5.0
Oct-82	0.5	0.9	18.2	2.4	18.6	9.0	26.7	-33.4	-263.6	5.6	7.4
Nov-82	0.4	0.7	17.6	1.8	12.8	11.5	20.3	-33.1	-261.0	6.9	10.4
Dec-82	0.3	0.5	13.5	1.3	8.5	13.5	15.1	-32.9	-257.6	8.2	12.9
Jan-83	0.3	0.4	8.3	0.9	5.5	14.0	13.7	-32.6	-254.7	8.9	13.6
Feb-83	0.2	0.4	6.5	0.7	4.8	12.9	19.2	-32.5	-252.7	8.5	12.6
Mar-83	0.3	0.4	7.8	0.9	7.0	10.9	26.7	-32.5	-253.1	7.2	10.3
Apr-83	0.3	0.3	10.0	1.2	10.6	9.5	30.7	-32.8	-256.1	5.9	8.6
May-83	0.4	0.4	11.8	1.5	13.1	9.4	30.2	-33.4	-260.7	5.0	8.3
Jun-83	0.4	0.5	14.6	1.8	14.9	10.5	42.5	-33.9	-265.3	4.2	9.2
Jul-83	0.4	0.6	19.9	2.1	16.7	11.3	46.7	-34.2	-267.7	3.8	9.9
Aug-83	0.4	0.8	23.6	2.3	17.9	11.0	47.4	-34.0	-267.4	4.3	9.5
Sep-83	0.6	0.9	22.2	2.4	17.8	10.6	37.2	-33.6	-263.9	5.6	9.1
Oct-83	0.7	1.0	15.8	2.5	18.0	11.6	41.0	-33.1	-259.4	7.7	10.0
Nov-83	0.7	0.9	9.9	2.6	18.7	14.9	35.9	-32.5	-254.3	10.4	13.4
Dec-83	0.5	0.8	11.9	2.4	17.2	18.1	26.0	-32.0	-249.9	12.6	16.7
Jan-84	0.4	0.7	21.5	1.7	11.6	19.6	12.2	-31.6	-246.9	13.9	18.7
Feb-84	0.3	0.5	29.5	1.1	7.2	18.6	17.7	-31.6	-246.2	13.6	18.0
Mar-84	0.3	0.4	29.8	1.0	7.0	16.6	20.9	-32.0	-249.3	12.1	16.0
Apr-84	0.3	0.3	25.0	1.1	9.5	13.7	25.4	-32.9	-255.3	9.6	12.9
May-84	0.2	0.3	25.0	1.3	11.6	10.7	24.6	-33.9	-264.0	6.9	9.7
Jun-84	0.1	0.4	31.9	1.5	12.7	8.0	24.7	-34.6	-270.8	4.6	6.9
Jul-84	0.1	0.5	39.7	2.0	16.7	6.9	44.4	-34.7	-273.8	4.5	5.5
Aug-84	0.2	0.8	40.0	2.8	23.4	7.9	52.8	-34.3	-270.3	5.1	5.9
Sep-84	0.5	0.9	32.1	3.1	25.9	10.1	53.3	-33.3	-262.2	6.7	7.9
Oct84	0.7	0.8	20.9	2.6	21.8	12.9	32.5	-32.1	-251.9	8.1	11.1

Nov-84	0.8	0.5	13.1	1.7	13.2	15.4	20.5	-31.2	-244.3	10.3	14.2
Dec-84	0.7	0.3	9.4	1.4	9.5	17.9	36.1	-31.0	-242.7	11.5	16.7
Jan-85	0.5	0.5	7.6	2.0	16.3	19.6	57.6	-31.4	-245.7	11.3	17.9
Feb-85	0.5	0.8	6.6	3.1	27.4	19.6	61.1	-32.1	-250.9	9.7	17.0
Mar-85	0.4	1.1	6.2	3.5	32.7	16.4	46.6	-32.9	-256.3	7.6	13.7
Apr-85	0.4	1.0	6.9	3.2	29.1	11.8	30.3	-33.8	-262.8	5.7	9.4
May-85	0.4	1.0	9.4	2.9	23.7	7.9	39.8	-34.5	-269.4	4.9	6.0
Jun-85	0.4	1.1	13.3	3.5	26.9	7.1	63.1	-35.0	-274.8	4.5	4.8
Jul-85	0.6	1.2	17.5	4.5	35.0	8.4	81.5	-35.1	-276.1	4.3	5.5
Aug-85	0.8	1.3	20.1	5.1	40.4	10.4	82.0	-34.7	-273.5	4.3	7.0
Sep-85	1.0	1.2	19.8	4.6	36.2	12.6	58.0	-33.9	-266.8	5.6	9.6
Oct-85	1.0	1.0	16.0	3.6	26.6	15.6	36.2	-32.9	-259.7	7.8	13.4
Nov-85	0.9	0.7	11.1	2.5	17.0	20.5	23.4	-32.3	-253.8	10.1	19.1
Dec-85	0.7	0.6	8.1	1.8	11.9	26.6	21.0	-32.2	-252.3	11.9	25.6
Jan-86	0.6	0.5	9.0	1.3	8.9	29.8	16.9	-32.7	-254.7	13.4	29.0
Feb-86	0.5	0.5	11.7	1.0	7.2	28.0	19.0	-33.6	-261.3	13.7	27.4
Mar-86	0.5	0.4	14.0	0.8	6.6	21.8	21.5	-34.6	-269.8	12.1	21.2
Apr-86	0.4	0.5	15.4	0.8	6.9	15.8	27.1	-35.7	-278.3	9.1	15.2
May-86	0.4	0.6	18.2	1.0	8.4	12.3	32.1	-36.5	-285.9	6.2	11.6
Jun-86	0.3	0.8	22.7	1.4	11.5	10.7	40.8	-37.1	-291.0	4.5	9.7
Jul-86	0.2	0.9	26.8	1.9	15.9	9.5	46.6	-37.3	-293.3	3.9	8.2
Aug-86	0.3	0.9	27.6	2.3	19.4	8.9	47.3	-37.1	-291.4	4.4	7.3
Sep-86	0.4	0.9	25.7	2.5	20.6	9.7	44.0	-36.7	-286.8	6.0	8.0
Oct-86	0.6	0.7	23.1	2.3	18.8	12.0	34.2	-36.4	-282.3	8.2	10.4
Nov-86	0.9	0.5	20.5	1.8	14.4	14.2	24.8	-36.2	-280.4	10.5	13.0
Dec-86	1.0	0.5	16.8	1.4	10.4	15.5	20.8	-36.2	-280.3	12.2	14.6
Jan-87	0.9	0.5	12.4	1.2	8.9	15.8	28.2	-36.2	-280.4	12.8	15.1

Feb-87	0.7	0.6	8.6	1.4	10.9	15.6	37.8	-36.0	-279.2	12.3	14.7
Mar-87	0.5	0.6	7.7	1.6	13.9	14.6	42.0	-35.8	-277.3	10.9	13.4
Apr-87	0.4	0.6	9.2	1.8	15.8	12.9	43.7	-35.6	-276.3	9.6	11.6
May-87	0.4	0.8	13.4	2.1	17.5	11.1	46.9	-35.6	-275.9	8.4	9.6
Jun-87	0.3	1.0	20.3	2.5	21.1	9.8	54.2	-35.5	-277.4	7.3	8.0
Jul-87	0.4	1.2	28.3	3.0	26.1	8.7	58.2	-35.6	-278.3	5.9	6.5
Aug-87	0.5	1.3	31.5	3.2	29.1	7.8	56.0	-35.4	-278.6	4.1	5.3
Sep-87	0.7	1.4	26.7	3.2	28.3	7.6	48.9	-35.1	-276.6	3.3	5.2
Oct-87	0.9	1.4	17.4	3.1	25.5	8.4	49.3	-34.7	-273.0	3.3	6.3
Nov-87	1.0	1.2	10.3	2.9	22.5	9.8	46.1	-34.4	-269.8	4.4	7.9
Dec-87	1.0	0.9	8.4	2.5	19.2	10.6	41.4	-34.3	-268.2	5.8	9.0
Jan-88	0.9	0.7	10.7	1.9	14.8	10.7	30.1	-34.3	-268.3	7.4	9.4
Feb-88	0.8	0.6	15.5	1.4	10.7	9.7	20.3	-34.2	-267.7	8.1	8.8
Mar-88	0.7	0.5	21.2	1.0	7.9	8.3	17.1	-34.0	-265.6	7.4	7.6
Apr-88	0.5	0.4	26.3	1.0	8.3	6.4	20.0	-33.6	-262.8	5.7	5.7
May-88	0.4	0.5	29.9	1.3	10.6	5.4	23.3	-34.0	-265.4	4.0	4.5
Jun-88	0.3	0.6	32.1	1.9	16.6	5.0	43.4	-33.5	-262.7	3.5	3.6
Jul-88	0.3	1.0	35.7	2.9	24.8	6.1	54.4	-33.0	-260.2	3.2	4.1
Aug-88	0.2	1.2	41.0	3.7	31.6	7.5	66.7	-32.3	-255.5	3.7	4.8
Sep-88	0.2	1.2	44.7	3.7	31.2	9.3	51.1	-32.4	-255.6	4.1	6.6
Oct-88	0.2	0.9	40.9	3.0	23.5	10.4	37.5	-32.3	-254.0	5.3	8.5
Nov-88	0.3	0.6	29.7	2.0	14.2	12.3	26.2	-31.7	-248.9	6.9	11.1
Dec-88	0.4	0.5	17.9	1.4	8.9	14.5	26.1	-31.7	-247.3	8.2	13.8
Jan-89	0.5	0.5	10.6	1.3	9.1	15.9	30.2	-32.3	-252.2	9.2	15.1
Feb-89	0.6	0.7	8.5	1.5	12.5	15.6	40.2	-33.5	-261.9	9.2	14.6
Mar-89	0.5	0.8	11.4	2.1	17.9	14.1	53.0	-34.5	-272.1	8.4	12.6
Apr-89	0.4	1.0	19.0	2.7	23.7	12.5	64.7	-35.3	-278.8	7.5	10.5

May-89	0.3	1.2	27.2	3.3	29.4	11.6	70.5	-35.5	-281.7	6.5	9.1
Jun-89	0.2	1.4	32.5	3.8	32.9	11.0	68.4	-35.5	-280.4	5.5	8.2
Jul-89	0.2	1.6	35.0	4.4	35.8	10.8	88.0	-34.9	-276.1	6.0	7.8
Aug-89	0.2	1.9	37.4	5.4	41.8	11.2	126.2	-34.0	-268.0	7.5	7.7
Sep-89	0.2	2.1	36.6	6.1	48.3	12.4	151.5	-32.8	-258.1	9.2	8.3
Oct-89	0.3	2.0	28.5	6.0	48.6	14.5	119.5	-31.7	-248.2	8.4	10.4
Nov-89	0.5	1.5	16.7	4.9	38.1	18.5	67.1	-31.0	-242.2	7.7	15.3
Dec-89	0.7	1.0	7.7	3.4	23.6	22.4	29.7	-30.9	-240.9	8.1	20.4
Jan-90	0.7	0.6	5.6	2.1	13.2	23.5	26.3	-31.3	-243.6	9.8	22.4
Feb-90	0.5	0.4	7.1	1.4	9.1	20.0	21.6	-31.9	-248.8	10.4	19.3
Mar-90	0.4	0.4	10.1	1.3	9.6	13.7	16.6	-32.6	-254.8	9.4	12.9
Apr-90	0.3	0.6	13.1	1.8	14.4	9.0	25.7	-33.3	-261.3	7.4	7.7
May-90	0.3	0.9	18.4	2.6	22.3	6.6	47.5	-33.8	-266.8	5.7	4.8
Jun-90	0.2	1.1	27.5	3.5	29.6	6.7	66.2	-34.1	-269.9	4.8	4.2
Jul-90	0.2	1.2	36.7	4.2	33.7	7.7	72.3	-33.8	-268.5	5.6	4.9
Aug-90	0.2	1.3	36.2	4.8	37.7	11.0	86.1	-33.0	-262.1	8.0	7.9
Sep-90	0.3	1.4	25.0	5.1	40.5	15.7	94.8	-31.8	-251.3	12.0	12.3
Oct-90	0.4	1.4	13.3	4.5	36.9	20.8	77.5	-30.6	-240.2	16.1	17.7
Nov-90	0.4	1.0	7.5	3.2	25.3	23.7	43.3	-29.9	-233.3	19.6	21.6
Dec-90	0.3	0.7	6.9	1.8	12.4	25.7	18.4	-30.1	-234.4	20.8	24.6
Jan-91	0.3	0.5	5.9	1.1	5.9	25.7	18.3	-31.1	-242.0	19.8	25.2
Feb-91	0.3	0.5	5.6	0.9	5.4	23.5	21.7	-32.5	-253.6	16.9	23.0
Mar-91	0.3	0.5	7.1	1.0	7.7	18.9	27.0	-34.0	-265.7	13.5	18.2
Apr-91	0.3	0.7	10.9	1.3	11.0	14.5	30.9	-35.1	-275.7	10.1	13.6
May-91	0.3	0.8	14.9	1.9	15.4	11.6	43.6	-35.8	-281.0	7.6	10.3
Jun-91	0.3	1.2	17.6	3.1	23.7	10.6	66.7	-35.7	-281.1	6.2	8.7
Jul-91	0.4	1.4	18.5	4.4	35.1	11.5	90.6	-35.4	-278.0	5.7	8.6
Aug91	0.5	1.6	19.0	5.1	42.7	13.0	82.4	-35.2	-274.5	5.4	9.4

Sep-91	0.6	1.1	18.6	3.8	32.7	13.2	61.4	-33.0	-256.6	6.3	10.5
Oct-91	0.6	0.7	15.7	2.2	19.2	15.2	36.0	-31.2	-243.2	8.7	13.6
Nov-91	0.6	0.3	11.1	0.8	7.7	21.1	29.7	-29.4	-230.4	12.4	20.5
Dec-91	0.4	0.3	7.5	0.8	8.3	30.3	22.2	-30.1	-235.2	16.4	29.6
Jan-92	0.3	0.3	6.6	0.8	7.7	34.1	19.3	-30.7	-239.1	18.3	33.5
Feb-92	0.3	0.4	7.4	0.7	6.7	30.1	18.0	-31.4	-245.1	17.4	29.5
Mar-92	0.3	0.4	9.2	0.7	6.7	21.2	22.3	-32.2	-251.9	13.2	20.7
Apr-92	0.3	0.4	11.3	0.9	9.0	13.8	30.6	-33.0	-258.3	8.7	13.0
May-92	0.3	0.6	12.1	1.4	13.0	10.5	38.2	-33.8	-264.2	5.9	9.4
Jun-92	0.4	0.8	12.2	1.9	16.9	10.7	41.5	-34.5	-270.3	4.6	9.3
Jul-92	0.4	0.9	13.9	2.2	18.9	14.7	40.5	-34.8	-273.2	4.5	13.2
Aug-92	0.5	0.9	19.4	2.2	19.0	19.2	41.5	-34.2	-270.1	4.9	17.6
Sep-92	0.8	0.9	24.7	2.2	18.6	22.3	42.8	-32.9	-259.9	6.4	20.7
Oct-92	1.1	0.9	24.6	2.0	17.3	22.8	39.0	-31.4	-246.9	8.8	21.4
Nov-92	1.1	0.8	18.8	1.7	13.5	23.0	28.3	-29.9	-234.4	11.6	21.8
Dec-92	0.9	0.6	11.7	1.2	9.1	24.0	20.0	-28.9	-224.6	13.6	23.2
Jan-93	0.6	0.4	8.2	0.9	6.4	25.1	17.6	-28.7	-222.2	14.7	24.6
Feb-93	0.4	0.3	8.9	0.9	6.8	25.2	23.0	-29.5	-230.2	14.2	24.6
Mar-93	0.4	0.4	12.1	1.0	8.8	23.5	25.8	-31.3	-245.2	13.0	22.7
Apr-93	0.3	0.5	16.6	1.3	11.3	21.6	29.0	-33.0	-260.1	11.1	20.6
May-93	0.3	0.7	22.2	1.5	12.8	20.3	26.4	-34.3	-269.9	8.2	19.2
Jun-93	0.2	0.7	30.2	1.6	12.6	19.8	28.3	-35.1	-276.8	5.7	18.7
Jul-93	0.2	1.0	39.0	1.7	13.2	18.4	35.4	-36.0	-283.8	3.6	17.3
Aug-93	0.2	1.2	43.2	2.1	16.7	17.9	51.9	-36.4	-288.6	2.9	16.5
Sep-93	0.3	1.5	38.4	2.7	22.6	18.8	61.2	-36.3	-288.0	3.3	16.9
Oct-93	0.4	1.6	26.4	3.0	25.4	20.9	51.9	-35.4	-280.9	5.2	18.8
Nov-93	0.5	1.3	14.8	2.6	21.8	22.3	33.7	-34.6	-272.5	9.2	20.5

Dec-93	0.5	0.9	8.0	1.9	14.8	24.3	19.6	-34.0	-267.1	13.2	23.1
Jan-94	0.5	0.5	5.9	1.2	8.9	25.3	18.0	-33.8	-264.5	15.7	24.6
Feb-94	0.5	0.5	5.8	1.0	8.0	24.1	21.9	-33.6	-263.5	15.2	23.4
Mar-94	0.4	0.5	7.3	1.2	10.6	20.1	33.5	-33.7	-262.7	12.4	19.2
Apr-94	0.3	0.6	11.9	1.6	14.2	15.8	44.6	-33.7	-263.5	8.7	14.6
May-94	0.3	0.7	19.3	2.3	19.2	12.8	65.5	-33.8	-265.1	6.4	11.2
Jun-94	0.3	1.0	26.7	3.3	25.5	11.0	78.8	-33.8	-266.6	4.9	8.9
Jul-94	0.4	1.5	30.5	4.5	35.1	10.1	97.9	-33.5	-264.8	5.0	7.2
Aug-94	0.5	1.8	29.5	5.3	43.3	11.0	98.0	-32.7	-259.0	4.7	7.3
Sep-94	0.7	1.8	25.2	5.3	44.9	13.0	78.2	-31.7	-250.2	5.8	9.2
Oct-94	0.9	1.4	20.2	4.2	35.6	16.6	49.0	-30.8	-242.7	8.5	13.6
Nov-94	0.8	0.9	16.4	2.8	21.7	20.9	26.2	-30.8	-241.6	12.3	19.1
Dec-94	0.7	0.7	14.6	1.6	10.8	24.7	23.3	-31.8	-248.6	17.6	23.8
Jan-95	0.5	0.5	14.5	1.1	6.8	26.7	21.8	-33.4	-261.3	21.0	26.1
Feb-95	0.4	0.4	15.7	0.9	6.1	25.8	19.3	-35.0	-273.1	21.7	25.3
Mar-95	0.4	0.4	17.5	1.0	6.7	22.2	16.7	-35.9	-281.4	18.3	21.6
Apr-95	0.6	0.6	19.2	1.3	9.7	17.8	28.4	-36.2	-284.2	13.5	17.0
May-95	0.7	0.9	22.6	1.8	15.1	14.0	58.7	-36.0	-283.1	9.7	12.7
Jun-95	0.6	1.1	30.2	2.5	23.3	11.9	77.3	-35.5	-279.2	7.0	10.0
Jul-95	0.5	1.2	43.3	3.1	29.1	11.2	77.7	-34.7	-274.0	5.8	8.7
Aug-95	0.4	1.3	51.4	3.5	31.7	12.4	58.1	-33.7	-267.5	5.4	9.8
Sep-95	0.5	1.2	46.5	3.4	29.0	15.2	44.8	-32.5	-258.0	7.0	12.8
Oct-95	0.7	1.0	30.6	3.0	24.2	18.4	34.7	-31.3	-246.7	11.2	16.4
Nov-95	0.9	0.9	17.3	2.4	19.1	21.3	29.6	-30.3	-237.1	16.3	19.7
Dec-95	0.9	0.7	13.0	2.0	15.5	22.8	31.2	-29.9	-232.3	20.1	21.5
Jan-96	0.7	0.7	14.9	1.8	14.5	23.4	37.6	-30.2	-234.5	20.0	22.2
Feb-96	0.5	0.7	17.7	1.8	15.1	22.5	40.9	-31.0	-240.3	16.6	21.3

Mar-96	0.5	0.6	20.0	2.0	16.9	20.0	39.6	-31.9	-246.9	11.5	18.6
Apr-96	0.4	0.7	21.2	2.1	17.9	16.3	51.1	-32.7	-253.5	6.9	14.8
May-96	0.4	0.7	21.1	2.4	19.0	12.7	69.8	-33.7	-261.2	4.1	11.1
Jun-96	0.4	1.0	19.4	3.0	23.5	11.4	84.1	-34.9	-271.6	3.2	9.3
Jul-96	0.5	1.5	16.3	4.6	33.8	11.5	65.0	-36.2	-281.9	3.7	8.6
Aug-96	0.6	2.1	13.6	6.2	48.1	11.7	47.8	-37.3	-290.8	6.2	7.5
Sep-96	0.8	2.2	12.2	6.8	52.6	11.2	36.5	-37.7	-295.2	10.8	6.8
Oct-96	0.9	1.8	11.3	5.5	42.4	10.4	43.4	-37.4	-292.3	14.2	6.9
Nov-96	0.8	1.4	9.7	3.6	25.8	12.4	45.9	-36.2	-283.0	13.5	10.2
Dec-96	0.6	1.2	7.5	2.1	14.8	16.2	46.0	-34.9	-272.4	9.4	15.0
Jan-97	0.4	1.2	6.5	1.8	13.8	19.6	46.7	-33.9	-265.2	5.3	18.4
Feb-97	0.3	1.1	7.2	1.8	15.5	19.5	42.4	-33.4	-261.7	3.2	18.2
Mar-97	0.2	1.0	8.5	1.9	18.0	16.3	39.6	-33.0	-258.9	2.6	14.7
Apr-97	0.3	0.9	8.8	2.1	20.2	12.5	34.3	-32.8	-256.9	2.8	10.8
May-97	0.2	1.0	7.5	2.2	21.2	9.4	27.6	-32.7	-256.2	3.0	7.6
Jun-97	0.2	1.1	6.4	2.1	20.5	7.2	25.9	-32.7	-256.9	3.6	5.5
Jul-97	0.2	1.3	7.6	2.0	17.9	6.8	25.6	-32.5	-256.0	4.2	5.3
Aug-97	0.3	1.4	11.9	2.0	15.1	7.4	26.6	-32.0	-252.9	5.1	6.2
Sep-97	0.4	1.3	17.4	1.9	12.9	9.4	23.2	-31.3	-247.6	6.4	8.3
Oct-97	0.5	1.2	20.1	1.8	12.3	12.7	19.7	-30.5	-241.2	9.5	11.7
Nov-97	0.6	1.1	18.2	1.6	11.4	17.3	18.8	-29.8	-235.8	13.0	16.4
Dec-97	0.5	1.2	13.1	1.3	9.6	21.1	21.4	-29.6	-232.7	14.5	20.3
Jan-98	0.3	1.1	8.7	1.0	7.3	22.4	23.8	-29.7	-233.0	12.3	21.8
Feb-98	0.2	0.9	8.4	0.8	6.8	21.2	22.3	-29.7	-232.3	8.1	20.7
Mar-98	0.3	0.6	13.5	0.9	8.4	18.0	16.6	-29.3	-228.7	4.4	17.3
Apr-98	0.3	0.4	23.4	0.9	9.9	13.3	12.2	-28.8	-223.8	2.6	12.5
May-98	0.4	0.4	34.3	0.8	9.4	8.7	13.2	-28.7	-222.9	2.0	7.9

Jun-98	0.5	0.3	40.7	0.7	7.4	5.9	22.2	-29.2	-227.8	2.3	5.2
Jul-98	0.6	0.3	39.2	0.8	7.1	5.1	33.0	-30.0	-236.1	3.2	4.5
Aug-98	0.8	0.5	31.3	1.1	9.9	5.5	53.9	-30.7	-242.7	5.3	4.6
Sep-98	0.8	0.8	22.2	1.8	14.8	6.8	63.1	-31.1	-245.5	9.3	5.6
Oct-98	0.8	1.0	15.5	2.4	19.8	9.6	57.6	-31.2	-246.5	14.3	8.0
Nov-98	0.7	1.0	11.7	2.5	20.6	13.3	36.3	-31.7	-249.4	17.9	11.6
Dec-98	0.6	0.8	9.5	2.1	16.9	16.3	21.4	-32.6	-256.4	18.4	14.9
Jan-99	0.4	0.7	8.4	1.5	11.1	16.7	20.4	-33.8	-265.0	16.1	15.7
Feb-99	0.3	0.6	8.5	1.1	8.0	14.6	28.6	-34.7	-271.9	12.8	13.9
Mar-99	0.2	0.7	10.1	1.4	10.5	12.0	44.7	-34.9	-273.2	10.9	11.1
Apr-99	0.3	1.1	12.5	2.2	18.5	10.3	62.5	-34.2	-268.2	7.9	8.6
May-99	0.3	1.6	15.3	3.2	29.2	9.9	81.3	-33.2	-259.9	6.4	7.3
Jun-99	0.3	1.9	19.3	4.1	37.5	9.9	82.4	-32.2	-253.1	4.1	6.6
Jul-99	0.3	1.8	23.1	4.5	39.8	10.5	77.5	-31.6	-249.1	4.7	7.2
Aug-99	0.5	1.5	23.5	4.2	35.9	11.6	59.7	-31.2	-247.2	5.0	8.6
Sep-99	0.7	1.2	19.6	3.5	27.9	12.7	42.9	-31.0	-245.6	6.0	10.4
Oct-99	0.8	1.0	13.6	2.6	19.7	13.9	31.1	-30.8	-244.5	7.8	12.2
Nov-99	0.6	0.8	8.2	1.9	13.9	16.1	25.2	-30.8	-243.1	10.8	15.0
Dec-99	0.4	0.6	4.8	1.5	10.9	19.3	24.1	-30.7	-241.6	13.7	18.4
Jan-00	0.3	0.5	4.2	1.2	9.1	20.6	22.2	-30.7	-240.8	16.2	19.8
Feb-00	0.3	0.4	6.0	1.1	8.2	18.7	23.3	-30.8	-241.0	15.8	18.0
Mar-00	0.4	0.6	8.1	1.2	9.2	15.1	28.9	-31.0	-242.0	14.1	14.3
Apr-00	0.4	1.0	9.0	1.3	11.3	12.3	31.1	-31.8	-247.5	11.0	11.3
May-00	0.4	1.4	8.9	1.7	14.2	11.3	42.4	-33.7	-262.5	8.7	10.1
Jun-00	0.3	1.6	11.2	2.2	17.3	11.1	49.4	-35.7	-279.9	6.2	9.7
Jul-00	0.3	1.8	23.1	2.7	21.9	11.3	64.9	-36.3	-285.9	4.6	9.5
Aug-00	0.3	2.0	42.5	3.0	24.4	11.6	50.9	-35.0	-275.3	3.7	9.6
Sep00	0.4	1.9	58.4	2.9	23.3	12.6	42.7	-33.1	-259.8	4.5	10.7

Oct-00	0.5	1.5	60.1	2.3	18.0	13.2	23.2	-32.0	-251.1	6.4	11.7
Nov-00	0.6	0.9	47.6	1.6	11.6	13.9	19.8	-31.8	-249.9	9.8	12.9
Dec-00	0.5	0.5	31.3	1.0	6.6	14.4	16.0	-32.1	-251.4	12.1	13.9
Jan-01	0.4	0.5	18.8	0.7	4.2	15.2	28.2	-32.6	-254.5	12.4	14.9
Feb-01	0.4	0.7	15.2	0.7	4.7	14.1	33.4	-33.3	-259.9	10.4	13.7
Mar-01	0.3	0.8	20.1	0.9	7.1	11.7	37.0	-34.1	-266.3	8.2	11.1
Apr-01	0.3	0.8	28.2	1.1	9.2	9.0	29.7	-34.5	-270.7	6.0	8.2
May-01	0.2	0.6	32.4	1.1	9.8	7.4	27.9	-34.6	-272.0	4.4	6.6
Jun-01	0.2	0.5	31.1	1.2	9.4	6.7	34.2	-34.4	-271.5	3.5	5.9
Jul-01	0.2	0.8	26.9	2.1	15.1	7.3	96.4	-34.1	-269.2	4.9	6.0
Aug-01	0.2	1.4	22.6	4.1	32.1	9.5	121.2	-33.3	-263.3	4.9	6.8
Sep-01	0.3	2.0	17.7	6.4	52.0	11.9	149.9	-32.3	-254.4	5.9	7.6
Oct-01	0.4	2.3	12.2	7.5	63.3	15.3	105.6	-31.3	-246.2	7.1	10.0
Nov-01	0.5	2.2	8.3	7.0	58.7	20.5	82.3	-30.8	-241.2	13.4	15.6
Dec-01	0.5	1.8	6.8	5.3	43.0	27.5	43.3	-30.7	-240.9	18.7	23.9
Jan-02	0.4	1.3	7.2	3.4	26.7	31.7	26.6	-31.1	-242.9	19.8	29.4
Feb-02	0.3	1.0	8.4	2.1	15.7	31.1	40.8	-31.7	-247.4	16.7	29.8
Mar-02	0.3	0.9	10.9	2.1	16.1	26.4	70.3	-32.4	-252.8	13.7	25.1
Apr-02	0.3	1.1	15.5	2.7	22.8	21.1	78.8	-33.0	-258.4	11.4	19.2
May-02	0.3	1.3	21.0	3.3	29.6	16.1	69.2	-33.4	-262.1	8.4	13.6
Jun-02	0.3	1.4	24.6	3.6	31.8	12.3	59.3	-33.4	-262.2	5.5	9.6
Jul-02	0.4	1.4	26.7	3.4	29.2	9.8	60.3	-32.7	-256.4	3.8	7.3
Aug-02	0.4	1.3	33.4	3.2	25.4	8.8	59.2	-31.5	-246.5	4.6	6.7
Sep-02	0.4	1.1	44.9	2.8	20.9	9.4	40.2	-30.1	-234.9	6.5	7.7
Oct-02	0.4	0.9	51.8	2.3	16.0	11.5	26.1	-28.8	-226.0	9.7	10.1
Nov-02	0.4	0.8	46.1	1.7	11.0	14.2	20.7	-28.1	-220.5	12.4	13.2
Dec-02	0.4	0.7	32.3	1.3	7.6	16.2	25.0	-27.9	-219.3	14.0	15.6

Jan-03	0.4	0.8	22.8	1.1	6.9	16.6	30.0	-28.1	-221.1	13.9	16.0
Feb-03	0.3	0.8	21.6	1.1	8.0	14.6	31.7	-28.6	-225.9	11.7	13.9
Mar-03	0.3	0.8	23.1	1.3	9.9	11.1	32.1	-29.6	-232.6	8.4	10.2
Apr-03	0.3	0.8	21.5	1.6	13.0	7.8	38.8	-30.8	-242.4	5.8	6.7
May-03	0.3	0.9	17.7	2.2	18.7	6.3	51.4	-32.3	-253.8	4.5	4.8
Jun-03	0.4	1.0	14.0	2.7	24.6	6.4	58.2	-33.7	-266.0	3.8	4.3
Jul-03	0.4	1.1	11.6	3.1	27.7	7.1	69.9	-34.8	-275.8	4.0	4.7
Aug-03	0.6	1.2	10.3	3.6	30.1	8.4	89.9	-35.3	-281.1	5.2	5.8
Sep-03	0.7	1.3	10.5	4.6	37.8	10.5	107.4	-35.2	-280.3	6.9	7.3
Oct-03	0.7	1.5	11.2	5.5	47.5	12.9	92.6	-34.4	-273.6	8.5	8.9
Nov-03	0.6	1.6	10.6	5.6	49.4	14.8	61.2	-33.4	-265.3	11.7	10.7
Dec-03	0.4	1.5	9.0	4.5	38.7	16.0	36.6	-32.8	-258.9	14.4	12.7
Jan-04	0.3	1.1	10.1	3.3	25.6	15.4	39.0	-32.8	-257.4	15.1	13.2
Feb-04	0.2	0.8	12.8	2.6	19.8	13.5	50.3	-33.1	-258.6	12.4	11.8
Mar-04	0.3	0.7	15.4	2.6	21.2	10.4	55.0	-33.7	-262.3	9.0	8.6
Apr-04	0.3	0.7	15.3	2.6	22.5	8.2	47.8	-34.5	-268.7	6.2	6.4
May-04	0.4	0.7	15.3	2.4	19.9	7.0	36.5	-35.6	-277.7	4.2	5.4
Jun-04	0.4	0.7	16.5	2.2	16.2	6.7	30.5	-36.4	-285.6	3.3	5.4
Jul-04	0.5	0.6	18.2	1.9	13.2	7.0	28.8	-36.6	-287.3	3.1	5.9
Aug-04	0.5	0.5	17.9	1.7	11.5	7.5	30.4	-35.7	-280.5	3.7	6.6
Sep-04	0.5	0.6	16.3	1.6	11.2	8.5	35.4	-33.9	-267.3	5.6	7.5
Oct-04	0.5	0.7	14.6	1.6	11.8	10.1	33.1	-32.1	-254.1	7.7	9.1
Nov-04	0.4	0.8	13.3	1.4	11.5	13.1	28.9	-31.2	-247.7	10.0	12.1
Dec-04	0.4	0.7	15.1	1.2	9.6	15.9	27.1	-31.8	-252.1	14.0	15.1
Jan-05	0.5	0.9	18.4	1.1	8.6	17.4	31.6	-33.3	-263.8	19.1	16.7
Feb-05	0.6	1.1	21.5	1.2	10.9	16.2	36.2	-34.7	-274.1	19.8	15.2
Mar-05	0.6	1.1	21.9	1.6	14.4	13.5	35.1	-34.9	-274.7	14.8	12.3

Apr-05	0.5	0.9	21.7	1.8	16.3	10.2	33.1	-34.2	-268.5	7.2	8.8
May-05	0.4	0.6	21.2	1.9	15.7	7.6	31.6	-33.8	-266.1	3.6	6.3
Jun-05	0.4	0.6	19.0	2.0	16.3	6.7	38.1	-34.2	-270.3	2.9	5.3
Jul-05	0.6	1.3	15.2	2.3	17.9	6.8	44.7	-34.4	-273.3	3.1	5.3
Aug-05	0.7	1.4	11.8	2.4	18.8	7.1	42.1	-33.9	-270.5	3.2	5.5
Sep-05	0.7	1.3	9.1	2.2	17.0	7.1	34.5	-32.8	-262.2	3.4	5.6
Oct-05	0.7	0.7	6.6	1.9	15.5	8.3	29.8	-31.6	-252.2	4.6	7.0
Nov-05	0.5	0.7	4.8	1.7	13.4	11.4	28.4	-31.1	-246.4	9.0	10.2
Dec-05	0.4	0.9	4.2	1.8	13.7	15.1	37.0	-31.2	-245.5	14.1	13.6
Jan-06	0.3	1.0	5.2	2.2	17.1	17.4	53.8	-31.8	-248.6	17.5	15.6
Feb-06	0.4	1.1	8.5	2.7	21.5	17.0	55.1	-32.2	-252.8	13.8	14.9
Mar-06	0.4	1.1	13.8	2.8	23.1	14.4	55.7	-32.8	-260.1	8.5	12.4
Apr-06	0.5	1.4	18.5	2.7	22.7	10.9	54.2	-33.9	-270.0	3.8	9.0
May-06	0.6	1.7	21.9	2.7	22.8	8.4	56.3	-34.7	-277.5	3.1	6.5
Jun-06	0.6	1.8	24.1	2.6	22.3	7.6	48.1	-34.7	-277.4	3.0	5.8
Jul-06	0.7	1.5	25.7	2.4	18.5	8.3	39.9	-33.6	-270.1	4.0	6.8
Aug-06	0.7	1.1	26.3	1.9	13.5	9.9	38.6	-31.8	-255.1	4.9	8.8
Sep-06	0.7	0.7	25.5	1.5	10.5	12.3	35.4	-29.8	-238.7	7.6	11.4
Oct-06	0.6	0.6	24.3	1.1	8.2	14.7	21.5	-28.8	-229.0	11.0	14.0
Nov-06	0.5	0.5	21.6	0.8	6.4	18.0	18.4	-29.3	-232.0	16.1	17.4
Dec-06	0.5	0.5	17.5	0.7	4.9	21.0	16.3	-30.9	-243.0	19.5	20.6
Jan-07	0.5	0.6	13.0	0.7	4.8	22.1	21.4	-32.3	-254.4	16.6	21.7
Feb-07	0.4	0.6	9.9	0.8	6.6	19.5	29.0	-33.3	-260.9	11.1	19.0
Mar-07	0.4	0.6	8.7	1.2	10.6	14.5	45.1	-34.0	-266.8	5.7	13.6
Apr-07	0.5	0.7	10.3	1.7	15.8	10.4	53.2	-34.9	-273.2	4.2	9.1
May-07	0.5	0.8	17.6	2.2	20.2	8.1	58.6	-35.5	-278.4	3.8	6.4
Jun-07	0.5	0.9	29.6	2.6	23.1	7.2	61.2	-35.7	-280.7	3.5	5.3

Jul-07	0.4	1.0	39.2	3.0	25.7	7.3	64.4	-35.1	-276.8	5.3	5.2
Aug-07	0.4	1.1	42.3	3.3	27.2	9.0	67.4	-33.3	-264.8	8.4	6.7
Sep-07	0.4	1.2	40.4	3.4	27.2	12.9	61.4	-31.0	-245.2	17.3	10.6
Oct-07	0.5	1.3	35.5	3.2	26.0	17.8	58.0	-29.1	-230.4	26.3	15.6
Nov-07	0.6	1.3	27.9	2.9	24.2	21.8	45.2	-28.5	-225.6	31.3	19.7
Dec-07	0.6	1.5	17.6	2.4	21.0	23.6	35.0	-28.8	-226.8	29.3	21.8
Jan-08		1.9		1.9	16.2	23.7	26.5	-29.2	-228.6	24.0	22.3
Feb-08		1.9		1.5	11.8	21.8	24.4	-29.7	-231.6	19.7	20.9
Mar-08		1.5		1.1	9.2	18.4	21.9	-30.9	-241.6	15.6	17.6
Apr-08		1.0		1.1	9.4	14.3	27.4	-32.6	-255.8	11.8	13.5
May-08		0.9		1.5	13.1	11.1	60.1	-34.3	-269.8	8.2	10.0
Jun-08		1.3		2.7	23.0	9.5	85.0	-35.6	-279.5	5.0	7.6
Jul-08		2.1		4.0	34.4	8.8	90.5	-36.7	-288.9	3.5	5.9
Aug-08		2.8		4.9	40.7	9.0	86.3	-37.7	-297.3	3.7	5.6
Sep-08		2.9		5.1	41.6	9.6	75.8	-37.2	-295.1	5.1	6.1
Oct-08		2.4		4.8	38.6	11.8	62.0	-35.2	-280.0	8.0	8.5
Nov-08		1.8		4.2	33.3	16.5	35.3	-33.0	-261.5	13.5	13.7
Dec-08		1.5		3.2	23.9	22.2	21.6	-32.3	-255.0	17.6	20.2
Jan-09		1.3		2.1	14.3	25.2	23.2	-33.0	-259.6	18.6	24.0
Feb-09		1.1		1.4	9.5	23.0	27.9	-34.2	-268.8	15.5	22.2
Mar-09		1.0		1.3	9.9	18.4	34.3	-35.3	-276.8	10.9	17.5
Apr-09		1.0		1.7	13.8	14.1	57.2	-35.8	-281.4	7.0	12.9
May-09		1.2		2.4	20.1	11.3	87.1	-35.9	-282.2	3.9	9.6
Jun-09		1.3		3.1	25.7	9.3	85.2	-35.9	-283.1	2.6	7.2
Jul-09		1.4		3.5	28.4	7.9	78.5	-35.8	-283.2	2.3	5.6
Aug-09		2.6		3.5	28.4	8.3	68.0	-34.8	-276.4	2.8	5.9
Sep-09		5.4		3.3	26.7	11.4	79.3	-32.9	-261.6	8.5	9.2
Oct09		9.0		3.0	23.3	17.3	63.7	-30.9	-244.9	16.9	15.4

Nov-09	10.8	2.3	17.2	24.3	48.8	-29.8	-235.7	25.5	22.9
Dec-09	9.6	1.7	10.7	29.8	39.8	-29.8	-235.5	27.5	29.0
Jan-10	6.7	1.1	6.1	32.4	44.6	-30.9	-242.7	26.8	31.8
Feb-10	4.0	0.8	4.3	31.7	34.0	-32.6	-256.2	23.8	31.3
Mar-10	2.4	0.7	4.2	28.7	33.6	-34.8	-273.0	22.7	28.4
Apr-10	1.4	0.7	4.8	24.6	34.8	-36.7	-289.5	16.6	24.2
May-10	1.0	1.0	7.2	19.8	45.7	-38.0	-300.8	11.0	19.2
Jun-10	1.1	1.7	12.0	15.5	88.1	-38.5	-305.5	4.9	14.5
Jul-10	1.5	3.4	23.7	12.0	160.5	-38.3	-304.5	3.3	10.0
Aug-10	2.2	5.7	41.6	10.2	229.6	-37.9	-301.0	3.1	6.7
Sep-10	3.1	8.5	65.4	9.7	244.6	-37.2	-296.3	3.1	4.2
Oct-10	3.8	10.6	85.6	9.8	206.4	-35.7	-283.9	4.8	3.1
Nov-10	4.3	12.1	98.4	10.1	161.2	-31.8	-253.6	7.4	2.3
Dec-10	4.7	12.6	102.8	10.5	125.7	-25.8	-205.7	11.1	1.9

Table A4: Monthly polynya total open water area (TOWA) and sea-ice extent (SIE) time series

Year	TOWA (km^2)	SIE (km^2)
Jan-79	20625	715625
Feb-79	43125	254375
Mar-79	1875	192500
Apr-79	0	961250
May-79	0	1146875
Jun-79	0	1233125
Jul-79	0	1461875
Aug-79	0	1908750
Sep-79	0	2093125
Oct-79	0	1976250
Nov-79	0	1828750
Dec-79	12500	1041875
Jan-80	45625	550625
Feb-80	51875	354375
Mar-80	10000	318125
Apr-80	0	519375
May-80	0	603125
Jun-80	0	851875
Jul-80	0	966250
Aug-80	0	1006875
Sep-80	0	1202500
Oct-80	0	1032500
Nov-80	625	1002500
Dec-80	25000	796250
Jan-81	43125	369375
Feb-81	58750	218125
Mar-81	0	129375
Apr-81	0	335625
May-81	0	762500
Jun-81	0	906875
Jul-81	0	1230625
Aug-81	0	1596250
Sep-81	0	1671875
Oct-81	0	1583750
Nov-81	0	1590000
Dec-81	6250	1219375
Jan-82	15625	576250
Feb-82	49375	201875
Mar-82	1250	380000
Apr-82	0	995625

May-82	0	1200625
Jun-82	0	1338125
Jul-82	0	1356875
Aug-82	0	1409375
Sep-82	0	1548750
Oct-82	0	1200000
Nov-82	0	1176875
Dec-82	11250	740625
Jan-83	18125	394375
Feb-83	65000	417500
Mar-83	0	388125
Apr-83	0	466875
May-83	1875	654375
Jun-83	0	968125
Jul-83	0	1207500
Aug-83	0	1452500
Sep-83	0	1570625
Oct-83	0	1698125
Nov-83	0	1610625
Dec-83	25000	1253125
Jan-84	33750	709375
Feb-84	23125	191875
Mar-84	0	151875
Apr-84	0	481250
May-84	0	888125
Jun-84	625	1026250
Jul-84	0	1235000
Aug-84	0	1571250
Sep-84	0	1923750
Oct-84	0	1986875
Nov-84	0	1456250
Dec-84	5625	1025000
Jan-85	26875	447500
Feb-85	34375	184375
Mar-85	625	216875
Apr-85	0	501875
May-85	0	842500
Jun-85	0	1038750
Jul-85	0	1450000
Aug-85	0	1813750
Sep-85	0	2025000
Oct-85	0	2039375
Nov-85	0	1580625

Dec-85	0	1199375
Jan-86	11250	658750
Feb-86	20625	298750
Mar-86	0	324375
Apr-86	0	817500
May-86	0	1070000
Jun-86	0	1575625
Jul-86	0	1834375
Aug-86	0	1822500
Sep-86	0	1925625
Oct-86	0	1725625
Nov-86	0	1509375
Dec-86	5000	1096250
Jan-87	26875	438750
Feb-87	43125	176875
Mar-87	0	587500
Apr-87	0	971875
May-87	0	1050625
Jun-87	0	1233750
Jul-87	0	1423750
Aug-87	0	1325000
Sep-87	0	1488125
Oct-87	0	1318750
Nov-87	2500	1161250
Dec-87	25000	1210625
Jan-88	41875	257500
Feb-88	38750	158125
Mar-88	0	308750
Apr-88	0	471250
May-88	0	806250
Jun-88	0	1038125
Jul-88	0	1119375
Aug-88	0	1250000
Sep-88	0	1166875
Oct-88	0	1336875
Nov-88	7500	1061875
Dec-88	18750	769375
Jan-89	26875	359375
Feb-89	31250	100625
Mar-89	625	140000
Apr-89	0	96875
May-89	0	708125
Jun-89	0	1118125

Jul-89	0	1416875
Aug-89	0	1609375
Sep-89	0	1908750
Oct-89	0	2021875
Nov-89	0	1805625
Dec-89	11250	1124375
Jan-90	13750	300000
Feb-90	19375	101875
Mar-90	0	116250
Apr-90	0	377500
May-90	0	843125
Jun-90	0	1458125
Jul-90	0	1816250
Aug-90	0	2033125
Sep-90	0	1877500
Oct-90	0	1933750
Nov-90	1875	1957500
Dec-90	24375	1363750
Jan-91	49375	410625
Feb-91	45000	110625
Mar-91	625	79375
Apr-91	0	375000
May-91	0	1050625
Jun-91	0	1087500
Jul-91	0	1275625
Aug-91	0	1605000
Sep-91	0	1705625
Oct-91	0	1575625
Nov-91	0	1351250
Dec-91	41875	697500
Jan-92	60000	81875
Feb-92	66250	70625
Mar-92	28750	144375
Apr-92	0	208750
May-92	0	464375
Jun-92	0	812500
Jul-92	0	871250
Aug-92	0	1073750
Sep-92	0	1395625
Oct-92	0	1370625
Nov-92	0	1343750
Dec-92	21875	833125
Jan-93	27500	256250

Feb-93	41250	100000
Mar-93	625	77500
Apr-93	0	386875
May-93	0	906875
Jun-93	0	1128125
Jul-93	0	1263750
Aug-93	0	1574375
Sep-93	0	1563750
Oct-93	0	1558125
Nov-93	3750	1353750
Dec-93	21875	980000
Jan-94	18750	202500
Feb-94	25625	100000
Mar-94	0	89375
Apr-94	0	173750
May-94	0	565000
Jun-94	0	1076875
Jul-94	0	1321250
Aug-94	0	1473750
Sep-94	0	1837500
Oct-94	0	1687500
Nov-94	5625	1231250
Dec-94	11250	713125
Jan-95	35000	420000
Feb-95	56875	80000
Mar-95	0	287500
Apr-95	0	599375
May-95	0	880625
Jun-95	0	1088125
Jul-95	0	1277500
Aug-95	0	1314375
Sep-95	0	1514375
Oct-95	0	1448125
Nov-95	625	1318125
Dec-95	21875	902500
Jan-96	31875	354375
Feb-96	41250	79375
Mar-96	0	228750
Apr-96	0	400625
May-96	0	927500
Jun-96	0	1305625
Jul-96	0	1444375
Aug-96	0	1745000

Sep-96	0	1882500
Oct-96	0	2015000
Nov-96	4375	2056875
Dec-96	57500	1195625
Jan-97	49375	391875
Feb-97	67500	129375
Mar-97	625	115000
Apr-97	0	678125
May-97	0	1030625
Jun-97	0	1166250
Jul-97	0	1467500
Aug-97	0	1749375
Sep-97	0	1761250
Oct-97	0	1125000
Nov-97	0	877500
Dec-97	15000	519375
Jan-98	25000	308125
Feb-98	35000	161250
Mar-98	0	176875
Apr-98	0	460000
May-98	0	680000
Jun-98	0	701250
Jul-98	0	1162500
Aug-98	0	1403125
Sep-98	0	1641250
Oct-98	0	1620000
Nov-98	0	1580625
Dec-98	16250	1338125
Jan-99	45625	319375
Feb-99	53125	133750
Mar-99	0	153125
Apr-99	0	648750
May-99	0	1155000
Jun-99	0	1444375
Jul-99	0	1475000
Aug-99	0	1801875
Sep-99	0	1660000
Oct-99	0	1565625
Nov-99	0	1509375
Dec-99	16250	1390625
Jan-00	40625	923750
Feb-00	56250	276250
Mar-00	0	156250

Apr-00	0	773750
May-00	0	1208125
Jun-00	0	1604375
Jul-00	0	1555625
Aug-00	0	1800000
Sep-00	0	1933125
Oct-00	0	1813125
Nov-00	0	1395625
Dec-00	4375	823125
Jan-01	20625	403750
Feb-01	31250	171875
Mar-01	0	176250
Apr-01	0	290000
May-01	0	672500
Jun-01	0	990625
Jul-01	0	1101250
Aug-01	0	1634375
Sep-01	0	1811875
Oct-01	0	1804375
Nov-01	6875	1966250
Dec-01	45625	1365625
Jan-02	49375	400625
Feb-02	36875	69375
Mar-02	0	110000
Apr-02	0	390000
May-02	0	670000
Jun-02	0	1098125
Jul-02	0	1563750
Aug-02	0	1621875
Sep-02	0	1293125
Oct-02	0	1198125
Nov-02	20000	1152500
Dec-02	50000	640625
Jan-03	53750	95000
Feb-03	67500	43750
Mar-03	1875	67500
Apr-03	0	77500
May-03	0	518750
Jun-03	0	880000
Jul-03	0	1167500
Aug-03	0	1589375
Sep-03	0	1826875
Oct-03	0	1796250

Nov-03	8750	1731875
Dec-03	23750	865000
Jan-04	28125	333125
Feb-04	42500	110625
Mar-04	0	160000
Apr-04	0	435625
May-04	0	839375
Jun-04	0	1109375
Jul-04	0	1371875
Aug-04	0	1690625
Sep-04	0	1918750
Oct-04	0	1787500
Nov-04	0	1417500
Dec-04	20625	1040000
Jan-05	25000	310000
Feb-05	43750	183125
Mar-05	0	236875
Apr-05	0	627500
May-05	0	1018125
Jun-05	0	1291875
Jul-05	0	1152500
Aug-05	0	1479375
Sep-05	0	1106250
Oct-05	0	1280000
Nov-05	4375	953125
Dec-05	15625	463125
Jan-06	23750	130000
Feb-06	20625	51875
Mar-06	1875	57500
Apr-06	0	428125
May-06	0	928750
Jun-06	0	1070000
Jul-06	0	1276875
Aug-06	0	1163750
Sep-06	0	1443750
Oct-06	0	1233125
Nov-06	8125	1313750
Dec-06	29375	451250
Jan-07	31250	191875
Feb-07	35000	61250
Mar-07	0	70625
Apr-07	0	166250
May-07	0	228750

Jun-07	0	702500
Jul-07	0	960625
Aug-07	0	1300000
Sep-07	0	1418750
Oct-07	0	1505625
Nov-07	3750	1330000
Dec-07	15625	929375
Jan-08	38125	279375
Feb-08	65625	49375
Mar-08	0	36875
Apr-08	0	263125
May-08	0	841875
Jun-08	0	1093125
Jul-08	0	1369375
Aug-08	0	1755625
Sep-08	0	1796875
Oct-08	0	1707500
Nov-08	10000	1414375
Dec-08	30625	888750
Jan-09	56250	314375
Feb-09	46875	57500
Mar-09	0	76875
Apr-09	0	296875
May-09	0	1053750
Jun-09	0	1482500
Jul-09	0	1563125
Aug-09	0	1598125
Sep-09	0	1836875
Oct-09	0	2046875
Nov-09	0	1818125
Dec-09	26875	895625
Jan-10	63750	205000
Feb-10	66875	10625
Mar-10	31250	0
Apr-10	0	114375
May-10	0	791875
Jun-10	0	1423750
Jul-10	0	1713750
Aug-10	0	1948125
Sep-10	0	2076250
Oct-10	0	2141875
Nov-10	1250	2175625
Dec-10	21250	1736250

Table A5: Annual chemistry for DIV2010, PIG2010, and THW2010 long cores

DIV2010

Year	MSA (ppb)	Na (ppb)	Ca (ppb)	Mg (ppb)	nssS (ppb)	S_{tot} (ppb)	δ18O (‰)	δD (‰)
1786	7.4	34.1	1.2	4.0	11.2	14.1	-26.5	-212.0
1787	7.5	39.9	1.4	5.0	10.6	14.0	-29.4	-235.6
1788	7.5	53.3	1.9	6.5	10.0	14.4	-30.1	-240.7
1789	7.6	23.7	1.1	2.9	8.5	10.5	-27.9	-223.2
1790	7.6	31.8	1.2	4.0	7.6	10.3	-28.0	-223.3
1791	7.7	13.3	0.4	1.7	11.4	12.6	-27.1	-217.1
1792	7.7	32.7	1.1	3.7	9.9	12.7	-27.6	-221.8
1793	7.8	29.4	1.1	3.4	10.9	13.4	-26.6	-213.7
1794	7.7	26.5	1.0	3.1	15.1	17.6	-26.4	-211.6
1795	6.7	34.7	1.2	4.2	10.0	12.9	-27.7	-222.2
1796	8.6	22.3	0.8	2.6	10.3	12.3	-27.9	-221.1
1797	7.5	52.1	2.0	6.0	12.6	16.9	-29.5	-237.1
1798	6.0	37.6	1.4	4.5	12.6	15.7	-28.8	-231.5
1799	4.5	24.6	0.8	2.9	9.9	12.0	-29.6	-237.7
1800	4.7	41.7	1.5	5.1	9.3	12.8	-28.8	-229.2
1801	4.6	36.8	1.3	4.6	8.0	11.1	-27.6	-221.1
1802	5.4	34.4	1.1	4.3	8.5	11.4	-28.8	-231.8
1803	5.7	18.7	0.7	2.3	9.2	10.8	-26.9	-215.1
1804	7.3	15.7	0.6	1.9	12.0	13.5	-27.7	-221.2
1805	6.7	40.1	1.5	4.6	9.9	13.3	-26.3	-209.1
1806	5.0	37.1	1.5	4.6	13.3	16.4	-27.8	-223.0
1807	7.4	63.4	2.4	7.7	10.7	16.0	-28.4	-226.5
1808	6.8	44.8	1.7	5.3	11.7	15.6	-26.9	-214.4
1809	4.6	24.5	1.0	3.3	12.2	14.2	-28.4	-224.7
1810	5.1	26.0	1.0	3.3	26.0	28.2	-29.1	-231.4
1811	7.0	49.8	1.7	6.1	21.0	25.2	-28.5	-227.1
1812	5.2	43.4	1.8	5.7	8.7	12.3	-29.0	-231.7
1813	6.6	42.0	1.7	5.3	9.2	12.9	-28.6	-228.3
1814	8.3	37.5	1.6	4.6	10.4	13.6	-28.2	-225.4
1815	6.9	28.2	1.1	3.6	12.6	15.0	-28.5	-228.0
1816	6.3	14.0	0.6	1.9	56.1	57.3	-27.1	-217.5
1817	5.2	18.5	0.6	2.3	27.9	29.4	-25.7	-205.9
1818	7.2	32.3	1.3	4.3	15.1	17.8	-26.2	-209.6
1819	9.1	33.0	1.3	3.8	12.7	15.5	-27.0	-214.7
1820	7.5	28.4	1.2	3.5	10.4	12.7	-25.8	-206.7
1821	6.4	32.7	1.3	4.1	9.4	12.2	-27.6	-220.2
1822	8.4	26.7	1.5	3.9	13.3	15.5	-28.2	-225.7
1823	7.4	26.9	1.1	3.3	11.7	13.9	-26.3	-210.5

1824	6.1	23.9	0.9	2.9	11.5	13.5	-26.6	-212.0
1825	6.1	26.0	1.1	3.2	8.3	10.4	-26.3	-209.8
1826	7.7	42.0	1.6	5.3	8.4	12.0	-27.8	-220.8
1827	6.4	23.5	0.7	2.7	9.0	11.0	-26.3	-208.0
1828	8.9	27.2	1.0	3.8	12.4	14.7	-28.3	-225.3
1829	5.5	18.9	0.7	2.4	8.8	10.4	-27.0	-215.0
1830	6.5	32.7	2.1	4.0	6.8	9.6	-26.6	-211.3
1831	7.4	40.9	4.4	5.0	9.5	12.9	-27.8	-220.2
1832	6.9	25.0	1.4	3.0	9.7	11.8	-28.6	-228.3
1833	8.1	30.6	1.1	3.9	11.6	14.2	-25.2	-200.3
1834	7.8	23.7	1.0	2.9	11.5	13.5	-25.3	-200.2
1835	7.2	20.7	1.3	2.5	11.0	12.8	-26.3	-206.6
1836	8.5	58.8	1.9	7.4	17.5	22.5	-27.5	-218.3
1837	12.7	49.0	1.7	6.3	19.6	23.7	-28.7	-228.8
1838	10.7	29.2	1.1	3.7	17.7	20.1	-26.2	-208.0
1839	9.7	22.6	1.0	2.8	13.9	15.8	-27.2	-213.7
1840	8.6	33.9	1.2	4.5	9.0	11.9	-28.9	-228.0
1841	6.1	30.1	1.0	3.8	9.1	11.6	-27.6	-219.5
1842	11.3	18.6	0.7	2.7	14.8	16.3	-26.9	-212.7
1843	6.1	15.9	0.5	1.8	7.2	8.5	-27.1	-213.3
1844	6.7	29.4	1.0	3.6	7.6	10.1	-26.7	-211.2
1845	9.4	14.8	0.5	1.9	10.1	11.4	-27.0	-213.8
1846	8.6	29.2	1.1	3.8	9.4	11.8	-27.8	-219.9
1847	6.5	19.0	0.6	2.7	10.6	12.2	-28.2	-223.1
1848	9.0	31.1	1.1	4.5	9.6	12.2	-28.2	-224.0
1849	7.1	31.1	0.9	3.3	9.2	11.8	-29.2	-230.2
1850	6.6	31.2	1.0	3.7	8.0	10.7	-28.8	-228.6
1851	5.6	35.3	1.1	4.6	7.0	9.9	-28.5	-225.0
1852	9.9	44.0	1.4	5.6	11.3	15.0	-29.2	-230.9
1853	7.5	26.5	0.9	3.6	9.3	11.5	-26.4	-208.2
1854	8.4	55.2	1.6	6.7	7.6	12.3	-26.8	-212.8
1855	7.2	34.9	1.5	4.2	9.0	12.0	-26.6	-211.8
1856	7.0	29.0	0.9	3.5	8.2	10.6	-28.0	-220.8
1857	4.4	62.2	1.9	7.7	4.1	9.3	-29.1	-230.1
1858	5.0	30.6	1.0	3.9	8.9	11.5	-28.7	-227.2
1859	7.7	27.9	0.9	3.3	13.1	15.5	-28.9	-228.9
1860	7.3	35.4	1.2	4.6	7.2	10.2	-29.2	-231.7
1861	6.3	31.0	0.9	3.9	8.7	11.3	-28.1	-222.9
1862	9.9	46.4	1.5	6.3	12.1	16.0	-28.1	-223.9
1863	9.2	18.4	0.6	2.3	17.2	18.7	-26.8	-212.7
1864	8.5	29.8	0.9	3.6	10.6	13.1	-27.8	-220.3
1865	9.3	21.4	0.7	2.9	13.8	15.5	-27.7	-219.1
1866	7.8	18.8	0.6	2.2	8.4	9.9	-27.0	-213.4

1867	6.2	21.1	0.6	2.3	6.1	7.8	-26.4	-209.1
1868	7.1	37.9	1.3	4.5	5.4	8.7	-29.1	-230.8
1869	6.4	33.5	1.1	4.5	7.2	10.0	-28.6	-227.8
1870	8.5	48.8	1.6	6.5	10.7	14.8	-28.8	-228.4
1871	6.8	29.0	0.9	3.4	9.1	11.5	-27.9	-220.9
1872	14.0	38.8	1.3	4.9	11.9	15.1	-28.1	-222.6
1873	9.7	21.3	0.7	2.6	11.1	12.9	-27.4	-216.4
1874	5.7	32.0	1.0	3.7	7.5	10.2	-27.2	-216.2
1875	6.2	42.0	1.4	4.8	10.0	13.5	-27.2	-215.7
1876	8.4	31.3	1.1	4.0	8.5	11.2	-28.2	-223.5
1877	13.2	25.7	0.9	3.0	14.3	16.5	-26.8	-213.1
1878	6.3	17.0	0.7	2.0	8.7	10.1	-29.1	-230.0
1879	8.7	31.5	1.0	4.1	10.2	12.8	-26.5	-209.3
1880	11.2	27.2	1.0	3.3	12.1	14.4	-26.5	-209.8
1881	5.3	17.6	0.7	2.3	9.5	10.9	-28.9	-230.7
1882	6.4	24.9	0.9	3.3	8.4	10.5	-26.9	-213.5
1883	6.8	14.5	0.6	1.8	9.7	10.9	-25.8	-206.0
1884	8.2	25.2	0.8	3.0	14.5	16.7	-27.6	-219.5
1885	7.2	22.3	0.8	2.9	18.8	20.6	-27.4	-218.0
1886	7.3	32.0	1.1	3.8	15.8	18.5	-26.3	-208.3
1887	6.9	26.8	1.1	3.3	13.6	15.8	-28.2	-224.8
1888	7.5	41.8	1.4	4.8	11.0	14.5	-26.6	-210.9
1889	5.5	20.0	0.7	2.4	7.6	9.3	-27.1	-213.7
1890	8.2	34.1	1.2	4.2	7.5	10.3	-28.3	-225.0
1891	7.3	37.0	1.2	4.5	8.9	11.9	-26.7	-211.5
1892	9.9	47.4	1.6	5.7	10.7	14.7	-28.5	-225.9
1893	6.4	35.6	1.2	4.3	8.9	11.9	-28.8	-228.4
1894	8.8	27.5	1.1	3.2	11.3	13.6	-27.0	-213.9
1895	8.8	20.8	1.0	2.8	15.9	17.6	-28.2	-223.3
1896	8.2	31.9	1.0	3.8	12.2	14.9	-27.9	-221.0
1897	9.0	17.0	0.6	2.4	11.8	13.3	-28.2	-223.1
1898	6.7	23.7	0.8	3.0	8.4	10.4	-26.7	-210.7
1899	7.4	41.2	1.5	5.3	6.9	10.4	-26.4	-208.1
1900	6.5	26.2	1.0	3.1	7.6	9.6	-27.2	-215.7
1901	4.8	22.6	0.8	2.9	6.5	8.4	-26.0	-206.5
1902	6.2	16.4	0.6	2.0	8.7	10.0	-26.2	-207.2
1903	12.4	29.4	1.0	3.6	12.3	14.9	-29.0	-230.0
1904	9.0	28.7	0.9	3.5	11.5	13.9	-26.6	-213.0
1905	8.2	59.9	2.0	7.2	9.9	14.9	-27.7	-219.6
1906	6.9	38.9	1.3	4.9	10.4	13.6	-29.0	-230.5
1907	6.6	37.1	1.0	2.8	9.5	12.6	-29.1	-231.3
1908	8.5	26.3	1.0	3.3	10.3	12.5	-27.9	-222.0
1909	8.9	33.4	1.1	3.8	11.5	14.4	-26.9	-213.2

1910	14.0	42.4	1.7	5.1	12.6	16.2	-27.1	-216.0
1911	8.1	28.6	1.1	3.5	10.5	13.0	-27.7	-220.0
1912	7.6	26.1	1.1	3.3	11.4	13.6	-26.4	-208.1
1913	6.7	24.5	1.1	3.0	11.7	13.7	-25.8	-203.2
1914	8.7	35.6	1.4	4.4	9.7	12.7	-28.4	-224.8
1915	9.4	19.8	1.0	2.6	14.5	16.1	-27.4	-216.8
1916	7.6	31.7	1.3	3.7	10.4	13.0	-27.9	-220.6
1917	9.2	31.1	1.1	3.8	10.6	13.2	-27.9	-220.0
1918	12.2	27.5	0.9	3.1	14.9	17.3	-27.6	-217.9
1919	10.6	32.1	1.1	3.8	11.6	14.3	-27.0	-211.9
1920	7.2	31.1	1.2	3.9	10.2	12.7	-27.6	-218.6
1921	7.5	42.2	1.7	5.3	6.7	10.1	-28.5	-225.5
1922	9.0	24.5	1.3	3.0	12.2	14.2	-26.4	-210.8
1923	9.3	26.8	0.9	3.4	11.2	13.4	-27.5	-216.8
1924	5.7	23.7	1.0	3.2	9.5	11.5	-27.7	-219.1
1925	8.2	35.1	1.3	4.3	8.1	11.1	-28.3	-223.9
1926	5.4	28.0	1.0	3.5	7.3	9.7	-26.0	-207.0
1927	6.7	18.8	0.8	2.3	8.9	10.5	-28.4	-224.5
1928	10.2	28.9	1.2	3.5	12.1	14.5	-27.3	-215.7
1929	9.0	21.7	0.9	2.7	14.2	16.0	-27.0	-212.6
1930	8.1	20.2	1.0	2.5	10.0	11.7	-27.8	-220.1
1931	8.2	28.9	1.1	3.6	9.9	12.3	-24.7	-195.4
1932	11.2	32.2	1.2	3.9	13.5	16.2	-26.4	-208.0
1933	9.4	24.8	1.0	3.1	12.3	14.4	-27.7	-218.1
1934	7.6	48.5	1.9	6.0	9.2	13.3	-27.2	-215.4
1935	10.8	27.7	1.2	3.7	12.4	14.7	-26.1	-207.6
1936	14.0	28.7	1.1	3.4	17.0	19.4	-26.8	-213.0
1937	7.8	32.1	1.2	3.8	13.8	16.5	-27.0	-215.2
1938	6.5	52.0	1.9	6.0	10.9	15.2	-26.4	-210.6
1939	5.1	40.9	0.9	2.8	7.8	11.3	-25.0	-198.9
1940	8.7	31.6	1.3	3.8	10.3	13.0	-26.8	-214.1
1941	8.1	11.3	0.6	1.4	9.9	10.9	-26.6	-210.8
1942	9.0	12.2	0.5	1.4	12.9	13.9	-27.2	-216.7
1943	10.8	42.9	1.5	5.1	11.0	14.6	-29.1	-231.9
1944	4.9	15.0	0.7	2.1	7.4	8.6	-26.9	-212.9
1945	5.1	14.8	0.7	1.9	8.6	9.9	-26.8	-212.5
1946	7.0	25.4	1.1	3.3	8.4	10.5	-26.8	-213.0
1947	6.8	28.2	1.1	3.3	9.0	11.4	-27.3	-215.2
1948	5.7	21.3	0.9	2.7	9.0	10.8	-28.1	-222.8
1949	3.6	21.6	1.0	2.8	5.7	7.5	-28.7	-227.6
1950	7.8	73.9	2.6	8.5	7.8	14.0	-27.4	-217.4
1951	7.7	27.7	1.2	3.5	20.1	22.4	-27.2	-217.3
1952	11.1	27.4	1.0	3.5	14.0	16.3	-27.3	-217.4

1953	6.6	24.9	1.1	3.2	8.1	10.4	-27.6	-218.9
1954	7.1	42.8	1.6	4.9	11.9	15.5	-27.8	-222.9
1955	6.2	39.6	1.4	4.4	7.8	11.1	-29.6	-237.7
1956	6.4	31.1	1.2	3.8	8.0	10.6	-27.9	-222.3
1957	5.6	32.4	1.1	3.8	9.1	11.8	-27.7	-221.0
1958	8.7	37.6	1.7	4.6	10.0	13.2	-30.4	-241.7
1959	7.6	24.5	0.9	2.9	7.8	9.9	-29.0	-229.9
1960	7.6	49.1	1.7	5.7	9.6	13.7	-27.5	-218.8
1961	9.7	17.9	0.7	2.2	10.1	11.6	-28.2	-224.4
1962	11.9	29.5	1.1	3.4	14.2	16.6	-27.3	-216.7
1963	5.8	22.1	0.9	2.6	9.4	11.2	-29.1	-230.7
1964	6.2	27.0	1.0	3.3	16.2	18.4	-28.8	-228.5
1965	7.7	15.1	0.5	1.9	15.2	16.5	-27.3	-216.8
1966	5.6	32.9	1.2	3.9	8.1	10.9	-26.7	-211.4
1967	7.1	37.8	1.4	4.6	9.0	12.2	-27.7	-220.7
1968	7.3	32.0	1.2	3.9	13.0	15.7	-27.6	-218.3
1969	6.5	23.0	0.9	2.7	10.0	11.9	-28.4	-226.3
1970	7.9	33.1	1.2	3.9	8.3	11.1	-27.7	-219.3
1971	6.4	21.2	0.7	2.6	7.6	9.4	-26.4	-210.2
1972	6.7	30.6	1.1	3.5	6.6	9.1	-27.3	-218.1
1973	7.6	59.7	2.1	6.6	11.7	16.7	-26.1	-207.9
1974	5.5	21.8	0.9	2.5	6.1	7.9	-29.3	-227.7
1975	7.9	35.6	1.3	4.0	6.5	9.5	-28.1	-222.9
1976	12.5	43.9	1.5	5.1	12.1	15.8	-26.3	-208.5
1977	10.4	29.8	1.0	3.5	13.1	15.6	-27.8	-221.1
1978	10.6	12.0	0.4	1.5	11.6	12.6	-26.8	-212.4
1979	6.6	20.2	0.7	2.4	7.5	9.2	-26.9	-213.6
1980	9.3	18.6	0.7	2.3	9.2	10.8	-26.3	-208.3
1981	6.8	26.2	1.0	3.3	8.1	10.3	-27.1	-215.2
1982	5.6	27.1	0.9	3.3	9.8	12.1	-27.0	-214.7
1983	8.1	27.1	1.0	3.4	13.6	15.9	-27.4	-218.3
1984	7.8	20.1	0.6	2.3	11.6	13.2	-25.6	-203.8
1985	4.6	25.7	0.9	2.7	7.1	9.3	-28.3	-225.3
1986	8.3	23.7	0.9	2.9	8.9	10.9	-28.5	-226.4
1987	9.1	32.5	1.1	3.9	9.3	12.0	-26.4	-210.1
1988	6.8	19.4	0.7	2.4	8.9	10.6	-26.1	-208.9
1989	5.7	32.6	1.2	3.8	9.2	12.0	-28.1	-222.7
1990	6.5	17.0	0.7	2.1	6.7	8.2	-26.9	-213.7
1991	6.6	18.0	0.9	2.3	8.2	9.7	-27.3	-215.4
1992	10.0	23.7	0.8	2.8	14.0	16.0	-27.7	-218.1
1993	9.8	22.0	0.7	2.6	15.3	17.1	-26.6	-210.6
1994	7.2	15.5	0.6	2.0	9.6	10.9	-28.3	-224.5
1995	18.4	26.4	1.2	3.3	16.6	18.9	-26.2	-208.3

1996	15.0	27.1	1.0	3.1	15.1	17.4	-26.9	-212.2
1997	7.6	31.4	1.1	3.7	8.1	10.7	-27.6	-217.8
1998	5.6	33.0	1.1	3.7	7.0	9.7	-26.2	-208.7
1999	7.1	28.6	0.9	3.3	8.2	10.6	-26.4	-210.7
2000	7.8	26.9	1.2	3.4	10.3	12.6	-25.0	-197.9
2001	9.9	42.0	1.5	4.7	12.4	15.9	-27.4	-217.8
2002	4.6	31.1	1.2	3.9	6.8	9.4	-28.6	-227.4
2003	7.9	27.4	0.9	3.4	10.3	12.6	-26.1	-207.3
2004	4.5	36.7	1.5	4.8	7.6	10.7	-29.4	-232.4
2005	5.1	46.1	1.7	5.7	8.3	12.1	-26.5	-211.9
2006	3.8	40.0	1.7	4.3	10.4	13.8	-25.1	-199.8
2007	5.7	18.1	1.5	2.4	11.1	12.6	-27.7	-217.4
2008	4.8	34.2	6.0	4.3	7.4	10.2	-27.6	-219.3
2009	6.5	26.7	5.1	3.6	10.3	12.5	-27.2	-215.1
2010	5.6	45.0	7.4	5.4	10.9	14.7	-28.8	-228.8

PIG2010

Year	MSA (ppb)	Na (ppb)	Ca (ppb)	Mg (ppb)	nssS (ppb)	S_{tot} (ppb)	δ18O (‰)	δD (‰)
1918		29.0	1.7	3.9	16.4	18.9	-31.4	-252.4
1919		21.6	1.2	2.9	11.0	12.8	-31.6	-253.9
1920		18.2	0.7	1.7	12.1	13.6	-31.0	-248.3
1921		41.1	7.5	3.8	12.3	15.7	-31.2	-249.1
1922		18.1	0.9	2.5	10.2	11.7	-31.2	-248.2
1923		16.0	1.9	2.3	8.0	9.3	-31.1	-247.2
1924		7.7	0.7	1.2	8.4	9.0	-31.0	-246.2
1925		16.0	1.9	2.0	10.0	11.5	-30.9	-245.2
1926		16.7	1.2	2.0	9.3	10.7	-30.5	-242.4
1927		13.3	0.9	1.7	11.2	12.3	-30.8	-244.9
1928		13.2	1.0	1.6	10.2	11.3	-32.2	-255.5
1929		24.6	1.5	3.3	10.9	13.0	-32.4	-257.4
1930		15.0	0.6	1.1	9.8	11.0	-32.6	-260.1
1931		11.7	0.4	0.6	11.0	12.0	-30.9	-245.9
1932		26.3	4.2	6.2	12.2	14.4	-32.8	-259.2
1933		35.7	18.0	1.5	14.8	17.7	-31.6	-249.9
1934		16.2	1.3	0.9	13.1	14.5	-32.1	-253.5
1935		25.3	41.8	7.5	11.6	13.7	-31.1	-248.4
1936		16.4	1.0	2.2	12.6	14.0	-31.1	-247.9
1937		15.6	1.6	2.6	12.4	13.7	-32.3	-255.4
1938		11.3	0.7	1.5	10.2	11.1	-31.8	-253.1
1939		16.6	1.0	2.1	11.0	12.4	-30.1	-237.6
1940		17.8	0.8	1.8	10.2	11.6	-30.6	-242.9
1941		12.1	1.5	1.6	12.2	13.2	-29.6	-235.3
1942		7.9	0.8	1.1	9.5	10.2	-31.1	-245.3

1943	21.9	1.1	3.0	11.1	12.9	-34.8	-277.0
1944	12.6	0.3	0.9	12.2	13.3	-32.0	-254.8
1945	11.9	1.4	2.4	16.4	17.4	-30.5	-243.3
1946	13.4	0.7	1.7	9.0	10.1	-31.3	-248.3
1947	17.5	0.9	2.3	9.7	11.1	-31.6	-250.0
1948	19.7	1.0	2.5	9.8	11.4	-32.3	-255.6
1949	9.8	0.6	1.3	9.0	9.8	-32.8	-259.9
1950	36.5	1.5	4.5	9.6	12.7	-31.8	-253.7
1951	22.1	1.3	3.2	10.8	12.7	-32.6	-259.2
1952	16.9	1.1	2.2	10.1	11.5	-33.8	-268.5
1953	12.1	0.9	1.6	9.3	10.3	-32.6	-259.1
1954	16.2	1.0	2.3	10.7	12.0	-32.9	-260.4
1955	16.6	0.9	2.1	11.4	12.8	-33.8	-269.5
1956	26.6	0.1	0.6	11.2	13.4	-33.1	-264.4
1957	12.4	2.6	6.3	10.7	11.7	-31.9	-254.4
1958	19.5	1.1	2.5	8.8	10.5	-33.6	-266.6
1959	19.3	2.1	2.3	10.6	12.2	-32.6	-257.9
1960	28.8	1.4	3.7	7.9	10.3	-32.6	-257.5
1961	15.2	1.0	2.1	11.8	13.1	-31.7	-252.5
1962	18.1	1.5	2.5	12.6	14.2	-32.4	-258.1
1963	18.4	1.0	2.4	12.5	14.1	-32.9	-260.9
1964	12.2	0.9	1.7	22.2	23.2	-32.1	-254.5
1965	13.5	0.6	1.8	17.6	18.8	-32.7	-259.2
1966	17.8	0.9	2.4	11.0	12.5	-32.4	-257.4
1967	27.3	1.2	3.9	11.5	13.8	-31.9	-255.0
1968	39.8	2.0	6.1	12.1	15.5	-34.1	-271.8
1969	14.3	0.9	2.0	11.8	13.0	-32.5	-258.0
1970	12.9	0.9	2.0	10.7	11.7	-33.3	-263.0
1971	19.4	1.0	2.9	10.5	12.1	-32.2	-255.1
1972	11.4	0.5	1.6	10.9	11.8	-32.0	-252.7
1973	19.6	0.8	2.6	11.0	12.7	-32.9	-262.4
1974	10.8	0.5	1.4	9.0	9.9	-33.6	-266.0
1975	17.8	0.8	2.4	11.1	12.6	-34.6	-272.7
1976	20.5	0.9	2.8	12.2	14.0	-31.9	-253.7
1977	22.9	0.9	3.1	11.5	13.4	-33.3	-264.2
1978	12.8	0.5	1.6	10.1	11.1	-31.2	-247.9
1979	22.4	1.3	3.0	8.9	10.8	-31.6	-252.5
1980	10.9	0.6	1.5	11.6	12.5	-31.1	-248.4
1981	10.6	0.5	1.4	8.1	9.0	-32.3	-258.6
1982	13.4	0.6	1.7	9.2	10.3	-31.8	-254.3
1983	12.3	0.5	1.5	10.1	11.1	-34.5	-274.8
1984	12.5	0.5	1.7	11.2	12.3	-31.9	-254.0
1985	18.6	1.4	2.5	8.5	10.0	-32.8	-262.0

1986		15.9	1.1	2.1	9.7	11.0	-33.7	-268.7
1987		14.5	0.6	2.0	9.9	11.1	-32.1	-256.8
1988		12.4	0.5	1.6	11.3	12.3	-31.7	-253.8
1989		24.0	1.1	3.1	9.7	11.8	-33.9	-270.8
1990		18.6	1.0	2.4	9.9	11.4	-34.3	-273.1
1991		16.9	0.8	2.3	15.2	16.6	-31.3	-249.4
1992		14.5	0.7	1.9	20.6	21.9	-31.0	-246.7
1993	11.5	9.9	0.6	1.2	20.8	21.6	-31.6	-250.2
1994	11.3	17.3	0.7	2.1	14.9	16.4	-32.3	-256.3
1995	10.1	14.4	0.7	1.8	12.0	13.2	-32.1	-255.9
1996	9.7	12.6	0.5	1.6	14.4	15.4	-32.3	-256.9
1997	12.1	29.0	1.0	3.4	12.0	14.4	-31.0	-245.4
1998	7.0	12.0	0.5	1.4	9.5	10.5	-30.1	-240.2
1999	8.6	22.7	2.6	2.9	9.6	11.5	-32.9	-261.5
2000	7.0	10.9	0.9	1.3	9.5	10.4	-30.4	-241.0
2001	10.6	27.7	1.1	3.4	13.0	15.3	-33.1	-264.9
2002	9.7	8.3	1.2	1.1	10.0	10.8	-32.9	-261.4
2003	6.7	21.9	1.0	2.6	8.3	10.1	-30.7	-244.5
2004	8.3	14.8	0.7	1.9	9.3	10.6	-32.7	-259.5
2005	8.6	15.7	0.7	1.9	11.4	12.7	-32.7	-260.2
2006	9.0	13.1	0.4	1.5	10.9	12.0	-32.5	-257.4
2007	9.4	12.4	0.7	1.5	11.7	12.7	-32.2	-256.0
2008	8.8	22.4	1.1	2.7	10.2	12.1	-32.1	-254.5
2009	9.4	26.8	14.2	3.7	15.9	18.2	-31.4	-250.4
2010	10.1	38.9	13.4	7.1	12.7	16.0	-33.7	-268.1

THW2010

Year	MSA (ppb)	Na (ppb)	Ca (ppb)	Mg (ppb)	nssS (ppb)	S_{tot} (ppb)	δ18O (‰)	δD (‰)
1867		17.4	0.7	2.4	10.2	11.6	-31.7	-251.6
1868		12.1	0.6	1.6	9.5	10.4	-33.1	-263.3
1869		29.4	1.2	3.9	10.1	12.6	-34.0	-271.7
1870		16.2	0.6	2.2	13.2	14.6	-34.8	-277.3
1871		20.4	0.7	2.6	10.3	12.0	-35.6	-284.0
1872		27.8	1.1	3.7	11.0	13.3	-34.0	-270.0
1873		20.2	0.7	2.6	10.3	12.0	-32.9	-260.6
1874		21.2	0.8	2.6	9.5	11.3	-32.0	-255.2
1875		33.4	1.5	4.5	7.5	10.3	-34.2	-272.1
1876		23.7	0.9	3.1	10.9	12.9	-31.0	-247.9
1877		21.6	0.9	2.6	12.2	14.1	-29.4	-235.5
1878		8.9	0.4	1.2	11.3	12.0	-29.4	-234.5
1879		24.6	0.9	2.9	10.0	12.0	-31.8	-252.2
1880		9.7	0.5	1.2	12.4	13.2	-32.4	-257.4
1881		16.4	0.6	2.2	12.9	14.2	-33.5	-266.7

1882	13.7	0.6	1.8	9.4	10.6	-31.9	-253.9
1883	11.9	0.6	1.6	8.7	9.7	-32.0	-255.2
1884	19.8	0.8	2.5	16.1	17.8	-31.7	-253.2
1885	17.2	0.7	2.3	23.5	24.9	-32.7	-261.0
1886	19.0	0.7	2.4	19.1	20.7	-31.6	-251.8
1887	24.0	0.9	3.0	13.8	15.8	-31.9	-255.4
1888	17.3	0.7	2.3	10.6	12.1	-31.2	-250.7
1889	15.7	0.5	2.0	9.6	10.9	-31.3	-250.3
1890	15.8	0.9	2.3	10.5	11.8	-33.4	-266.8
1891	15.0	0.6	2.0	10.9	12.1	-32.2	-257.3
1892	29.5	1.3	4.2	12.0	14.5	-32.4	-258.6
1893	24.5	0.9	3.0	7.4	9.5	-33.1	-262.1
1894	12.8	0.5	1.7	12.4	13.5	-33.7	-268.5
1895	15.1	0.5	2.2	12.9	14.2	-33.7	-269.5
1896	26.8	1.0	3.4	9.3	11.5	-32.4	-258.6
1897	27.4	1.2	3.5	9.9	12.2	-32.0	-255.8
1898	9.5	0.3	1.3	8.7	9.5	-31.9	-255.6
1899	17.2	0.6	2.1	9.5	10.9	-31.4	-251.6
1900	9.2	0.3	1.2	9.6	10.4	-31.9	-254.2
1901	10.3	0.3	1.2	9.2	10.1	-32.3	-255.7
1902	11.1	0.4	1.4	10.1	11.1	-31.6	-250.7
1903	21.9	0.9	2.7	13.8	15.6	-33.2	-262.0
1904	17.8	0.7	2.5	13.6	14.9	-31.1	-247.8
1905	27.1	1.2	3.4	10.7	12.9	-32.7	-260.1
1906	13.8	0.6	2.0	10.3	11.5	-33.0	-262.1
1907	17.0	0.6	2.1	9.5	10.9	-32.2	-255.4
1908	20.4	0.9	2.5	8.7	10.4	-33.8	-268.6
1909	28.1	1.1	3.7	10.8	13.1	-34.1	-270.9
1910	12.9	0.6	1.7	12.5	13.6	-33.7	-267.6
1911	20.9	0.7	2.5	9.8	11.6	-32.1	-254.2
1912	15.1	0.5	2.0	10.5	11.7	-30.7	-243.9
1913	14.9	0.6	1.9	11.7	13.0	-32.0	-253.9
1914	13.0	0.5	1.7	10.9	12.0	-33.1	-262.7
1915	22.5	0.8	3.0	10.9	12.8	-33.2	-264.1
1916	25.1	0.9	3.2	9.2	11.3	-32.1	-255.6
1917	23.4	1.0	3.0	11.9	13.9	-32.7	-259.1
1918	11.9	0.4	1.6	11.7	12.7	-32.0	-253.9
1919	13.0	0.6	1.7	10.0	11.1	-32.0	-253.2
1920	14.9	0.6	1.8	8.5	9.7	-33.3	-265.4
1921	45.0	2.1	6.8	6.5	10.3	-34.1	-272.2
1922	21.9	0.9	2.7	11.6	13.5	-33.4	-264.0
1923	15.0	0.6	1.8	10.6	11.8	-31.8	-250.5
1924	15.0	0.7	1.9	8.1	9.4	-33.0	-260.1

1925		21.3	0.9	2.7	9.6	11.5	-34.6	-272.6
1926		22.3	0.9	2.7	8.4	10.3	-32.6	-257.5
1927		27.4	1.2	3.4	12.7	15.1	-32.4	-256.0
1928		13.9	0.7	1.6	24.6	25.8	-31.9	-250.7
1929		17.9	0.8	2.2	24.0	25.5	-33.1	-261.3
1930		20.7	0.9	2.5	12.9	14.7	-32.6	-257.9
1931		15.2	0.7	1.8	7.5	8.7	-32.4	-255.9
1932		28.5	1.2	3.6	8.2	10.6	-33.9	-267.1
1933		17.1	0.7	2.0	6.9	8.4	-32.5	-257.1
1934		21.5	1.0	3.0	6.3	8.0	-32.1	-251.9
1935		21.7	0.8	2.6	5.9	7.8	-31.8	-251.8
1936		22.3	0.9	2.7	9.3	11.2	-34.0	-268.2
1937		29.2	1.3	3.6	11.5	13.9	-32.1	-254.0
1938		25.2	1.1	3.1	9.2	11.3	-32.0	-253.3
1939		20.3	0.7	2.4	7.5	9.2	-31.4	-247.8
1940		12.1	1.5	1.6	10.5	11.5	-30.9	-244.2
1941		19.9	0.9	2.4	7.9	9.6	-30.7	-242.1
1942		18.9	0.8	2.2	9.4	11.0	-30.9	-243.0
1943		51.2	2.1	6.7	11.6	15.9	-33.7	-266.5
1944		17.1	0.8	2.2	12.3	13.7	-31.4	-247.9
1945	9.2	24.1	1.4	3.1	13.5	15.6	-32.3	-256.6
1946	8.8	18.8	0.9	2.4	10.4	12.0	-31.5	-248.5
1947	8.3	16.9	0.7	2.1	9.8	11.2	-33.3	-264.4
1948	7.8	10.0	0.5	1.2	9.7	10.5	-32.4	-254.3
1949	7.4	18.3	0.7	2.2	9.7	11.2	-31.6	-250.0
1950	8.7	27.1	1.0	3.4	8.8	11.1	-34.0	-269.0
1951	11.7	24.4	1.0	3.0	12.5	14.6	-32.9	-260.3
1952	9.0	19.3	0.8	2.4	10.8	12.4	-33.6	-267.4
1953	8.8	21.7	0.9	2.7	13.3	15.1	-33.5	-264.8
1954	11.0	25.3	1.2	3.0	16.6	18.7	-33.4	-264.5
1955	10.1	18.0	0.8	2.2	13.7	15.3	-34.0	-268.7
1956	9.5	37.7	1.5	4.6	11.6	14.9	-33.5	-263.6
1957	10.5	25.7	1.0	3.1	14.3	16.5	-33.1	-261.3
1958	9.8	26.3	1.0	3.0	13.3	15.5	-33.4	-264.0
1959	7.5	20.5	1.4	2.7	10.7	12.4	-33.8	-267.2
1960	8.0	26.1	1.1	3.2	11.3	13.5	-33.0	-261.4
1961	8.9	21.5	0.9	2.5	10.2	12.0	-33.7	-267.1
1962	10.2	14.0	0.8	1.8	11.4	12.6	-33.4	-265.3
1963	10.5	14.3	1.3	1.7	12.4	13.6	-32.9	-260.8
1964	7.9	14.8	0.7	1.8	20.3	21.5	-34.7	-273.8
1965	8.2	11.4	0.7	1.4	18.0	19.0	-32.7	-257.6
1966	7.2	21.2	1.0	2.5	10.9	12.7	-32.5	-256.4
1967	8.7	19.9	0.9	2.5	12.1	13.8	-31.8	-250.0

1968	6.9	22.1	0.9	2.8	10.8	12.6	-34.6	-270.0
1969	7.4	25.2	1.1	3.1	10.4	12.5	-33.8	-266.1
1970	7.5	19.4	0.9	2.3	8.9	10.5	-33.3	-260.7
1971	10.4	15.8	0.7	2.0	10.1	11.4	-32.9	-257.5
1972	7.3	9.6	0.5	1.2	10.0	10.8	-32.8	-257.6
1973	8.1	37.6	1.5	4.5	10.7	13.8	-33.8	-266.5
1974	7.4	24.0	1.1	3.2	8.3	10.4	-34.1	-268.0
1975	8.6	38.4	1.6	5.0	13.3	16.5	-33.5	-264.0
1976	13.2	35.6	1.6	4.7	13.6	16.6	-35.0	-274.6
1977	11.8	28.6	1.3	3.7	12.6	15.0	-33.7	-265.2
1978	9.6	10.8	0.5	1.5	11.0	11.9	-34.9	-274.5
1979	7.8	28.1	1.1	3.5	9.6	11.9	-33.9	-267.3
1980	6.3	22.4	0.8	2.6	7.5	9.4	-32.9	-258.7
1981	6.0	18.6	0.8	2.4	8.6	10.2	-32.7	-256.4
1982	6.6	16.8	0.7	2.0	11.9	13.3	-32.9	-258.7
1983	7.0	13.6	0.6	1.8	10.9	12.1	-33.1	-258.8
1984	9.0	13.8	0.5	1.7	12.0	13.2	-32.8	-256.2
1985	7.2	27.1	1.0	3.4	12.3	14.6	-33.4	-261.9
1986	8.7	12.4	0.6	1.5	14.8	15.9	-35.8	-279.7
1987	7.3	20.0	1.0	2.4	9.4	11.1	-35.4	-275.9
1988	5.7	16.8	0.7	2.1	7.3	8.7	-33.1	-259.4
1989	7.8	30.4	1.3	3.8	11.7	14.2	-33.5	-263.4
1990	10.9	23.6	0.9	3.0	13.4	15.4	-32.2	-252.8
1991	10.6	17.8	0.8	2.2	15.8	17.3	-33.2	-259.9
1992	9.9	13.1	0.7	1.5	19.6	20.7	-32.3	-253.5
1993	8.7	14.6	0.9	1.8	20.2	21.4	-33.7	-265.3
1994	9.7	23.1	1.0	2.9	15.2	17.2	-32.8	-257.3
1995	13.4	18.0	0.9	2.1	16.9	18.4	-33.8	-265.2
1996	10.3	27.0	1.2	3.5	12.5	14.8	-34.5	-268.8
1997	6.0	15.8	1.2	1.9	12.1	13.4	-32.0	-251.7
1998	8.4	11.7	0.7	1.3	11.2	12.2	-30.2	-236.8
1999	8.7	21.7	1.1	2.6	11.2	13.1	-32.5	-255.5
2000	9.5	14.6	1.2	1.8	12.7	13.9	-32.8	-257.2
2001	8.2	26.3	1.2	3.2	10.7	12.9	-33.0	-259.1
2002	10.5	20.4	1.1	2.6	15.8	17.5	-31.2	-244.1
2003	8.2	26.5	1.1	3.1	8.8	11.0	-32.4	-256.5
2004	7.5	15.7	0.7	2.0	9.0	10.3	-33.9	-266.1
2005	8.8	14.7	0.9	1.8	9.3	10.6	-33.4	-264.3
2006	9.5	16.1	1.1	2.0	11.9	13.3	-32.0	-254.3
2007	13.5	19.6	0.9	2.3	13.0	14.6	-32.7	-257.4
2008	11.3	24.7	1.9	3.0	12.6	14.6	-33.7	-265.1
2009	12.0	18.8	3.9	2.4	15.2	16.7	-33.7	-265.8
2010	11.6	37.9	2.9	4.9	14.9	18.0	-35.1	-277.9

Appendix A2

Supplemental Material for Chapter 2: Ice sheet record of recent sea-ice behavior and polynya variability in the Amundsen Sea, West Antarctica

MSA and polynya correlations

DIV2010S MSA fluxes, annually-summed MSA concentrations, and annual maximum MSA concentrations were correlated with annually-integrated total open water area within the Amundsen Sea and Pine Island Bay polynyas (TOWA), annual maximum open water area within the polynyas, and number of days per year the polynyas were open (open water days defined in methods of Criscitiello et al., 2013a). These correlations were performed to determine which MSA records (concentrations, maxima, fluxes) were most strongly linked with various polynya characteristics (TOWA, maximum open water area, duration).

Supplemental Tables

	2002-2003	2003-2004	2004-2005	2005-2006	2006-2007	2007-2008	2008-2009	2009-2010
TOWA (km^2)	248188	177843	172082	147290	182043	221661	222376	223874
Max Open Water (km^2)	61875	54570	59063	43984	55547	61914	58242	60742
Duration (days)	129	107	86	67	91	113	115	106
Max MSA (ppb)	22	18	18	17	14	25	23	17
MSA Summed (ppb)	81	38	59	59	37	139	58	85
MSA Flux ($g/cm^2/yr$)	3E-06	4E-06	2E-06	2E-06	2E-06	6E-06	3E-06	2E-06

Table 1. Table of annual DIV2010S MSA fluxes, annually-summed MSA concentrations, and annual maximum MSA concentrations; annually-integrated total open water area within the Amundsen Sea and Pine Island Bay polynyas (TOWA),

annual maximum open water area within the polynyas, and number of days per year the polynyas were open (duration).

Supplemental Figures

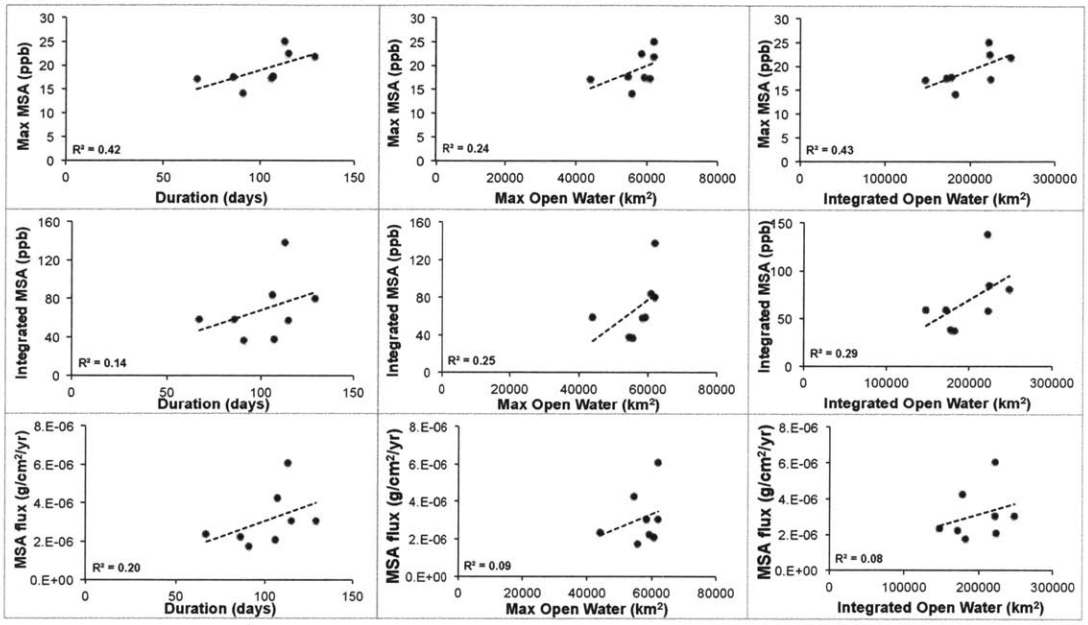

Figure 1. MSA variables (maximum MSA, integrated MSA, MSA flux) plotted against polynya variables (TOWA, maximum open water area, duration). R^2 values are shown on plots.

Appendix A3
Supplemental Material for Chapter 3: Tropical Pacific influence on source and transport of marine aerosols to West Antarctica

Oxygen isotope records and firn-core dating

We analyzed oxygen isotopes in all firn cores except UPT2009 (5-cm minimum resolution) using a Picarro cavity ring-down spectroscopy analyzer linked directly with a continuous ice-core melter system. Sample isotope ratios were standardized using three working standards calibrated against the IAEA standards VSMOW and SLAP. Final $\delta^{18}O$ values are on the VSMOW/SLAP scale. The $\delta^{18}O$ record for UPT2009 was analyzed as discrete samples at the UC Davis Stable Isotope Facility using similar analytical methods. We established an age-depth relationship and determined accumulation rates by matching the $\delta^{18}O$ firn-core records with regional surface temperature data for the UPT2009 record, and with summer and winter solstice dates for the other three core sites (linearly interpolating between solstices). Where $\delta^{18}O$ records were ambiguous, we additionally used the nssS/Na summer peak (indicative of summer solstice) to pin the annual $\delta^{18}O$ maxima.

Statistical significance in monthly figures

Statistical significance for the monthly correlations (where autocorrelation is a concern) was determined using 1,000 Monte-Carlo simulations; $p < 0.1$; Ebisuzaki 1997). This statistical test produces random time series with the same autocorrelation as the original time series by adding a random phase in Fourier-space, directly accounting for the autocorrelation characteristics of the time series when assessing the confidence

level of correlations (Ebisuzaki 1997). Within the annual cycle, we estimate a maximum possible error in the interpolated age scale of ±2 months, similar to others who utilize the same methods (e.g., Abram et al. 2011), which may weaken some monthly correlations.

References

Abram, N. J., R. Mulvaney, and C. Arrowsmith, 2011: Environmental signals in a highly resolved ice core from James Ross Island, Antarctica. *J. Geophys. Res.*, **116**, D20116.

Ebisuzaki, W., 1997: A method to estimate the statistical significance of a correlation when the data are serially correlated. *J. Climate*, **10**, 9, 2147-2153.

Supplemental Figures

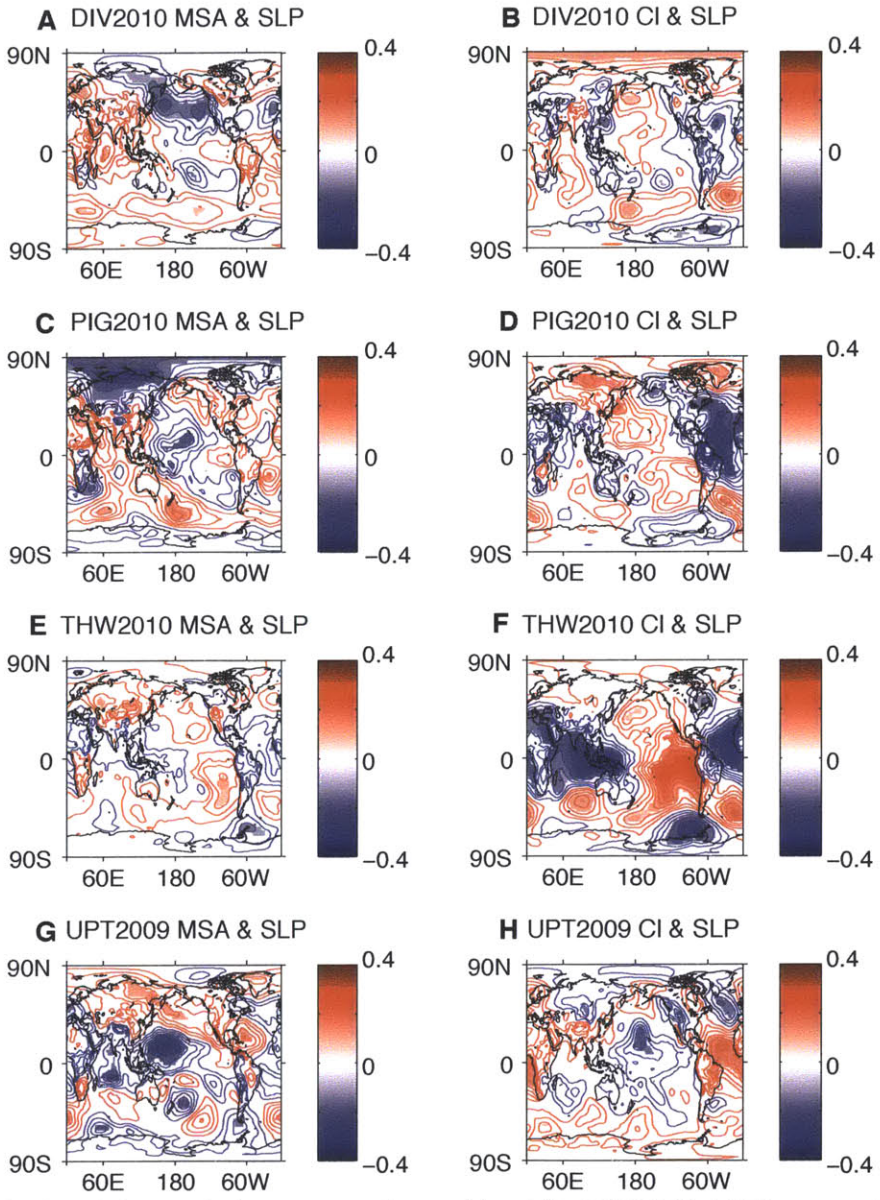

Figure 1. Spatial correlation maps of monthly (A) DIV2010 MSA anomalies, (B) DIV2010 Cl^- anomalies, (C) PIG2010 MSA anomalies, (D) PIG2010 Cl^- anomalies, (E) THW2010 MSA anomalies, (F) THW2010 Cl^- anomalies, (G) UPT2009 MSA anomalies, and (H) UPT2009 Cl^- anomalies with monthly SLP anomalies. Filled in regions indicate >90% significance (confidence determined using Monte-Carlo simulations; Ebisuzaki 1997).

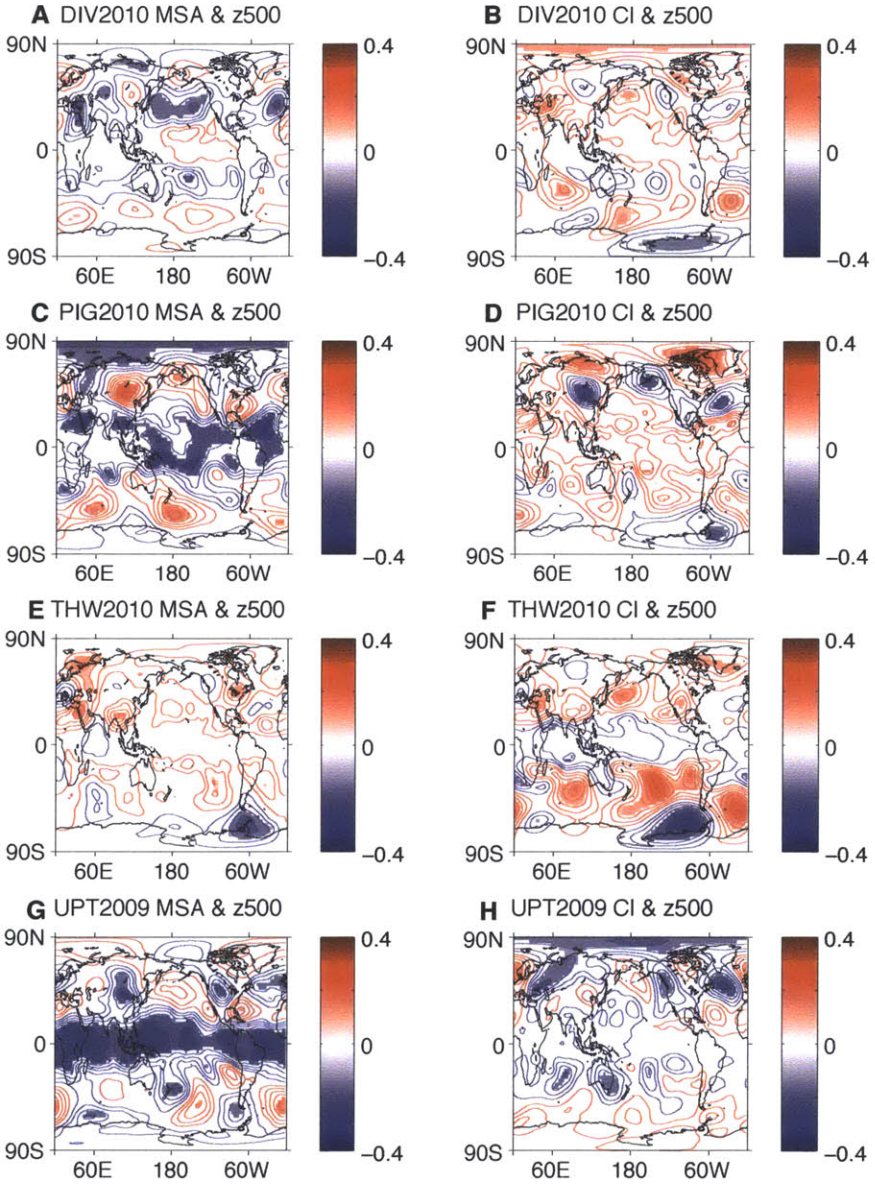

Figure 2. Spatial correlation maps of monthly (A) DIV2010 MSA anomalies, (B) DIV2010 Cl^- anomalies, (C) PIG2010 MSA anomalies, (D) PIG2010 Cl^- anomalies, (E) THW2010 MSA anomalies, (F) THW2010 Cl^- anomalies, (G) UPT2009 MSA anomalies, and (H) UPT2009 Cl^- anomalies with monthly 500 hPa GH (z500) anomalies. Filled in regions indicate >90% significance (confidence determined using Monte-Carlo simulations; Ebisuzaki 1997).

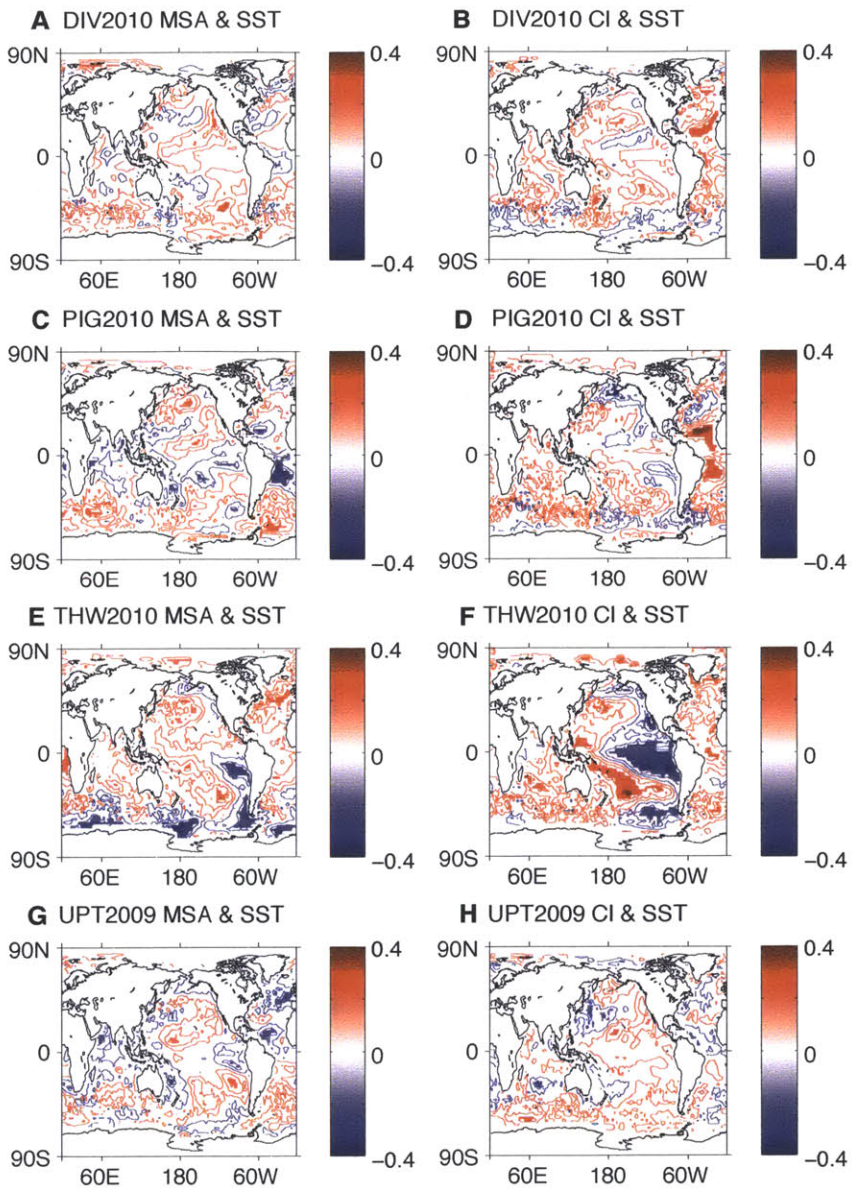

Figure 3. Spatial correlation maps of monthly (A) DIV2010 MSA anomalies, (B) DIV2010 Cl^- anomalies, (C) PIG2010 MSA anomalies, (D) PIG2010 Cl^- anomalies, (E) THW2010 MSA anomalies, (F) THW2010 Cl^- anomalies, (G) UPT2009 MSA anomalies, and (H) UPT2009 Cl^- anomalies with monthly SST anomalies. Filled in regions indicate >90% significance (confidence determined using Monte-Carlo simulations; Ebisuzaki 1997).

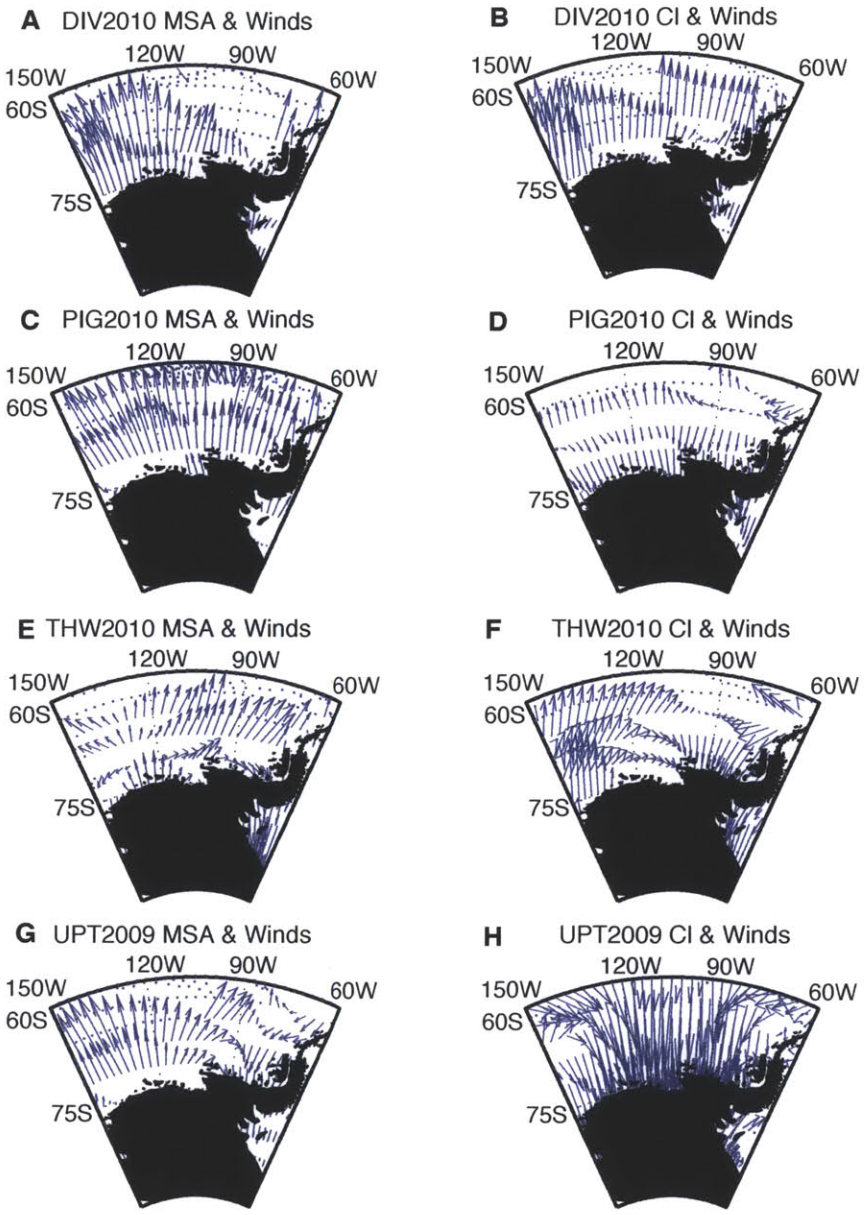

Figure 4. Regression of monthly wind anomalies on (A) DIV2010 MSA anomalies, (B) DIV2010 Cl^- anomalies, (C) PIG2010 MSA anomalies, (D) PIG2010 Cl^- anomalies, (E) THW2010 MSA anomalies, (F) THW2010 Cl^- anomalies, (G) UPT2009 MSA anomalies, and (H) UPT2009 Cl^- anomalies.

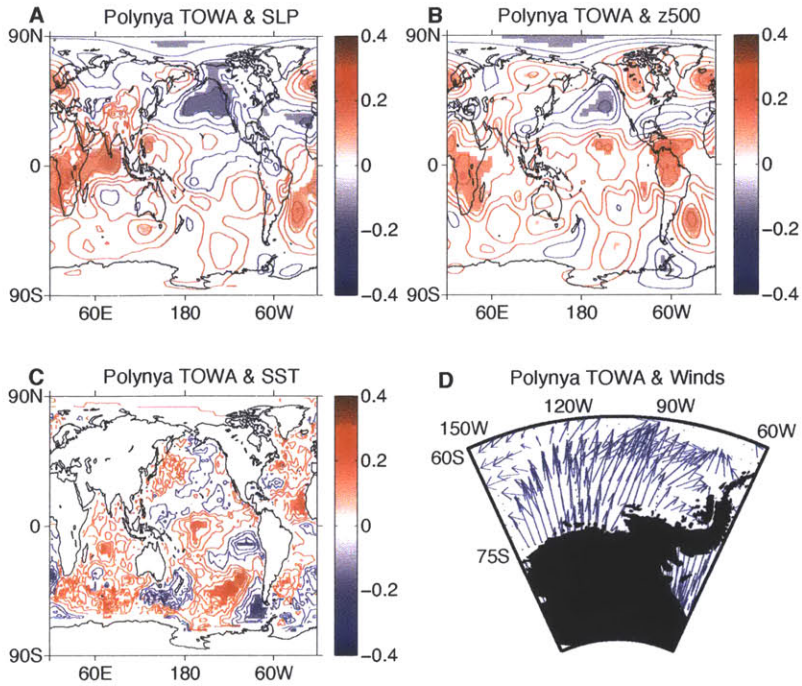

Figure 5. Spatial correlation maps of monthly polynya total open water area (TOWA) and monthly (A) SLP, (B) 500 hPa GH (z500), and (C) SST. Filled in regions indicate >90% significance (confidence determined using Monte-Carlo simulations; Ebisuzaki 1997). (D) Regression of monthly wind anomalies on TOWA anomalies.

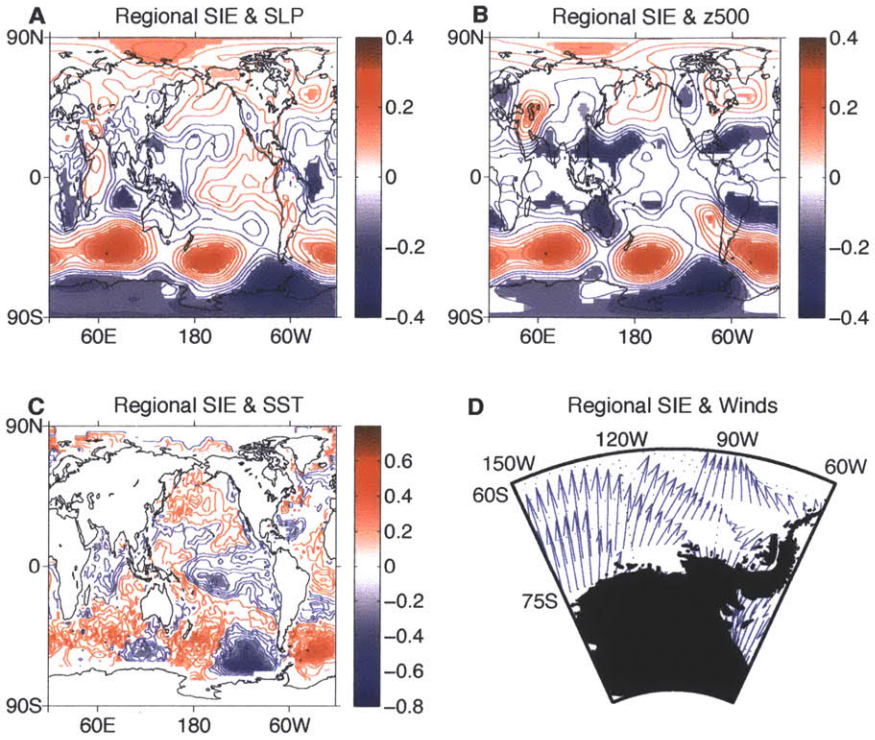

Figure 6. Spatial correlation maps of monthly regional sea ice extent (SIE, for the region between 80°W–140°W and 60°S–71°S) and (A) SLP, (B) 500 hPa GH (z500), and (C) SST. Filled in regions indicate >90% significance (confidence determined using Monte-Carlo simulations; Ebisuzaki 1997). (D) Regression of monthly wind anomalies on SIE anomalies.